Report No. FAA-74-75, I

MULTIPATH IN AIR TRAFFIC CONTROL FREQUENCY BANDS

Volume I - Classification of Multipath, Effects of Multipath on Systems, and Causes of Multipath

Edited by William J. Hartman

U. S. Department of Commerce
Office of Telecommunications
Institute for Telecommunication Sciences
Boulder, Colorado

July 1974

Document is available to the public through the
National Technical Information Service,
Springfield, Virginia 22151

Prepared for

U.S. DEPARTMENT OF TRANSPORTATION
FEDERAL AVIATION ADMINISTRATION
Systems Research & Development Service
Washington, D.C. 20590

NOTICE

This document is disseminated under the sponsorship of the Department of Transportation in the interest of information exchange. The United States Government assumes no liability for its contents or use thereof.

TECHNICAL REPORT STANDARD TITLE PAGE

1. Report No.	2. Government Accession No.	3. Recipient's Catalog No.
FAA-RD-74-75 ,I		

4. Title and Subtitle	5. Report Date
Multipath in the Air Traffic Control Frequency Bands Vol. I	July 1974
	6. Performing Organization Code
7. Author(s)	8. Performing Organization Report No.
Hartman, William J. (Editor)	
9. Performing Organization Name and Address	10. Work Unit No.
Office of Telecommunications, Institute for Telecommunication Sciences, U. S. Dept. of Commerce, Boulder, Colorado 80302	11. Contract or Grant No. DOT-FA72WAI-239
	13. Type of Report and Period Covered
12. Sponsoring Agency Name and Address **U.S. Department of Transportation** **Federal Aviation Administration** **Systems Research and Development Service** **Washington, D.C. 20590**	14. Sponsoring Agency Code ARD-60

15. Supplementary Notes

Vol. I - Classification of Multipath, Effects of Multipath on Systems, and Causes of Multipath

16. Abstract

Historically, multipath problems have been handled on an ad hoc basis requiring liberal portions of hindsight, engineering ingenuity and serendipity. However, as is often the case, once the underlying principles are identified, theoretical developments advanced rapidly. Implementation of the techniques suggested by the theory has proceeded more slowly. Thus, many theoretical results remain unverified or only partially substantiated by experiment. In this handbook, we have collected theories and techniques which have one or more of the following qualities: It has been in frequent use by engineers; it has been shown to be accurate; it can be applied to a wide variety of problems; it offers an easily obtainable upper or lower bound.

Most of the problems arising because of multipath cannot be solved or described precisely, but instead involve assumptions or approximations, the effects of which cannot be quantified. The responsibility for the decision on which approximation or assumption to use for a particular problem is with the reader.

Since the handbook is directed toward air traffic control (ATC) frequencies, most of the material presented is oriented toward frequencies above VHF, and toward line-of-sight paths. Two special sections, one on Omega and one on Loran are included. No information on HF propagation or ionospheric scatter is included.

Finally, selection of the material in this handbook has been heavily influenced by the systems presently used by the FAA.

17. Key Words	18. Distribution Statement
Multipath; Air-traffic-control frequencies; Doppler; Diversity; Path-loss calculations; Radar refractivity; Scintillation calculations; Omega; Loran	Document is available to the public through the National Technical Information Service, Springfield, Virginia 22151.

19. Security Classif. (of this report)	20. Security Classif. (of this page)	21. No. of Pages	22. Price
UNCLASSIFIED	UNCLASSIFIED	300	

Form DOT F 1700.7 (8-69)

William J. Hartman, Editor*

The following contributed chapters or significant portions of chapters in this handbook

Crary, James H. **

Dutton, Evan J.*

Gierhart, Gary D.*

Hartman, William J.*

Hufford, George A.*

Johnson, Mary Ellen*

Liebe, Hans J.*

Ma, Mark T.*

Pope, Joseph H.***

Spaulding, Arthur D.*

Wieder, Bernard*

---

*Office of Telecommunications, Institute for Telecommunication Sciences, Boulder Laboratories, Boulder, Colorado 80302

**947 Crestmoor Drive, Boulder, Colorado

***Space Environment Laboratory, Environmental Research Laboratory, National Oceanic and Atmospheric Administration, Boulder, Colorado 80302

TABLE OF CONTENTS

Multipath in Air Traffic Control Frequency Bands

VOLUME I

LIST OF FIGURES

PREFACE

Historically, multipath problems have been handled on an ad hoc basis requiring liberal portions of hind-sight, engineering ingenuity and serendipity. However, as is often the case, once the underlying principles are identified, theoretical developments advance rapidly. Implementation of the techniques suggested by the theory has proceeded more slowly. Thus, many theoretical results remain unverified or only partially substantiated by experiment. In this handbook, we have collected theories and techniques which have one or more of the following qualities: It has been in frequent use by engineers; it has been shown to be accurate; it can be applied to a wide variety of problems; it offers an easily obtainable upper or lower bound.

Most of the problems arising because of multipath cannot be solved or described precisely, but instead involve assumptions or approximations, the effects of which cannot be quantified. The responsibility for the decision on which approximation or assumption to use for a particular problem is with the reader.

Since the handbook is directed toward air traffic control (ATC) frequencies, most of the material presented is oriented toward frequencies above VHF, and toward line-of-sight paths. Two special sections, one on Omega and one on Loran are included. No information on HF propagation or ionospheric scatter is included.

Finally, selection of the material in this handbook has been heavily influenced by the systems presently used by the FAA.

AI. CLASSIFICATIONS OF MULTIPATH

AI-A. Introduction

Multipath as used here will be interpreted to include propagation over paths passing through different parts of space, paths with different physical properties, paths which are changing with time, or combinations of these (see fig. 1). The purpose of this chapter is to develop methods which permit a mathematical description or classification of this multipath, which is independent of the signals experiencing the multipath, but one which is useful for describing the effects of this multipath on these signals.

Most analytical treatments of multipath problems are either based on or can be formulated in terms of a linear, time-variant, impulse response function. The purpose of this chapter is to describe such functions and approximations to these functions in a variety of ways that will facilitate identification with predicted or measured quantities.

For system evaluation, it is necessary to have additional information, not covered here, such as a description of the signal, the additive noise, the signal processing, etc. The full generality of the mathematical

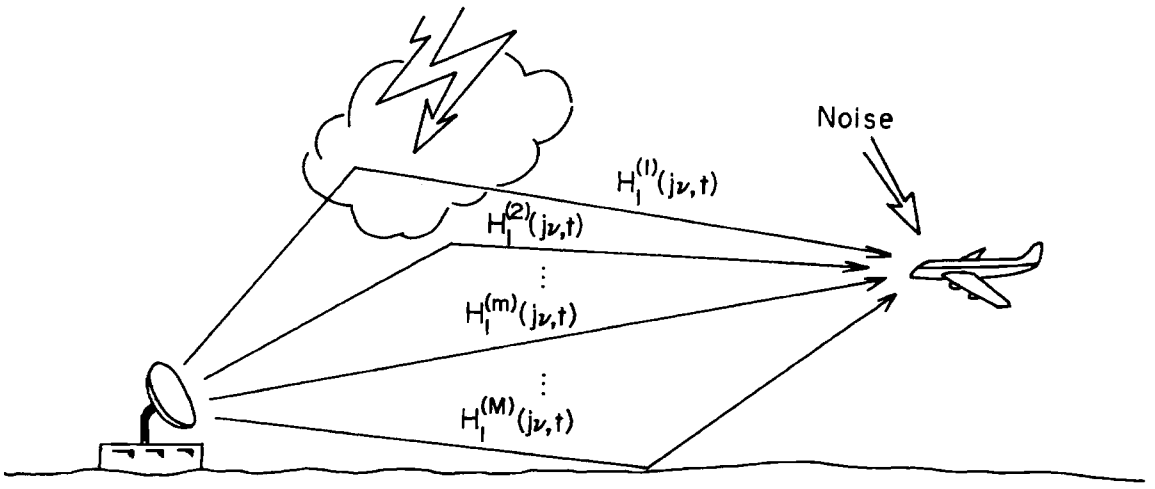

Figure AI-1. An example of assigning a system function to each path. An alternate approach would assign a single system function.

formulation in section B below is seldom used for systems evaluation, primarily because of insufficient information for the description of the impulse response function, but also because of mathematical difficulties associated with the analytical representation of the signal. However, it is useful for providing insight into the nature of multipath problems.

In the implementation of the approach to the channel as a time-variant linear filter, the basic techniques employed in this chapter are essential. The input signal is considered to be made up of a sum of appropriately weighted elementary components, such as impulse functions of time (a pulse of infinitesimal duration) or frequency (a sinusoid of infinitesimal line width). For a linear transmission medium, the function of time or frequency (or both) that describes the manner in which the medium modifies each elementary component employed in the representation of the input signal in order to yield the response embodies all of the characteristics of the medium, and it may be called the impulse response function or the transfer function of the medium. The channel is thus represented by one of a set of time-variant transfer functions, each defined as the characteristic response to a specified elementary excitation.

AI-B. The Impulse Response Function

If the output of a channel is known for a sufficiently large class of input signals then the channel characteristics can, in theory, be completely specified. Since the input signals of interest can be represented as sums of weighted impulses, the response to an impulse will be used as the primary characterization of the multipath. Here, an impulse is defined as the Dirac delta function $\delta(t)$ (see e.g., Vander Pol and Bremmer [1959], and Schwartz [1959]). For multipath problems, we assume that the channel is linear, i.e., if any two input signals $x_1(t)$ and $x_2(t)$ result in the two output $y_1(t)$ and $y_2(t)$, then the composite input signal $x_1(t) + x_2(t)$ results in the output signal $y_1(t) + y_2(t)$. This assumption is reasonable for most situations.

Finally, we assume that the channel cannot have a response before an input signal is applied.

Following the notation of Kailath [1961], we define the impulse response $h_1(t,\tau)$ as the output measured at time t in

response to a unit impulse applied at time τ. Then, if $x(t)$ is the input signal, the output $y(t)$ is given by

$$y(t) = \int_{-\infty}^{\infty} x(\tau) h_1(t, \tau)\, d\tau \tag{1}$$

Zadeh [1950] has also defined the system function

$$H_1(j\nu, t) = \int_{-\infty}^{\infty} h_1(t, \tau)\, e^{-j2\pi\nu(t-\tau)}\, d\tau \tag{2}$$

which has the interpretation

$$H_1(j\nu, t) = \frac{\text{response of the network to } \exp(j\,2\pi\,\nu\,t)}{\exp(j\,2\pi\,\nu\,t)} \quad . \tag{3}$$

and the bifrequency function is

$$\Gamma(j\nu, j\mu) = \int_{-\infty}^{\infty}\int_{-\infty}^{\infty} h_1(t, \tau)\, e^{j2\pi\nu\tau}\, e^{-j2\pi\mu t}\, d\tau dt \,. \tag{4}$$

The spectrum of $x(t)$ is given by

$$X(j\nu) = \int_{-\infty}^{\infty} x(t)\, e^{-j2\pi\nu t}\, dt \quad . \tag{5}$$

Then, the output y(t), or its spectrum Y(ju) are given by the formulas

$$y(t) = \int_{-\infty}^{\infty} H_1(j\nu, t)\, X(j\nu)\, e^{j2\pi\nu t}\, d\nu \quad , \tag{6}$$

and

$$Y(j\mu) = \int_{-\infty}^{\infty} \int_{-\infty}^{\infty} H_1(j\nu, t)\, X(j\nu)\, e^{j2\pi\nu t}\, e^{-j2\pi\mu t}\, d\nu\, dt$$

$$= \int_{-\infty}^{\infty} H_1\left[j\nu,\ j(\mu - \nu)\right] X(j\nu)\, d\nu \quad , \tag{7}$$

where

$$H_1(j\nu, j\mu) = \int_{-\infty}^{\infty} H_1(j\nu, t)\, e^{-j2\pi\mu t}\, dt \tag{8}$$

or

$$\Gamma(j\nu, j\mu) = H_1\left[j\nu,\ j(\mu - \nu)\right] . \tag{9}$$

It is convenient to relate ν to the input frequencies, and μ to the rate of variation caused by the multipath.

AI-C. Time Invariant Transfer Functions

Because of the many interesting theorems and physical interpretations that can be obtained when time invariance is assumed, this special case is singularly important. The definition of time invariance is: If the input $x(t)$ yields the output $y(t)$, then the input $x(t+\tau)$ yields the output $y(t+\tau)$.

With this assumption the impulse response function becomes simply $h(\tau)$, and the output $y(t)$ correspondingly to the input $x(t)$ is given by*

$$y(t) = \int_{-\infty}^{\infty} x(\tau)h(t-\tau)d\tau \quad ,$$

$$= \int_{-\infty}^{\infty} x(t-\tau)h(\tau)d\tau \quad . \qquad (10)$$

The spectra then are related by the formula

$$Y(j\nu) = X(j\nu)H(j\nu) \quad , \qquad (11)$$

*The restrictions that must be placed on $x(t)$ and $h(t)$ in order for the following results to be true are important mathematically but seldom are required for practical problems. See Siebert (1961) for a precise statement of these conditions.

or in the more familiar form

$$Y(\omega) = X(\omega) H(\omega) \tag{12}$$

where

$$x(t) = \frac{1}{2\pi} \int_{-\infty}^{\infty} X(\omega)\, e^{jwt}\, d\omega \ . \tag{13}$$

It is because of the form of (12) that multipath disturbances are often called multiplicitive noise, although it is clear from (6) that, for time varying systems, multiplicative is not an accurate description.

If $x(t)$ has a sufficiently broad spectrum $X(\omega)$, and the spectrum $Y(\omega)$ can be determined, $H(\omega)$ can be readily determined using (12). Ideally, $x(t)$ would be an impulse with a constant spectrum extending over all frequencies. However, in the practical situation where $x(t)$ is band-limited, i.e., $X(\omega) = 0$ for $|\omega| > \omega_0$, $H(\omega)$ can only be approximately determined, and no information is available for $|\omega| > \omega_0$. This implies that $h(t)$ will be ambiguous or undetermined for small values of t.

Anticipating later requirements, a maximum delay spread is defined as either

$$\min_{t_o} t_o \text{ such that } x(t) = 0 \ , \text{ for } t > t_o \ , \tag{14}$$

or

$$\min_{t_o} t_o \text{ such that } x(t) < \epsilon \ , \text{ for } t > t_o \ . \tag{15}$$

depending on whether small components ($<\epsilon$) are important or not.

Practical applications of the time invariant case include the system evaluation for slow-flat fading covered in Chapter BI.

AI-D. Simple Doppler

The case of a single path which changes with time can be treated within the framework of the impulse response function theory only if the change is linear with time, or if it can be modeled as piece-wise linear. This assumption is also necessary for the statistical development in sec AI-F.

For the single path case, the impulse response is given by $\delta(At-\tau)$ where A is the appropriate doppler factor. For the non-relativistic case $A = 1 - v/c$, where v is the radial velocity between the transmitter and receiver, negative in the outgoing direction, and c is the speed of light.

Then, the output $y(t)$ is given by

$$y(t) = x(At), \text{ with spectrum}$$

$$Y(\omega) = \frac{X(\omega/A)}{A},$$

which shows that both the width and the amplitude of the spectrum are changed. However, A is usually close to 1, and

the amplitude change is negligible, and the spectral change can frequently be approximated by a simple shift, neglecting the spread change. That is, if ω_o is the center frequency of the narrow band signal $X(\omega)$,

$$Y(\omega) \simeq X(\omega_o + \omega_d)$$

where $\omega_d = v/c\ \omega_o$.

Chapter DI contains methods for calculating Doppler and the effects of Doppler whenever this approximation is valid.

AI-E. Discrete Multipath

One of the most useful models of multipath for line-of-sight paths is the discrete model,

$$h(t,\tau) = \sum_{i=0}^{N} a_i\, \delta(t - \tau_i) \qquad (16)$$

where the a_i and τ_i may vary with time, subject to the restriction mentioned in the last section, that the τ_i are piece-wise linear functions of t at least to a close approximation. However, utilizing this impulse response function with the input signal $x(t) = x_o(t)\ell^{j\omega_o t}$, we obtain the output

$$y(t) = \sum_{i=0}^{N} a_i\, x_o(t - \tau_i)\, \ell^{j\omega_o(t - \tau_i)} \qquad (17)$$

and we may dispense with the restriction on τ_i utilizing this form (17). For most line-of-sight paths, we may use the specialized form

$$y(t) = A_0 x(t - \tau_0) + \sum_{i=1}^{N} a_i x(t-\tau_i) \qquad (18)$$

where the first term on the right-hand side represents the direct path, where slight perturbations on the amplitude (for example attenuation caused by absorption) and phase (for example path length changes due to changes in the refractive index along the path) are possible. For many problems of interest it is reasonable to assume $A_0 = 1$ and $\tau_0 = 0$.

The special case N=1, the two-path model, is treated in detail from the physical viewpoint in Chapter CI, and is illustrated from a system performance evaluation point of view in Chapter BIII. Many line-of-sight paths such as paths over a calm ocean and paths experiencing specular reflection from a smooth atmospheric layer, fit a two-path model where the differential path delays vary slowly.

Figure 2(a) shows a graphical representation of a single (time invariant) path, and figure 2(b) shows a two-path model. Figure 3 shows the power spectrum of a white noise signal of bandwidth $2(B)f_c$ where B is given as a fraction (0.1) of the carrier frequency f_c, for different differential delays between two paths corresponding to a ground-to-air path discussed in Chapter CII. In this

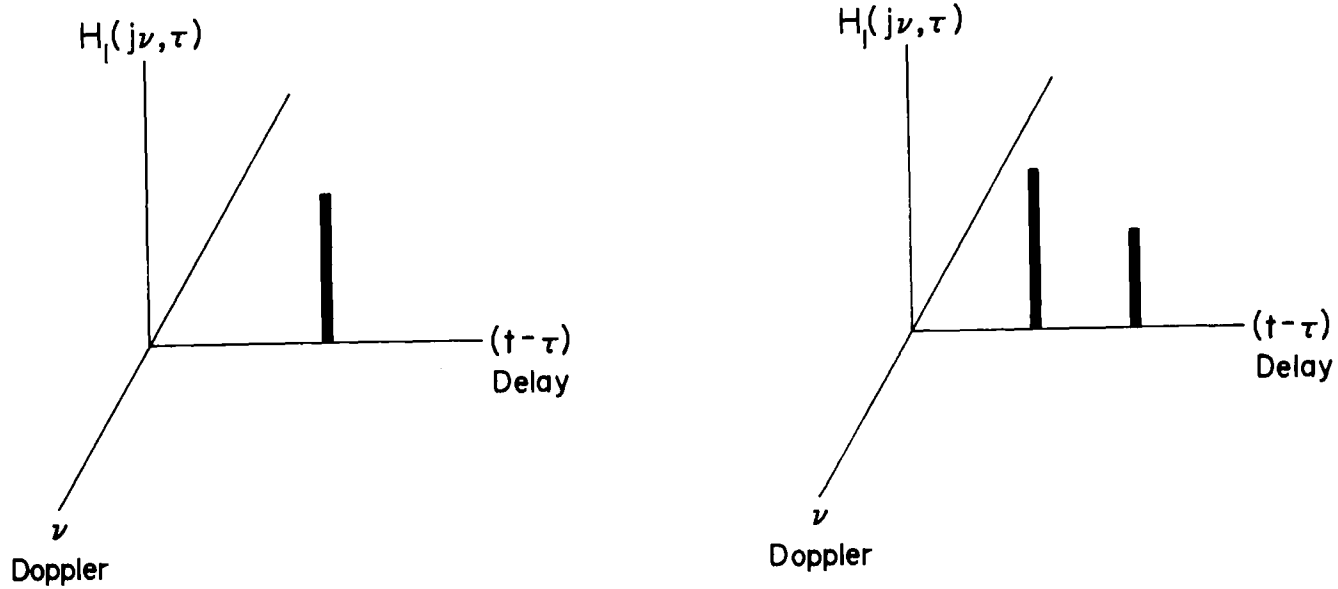

a) Flat-Flat Fading

b) Two-Path Model

Figure AI-2. (a) A representation of a system function for a time invariant single path. (b) A representation for a time invariant two path model.

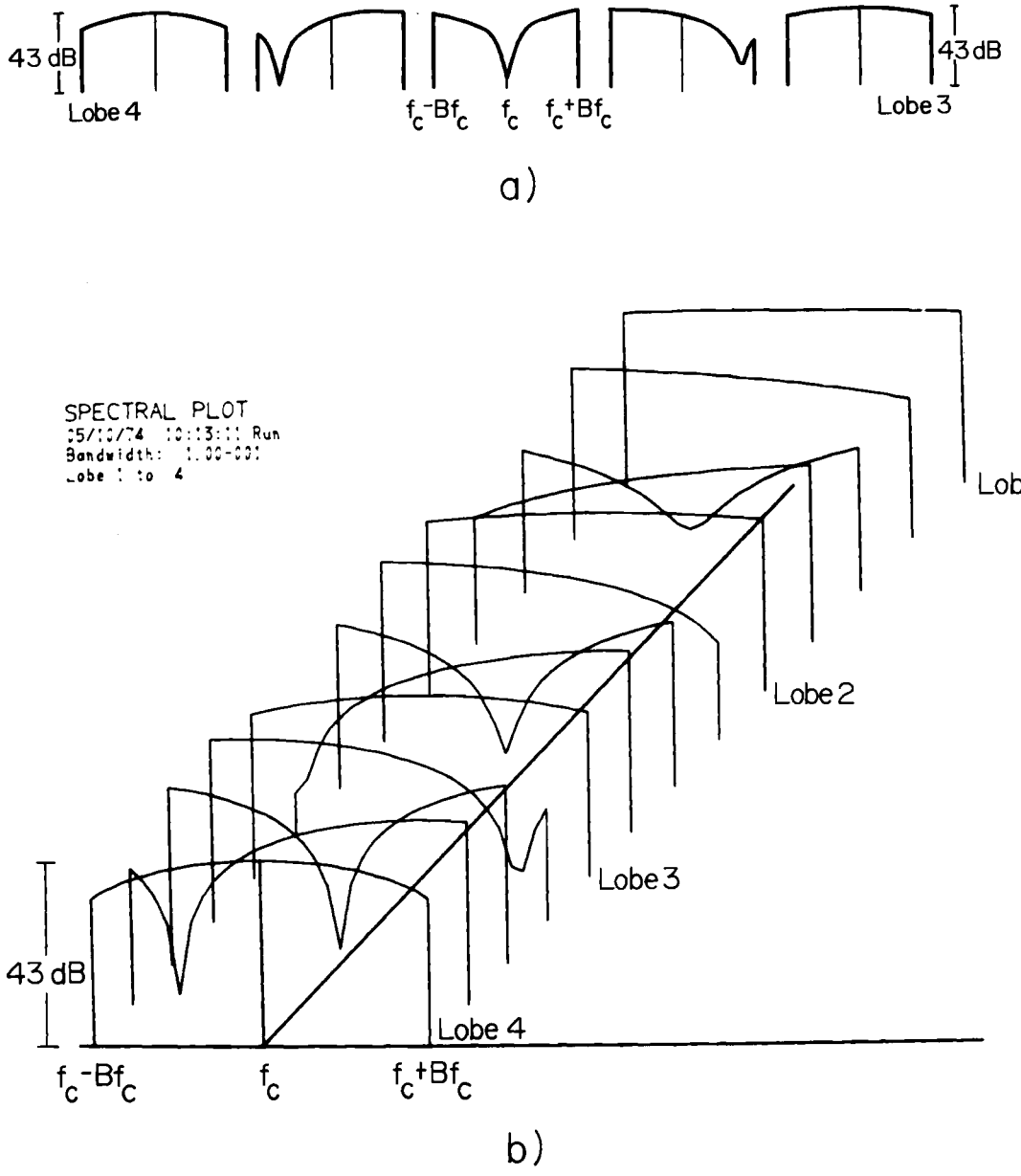

Figure AI-3. The effect of two path multipath on a signal of bandwidth $(2 f_c)(0.1) = 20$ percent of the carrier frequency and a flat spectrum. These represent points along a ground-air path described in Chapter CII. (a) shows the first five spectra shown in the composite (b).

figure, the frequency dependence of the fading is obvious. Figure 4 shows the same physical paths, for signal of smaller bandwidth ($B=10^{-5}$), and the frequency dependence of the fading is hardly noticeable. The total range of each of the figures 3 and 4 is 43 dB.

Returning to (17), if N is very large, and the a_i and $\varphi_i=\omega_o\tau_i$ are appropriately distributed so that the central limit theorem applies [see Rice (1944), Beckmann (1967), pp. 118 ff)], then both the real and imaginary part of the sum in eq (18) are normally distributed with mean zero, and variance σ^2. In addition, the amplitude of the sum is Rayleigh distributed. Thus, the amplitude of the total signal $|y(t)|$ has a Nakagami-Rice distribution. If flat fading can be assumed, and it appears from the following discussion that such an assumption is not compatible with the derivation of the distribution, then the methods of Chapter BI can be applied, and the Nakagami-Rice, flat-fading case is discussed there.

However, if the summation is independent of, or at least uncorrelated with the specular term, the summation may be treated as additive noise, and the methods of Chapter BII apply.

Distributions for various assumptions for which the central limit theorem does not apply are given in Beckmann [1967], pp. 128 ff, and in chapter BII.

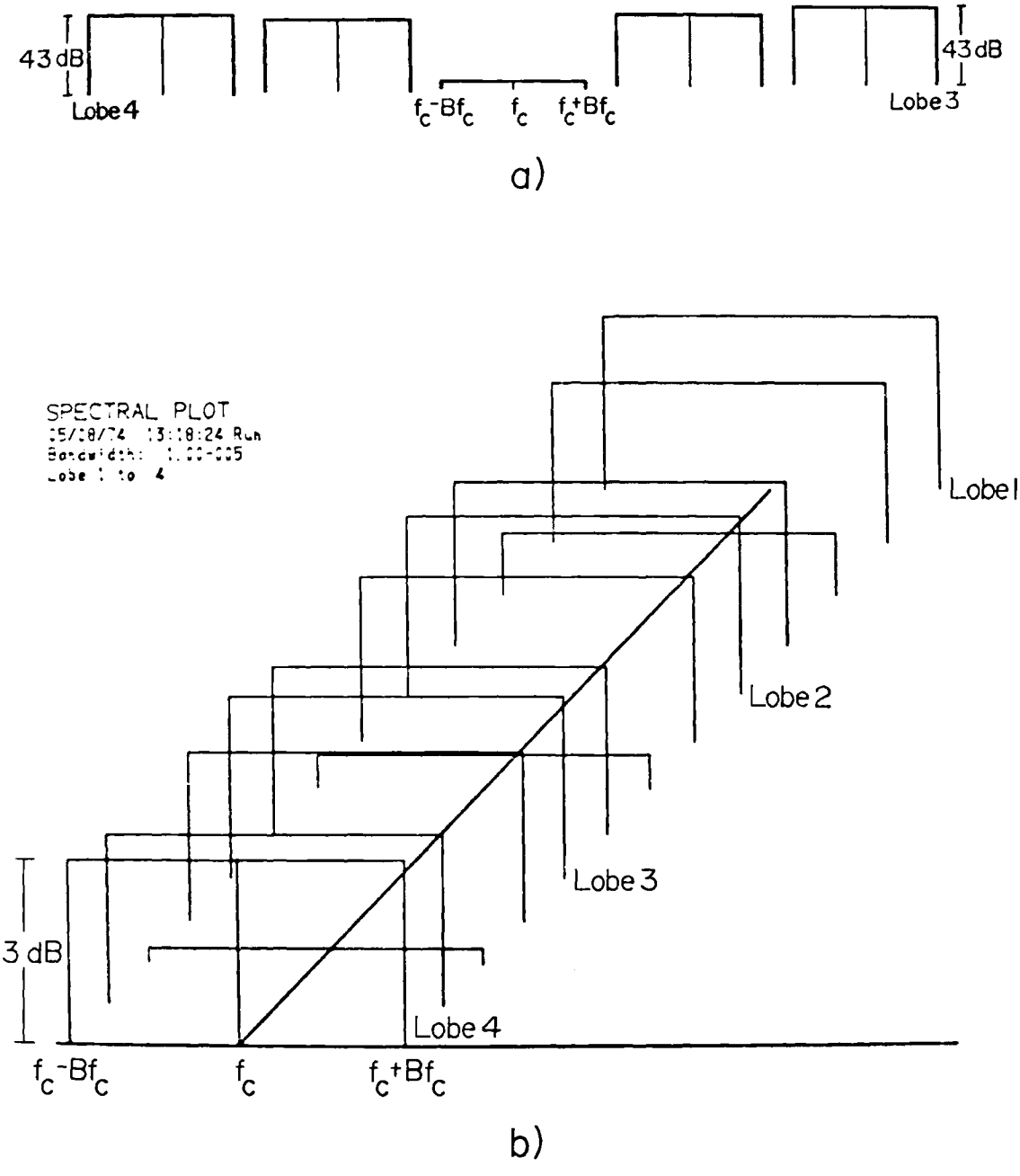

Figure AI-4. The effect of two path multipath on a signal of bandwidth $2 f_c (10^{-5}) = 0.002$ percent of the carrier frequency and a flat spectrum. These represent points along a ground-air path described in Chapter CII. (a) shows the first five spectra shown in the composite (b).

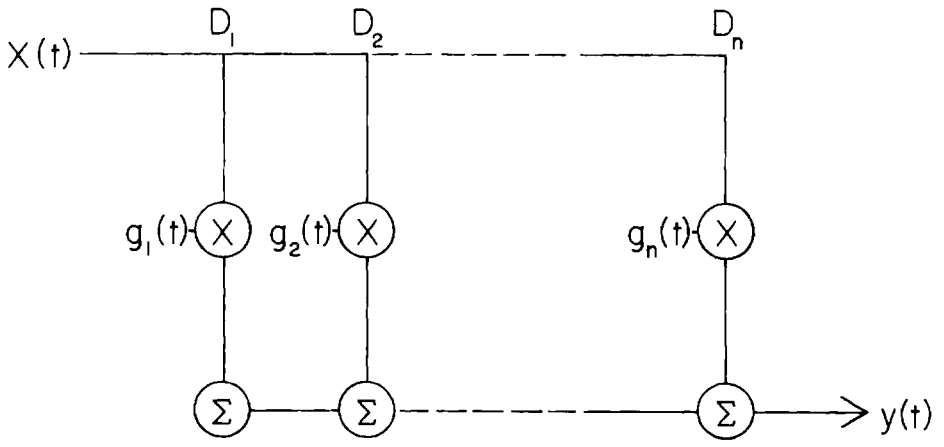

Figure AI-5. A general tap delay line model with variable delays Di and gains gi.

AI-F. Sampling Theorems and Tap Delay Line Models

The form of (17) suggests that a physical model of the impulse response function might be constructed as in figure 5, where the delays D_i may vary with time. However, it is difficult to obtain variable delays, and implementation of the model has involved various types of approximations.

One such approximation that is widely used is based on the sampling theorem, or other forms of interpolating functions (see Temes et al. [1973]). A familiar form of the sampling theorem is as follows. Let $x_o(t)$ be a low pass signal with spectrum band-limited to $(-\omega_o, \omega_o)$, i.e., $x(\omega) = 0$ for $|\omega| > \omega_o$. Then

$$x_o(t - \tau) = \sum_{k=-\infty}^{\infty} x_o(t - k\tau_o) \sin c\,(\tau/\tau_o - k) \qquad (19)$$

where $\tau_o = \frac{1}{2\omega_o}$

and

$$\sin cx = \frac{\sin \pi x}{\pi x} \qquad (20)$$

This implies that a band-limited signal can be completely reconstructed from samples taken at appropriate, equally spaced intervals. The received signal can be written in the form

$$y(t) = \mathrm{Re} \int_{-\infty}^{\infty} x_o(t - \tau)\, e^{i\omega_c (t - \tau)}\, h_1(t, t - \tau)\, dt \qquad (21)$$

Then a sampled version of y(t) would be given by combining (19) and (21) to obtain

$$y(t) = \mathrm{Re}\left\{ \sum_{k=-\infty}^{\infty} x_o(t - k\tau_o) \int_{-\infty}^{\infty} \mathrm{sinc}(\tau/\tau_o - k)\, \ell^{i\omega_c(t-\tau)} h_l(t, t-\tau)\, d\tau \right\}$$

$$= \mathrm{Re} \sum_{k=-\infty}^{\infty} b_k(t)\, x_o(t - k\tau_o) \qquad (22)$$

(22)

where

$$b_k = \int_{-\infty}^{\infty} \mathrm{sinc}(\tau/\tau_o - k)\, \ell^{i\omega_c(t-\tau)} h_l(t, t-\tau)\, d\tau \qquad (23)$$

is the tap gain function. If only a finite number of terms of the series (22) is used, an approximation is obtained.

A second approximation that is used when average delays are known is to construct a tapped delay line with these average delays, and approximate the changes in delay by imposing a phase modulation on each tap together with an appropriate amplitude modulation.

In most simulation applications the tap gain functions are generated as random time variables with statistical parameters chosen to match the physical situation to be simulated. An example of a simulator is given in section H.

AI-G. Statistical Models*.

Often, the information available for the specification of the impulse response function or the system function of section B is either inadequate, or too complicated to be useful in this form. For these cases, statistical methods have been developed.

It is convenient here to define $h_2(\tau,t)$ as the response measured at time $t+\tau$ to a unit impulse applied at time t, and the corresponding time-varying frequency response

$$H_2(f,t) = \int_{-\infty}^{\infty} h_2(\tau,t) \exp(-j2\pi f\tau)\, d\tau \tag{24}$$

Then

$$y(t) = \int_{-\infty}^{\infty} h_2(\tau,t)\ x(t-\tau)\, d\tau \tag{25}$$

We now assume that $H_2(f,t)$ is a stationary random process which can be completely described by its first and second moments. In particular, we assume $E[H_2(f,t)] = 0$ where E denotes expected value. Although the theory can be described in terms of expected values, it is convenient to

*The material in sections AI-G and AI-H was reproduced with the permission of C. C. Watterson, J. R. Juroshek and W. D. Bensema [See Watterson et al. (1969)].

assume ergodicity so that time averages can also be used to facilitate comparison with measurements. For this model, the channel correlation function can be defined as

$$R(\Delta f, \Delta t) = \overline{H_2^*(f,t)\, H_2(f + \Delta f,\ t + \Delta t)} \ , \qquad (26)$$

where the long bar indicates an average in the frequency-time plane, and the asterisk indicates the complex conjugate of the function. The function $R(\Delta f, \Delta t)$ is not one of frequency, f, or time, t, when $H(f,t)$ is stationary in these variables, but depends only upon the frequency and time displacements, Δf and Δt.

Since fewer independent measurements can be made over the band of interest at one time than can be made in time at any one frequency, it is convenient to define $R(\Delta f, \Delta t)$ more explicitly as an integral in the time domain,

$$R(\Delta f,\ \Delta t) = \lim_{t_1 \to \infty} \frac{1}{t_1} \int_{-t_1/2}^{t_1/2} H_2^*(f,t)\, H(f + \Delta f,\ t + \Delta t)\, dt \ . \qquad (27)$$

The channel scatter function then is defined as the double Fourier transform on Δf and Δt of $R(\Delta f, \Delta t)$,

$$s(\tau, \upsilon) = \int_{-\infty}^{\infty} \int_{-\infty}^{\infty} R(\Delta f, \Delta t)\, \exp(j2\pi\tau\Delta f - j2\pi\upsilon\Delta t)\, d\Delta f\, d\Delta t \ . \qquad (28)$$

At this point, it is convenient to consider dimension. A continuing signal expressed as a real function of time has the dimensions of voltage or current. When it is autocorrelated to obtain a correlation function (with unit resistance assumed), and the result is Fourier transformed to obtain a spectrum, the correlation function has the dimensions of power and the spectrum has the dimensions of power per unit frequency (power density). In the preceding equations, $H_2(f,t)$ is not a signal, but a dimensionless ratio of two amplitude spectra; consequently, $R(\Delta f, \Delta t)$ is dimensionless. It is convenient, however, to think of it as a power ratio. The channel scatter function, $s(\tau,\upsilon)$, is also dimensionless, but it is useful to think of it as a power ratio per unit time per unit frequency. It is the ratio of the channel output power per unit time delay, τ, per unit frequency offset, υ, to the channel input power. If the channel scatter function in (28) is integrated over its domain, it is easy to show that

$$\int_{-\infty}^{\infty}\int_{-\infty}^{\infty} s(\tau,\upsilon)\, d\tau\, d\upsilon = R(0,0) \quad , \tag{29}$$

and $R(0,0)$ is thus the ratio of the channel output power to the channel input power.

If the ratio of the channel output power to the channel input power is set equal to one, to define normalized funcitons, then the normalized channel correlation function is

$$\bar{R}(\Delta f, \Delta t) = R(\Delta f, \Delta t)/R(0,0) \quad , \qquad (30)$$

and the normalized channel scatter function is

$$\bar{s}(\tau, \upsilon) = s(\tau, \upsilon)/R(0,0) \quad . \qquad (31)$$

In addition to the previous functions that have been discussed by other authors, some additional functions describing stationary time varying channels are also useful. Define the channel time-scatter function as

$$u(\tau) = \int_{-\infty}^{\infty} s(\tau, \upsilon)\, d\upsilon \quad . \qquad (32)$$

When (28) is substituted in (32), the latter becomes

$$u(\tau) = \int_{-\infty}^{\infty}\int_{-\infty}^{\infty}\int_{-\infty}^{\infty} R(\Delta f, \Delta t)\, \exp(j2\pi\tau\Delta f - j2\pi\nu\Delta t)\, d\Delta f\, d\Delta t\, d\nu \quad . \qquad (33)$$

Equation (33) can be integrated with respect to υ and Δt, in turn, to obtain

$$u(\tau) = \int_{-\infty}^{\infty} R(\Delta f, 0)\, \exp(j2\pi\tau\Delta f)\, d\Delta f \qquad (34)$$

Then

$$u(\tau) = F_{\Delta f}^{-1}\left[R(\Delta f, 0)\right] \quad , \qquad (35)$$

where $F_{\Delta f}^{-1}$ means the inverse Fourier transform on Δf. The channel time-scatter function, $u(\tau)$, has the dimension of frequency or inverse time and can be viewed as a power ratio per unit time. It is the ratio of the channel output power per unit time delay, τ, to the channel input power.

From (31) and (32), the normalized channel time-scatter function is

$$\bar{u}(\tau) = \int_{-\infty}^{\infty} \bar{s}(\tau, \nu)\, d\nu = u(\tau) / R(0, 0) \quad . \tag{36}$$

Define the channel frequency-scatter function as

$$v(\nu) = \int_{-\infty}^{\infty} s(\tau, \nu)\, d\tau \quad . \tag{37}$$

To evaluate (37) for any stationary time-varying channel, substitute (28) in (37) to obtain

$$v(\nu) = \int_{-\infty}^{\infty}\int_{-\infty}^{\infty}\int_{-\infty}^{\infty} R(\Delta f, \Delta t) \exp(-j2\pi\nu\Delta t + j2\pi\tau\Delta f)\, d\Delta t\, d\Delta f\, d\tau \tag{38}$$

Now integrate (38) with respect to $\Delta\tau$ and Δf, in turn, to obtain

$$v(\nu) = \int_{-\infty}^{\infty} R(0, \Delta t) \exp(-j2\pi\nu\Delta t)\, d\Delta t \quad ; \tag{39}$$

consequently,

$$v(\nu) = F_{\Delta t}\,[R(0, \Delta t)] \ . \tag{40}$$

The channel frequency-scatter function, $v(\upsilon)$, has the dimension of time or inverse frequency and can be viewed as a power ratio per unit frequency, i.e., it is the ratio of the channel output power per unit frequency offset, υ, to the channel input power.

From (31) and (37), the normalized channel frequency-scatter function is

$$\bar{v}(\nu) = \int_{-\infty}^{\infty} \bar{s}(\tau, \nu)\, d\tau = v(\nu)/R(0, 0) \ . \tag{41}$$

Now define the <u>channel time delay</u> as the first moment of the normalized channel time-scatter function,

$$\hat{\tau} = \int_{-\infty}^{\infty} \tau\, \bar{u}(\tau)\, d\tau \ , \tag{42}$$

which has the dimension of time and is a measure of the average time delay in the channel. To relate the channel time delay to the channel correlation function, substitute (35) in (36) to obtain

$$F_{\Delta f}^{-1}\,[R(\Delta f, 0)] = R(0, 0)\, \bar{u}(\tau) \ . \tag{43}$$

Then (43) can be written as the direct Fourier transform

$$R(\Delta f, 0) = R(0, 0) \int_{-\infty}^{\infty} \bar{u}(\tau) \exp(- j2\pi\Delta f\tau)\, d\tau \ . \qquad (44)$$

Now substitute (44) in (30) with $\Delta t = 0$ and differentiate result with respect to Δf to obtain

$$\frac{dR(\Delta f, 0)}{d\Delta f} = -j2\pi \int_{-\infty}^{\infty} \tau\, \bar{u}(\tau) \exp(-j2\pi\Delta f\tau)\, d\tau \ . \qquad (45)$$

If (45) is evaluated at $\Delta f = 0$ and combined with (42),

$$\hat{\tau} = \frac{j}{2\pi} \left[\frac{d\bar{R}(\Delta f, 0)}{d\Delta f} \right]_{\Delta f=0} . \qquad (46)$$

Now define

$$\phi R(\Delta f, 0) = \tan^{-1} \left\{ \mathrm{Im}[\bar{R}(\Delta f, 0)] / \mathrm{Re}[\bar{R}(\Delta f, 0)] \right\} . \qquad (47)$$

It can be shown that $\mathrm{Re}[\bar{R}(\Delta f, 0)]$ is an even function with a derivative of zero at $\Delta f = 0$, providing $\bar{u}(\tau)$, the inverse Fourier transform of $\bar{R}(\Delta f, 0)$, decreases at a rate greater than $1/|\tau|^2$ as $|\tau| \to \infty$. Under this condition, and since $\mathrm{Im}[\bar{R}(\Delta f, 0)]$ is an odd function with a zero value at $\Delta f = 0$ and $R(0, 0) = 1$, (47) can be differentiated with respect to Δf and evaluated at $\Delta f = 0$ to obtain

$$\left[\frac{d\phi\bar{R}(\Delta f, 0)}{d\Delta f} \right]_{\Delta f=0} = -j \left[\frac{d\bar{R}(\Delta f, 0)}{d\Delta f} \right]_{\Delta f=0} . \qquad (48)$$

Substitute (48) in (46) then to obtain

$$\hat{\tau} = \frac{-1}{2\pi} \left[\frac{\partial \Phi \bar{R}(0, 0)}{\partial \Delta f} \right] . \tag{49}$$

In a similar way, define the channel frequency shift as the first moment of the normalized channel frequency-scatter function,

$$\hat{\nu} = \int_{-\infty}^{\infty} \nu \, \bar{v}(\nu) \, d\nu , \tag{50}$$

which has the dimension of frequency and is a measure of the average frequency offset in the channel. Relate the channel frequency shift to the channel correlation function, in a manner analogous to the development of equations (42) through (49), to obtain

$$\hat{\nu} = \frac{1}{2\pi} \left[\frac{\partial \Phi \bar{R}(0, 0)}{\partial \Delta t} \right] . \tag{51}$$

Define the channel time spread as two times the square rcot of the second central moment of the normalized channel time-scatter function.

$$2\rho = 2 \left[\int_{-\infty}^{\infty} (\tau - \hat{\tau})^2 \, \bar{u}(\tau) \, d\tau \right]^{\frac{1}{2}} , \tag{52}$$

which has the dimension of time and is a single-number measure of the time-scatter on the channel. To relate it to the channel correlation function, differentiate (45) with respect to Δf and evaluate at $\Delta f = 0$ to obtain

$$\left[\frac{d^2 \bar{R}(\Delta f, 0)}{d\Delta f^2} \right]_{\Delta f=0} = -4\pi^2 \int_{-\infty}^{\infty} \tau^2 \, \bar{u}(\tau) \, d\tau \, . \tag{53}$$

Now square (52), expand the integrand to three terms, and substitute (42), (46), and (53) in the result to obtain

$$(2\rho)^2 = \frac{1}{\pi^2} \left\{ - \frac{d^2 \bar{R}(\Delta f, 0)}{d\Delta f^2} + \left[\frac{d\bar{R}(\Delta f, 0)}{d\Delta f} \right]^2 \right\}_{\Delta f=0} . \tag{54}$$

It can be shown however that the second derivative of the magnitude of $\bar{R}(\Delta f, 0)$ with respect to Δf, at $\Delta f = 0$, is

$$\left[\frac{d^2 \left| \bar{R}(\Delta f, 0) \right|}{d\Delta f^2} \right]_{\Delta f=0} = \left\{ \frac{d^2 \bar{R}(\Delta f, 0)}{d\Delta f^2} - \left[\frac{d\bar{R}(\Delta f, 0)}{d\Delta f} \right]^2 \right\}_{\Delta f=0} . \tag{55}$$

We can then combine (55) with (54) to obtain

$$2\rho = \frac{1}{\pi} \left[- \frac{\partial^2 \left| \bar{R}(0, 0) \right|}{\partial \Delta f^2} \right]^{\frac{1}{2}} . \tag{56}$$

Similarly, define the channel frequency spread as twice the square root of the second central moment of the normalized channel frequency-scatter function,

$$2\sigma \equiv 2\left[\int_{-\infty}^{\infty} (\nu-\hat{\nu})^2\ \bar{v}(\nu)\ d\nu\right]^{\frac{1}{2}}, \tag{57}$$

which has the dimension of frequency and is a single-number measure of the frequency-scatter on the channel. Relate it to the channel correlation function, in a manner that is analogous to the development of equations (52) through (56), to obtain

$$2\sigma = \frac{1}{\pi}\left[-\frac{\partial^2 \left|\bar{R}(0,0)\right|}{\partial \Delta t^2}\right]^{\frac{1}{2}} . \tag{58}$$

AI-H. Statistical Tapped Delay Line Model

AI-H.1. General

The complex time-varying frequency response of a stationary tapped-delay-line model is (see fig. 6)

$$H_2(f, t) = \sum_{i=1}^{n} G_i(t) \exp(-j2\pi\tau_i f) , \qquad (59)$$

where i is an integer that numbers the tap or path, τ_i is the time delay on the i-th path, and n is the total number of paths. Each exponential function defines the time delay of a path and is a function of frequency only, since it does not change with time. Each tap-gain function $G_i(t)$ is a complex function that is constant in frequency but varies in time; i.e., each tap-gain function varies the amplitude and phase of each spectral component of the delayed signal at its tap by the same amount continuously with time.

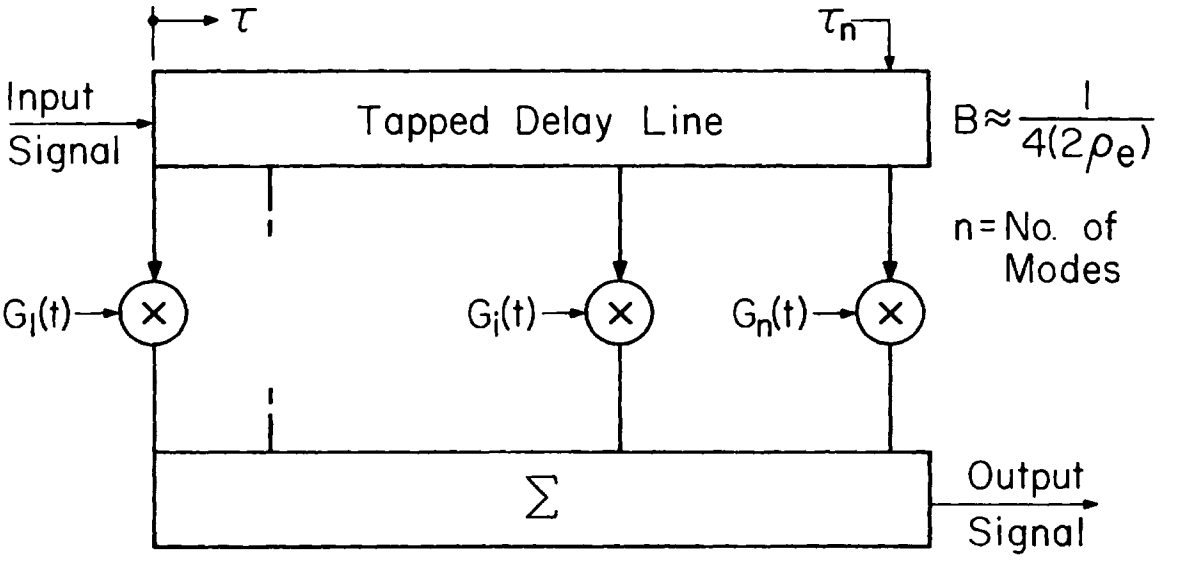

Figure AI-6. Block diagram of channel model.

Equation (59) can be substituted in (27) to obtain the channel correlation function for the general stationary model of figure 6,

$$R(\Delta f, \Delta t) = \lim_{t_1 \to \infty} \frac{1}{t_1} \int_{-t_1/2}^{t_1/2} \sum_{i=1}^{n} \sum_{\ell=1}^{n} G_{\ell}^{*}(t)\, G_i(t+\Delta t) \exp\left[j2\pi(\tau_{\ell} - \tau_i) f - j2\pi\tau_i \Delta f \right] dt \,. \tag{60}$$

The order of integration and summation can be changed to give

$$R(\Delta f, \Delta t) = \sum_{i=1}^{n} \exp(-j2\pi\tau_i \Delta f) \sum_{\ell=1}^{n} \exp[j2\pi(\tau_\ell - \tau_i)f] \lim_{t_1 \to \infty} \frac{1}{t_1} \int_{-t_1/2}^{t_1/2} G_\ell^*(t)\, G_i(t+\Delta t)\, dt \tag{61}$$

Now assume that the cross correlations between all pairs of tap-gain functions are zero. For the terms where $i = \ell$, the exponential function preceding the integral becomes one. Then (61) becomes

$$R(\Delta f, \Delta t) = \sum_{i=1}^{n} \exp(-j2\pi\tau_i \Delta f) \lim_{t_1 \to \infty} \frac{1}{t_1} \int_{-t_1/2}^{t_1/2} G_i^*(t)\, G_i(t+\Delta t)\, dt\,. \tag{62}$$

Because of its form, the integral in (62) is conveniently defined as the tap-gain correlation function

$$C_i(\Delta t) = \lim_{t_1 \to \infty} \frac{1}{t_1} \int_{-t_1/2}^{t_1/2} G_i^*(t)\, G_i(t+\Delta t)\, dt\,, \tag{63}$$

which differs from the one given by Gallager (1964). The latter function is the single Fourier transform on Δf of $R(\Delta f, \Delta t)$ and a continuous function of τ and Δt. It is applicable to a model with a large number of equally spaced taps as the number of taps approaches infinity. The

definition in (63) is more useful for models with a finite number of spaced taps.

Like $R(\Delta f,\Delta t)$, $C_i(\Delta t)$ is dimensionless, but it can also be viewed as a power ratio with $C_i(0)$ the ratio of the i-th path output power to the channel input power. The normalized tap-gain correlation function is defined as

$$\overline{C}_i(\Delta t) = C_i(\Delta t)/C_i(0) . \tag{64}$$

To continue with $R(\Delta f,\Delta t)$, when (63) is substituted in (44), the channel correlation function for the general stationary model of figure 6 becomes

$$R(\Delta f,\ \Delta t) = \sum_{i=1}^{n} \exp(-j2\pi\tau_i \Delta f)\ C_i(\Delta t) . \tag{65}$$

The normalized channel correlation function $R(\Delta f,\Delta t)$, can be obtained by substituting (65) into (30).

The <u>tap-gain spectrum</u> for the i-th path is defined as the Fourier transform of the tap-gain correlation function for the i-th path,

$$v_i(\nu) = \int_{-\infty}^{\infty} C_i(\Delta t) \exp(-j2\pi\nu\Delta t)\, d\Delta t . \tag{66}$$

The function $v_i(\upsilon)$ has the dimension of time or inverse frequency and can be viewed as a power ratio per unit frequency. It is the ratio of the i-th path output power per unit frequency offset, υ, to the channel input power. The normalized tap-gain spectrum, corresponding to the normalized tap-gain correlation function, is

$$\bar{v}_i(\nu) = v_i(\nu)/C_i(0) . \tag{67}$$

To obtain the channel scatter function for the general stationary channel model of figure 6, substitute (65) in (28) to obtain

$$s(\tau, \nu) = \sum_{i=1}^{n} \int_{-\infty}^{\infty} d\Delta f \exp[j2\pi(\tau - \tau_i)\Delta f] \int_{-\infty}^{\infty} d\Delta t \, C_i(\Delta t) \exp(-j2\pi\nu\Delta t) . \tag{68}$$

Equation (66) can be substituted in (68) and the remaining integration performed to obtain

$$s(\tau, \nu) = \sum_{i=1}^{n} \delta(\tau - \tau_i) \, v_i(\nu) . \tag{69}$$

The normalized channel scatter function, $s(\tau,\upsilon)$, can be obtained by substituting (69) in (31).

The channel time-scatter function is obtained when (65), with $\Delta t = 0$, is substituted in (34) and integrated to give

$$u(\tau) = \sum_{i=1}^{n} C_i(0)\, \delta(\tau - \tau_i) . \tag{70}$$

The normalized channel time-scatter function is obtained by substituting (70) in (36).

The channel frequency-scatter function is obtained when, at $\Delta f = 0$, we substitute (65) in (39) and then (66) into the result

$$v(\nu) = \sum_{i=1}^{n} v_i(\nu) . \tag{71}$$

Substituting (71) in (41) yields the normalized channel frequency-scatter function.

The channel time delay is given by

$$\hat{\tau} = [\, 1/R(0,0)] \sum_{i=1}^{n} C_i(0)\, \tau_i . \tag{72}$$

To specify the channel frequency shift, define for each path the tap-gain frequency shift as the first moment of the normalized tap-gain spectrum,

$$\nu_i = \int_{-\infty}^{\infty} \nu\, v_i(\nu)\, d\nu , \tag{73}$$

which has the dimension of frequency and is a measure of the average frequency offset on the path. For each path, the tap-gain frequency shift is related to the tap-gain correlation function by

$$\nu_i = \frac{1}{2\pi}\left[\frac{d\phi\bar{C}_i(0)}{d\Delta t}\right]. \tag{74}$$

It follows that the channel frequency shift is

$$\hat{\nu} = [1/R(0,0)]\sum_{i=1}^{n} C_i(0)\,\nu_i\ . \tag{75}$$

The channel time spread can be written directly as two times the square root of the difference between the second moment of the normalized channel time-scatter function, (70) divided by R(0,0), and the square of its first moment, the channel time delay,

$$2\rho = 2\left\{[1/R(0,0)]\left[\sum_{i=1}^{n} C_i(0)\,\tau_i^2\right] - \hat{\tau}^2\right\}^{\frac{1}{2}}. \tag{76}$$

To specify the channel frequency spread define for each path the tap-gain frequency spread as twice the square root of the second central moment of the normalized tap-gain spectrum,

$$2\sigma_1 = 2\left\{\int_{-\infty}^{\infty}(\nu-\nu_i)^2\,\bar{v}_i(\nu)\,d\nu\right\}^{\frac{1}{2}}, \tag{77}$$

which has the dimension of frequency and is a single-number measure of the frequency scatter on the path. for each path, we can relate the tap-gain frequency spread to the tap-gain correlation function by analogy to (57) and (58) to obtain

$$2\sigma_i = \frac{1}{\pi}\left[\frac{-d^2\,|\bar{C}_i(0)|}{d\Delta t^2}\right]^{\frac{1}{2}} . \tag{78}$$

The channel frequency spread then can be written as twice the square root of the difference between the second moment of the normalized channel frequency-scatter function and the square of its first moment,

$$2\sigma = 2\left\{\sum_{i=1}^{n}\left[C_i(0)/R(0,0)\right]\left(\nu_i^2+\sigma_i^2\right) - \left[\sum_{i=1}^{n}\left[C_i(0)/R(0,0)\right]\nu_i\right]^2\right\}^{\frac{1}{2}} . \tag{79}$$

The first summation in (79) is the second moment of the normalized channel frequency-scatter function and is the sum of the weighted second moments of the tap-gain spectra in terms of their frequency shifts and frequency spreads. The second summation in (79) is the corresponding first moment.

AI-H.2. A Specific Tapped Delay Line Model

On the basis of experimental evidence the best choice for tap-gain functions in the specific channel model are independent baseband complex bivariate Gaussian random functions with zero mean values and quadrature components with equal rms (root mean square) values, so that signals on each path in the model would have independent fading with a Rayleigh amplitude distribution and a uniform phase distribution.

In addition to deciding that the tap-gain functions would have a Rayleigh amplitude distribution and a uniform phase distribution, the spectra of the tap-gain functions had to be specified. Since the ionosphere can introduce frequency shifts on signals, as well as fading that results in frequency spreads, such shifts also had to be included in the tap-gain spectra. In addition, two magnetoionic components of a mode can produce different frequency shifts, and the difference of the two shifts can at times be greater than the frequency spreads of the magnetoionic components (Davies, 1962). Therefore the tap-gain spectra in general need two components--one for each magnetoioinic component. It was also necessary to specify the shapes of the tap-gain

spectrum for the two magnetoionic components, since it is known that these shapes can have a considerable influence on the distortion characteristics of a channel.

We selected a Gaussian spectrum of the form $\exp(-\xi_2 v^2)$. To be explicit, the channel model selected has independent tap-gain functions, each of which is defined by

$$G_{si}(t) = G'_{sia}(t) \exp(j2\pi\nu_{sia} t) + G'_{sib}(t) \exp(j2\pi\nu_{sib} t) , \qquad (80)$$

where the s subscripts designate quantities for the statistical channel model, the i subscripts denote the path number, and the a and b subscripts identify the magnetoionic components. $G'_{sia}(t)$ and $G'_{sib}(t)$ are sample functions of two independent complex Gaussian stationary ergodic random processes, each with zero mean values and independent quadrature components with equal rms values. Specifically, if $G'_{sia}(t)$ is defined in terms of its real and imaginary components by

$$G'_{sia}(t) = \underline{g}'_{sia}(t) + j\, \underline{\underline{g}}'_{sia}(t) , \qquad (81)$$

then g'_{sia} and g'_{sib} have a joint probability density function

$$p(\underline{g}'_{sia}, \underline{\underline{g}}'_{sib}) = \frac{1}{\pi C_{sia}(0)} \exp\left[- \frac{\underline{g}'^2_{sia} + \underline{\underline{g}}'^2_{sia}}{C_{sia}(0)} \right] , \qquad (82)$$

where $C_{sia}(0)$ is the autocorrelation function of $G'_{sia}(t)\exp(j2\pi\upsilon_{sia}t)$ at zero displacement ($\Delta t = 0$) and specifies the ratio of the channel output power delivered by the magnetoionic component to the channel input power. With a suitable change in the a subscripts, (81) and (82) also apply to $G'_{sia}(t)$.

To explain the exponential factors in (80), consider $E[G'_{sia}{}^{*}(t)\ G'_{sia}(t+\Delta t]$. When this autocorrelation function is computed in terms of the real and imaginary components in (63), the cross products will have zero averages because the real and imaginary components are independent. The resulting correlation function will be real and have even symmetry about $\Delta t = 0$. Its Fourier transform, the spectrum of $G'_{sia}(t)$, must then have even symmetry about $\upsilon = 0$. The same is true for $G'_{sib}(t)$, and the primes in (80), (81), and (64) indicate the functions have spectra with even symmetry about $\upsilon = 0$. Therefore, the exponential factors in (80) were incorporated to provide the desired frequency shifts, υ_{sia} and υ_{sib}, for the magnetoionic components in the tap-gain spectrum.

The tap-gain correlation function corresponding to (62) is

$$C_{si}(\Delta t) = \left\{ \begin{array}{l} C_{sia}(0)\exp[-2\pi^2\sigma_{sia}^2(\Delta t)^2 + j2\pi\nu_{sia}\Delta t] \\ \quad + C_{sib}(0)\exp[-2\pi^2\sigma_{sib}^2(\Delta t)^2 + j2\pi\nu_{sib}\Delta t] \end{array} \right\} \qquad (83)$$

and the tap-gain spectrum is

$$\nu_{si}(\nu) = \left\{ \begin{array}{l} [\, C_{sia}(0)/(2\pi\sigma_{sia}^2)^{\frac{1}{2}}] \ \exp[\, -(\nu - \nu_{sia})^2/(2\sigma_{sia}^2)] \\ \quad + [\, C_{sib}(0)/(2\pi\sigma_{sib}^2)^{\frac{1}{2}}] \exp[\, -(\nu - \nu_{sib})^2/(2\sigma_{sib}^2)] \end{array} \right\}, \quad (84)$$

where

$$C_{si}(0) = C_{sia}(0) + C_{sib}(0)\,, \quad (85)$$

and σ_{sia} and σ_{sib} are the standard deviations of the two Gaussian components of the spectrum. A graphical representation of a tap-gain spectrum is shown in figure 7a. In general, the two Gaussian components in a tap-gain spectrum have different power ratios, frequency shifts, and frequency spreads. There are times, however, when the shifts and spreads of the two magnetoionic components in an ionospheric channel are approximately equal, when the two components are effectively one. For these times, $C_{sib}(0)$ becomes zero in (80) and (83) through (85) and the "a" subscript is dropped, causing the tap-gain spectrum to appear as in figure 7b.

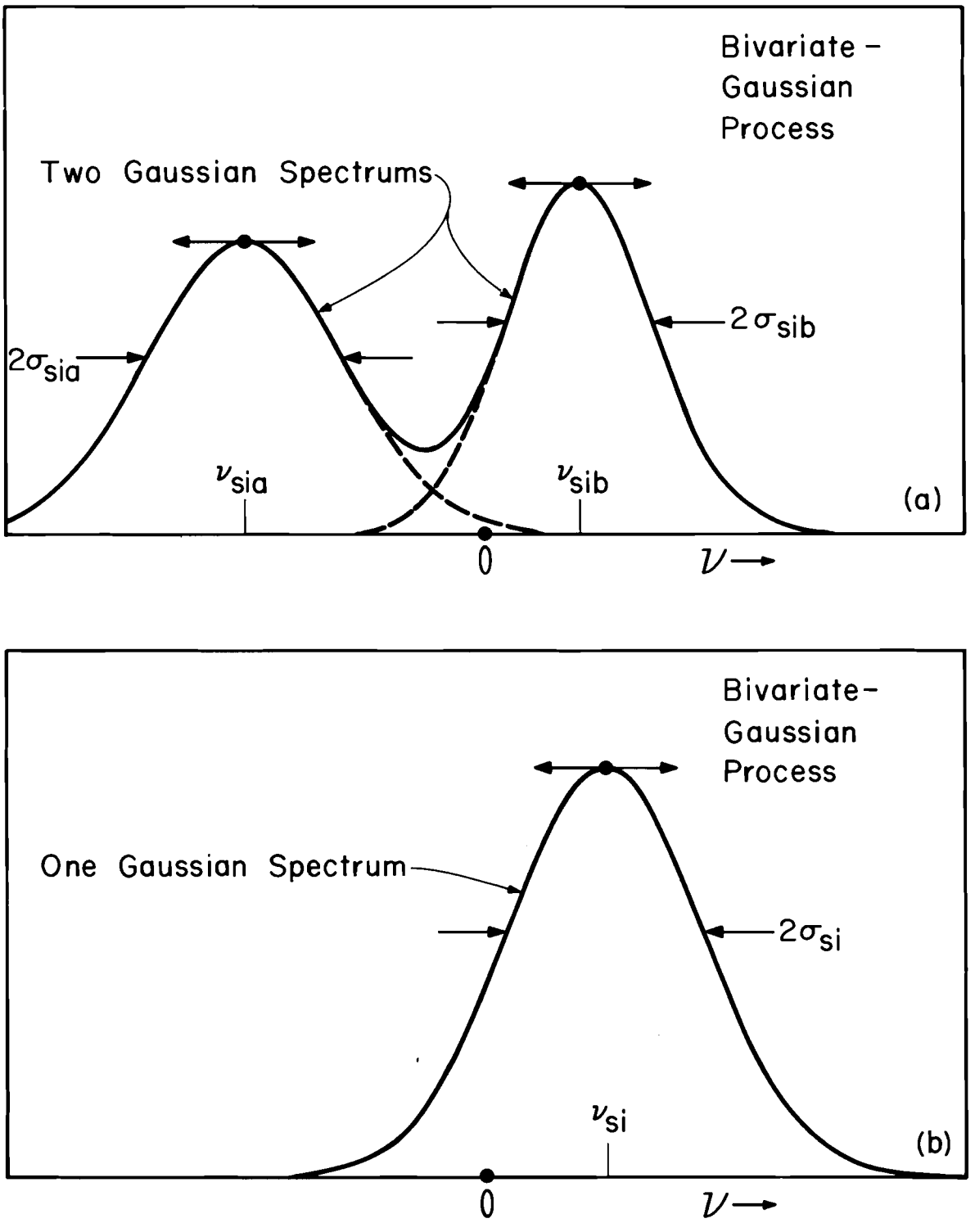

Figure AI-7. Tap-gain spectra in chosen model.

AI-I. A Flat Fading Model for Tropospheric Line-of-Sight Paths

Many measurements have been made of amplitude and phase fluctuations over tropospheric line-of-sight paths. Statistical information from these data in the form of amplitude distributions, spectra of phase fluctuations, spectra of amplitude fluctuations and other parameters are useful for system evaluation if (frequency) flat fading can be assumed. Examples of these data are shown in figures 8, 9, 10 and 11 [Janes et al., 1970]. Since the signal used to obtain this type of measurement has typically been an unmodulated carrier, $e^{i\omega_o t}$, the output is given as

$$A(t)e^{i\varphi(t)}\, e^{i\omega_o t} \quad , \quad (86)$$

where $A(t)$ then gives the amplitude and $\varphi(t)$ the phase variation. For the flat fading assumption, using equations (1) (2) and (3), we obtain

$$A(t)\, e^{i\varphi(t)}\, e^{i\omega_o t} = \int_{-\infty}^{\infty} e^{i\omega_o \tau}\, h_1(t,\tau)\, d\tau = H_1\left(\frac{j\omega_o}{2\pi},\, t\right) e^{i\omega_o t} \quad . \quad (87)$$

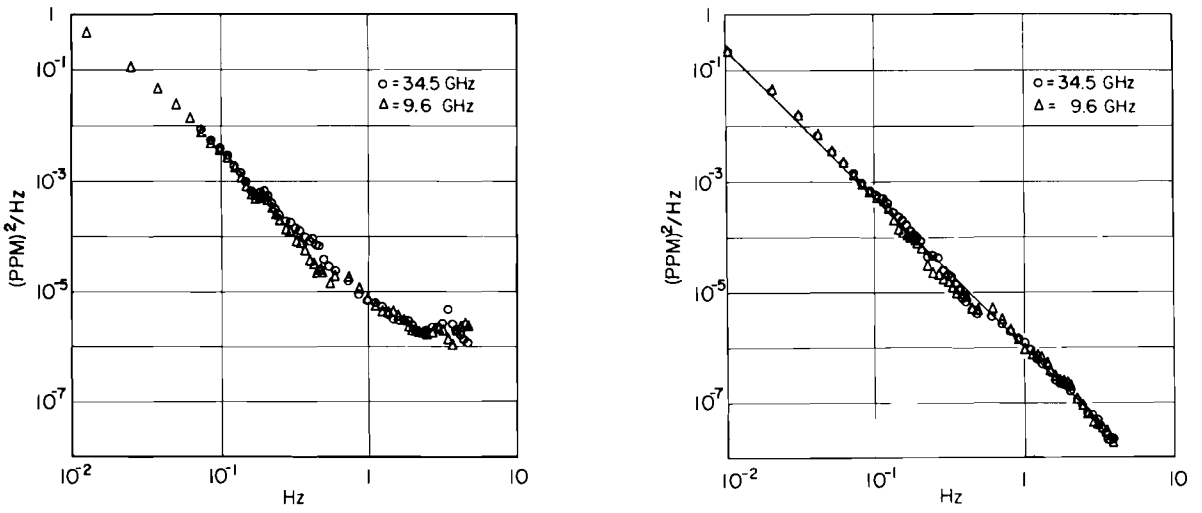

Figure AI-8. Spectra of phase variations at 9.6 and 34.52 GHz, 1457-1520, February 14, 1967.

Figure AI-9. Spectra of phase variations at 9.6 and 34.52 GHz, 1453-1523, June 7, 1967.

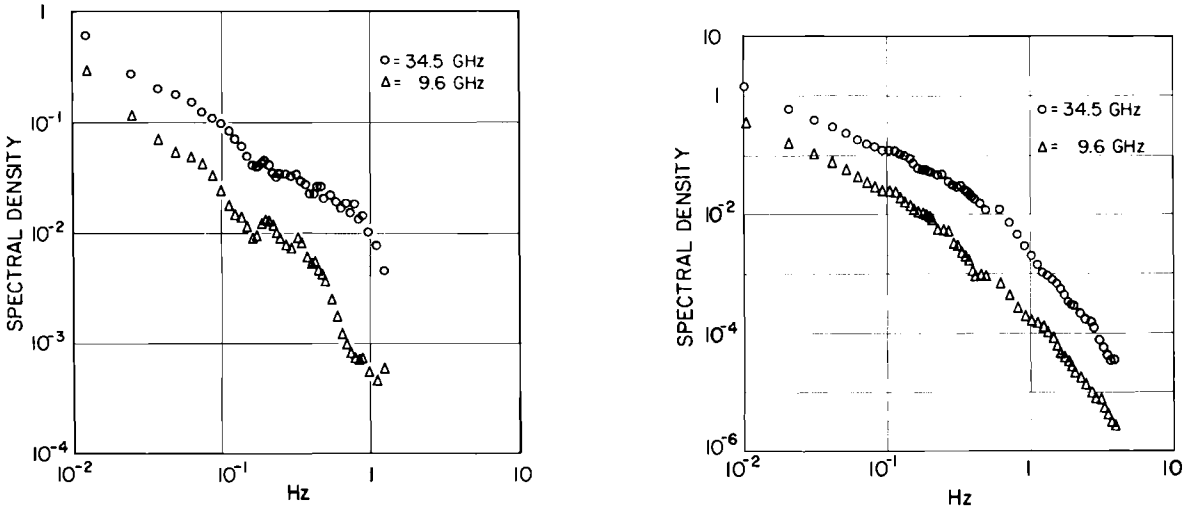

Figure AI-10. Spectra fading at 9.6 and 34.52 GHz, 1457-1520, February 14, 1967.

Figure AI-11. Spectra of fading at 9.6 and 34.52 GHz, 1453-1523, June 7, 1967.

The flat fading assumption further implies that $A(t)$ and $\phi(t)$ are frequency independent and hence,

$$H_1\left(\frac{j\omega_o}{2\pi}, t\right) = H_1\left(\frac{j\omega}{2\pi}, t\right) \qquad (88)$$

for all ω. Thus

$$h_1(t, \tau) = \delta(t - \tau)\, A(t)\, e^{i\varphi(t)} , \qquad (89)$$

and for any input signal $x(t)$, the output $y(t)$ is given by

$$y(t) = x(t)\, [A(t)\, e^{i\varphi(t)}] . \qquad (90)$$

AI-J. Other Definitions of Frequency Spread and Time Spread

The definitions of "spread" used in section AI-G [eqs (52) and (57)] are convenient because of the ease of obtaining a physical integration for them. However, for some purposes, other definitions are desirable. A discussion of some additional definitions is contained in Lerner [1961]. One of these sets of definitions is utilized below to derive conditions for making simplifying assumptions for the scattering function $\overline{s}(\tau,\upsilon)$ of eq (31).

Using equation (41) we define doppler spread, B, as

$$B = \left[\int_{-\infty}^{\infty} \overline{v}^2(\upsilon)\, d\upsilon \right]^{-1} . \quad (91)$$

Using (36), we define the multipath spread, L, as

$$L = \left[\int_{-\infty}^{\infty} \overline{u}^2(t)\, dt \right]^{-1} . \quad (92)$$

The total spread S using eq (31) is

$$S = \left[\int_{-\infty}^{\infty} \int_{-\infty}^{\infty} \overline{s}^2(t,\upsilon)\, dt\, d\upsilon \right]^{-1} . \quad (93)$$

We now wish to define the time duration T and bandwidth w of a signal consistent with the above quantities.

If $x(t)$ is the complex envelope of a signal, the following are found to be sufficient:

$$T = \left[\int_{-\infty}^{\infty} |x(t)|^4 \, dt \right]^{-1}, \quad (94)$$

and

$$W = \left[\int_{-\infty}^{\infty} |\underline{\overline{X}}(f)|^4 \, df \right]^{-1} . \quad (95)$$

With this background notation is it possible to characterize certain types of channels and also to give some gross estimates of system performance.

1. A non-dispersive channel is defined by

$$\overline{s}(t, \upsilon) = \delta(t) \, \delta(\upsilon)$$

and is sometimes called a flat-flat fading channel.

2. A time-dispersive channel is defined by

$$\overline{s}(t, \upsilon) = \delta(\upsilon) \overline{u}(t)$$

and is called a time-flat fading, or a frequency-selective fading channel. There is also the time-invariant channel of eq 10.

3. A frequency dispersive channel is defined by

$$\overline{s}(t,\upsilon) = \delta(t)\,\overline{v}(\upsilon)$$

and is called either a time-selective fading or a frequency flat fading channel.

4. A doubly dispersive channel is one which is dispersive in both time and frequency.

These classifications have derived from the <u>effects</u> of the multipath on the signal. Note that the multipath itself is the same, regardless of which method is used to name it. Figure 12 shows several examples of scattering functions with the appropriate nomenclature. Example a is a type of scattering function that is frequently associated with HF ionospheric propagation, discussed in connection with the specific tap-delay line of AI-H.2.

In practice, no channel has exactly impulsive response characteristics in either time or frequency and many of the problems encountered consist of determining when an impulse function is a good approximation to the actual problem. Thus, for one system it may be possible to use a non-

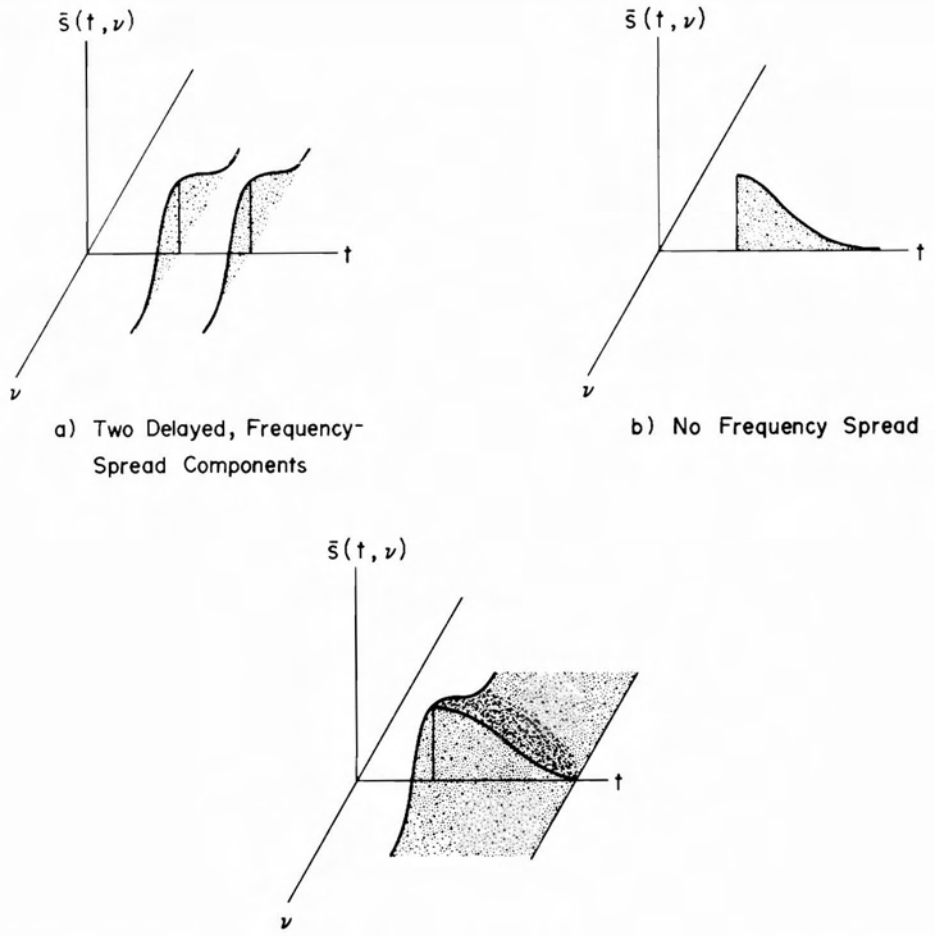

Figure AI-12. Illustrations of scattering functions. (a) The two-delay, frequency spread channel for the mode of section H. (b) Time spread, no frequency spread that might be observed from a diffuse scatterer. (c) Totally dispersive channel such as a tropo-scatter channel.

dispersive classification for the channel while for a different system it would be necessary to classify the same channel as one of the forms of a dispersive channel. For the purposes of determining when an approximation can be used, table 1 shows the relations between the channel parameters B, L and S to the signal parameters T and W.

BECKMANN, P. (1967),
PROBABILITY IN COMMUNICATION ENGINEERING,
(HARCOURT, BRACE AND WORLD, INC, NEW YORK)

BELLO, P.A. (1963),
CHARACTERIZATION OF RANDOMLY TIME-VARIANT LINEAR CHANNELS,
IEEE TRANS. COMM. SYSTEMS CS-11, NO. 4, 360-393.

DAVIES, K. (1962),
THE MEASUREMENT OF IONOSPHERIC DRIFTS BY MEANS OF A DOPPLER SHIFT TECHNIQUE,
J. GEOPHYS. RES. 67, NO. 12 4909-4913

GALLAGER, R.G. (1964),
CHARACTERIZATION AND MEASUREMENT OF TIME-AND FREQUENCY-SPREAD CHANNELS,
TECH. REPT. 352, LINCOLN LABORATORY, M.I.T., 1-34.

HAGFORS, T. (1961),
SOME PROPERTIES OF RADIO WAVES REFLECTED FROM THE MOON AND AND THEIR RELATION TO THE LUNAR SURFACE,
J. GEOPHYS. RES. 66, 777-785.

JANES, H.B., M.C. THOMPSON, JR., D. SMITH AND A.W. KIRKPATRICK (1970),
COMPARISON OF SIMULTANEOUS LINE-OF-SIGHT SIGNALS AT 9.6 AND 34.5 GHZ,
IEEE TRANS. ANT. AND PROP., VOL. AP-18,
NO. 4, 447-451, JULY 1970.

KAILATH, T. (1961),
CHANNEL CHARACTERIZATION, TIME-VARIANT DISPERSIVE CHANNELS,
LECTURES ON COMM. SYSTEMS THEORY, ED.- E.J. BAGHDADY, 95-123
(MCGRAW-HILL BOOK CO., NEW YORK).

LERNER, R.M. (1961),
REPRESENTATION OF SIGNALS, P.203,
LECTURES ON COMMUNICATION SYSTEM THEORY,
ED. E.J. BAGHDADY,
(MC GRAW-HILL).

RICE, S.O. (1944),
MATHEMATICAL ANALYSIS OF RANDOM NOISE,
BELL SYSTEM TECH. J. 23, 282-332/ALSO SAME JRNL (1945) 24, 46-156.

SCHWARTZ, MISCHA (1959),
INFORMATION TRANSMISSION, MODULATION AND NOISE,
(MC GRAW-HILL BOOK CO, INC., NEW YORK).

SHERMAN, H. (1961),
CHANNEL CHARACTERIZATION-RAPID MULTIPLICATIVE PERTURBATION,
LECTURES ON COMMUNICATION SYSTEMS THEORY, ED.-E.J. BAGHDADY, 71-73
(MCGRAW-HILL BOOK CO., NEW YORK).

SIEBERT, W. (1961),
STASTICAL DECISION THEORY AND COMMUNICATIONS, THE
SIMPLE BINARY DECISION PROBLEM,
LECTURES ON COMM. SYSTEM THEORY, ED. E.J. BAGHDADY 177-190
(MC GRAW HILL BOOK CO., INC., NEW YORK).

TEMES, G.C., V. BARCILON, AND F.C. MARSHALL, III (1973),
THE OPTIMIZATION OF BANDLIMITED SYSTEMS,
PROC. IEEE, VOL. 61, NO. 2. PP. 196-234.

VANDERPOL, BALTH, AND H. BREMMER (1959),
OPERATIONAL CALCULUS,
CAMBRIDGE UNIVERSITY PRESS, CAMBRIDGE, ENGLAND)

WATTERSON, C. C., J. R. JUROSHEK AND W. D. BENSEMA (1969),
EXPERIMENTAL VERIFICATION OF AN IONOSPHERIC CHANNEL MODEL,
ESSA TECHNICAL REPORT ERL 112-ITS-80,
U. S. GOVERNMENT PRINTING OFFICE, WASHINGTON, D.C. 20402.

ZADEH, L.A. (1950), FREQUENCY ANALYSIS OF VARIABLE
NETWORKS, PROC. IRE,VOL. 38, 291-299.

B. EFFECTS OF MULTIPATH ON SYSTEMS

The transfer function approach given in A, is a very general method of evaluating system performance, but because of this great generality, it is usually the case that some simplifying assumptions must be made. The first two chapters in this section offer very attractive solutions to the systems evaluations problems whenever the underlying assumptions can be justified. Both of these chapters utilize methods which derive the performance with multipath from the performance curves under steady (without multipath) conditions. Hence it is not necessary (for example) to have detailed knowledge of the signal structure or the specific receiver characteristics.

In contrast, the later chapters, where the classifications of multipath are more complex, give only examples of system evaluation with assumptions pertinent only to specific systems.

BI. SYSTEMS EVALUATION FOR SLOW-FLAT FADING

BI-A. INTRODUCTION

In this section we will develop the simple technique to determine the performance of a telecommunications system with a slow-flat fading signal once a performance characteristic is known for the constant signal. The "slow" in slow-flat fading means the signal amplitude fades slowly enough in time that the signal can be regarded as constant over some time period of interest (such as the time of a signal element in a digital system). The "flat" refers to the spectral behavior of the fading, and implies that the entire signal spectrum fades up and down uniformly so as not to distort the signal.

The physical processes that cause fading fall into two broad catagories: (1) absorption and other large volume effects, which result in a random signal normally called scatter; (2) the other category is comprised of numerous specular modes of propagation. The separation of the modes may take place at sharp boundaries of charged particles or reflections from isolated objects, etc. We have an assortment of distinct paths that the wave fronts may take in propagating from the transmitter to the receiver. This phenomenon is commonly called multipath and each path may contain some specular and scatter contributions. In any case, the fading signal received at the receiver becomes random and can be treated only in statistical terms.

In order to understand how a system's performance is degraded by the slow-flat fading signal compared with the performance for a constant signal of the same average power, and how the degree of degradation can be easily calculated,

we will first consider a simple, but practical example. This will enable us not only to understand the technique, but also to see why the technique will not work for other kinds of fading signals (for example, frequency selective fading, leading to signal distortion).

We will analyze the performance of a binary coherent phase shift keying (CPSK) digital system first, when the signal is constant, and then, from the probability of error characteristic obtained for this constant signal, we will obtain the system performance for slow-flat fading signals. We will do this for all the types of slow-flat fading signals generally considered, starting at the very beginning and analyzing the system's performance using a geometrical approach. This will enable us to picture what is going on in the signal-receiving process.

BI-B. CONSTANT SIGNAL PERFORMANCE

To represent a digital system geometrically, we make use of the following fact:

> Any finite set of physical waveforms of duration T, say $S_1(t)$, $S_2(t)$, ..., $S_m(t)$, may be expressed as a linear combination of k orthonormal waveforms $\phi_1(t), \phi_2(t), \ldots \phi_k(t)$, where $k \leq m$.

That is, each signal, $S_i(t)$ can be written as

$$S_i(t) = a_{i1}\phi_1(t) + a_{i2}\phi_2(t) + \ldots + a_{ik}\phi_k(t) \quad , \quad \text{(BI-1)}$$

where the coefficients a_{ij} are given by

$$a_{ij} = \frac{1}{T} \int_0^T S_i(t)\phi_j(t)\, dt.$$

Here the basic waveforms, $\phi_j(t)$, being orthonormal means that

$$\frac{1}{T}\int_0^T \phi_i(t)\phi_j(t)dt = 1 \quad i = j$$
$$= 0 \quad i \neq j \ .$$

While the above representation looks similar to the familiar Fourier expansion of a waveform, it is different in two important respects. The waveforms $\phi_i(t)$ are not restricted to sine and cosine waveforms, and (BI-1) is exact, even though only k terms are used.

Because of the above, our signaling waveforms, $S_i(t)$, can be represented in the k-dimensional signal space, $\phi_j(t)$, with coordinates given by the a_{ij}. For example, consider a set of signals for which k = 2, then the signals, $S_i(t)$, are given by vectors in the space $\phi_1(t)$, $\phi_2(t)$ as in figure BI-1.

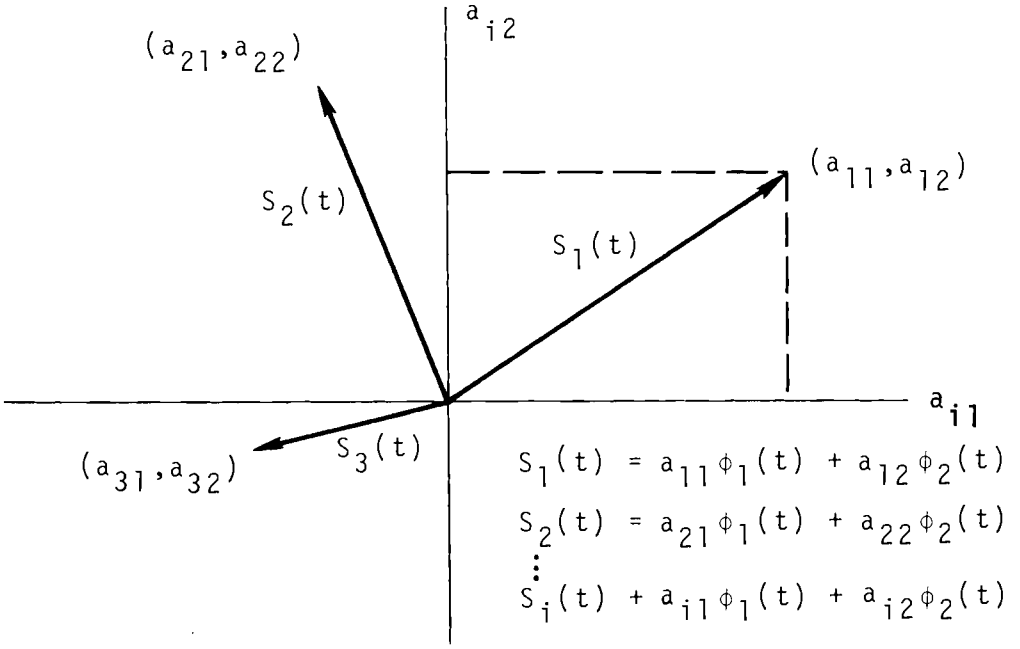

Figure BI-1. Signals represented as vectors in a signal space, k = 2.

As we shall see, the above representation not only allows visualization of what is actually going on in the receiving process, but also allows the variable t, time, to be removed from the problem. Our signals are now represented by simple vectors in ordinary Cartesian coordinates. That is, each signal is now represented by a point in the signal space with coordinates a_{ij}. All the rules of ordinary geometry apply, for example, the "distance" between signals is simply the ordinary distance between the corresponding signal points.

Digital receivers, by various means, actually compute the coordinates of a received signal and then make a decision based on these coordinates. One obvious receiver implementation is shown in figure BI-2. The actual physical implementations of the digital receiver may be, as in figure BI-2, a matched filter form, etc., but all these forms accomplish precisely the same thing, i.e., compute the signal coordinates, a_{ij}, and then make a decision as to which signal was sent, based on these a_{ij}.

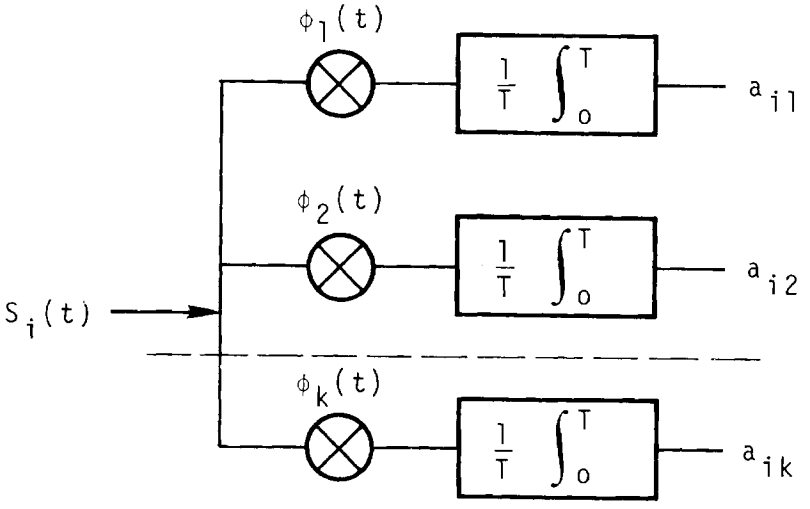

Figure BI-2. Product integrators used to calculate the signal space coordinates of signal $S_i(t)$.

The additive noise, which interferes without signal and causes the receiver to make errors when it tries to decide which one of the m-signalling waveforms was transmitted, also is represented by a point in the receiver's signal space. If n(t) is the received random-noise waveform, then it (like the signal) goes through the product integrators (or whatever), with the result that, as far as the receiver is concerned, the interfering noise is given by

$$n(t) = n_1\phi_1(t)+n_2\phi_2(t)+\ldots+n_k\phi_k(t) \ . \qquad \text{(BI-2)}$$

Therefore, if the receiver received noise only, the noise would also be represented by a point in the receiver's signal space, the noise coordinates given by $n_1, n_2, \ldots, n_k$.

Each of our m signals is represented by a unique point in the signal space. When signal plus noise is received, the result is a point (signal-plus-noise point) that can be anywhere in the signal space, depending on the noise. If each of our m signals is equally apt to have been sent, and are of equal power, the receiver, in order to minimize the average probability of error when it guesses what signal was transmitted, simply guesses the signal whose "point" is closest to the received signal-plus-noise point.

To take a specific example, consider coherent phase-shift-keyed signals. Our m signals are now, say

$$\begin{aligned} S_i(t) &= \sqrt{2W}\cos\left(\omega_o t+\frac{2\pi i}{m}\right) \ , \ 0\leq t<T \\ &= 0 \quad \text{elsewhere} \\ i &= 1,2, \ldots, m, \end{aligned} \qquad \text{(BI-3)}$$

where W is the power of $S_i(t)$ in Watts, and $\omega_o = 2\pi\ell/T$, for some fixed integer ℓ.

We can choose, then, for our basic waveforms

$$\phi_1(t) = \sqrt{2} \cos \omega_0 t$$
$$\phi_2(t) = \sqrt{2} \sin \omega_0 t \quad .$$

Note that our signal space is two-dimensional (k = 2) no matter what m is.

Consider m = 2, now

$$a_{11} = \frac{1}{T}\int_0^T \sqrt{2W} \cos (\omega_0 t+\pi) \sqrt{2} \cos \omega_0 t \, dt = -\sqrt{W}$$

$$a_{12} = \frac{1}{T}\int_0^T \sqrt{2W} \cos (\omega_0 t+\pi) \sqrt{2} \sin \omega_0 t \, dt = 0$$

Likewise, $a_{21} = \sqrt{W}$, $a_{22} = 0$. Therefore, the space and the points representing the two signals are as shown in figure BI-3. The point (n_1, n_2) corresponding to additive noise alone is also shown on figure BI-3.

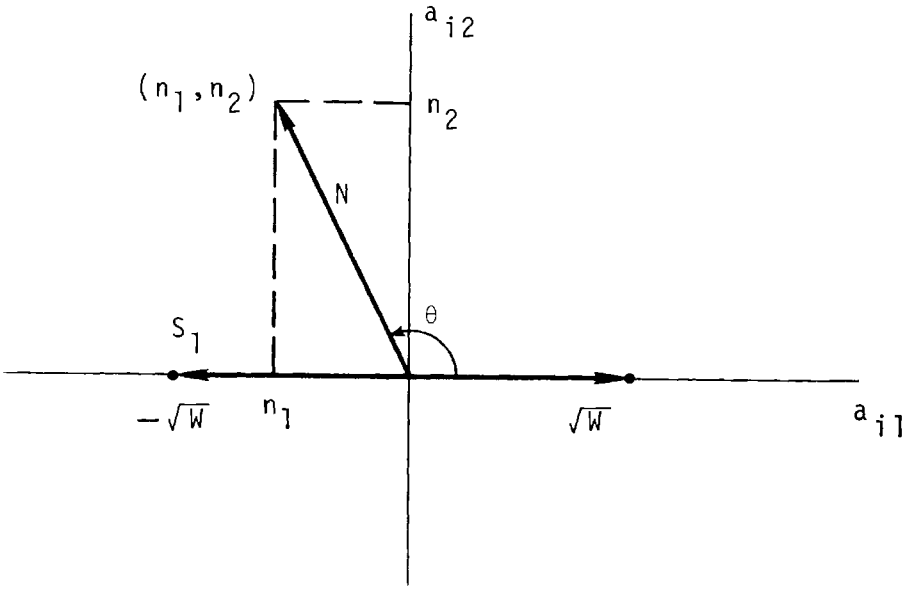

Figure BI-3. The signal space and signal points for binary CPSK, and the noise point (n_1, n_2).

Let the interfering noise be zero mean, white Gaussian, such as it would be if the noise were galactic or receiver front-end noise. N, the noise amplitude after it goes through the receiver and appears on the signal space (fig. BI-3), is Rayleigh distributed. Its probability density function is

$$p_N(y) = \frac{2y}{N_o B} \exp\left[-\frac{y^2}{N_o B}\right], \quad y \geq 0 . \qquad \text{(BI-4)}$$

This says that the probability that the noise amplitude N has a value in the range Y - dy/2 and y + dy/2 is given by $p_N(y)dy$, where N_o is the noise power spectral density (Watts/Hz) and B is the bandwidth (Hz), i.e., $N_o B$ is the noise power. The phase angle θ is uniformly distributed; i.e., its probability density function is

$$p_\theta(x) = \frac{1}{2\pi}, \quad -\pi < x \leq \pi ,$$

and θ has equal probability of being anything between $-\pi$ and π. The coordinate points are given by $n_1 = N \cos\theta$ and $n_2 = N \sin\theta$. This results in the coordinate points, n_1 and n_2, having zero mean normal distributions,

$$p_{n_1}(x) = \frac{1}{\sqrt{\pi N_o B}} \exp\left[-\frac{x^2}{N_o B}\right], \quad -\infty < x < \infty . \qquad \text{(BI-5)}$$

Note that since our development led to the signal being represented on the signal space by a vector of length $\sqrt{W}$, i.e., an rms voltage, the noise appears on the signal space in similar terms. That is, N or the variable y in (BI-4) is the instantaneous rms amplitude of the noise envelope.

Now let us consider the situation where S_2 is sent and we want to compute the probability that the receiver will decide S_1, and thus make an error. The situation is shown in

figure BI-4. If the resultant signal-plus-noise point lies in the shaded region (the region whose points are closest to the S_1 point), then the receiver will decide S_1, and make an error. This will happen whenever $\sqrt{W} + n_1$ is less than zero, or p_e = probability of error given that S_2 is transmitted = probability that $\sqrt{W} + n_1 < 0$. The probability, or likelihood, that $\sqrt{W} + n_1 < 0$ depends on the probability distribution of n_1.

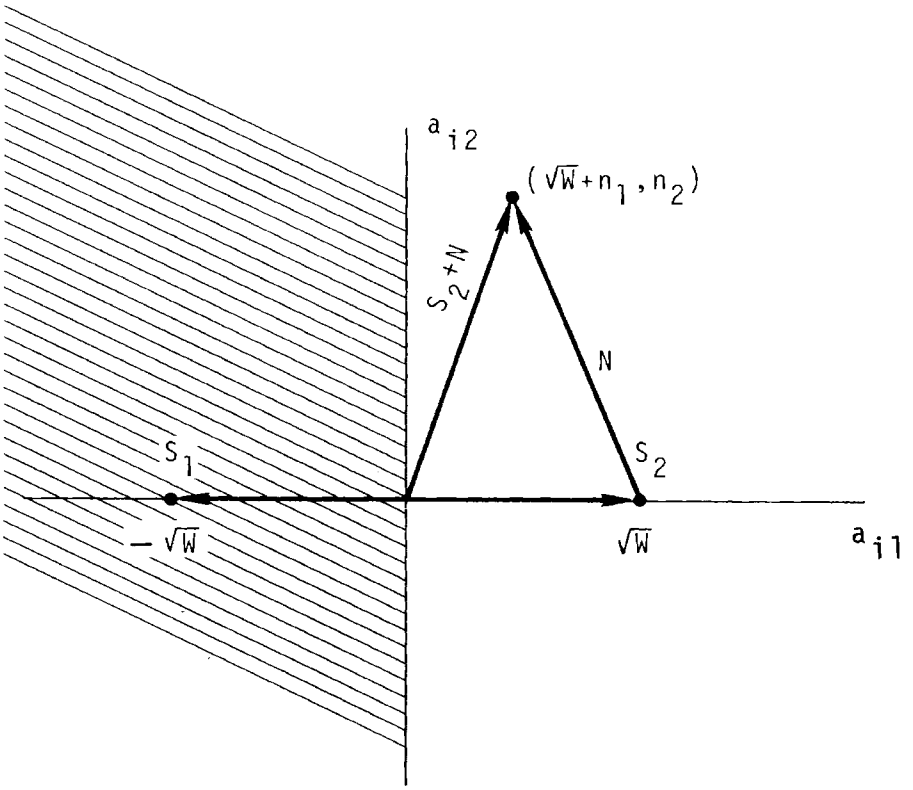

Figure BI-4. The signal-plus-noise point, given that S_2 was transmitted.

In our case

$$p_e = \text{prob}\left[\sqrt{W} + n_1 < 0\right] = \text{prob}\left[n_1 < -\sqrt{W}\right],$$

or, from (BI-5)

$$p_e = \int_{-\infty}^{-\sqrt{W}} \frac{1}{\sqrt{\pi N_o B}} \exp\left(-\frac{x^2}{N_o B}\right) dx \quad ,$$

or

$$p_e = \frac{1}{\sqrt{\pi}} \int_{\sqrt{\frac{W}{N_o B}}}^{\infty} e^{-y^2} dy \quad . \qquad \text{(BI-6)}$$

The performance p_e is a function of the signal-to-noise ratio W/N_oB. It is common to express the signal-to-noise ratio (SNR) as signal energy E (Joules or Watt seconds) to noise power spectral density N_o. For this system, the following are all identical expressions for the SNR:

$$\text{SNR} = \frac{E}{N_o} = \frac{W}{N_o B} = \frac{E}{N_o B T} \quad .$$

The integral (BI-6) can be given in terms of the standard tabulated function called the error function (erf) or

$$p_e = \frac{1}{2}\left[1 - \text{erf}\sqrt{\frac{E}{N_o}}\right] \quad , \qquad \text{(BI-7)}$$

where

$$\text{erf}(x) = \frac{2}{\sqrt{\pi}} \int_0^x e^{-y^2} dy \quad .$$

Let us look more closely at what the above result (BI-6) actually says. If we have in, say the i^{th} bit, the signal

level represented by $\sqrt{W}$, and the noise level (in this case represented by n_1), there will or will not be an error in this i^{th} bit, depending on the size of n_1. The integral in (BI-6) says that we are taking an average over an infinity of such i^{th} bits, weighted according to the probability or likli-hood that n_1 is of proper size to cause an error. That is, p_e in (Bi-6) represents an <u>average</u> probability of error given that S_2 is sent. If p_e is 10^{-3}, say, then out of m such bits, with m being very, very large, essentially m x 10^{-3} of these bits will be in error. Of course, there is no way of telling which bits will be in error, only the average number. We have considered the above case in which only S_2 was sent. If we repeat for the signal S_1, we obtain the same result. So the probability of error, p_e (BI-6) is the average probability of error for the system.

All digital systems can be put in the above framework and their performance for a constant signal level and for arbitrary additive noise calculated (although, perhaps not so easily as above). Note that for the noise, we required knowledge of the noise <u>as seen by our receiver</u>, how big it was, i.e., its spectral density, N_o, and the probability density of its amplitude. Note also that the performance turned out to be a function of the signal-to-noise ratio E/N_o (or $\frac{W}{N_o B}$).

BI-C. FADING SIGNAL PERFORMANCE

We now consider the case where the signal is not constant but fading. Suppose, however, that our signal is not distorted by the fading and that the fading is slow enough that we can consider the signal constant over an appropriate period of time (T seconds in our example). For our example, we still have the same "signal space" representation of the system, but now our two signals are given by (see (BI-3))

$$S_1(t) = -\sqrt{2W_j}\cos\omega_o t \ , \ o \leq t \leq T \qquad \text{(BI-8)}$$

$$S_2(t) = \sqrt{2W_j}\cos\omega_o t \ , \ o \leq t \leq T$$

where the subscript j denotes the signal level in the j^{th} bit. Note that the only change we have allowed is in the signal amplitude and we require W_j to be constant over the time period occupied by bit j. Having pointed out what, precisely, the "slow-flat" fading rules are, we generally now drop the subscript j, and simply say that the signal amplitude varies according to some fading distribution. This says that now the signal amplitude, just as the noise before, is random and we can only specify the likelihood or probability of it having particular values.

Previously (see fig. BI-3), as we went from bit to bit in our bit stream, the signal points on the a_{i1} axis remained fixed, while the noise point of interest (the coordinate n_1) moved randomly up and down the a_{i1} axis. We computed the average probability of error by averaging over many, many situations (bits) taking into account the probability of n_1 having values which would cause errors.

Now with the fading signal, the signal point also moves randomly up and down the a_{i1} axis as we go from bit to bit. Figure BI-5 shows the situation for three successive bits, considering signal S_2.

As before with the noise, to obtain the average probability of error, we must average over many such bits, taking into account now, the variable signal point (i.e., the probability distribution of the signal amplitude) as well as the variable noise point. This means that our average must now consider both the signal distribution and the noise distribution. Fortunately, this can be accomplished quite easily using the following rule from probability theory:

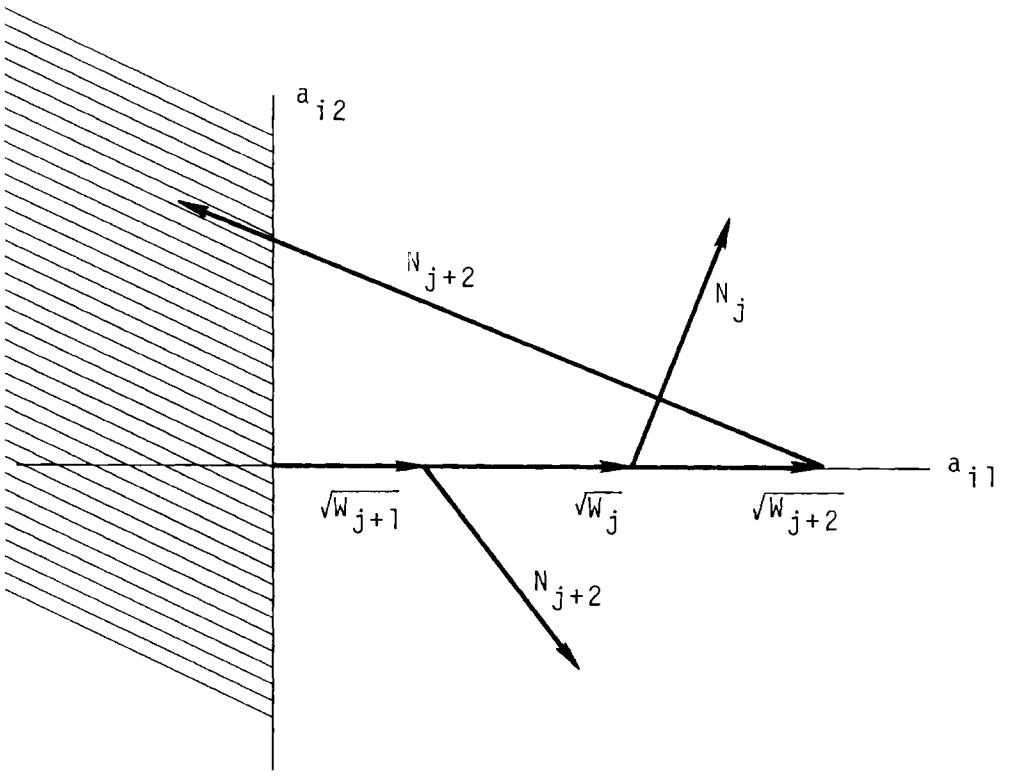

Figure BI-5. Signal plus noise, signal fading.

$$P[A] = \int_{-\infty}^{\infty} P[A|B=x]\ p_B(x)\ dx\ ,$$

that is, the probability of event A is given by the probability of event A, given that B has the value x, averaged over all values that B can have.

For our system, we have calculated the performance, given a signal energy E (or power, W) namely, p_e. The above says that for fading signal, we need only multiply the constant signal performance by the probability density function of the fading signal energy and then average (integrate) over all possible values of the signal energy. Therefore, from (BI-7), we have

$$P_e(\text{fading signal}) = \int_0^\infty 1/2 \left[1-\text{erf}\sqrt{\frac{x}{N_o}}\right] p_E(x)dx \ , \qquad \text{(BI-9)}$$

where, in order to keep the variables straight, we have used a "dummy" variable of integration, and $p_E(x)$ denotes the probability density function of E.

Equation (BI-9) gives the solution for the p_e for a fading distribution of signal energy E. Quite often we have given to us, instead, a fading distribution of signal power W or signal amplitude S, where $W = S^2/2$. Then, in terms of power, (BI-9) becomes

$$p_e(\text{fading signal}) = \int_0^\infty \frac{1}{2} \left[1-\text{erf}\sqrt{\frac{x}{N_oB}}\right] p_W(x)dx \ , \qquad \text{(BI-10)}$$

where $p_W(x)$ is the fading distribution of signal power W. Note that, of course, (BI-9) and (BI-10) are identical in form. For signal amplitude S,(BI-9) becomes

$$p_e(\text{fading signal}) = \int_0^\infty \frac{1}{2} \left[1-\text{erf}\frac{x}{\sqrt{2N_oB}}\right] p_S(x)dx \ , \qquad \text{(BI-11)}$$

where $p_S(x)$ denotes the distribution of signal amplitude. In (BI-10) the variable of integration x represents signal power W, while in (BI-11), the variable of integration x represents signal amplitude S ($W = S^2/2$).

The question now becomes, what $p_W(x)$ or $p_S(x)$ should we use? Let us first consider the case of a signal whose amplitude fades according to the Rayleigh distribution:

$$p_S(x) = \frac{x}{W_o} e^{-x^2/2W_o} \ , \qquad \text{(BI-12)}$$

where W_o denotes the mean power of the signal; i.e., the mean value of W. Of course, for constant signal, $W_o = W$. We will see later why the Rayleigh distribution is sometimes a good one to use for multipath signals.

Equation (BI-11) now gives us

$$p_e = \frac{1}{2} \int_0^\infty \left[1\text{-erf} \frac{x}{\sqrt{2N_oB}} \right] \frac{x}{W_o} e^{-x^2/2W_o} \, dx \; . \quad \text{(BI-13)}$$

This integral is easily evaluated (especially with a good table of integrals) to give the known result

$$p_e = \frac{1}{2} \left(1 - \frac{\sqrt{\frac{W_o}{N_oB}}}{\sqrt{\frac{W_o}{N_oB} + 1}} \right) \quad \text{(BI-14)}$$

Again, our result came out in terms of the SNR. As discussed previously, the signal power to noise power ratio, W_o/N_oB is equal to the signal energy to noise power spectral density ratio, E_o/N_o, (E_o = mean value of E) for this system.

What we have shown is that the performance of any system with slow flat-fading signal can be calculated using the system performance characteristic in constant signal and the probability distribution of the fading signal. For example, if we had available for an analog system (such as voice) some constant signal performance characteristic (such as articulation index) as a function of signal-to-noise ratio, then we could compute the performance for fading signal as above. We would need to be sure, however, that all the assumptions inherent in "slow" and "flat" were met or were reasonable approximations to the actual physical situation.

In summary, if $g_c(W/N_oB)$ denotes the performance for constant signal, and if $p_W(x)$ denotes the probability density of the signal power W, then the performance of the system in fading signal, $g_f(W_o/N_oB)$, is given by the average over all possible values of W,

$$g_f(W_o/N_oB) = \int_{\text{all } W} g_c(x/N_oB)p_W(x)\,dx \quad . \qquad \text{(BI-15)}$$

If $p_S(x)$ is the probability density of the signal amplitude S,

$$gf(W_o/N_oB) = \int_{\text{all } S} g_c(x^2/2N_oB)\,p_S(x)\,dx \quad . \qquad \text{(BI-16)}$$

Consider now the cases where either the "slow" assumption, or the "flat" assumption, or both, is not valid. Our receiver will still calculate a signal point no matter what kind of distorted signal the receiver receives. Now, however, the signal points will move randomly and rapidly all over the signal space and the computations of the statistics of such motion will be extremely difficult. Also, the signals are usually spread in time (also frequency), resulting in the received signals occupying more than their allotted (0,T) time slot. The result is that, if we are looking at bit j, for example, there is some signal from bit j-1 still going on, causing interference, i.e., intersymbol interference. This, as well as other problems, indicates why the straightforward approach given in (BI-15,16) cannot be used. For this reason we like to use slow-flat fading approximations whenever possible. The procedures required for system performance calculations in the case of "slow and flat" not being valid are covered in subsequent sections.

BI-D. FADING SIGNAL DISTRIBUTIONS

When the signal is propagated from the transmitter to the receiver, it is modified by the propagation media. Quite often the signal travels to the receiver via one, two, or any number of separate paths. If the signal from each of these multipaths is represented by a signal vector, then the receiver sees the vector sum of these signal vectors. The phase angle between any two such vectors is generally, on the average, uniformly distributed; i.e., the phase angle has equal chance of being anything between $-\pi$ and π radians. We are interested then in the probability distribution of the amplitude (or power) of the received signal, i.e., the above vector sum.

As mentioned earlier, each path may have some specular and scatter contributions. Scatter comes from large volume effects, and means the signal is scattered into many, many small signal vectors. That is, it is equivalent to multipath with many, many paths such that none of these many, many received signal vectors dominate the others (i.e., sticks out like a "sore thumb"). If we have such a sum of many more or less equal-sized vectors with uniform phase between them, then the amplitude of the vector sum has a Rayleigh distribution. Figure BI-6 (from Nesenbergs, 1967) shows the probability-density function of n equal-sized vectors for n = 1, 2, 3, 4, and 6 along with the Rayleigh limit ($n \to \infty$). We see that the "many many" above need only be 5 or 6 before the Rayleigh distribution is a reasonable approximation. In other words, the situation where we have, say 6 or more distinct paths, and the signal components from these paths are essentially equal, then the received signal amplitude is approximately Rayleigh distributed.

Suppose, instead, that we have one specular path (due, for example, to a direct line-of-sight path) and a scatter path,

or, equivalently, a number of other paths from which the received signals are more or less equal and small compared to the main signal. An example of one such situation would be "constant groundwave plus Rayleigh fading skywave". There are, of course, many other possibilities. In this case, the received signal amplitude has a Nakagami-Rice distribution,

$$p_S(x) = \frac{x}{\alpha} \exp\left[\frac{-x^2+2\beta}{2\alpha}\right] I_o\left(\frac{\sqrt{2\beta}\ x}{\alpha}\right) \qquad \text{(BI-17)}$$

where α is the power in the Rayleigh vector, β is the power in the constant vector, and I_o is the zero-order modified Bessel function.

If, as before, N_o denotes the noise power spectral density, then the signal-to-noise ratio is

$$\frac{W}{N_o B} = \frac{\alpha+\beta}{N_o B} \qquad \text{(BI-18)}$$

The distribution of signal amplitude for the general case of the sum of any number of such Nakagami-Rice vectors and resulting special cases is given by Nesenbergs (1967).

Consider the case where we have a direct ray and a single other path, resulting from a ground reflection. The probability density for the received signal power, W, is then

$$p_W(x) = \frac{1}{\pi} \frac{1}{\sqrt{4k^2\gamma_o^2-(x-(k^2+1)\gamma_o)^2}} ,$$

$$\gamma_o(1-k)^2 \leq x \leq \gamma_o(1+k)^2 , \qquad \text{(BI-19)}$$

where γ_o is the power of the direct ray and k is the voltage-amplitude ratio of the reflected-to-direct ray (reflection coefficient). The total mean power in the received signal is $\gamma_o(1+k^2)$, or the signal-to-noise ratio is

$$\frac{W}{N_o B} = \frac{\gamma_o(1+k^2)}{N_o B} \qquad \text{(BI-20)}$$

Experimental observations of received fading-signal amplitudes over various communication circuits have shown that the signal amplitude, when expressed in decibels, can sometimes be approximated by a normal distribution. That is, the signal amplitude has a log-normal distribution. If, for the signal amplitude, S, we let Y = 20 log S, then

$$p_Y(y) = \frac{1}{\sigma\sqrt{2\pi}} e^{-\frac{1}{2}\left(\frac{y-\mu}{\sigma}\right)^2} \quad , \quad -\infty<y<\infty \quad , \qquad \text{(BI-21)}$$

where μ is the mean value of Y(dB) and σ is the standard deviation (dB). The signal distribution for use in (BI-16) is then

$$p_S(x) = \frac{8.686}{x\sqrt{2\pi\sigma^2}} e^{-\frac{1}{2}\left(\frac{20\log x-\mu}{\sigma}\right)^2} \quad , \quad 0\leq x<\infty \quad . \qquad \text{(BI-22)}$$

For log-normal fading signal, the σ is usually given in terms of the "fading range". The fading range is the difference (in dB) between the upper and lower decile values. The upper decile is that value which is exceeded only 10 percent of the time, and the lower decile is that value which is exceeded 90 percent of the time. In terms of the fading range, 2.54 σ = fading range. The average received signal power is

$$W_o = 10^{0.1\mu+0.0115\sigma^2} \qquad \text{(BI-23)}$$

and the signal-to-noise ratio is W_o/N_oB.

The above distributions (BI-12, 17, 19, and 22) pretty well cover all the signal distributions that are generally considered for slow-flat fading. Which one to use depends on the particular kind of propagation path one is interested in. The

above distributions of the fading signal say nothing as to how "fast" the signal fades up and down. Therefore, consideration must be given to more than the fading distribution when trying to decide if a slow-flat assumption is valid.

BI-E. EXAMPLES AND REFERENCES

In this section we will give the results for our example system (CPSK) for all of the fading distributions considered above. An example for a voice system will also be given.

Figure BI-7 shows the results for the binary CPSK system for constant signal (BI-7), Rayleigh fading signal (BI-14), Nakagami-Rice fading (BI-17) with the power of the constant vector 10 dB above the average power of the Rayleigh vector, Nakagami-Rice fading with the power of the constant vector equal to the average power of the Rayleigh vector, and log-normal fading (BI-22), using a 13.4 dB fading range. Note that Rayleigh fading also has a 13.4 dB fading range.

Figure BI-8 shows the results for the binary CPSK system for the case of constant signal vector plus reflected signal vector. Results are given for constant signal (k=0), and for k = 0.2, 0.6, 0.8, and 0.9. We see from figures BI-7 and BI-8 that a very wide range of system performances can be obtained depending on the particular kind of signal fading present.

In order to show the results of using (BI-16) for a voice system, figure BI-9 is included. It shows the performance of a double-sideband AM system in white Gaussian noise and Rayleigh-fading signal. The calculations, via (BI-16), are from the performance in constant signal for a 5.2 kHz IF bandwidth (Cunningham et al., 1947). The performance is given in terms of the phonetically balanced word articulation index.

For the nature of fading signals, extensive bibliographies (Nupen, 1960; Salaman, 1962) are available. A historically significant survey was performed by the National Bureau of Standards (NBS, 1948). A number of good comprehensive texts are also available (Davies, 1965, for example).

The representation of digital systems in geometric terms is covered quite well by Arthers and Dym (1962). Performance characteristics for systems in fading signal and in nonGaussian impulsive noise (as well as Gaussian noise) are available (Bello, 1965; Conda, 1965; Halton and Spaulding, 1966; Akima et al., 1969; Akima, 1970; etc.

The following list of references includes additional references not cited above. The list is hardly complete, but will provide a great deal of additional information concerning the characterization of the fading channel, and the performance of a wide variety of systems with both constant and fading signal.

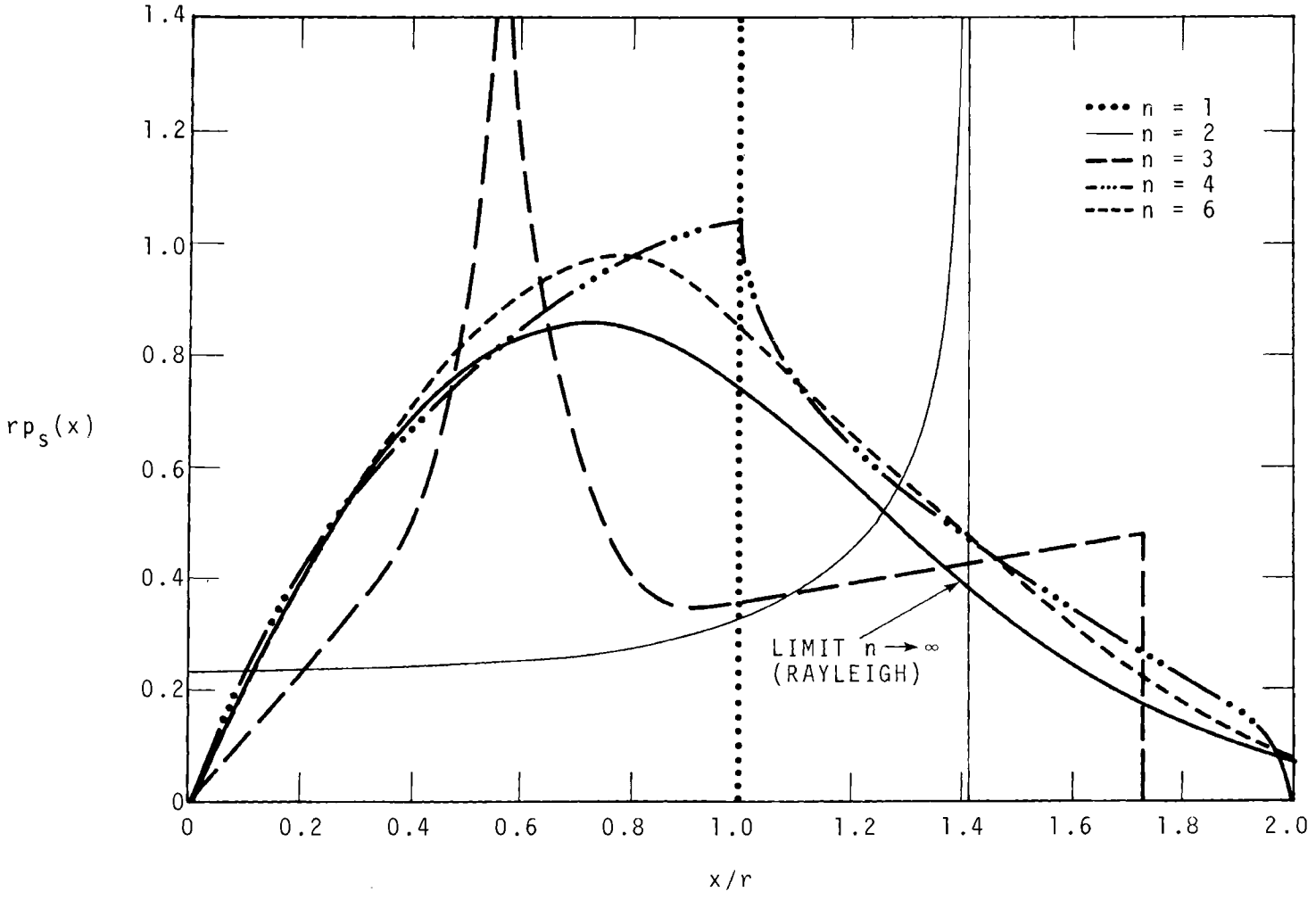

Figure BI-6. Amplitude probability density for sum of n equi-power constant signal vectors. The density functions are given in normalized form where r^2 = total signal power = nr_1^2, r_1^2 = power in each of the n-signal vectors.

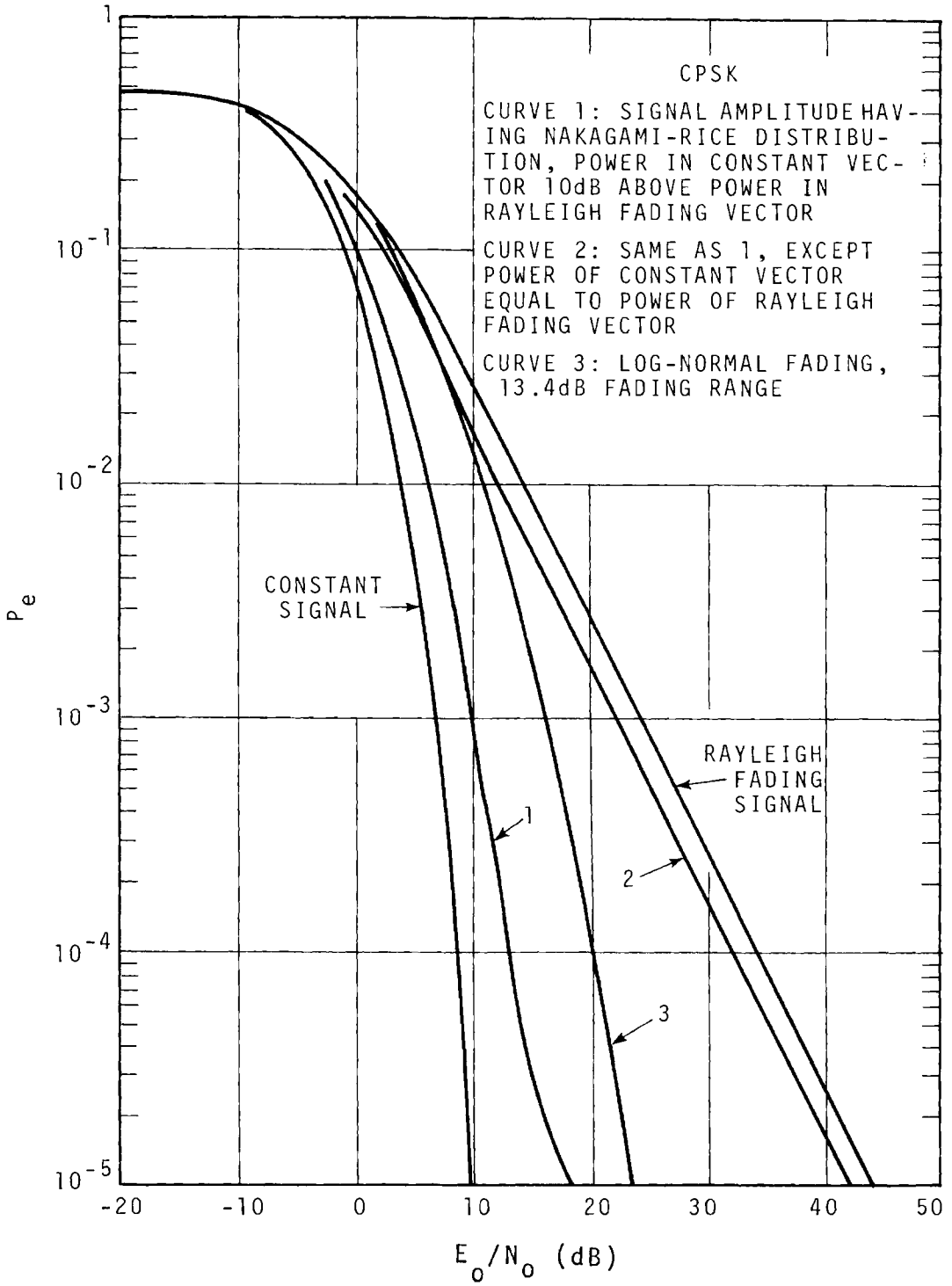

Figure BI-7. Average probability of error vs. signal energy to noise power spectral density ratio for constant signal and various types of fading signals for a binary coherent phase shift keying system. The noise is Gaussian.

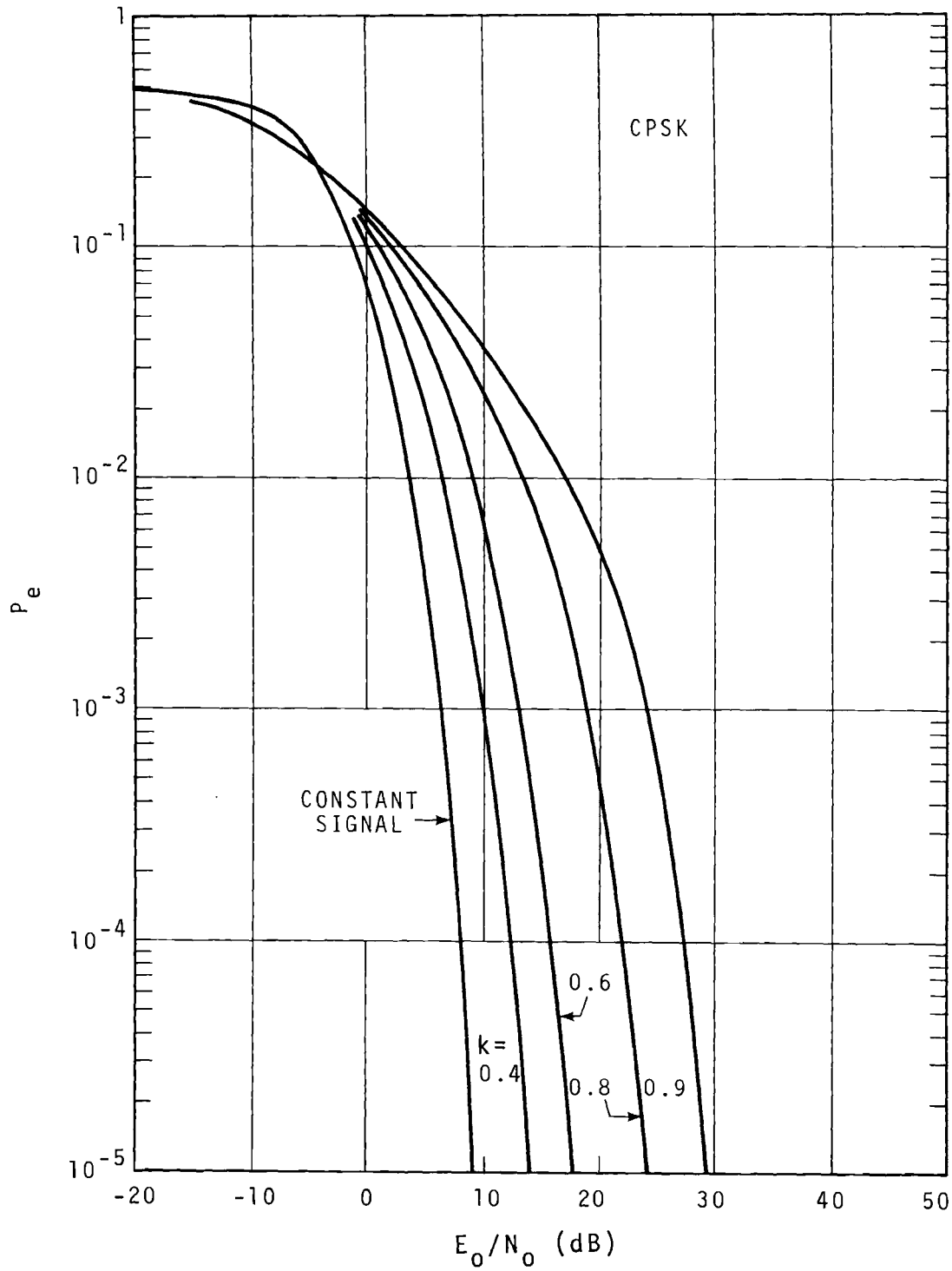

Figure BI-8. Average probability of error vs. signal energy to noise power spectral density ratio for constant signal and fading signal, where the fading signal is composed of a constant signal vector plus a reflected vector with reflection coefficient k. The noise is Gaussian.

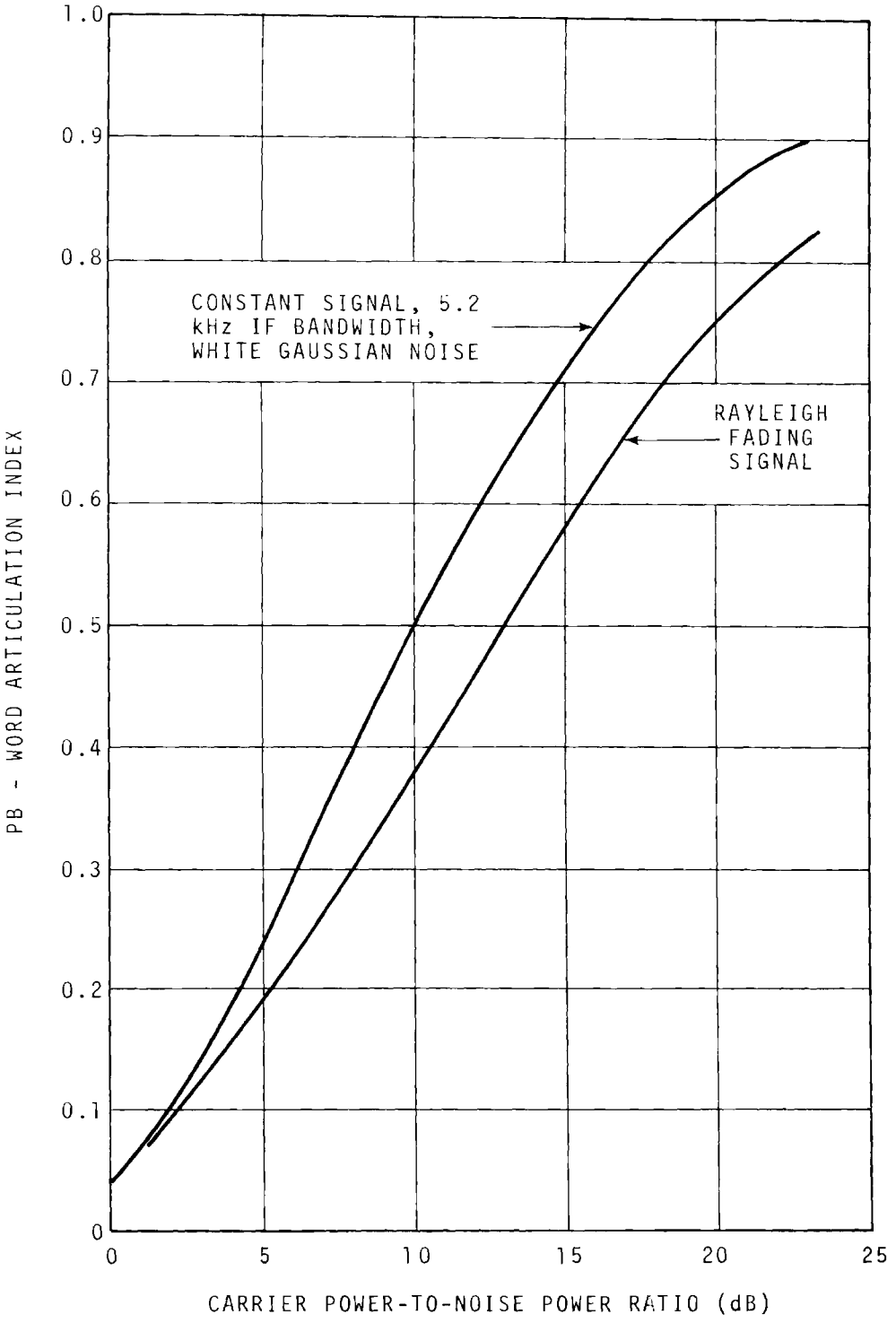

Figure BI-9. Phonetically balanced word articulation index vs. carrier power-to- voice power ratio for DSB-AM constant signal and Gaussian noise (after Cunningham et al., 1947) and for Rayleigh-fading signal.

BI-F. REFERENCES

AKIMA, H. (1970),
MODULATION STUDIES FOR IGOSS
ESSA TECHNICAL REPORT ERL 172-ITS 110
U.S. GOV T. PRINTING OFFICE, WASHINGTON, D.C. 20402, PRICE $0.55.

AKIMA, H., G. AX, AND W.M. BERRY (1969),
REQUIRED SIGNAL-TO-NOISE RATIOS FOR HF COMMUNICATION SYSTEMS
ESSA TECHNICAL REPORT ER 131-ITS 92
U.S. GOV T. PRINTING OFFICE, WASHINGTON, D.C. 20402, PRICE $0.60.

ARTHURS, E. AND H. DYM (1962),
ON THE OPTIMUM DETECTION FOR SIGNALS IN THE PRESENCE OF
WHITE GAUSSIAN NOISE
A GEOMETRIC INTERPRETATION AND A STUDY OF THREE BASIC DATA
TRANSMISSION SYSTEMS,
IRE TRANS. ON COMM. SYSTEMS, PP 336-372, DECEMBER.

BELLO, P.A. (1965),
ERROR PROBABILITIES DUE TO ATMOSPHERIC NOISE AND FLAT FADING IN
HF IONOSPHERIC COMMUNICATIONS SYSTEMS
IEEE TRANS. ON COMMUNICATIONS TECH., VOL. 13, NO. 3, PP 266-279.

CORDA, A.M. (1965),
THE EFFECT OF ATMOSPHERIC NOISE ON THE PROBABILITY OF ERROR FOR
AN NDFSK SYSTEM
IEEE TRANS. ON COMMUNICATIONS TECH., VOL. 13, NO. 3, PP 280-283.

CUNNINGHAM, W.T., S.J. GOFFARD, AND J.C.R. LICHLIDER (1947),
THE INFLUENCE OF AMPLITUDE LIMITING AND FREQUENCY SELECTIVITY
UPON THE PERFORMANCE OF RADIO RECEIVERS IN NOISE.
PROC. IRE35, 1021-1025.

FARROW, J.E., R.E. SKERJANEC, AND A.P. BORSIS (1971),
A DISCUSSION OF PERFORMANCE PREDICTIONS AND STANDARDS FOR
TROPOSPHERIC TELECOMMUNICATIONS SYSTEMS
OFFICE OF TELECOMMUNICATIONS TECHNICAL MEMORANDUM 62.

FLORMAN, E.F. AND J.J. TARY (1962),
REQUIRED SIGNAL-TO-NOISE RATIOS, RF SIGNAL POWER, AND BANDWIDTH
FOR MULTICHANNEL RADIO COMMUNICATIONS SYSTEMS
N.B.S. TECHNICAL NOTE 10
U.S. GOV T. PRINTING OFFICE, WASHINGTON D.C. 20402, PRICE $1.00.

GIERHART, G., R.W. HUBBARD, AND D.V. GLEN (1970),
ELECTROSPACE PLANNING AND ENGINEERING FOR THE AIR TRAFFIC
ENVIRONMENT
REPORT NO. FAA-RD-70-71,
U.S. GOV T. PRINTING OFFICE, WASHINGTON D.C. 20402, PRICE $2.25.

HALTON, J.H. AND A.D. SPAULDING (1966),
ERROR RATES IN DIFFERENTIALLY COHERENT PHASE SYSTEMS IN NON-GAUSSIAN NOISE
IEEE TRANS. ON COMM. TECH., VOL. COM-14, NO. 5, PP 594-601.

HUBBARD, R.W., D.V. GLEN, AND W.J. HARTMAN (1970),
MODULATION CHARACTERISTICS CRITICAL TO FREQUENCY PLANNING FOR THE AERONAUTICAL SERVICES
ESSA TECH. MEMO. ERLTM-ITS 232, FAA CONTRACT NO. FA67-WAI 134, FAA SYSTEMS RESEARCH AND DEV. SERVICES, SPECTRUMS PLANS AND PROGRAMS BRANCH RD-510, WASHINGTON D.C. 20553.

NATIONAL BUREAU OF STANDARDS (1948),
IONOSPHERIC RADIO PROPAGATION,
N.B.S. CIRCULAR NO. 462
U.S. GOV T. PRINTING OFFICE, WASHINGTON D.C. 20402.

NESENBERGS, M. (1967),
SIGNAL AMPLITUDE DISTRBUTION FOR STATIONARY RADIO MULTIPATH CONDITIONS.
ESSA TECHNICAL REPORT IER44-ITSA44
SUPERINTENDENT OF DOCUMENTS, U.S. GOV T. PRINTING OFFICE, WASHINGTON, D.C. 20402, PRICE $0.50.

NUFER, W. (1960),
BIBLIOGRAPHY ON IONOSPHERIC PROPAGATION OF RADIO WAVES (1923-1960),
N.B.S. TECH. NOTE NO. 84
U.S. GOV T. PRINTING OFFICE, WASHINGTON, D.C. 20402.

SALAMAN, R.K. (1962),
HISTORICAL SURVEY OF FADING AT MEDIUM AND HIGH FREQUENCIES.
N.B.S. TECH. NOTE NO. 133
U.S. GOV T. PRINTING OFFICE, WASHINGTON, D.C. 20402.

SALAMAN, R.K., G. AX, AND A.C. STEWART (1971),
RADIO CHANNEL CHARACTERIZATION
TELECOMMUNICATIONS TECHNICAL MEMORANDUM
OFFICE OF TELECOMMUNICATIONS/ITSTM 27.

BII. SYSTEMS EVALUATION FOR NOISE-LIKE MULTIPATH

BII-A. INTRODUCTION

From the model for discrete multipath, chapter AI-E equation AI (17),

$$y(t) = \sum_{i=0}^{N} a_i x_o(t - \tau_i)$$

$$= a_o x_o(t) e^{j\omega_o t} + \sum_{i=1}^{N} a_i x_o(t - \tau_i) e^{i\omega_o(t-\tau_i)} \qquad (1)$$

$$= a_o x_o(t) e^{j\omega_o t} + m(t) \quad ,$$

one can obtain a simple method for evaluating system performance under certain conditions which permit the summation in (1) to be treated as a random variable. Even when these conditions are not satisfied, the simplicity of the method makes it useful for obtaining quick approximations for bounds on performance.

BII-B. THE BASIC MODEL

In chapter BI, examples of system performance evaluations were given for an undistorted signal in the presence of white Gaussian noise n(t). If m(t) in eq (1) satisfies the conditions: (a) the real and imaginary parts are Gaussian, uncorrelated random variables with zero mean

and equal standard deviations, and (b) $m(t)$ is uncorrelated with $x_0(t)e^{i\omega_0 t}$, then exactly the same techniques used in chapter BI for noise only can be used to evaluate the system performance. We may write (1), with the noise term $n(t)$ added, in the form

$$y(t) = a_0 x_0(t) e^{i\omega_0 t} + m(t) + n(t) \qquad (2)$$

Then the real and imaginary parts, $m(t) + n(t)$, are also Gaussian random variables with zero means, and standard deviations which are the sum of the standard deviations of the real and imaginary parts of $m(t)$ and $n(t)$ [Beckmann, 1967]. One important difference however, between $m(t)$ and $n(t)$ is that the mean squared value of $m(t)$ is proportional to the power in the signal, while that of $n(t)$ is fixed. Expressed another way, with the above assumptions it is possible to define a noise power spectral density M_0 corresponding to $m(t)$ in the same way N_0 is defined in chapter BI, and E/M_0 will be fixed while E/N_0 varies. Thus, the performance curves for this case can be calculated from the non-fading curves of chapter BI, or from similar curves obtained from back-to-back measurements by the following method:

If E/N_0 and E/M_0 are given as power ratios, calculate

$$\frac{1}{\left(\frac{1}{E/N_0}\right) + \left(\frac{1}{E/M_0}\right)}$$

and read the appropriate curve at this point and plot at the ordinate E/N_0.

If E/N_0 and E/M_0 are given in dB, calculate

$$10 \log \frac{1}{10^{-E/10N_o} + 10^{-E/10M_o}}$$

read the value from the curve at this ordinate, and plot this point at the ordinate E/N_0(dB). For a fixed E/M_0, it is clear that, as E/N_0 increases, the best performance that can be achieved is that obtained from the curve read at the value $E/N_0 = E/M_0$. Figures (1) and (2) show examples corresponding to the constant signal curves of figures BI-8 and BI-9, for two values of E/M_0, 5 dB and 10 dB.

It is difficult to state precisely when conditions (a) and (b) are valid, but guidelines are available. Condition (b), stating that m(t) is uncorrelated with the signal is met if the differential delays between the direct component and the components of m(t) are large compared to the correlation time of the signal. Although this is sufficient to insure no correlation, it is not necessary, and for many practical situations, condition (b) will hold for shorter delays.

BII-C EXAMPLES FOR CONDITION (a) NOT SATISFIED

When the in-phase and quadrature components of $m(t)$ are correlated and have unequal variances, representing a situation where the multipath component has a preferred phase, one can use the methods of BII-B for a coherent binary phase shift key system. However, other systems are not, in general, amenable to these simplified methods.

Let the in-phase and quadrature components of $m(t)$ be $u_1(t)$ and $v_1(t)$ respectively, and of $n(t)$ be $u_2(t)$ and $v_2(t)$ respectively.

Let the variance of $x(t) = u_1(t) + u_2(t)$ be s_1, and of $y(t) = v_1(t) + v_2(t)$ be s_2, and the correlation between x and y be ρ. Note that ρ comes from correlation between u_1 and v_1 since it is still assumed that the noise components are uncorrelated with equal variances.

The probability density function for this case is

$$p_{xy}(x, y) = \frac{1}{2\pi \sqrt{s_1 s_2}\sqrt{1 - s^2}} \exp\left\{-[2(1 - s^2)]^{-1}\left[\frac{x^2}{s_1} - \frac{2\rho\, xy}{\sqrt{s_1}\sqrt{s_2}} + \frac{y^2}{s_2}\right]\right\}$$

For the binary CPSk, we need

$$\frac{1}{2}\ \text{prob}[x < -\sqrt{w}\ ] + \frac{1}{2}\ \text{prob}[x > \sqrt{w}]$$

where w is the signal power in watts. Integrating over y, we obtain

$$p_x(x) = \frac{1}{\sqrt{2\pi s_1}} e^{-x^2/2s_1} \quad ,$$

so that the probability of error as derived in BI for this case depends only on s_1, and is independent of s_2 and ρ. Therefore, we may use the curves of figure 1.

For other systems however, p_e will depend on s_1, s_2 and ρ, and no convenient method of calculation is available.

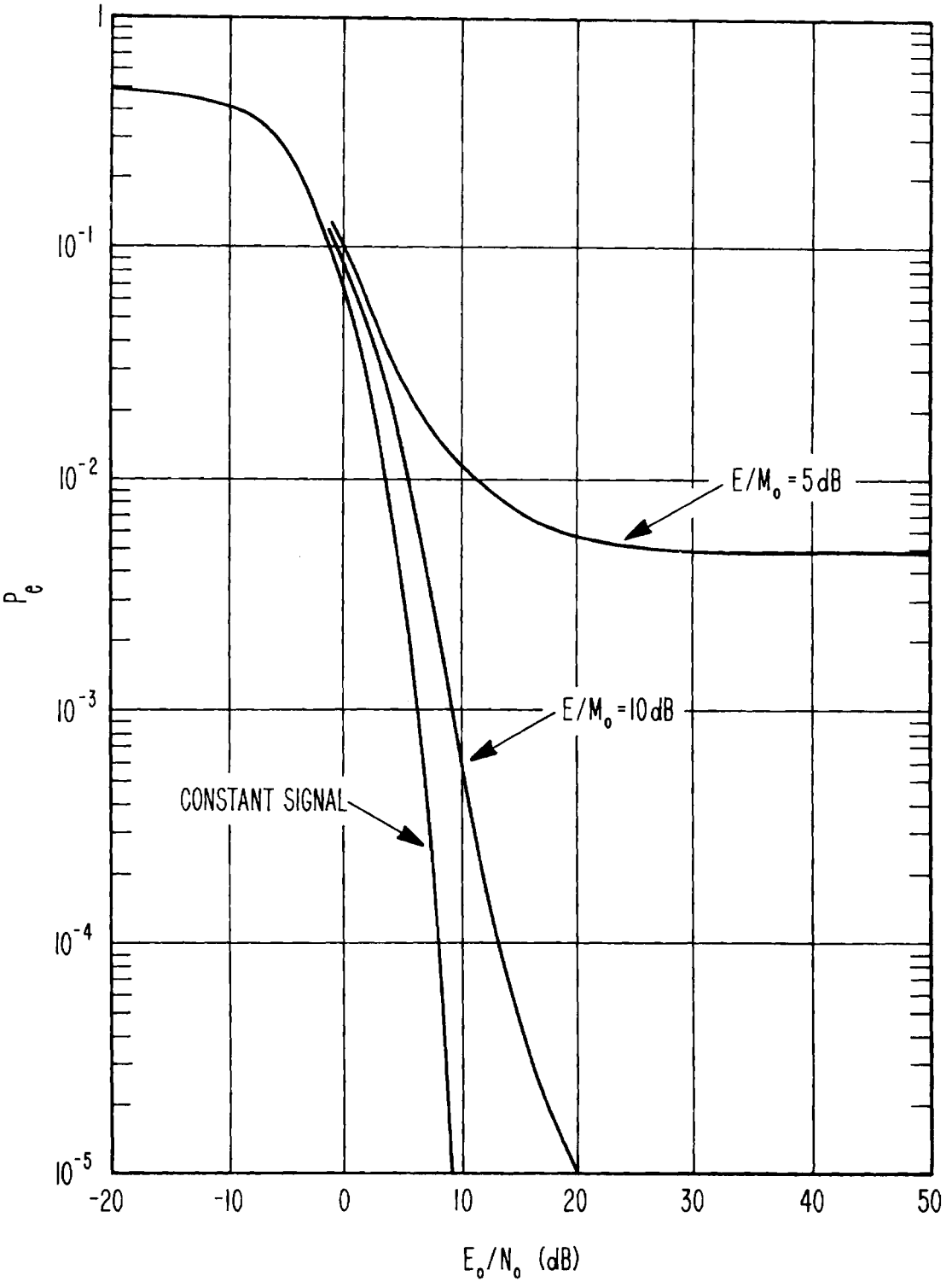

Figure BII-1. Average probability of error vs. signal energy to noise power spectral density ratio for constant signal curve of figure BI-8 and for two different values of signal interference ratios.

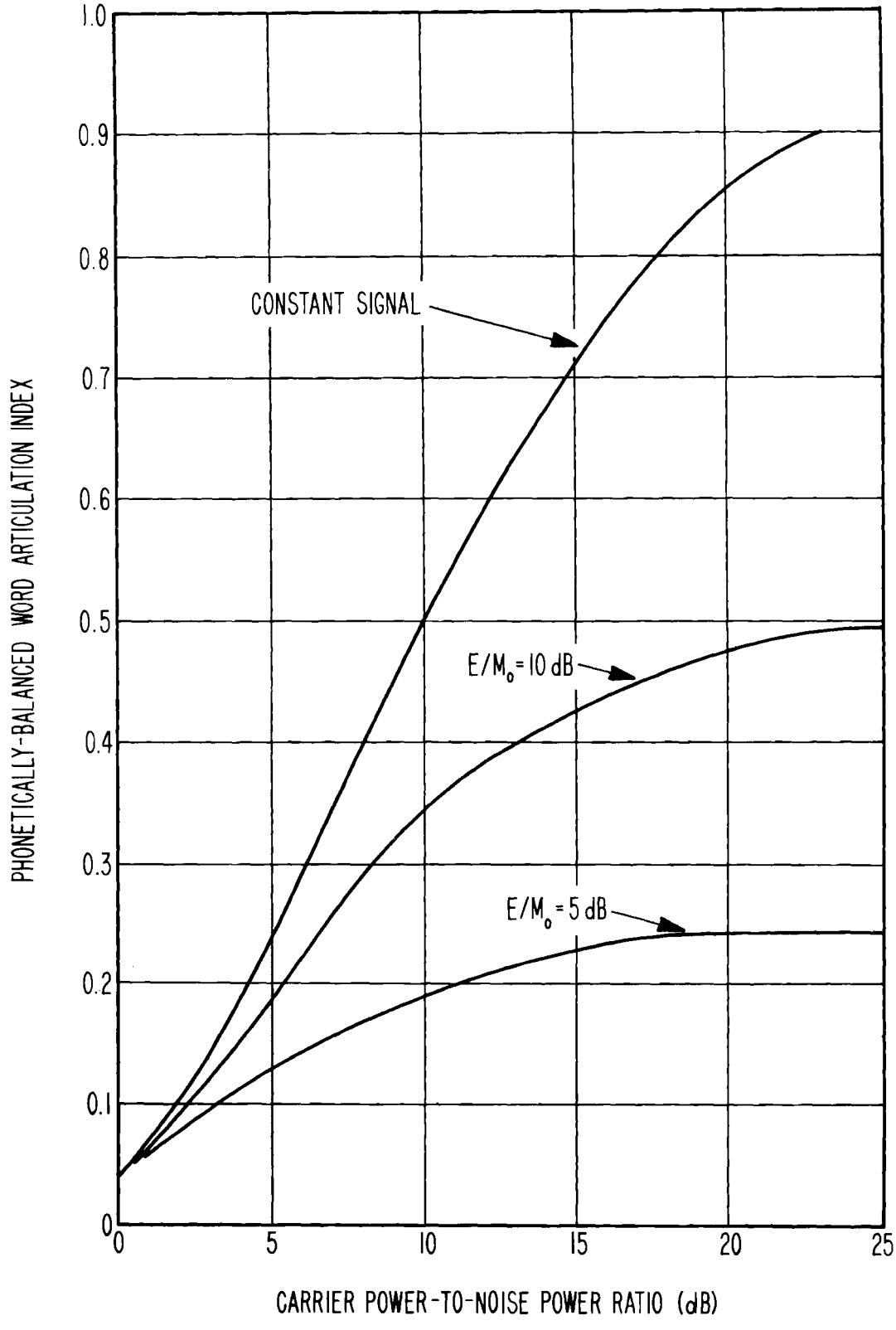

Figure BII-2. Phonetically balanced word articulation index vs. carrier power-to-voice power ratio for DSB-AM constant signal of figure BI-9 and two different values of signal to interference ratios.

ABRAMOWITZ, M., AND I.A. STEGUN (1964),
HANDBOOK OF MATHEMATICAL FUNCTIONS,
NBS APPL. MATH. SERIES 5-5
(GPO, $6.50)

BECKMANN, P. (1967),
PROBABILITY IN COMMUNICATION ENGINEERING
(HARCOURT, BRACE AND WORLD, INC., NEW YORK)

BIII. PHASE SHIFT KEY PERFORMANCE FOR NON-FLAT FADING

BIII-A. Introduction

When the methods of chapters BI and BII are not applicable additional complications arise in the study of system performance estimation. This chapter illustrates some of the methods used for coherent phase shift key systems for three different classifications of multipath.

The first two cases are similar, both two path models, one with a specular second path and the other with a time spread second path. The statistics enter into these cases through the probability that a particular delay will occur. The third case involves a scattering function, dispersive in time and frequency, under the assumption that the statistical process is a zero-mean homogeneous Gaussian process.

BIII-B. Two Path Specular Model

We consider first the simple case of two-path model without spread. Under this condition, the system impulse function may be written as

$$h(t) = \delta(t) + A\delta(t-\tau_d) \quad , \quad 0 \leq t \leq T, \tag{1}$$

where A and τ_d are respectively the interference-to-signal-voltage ratio (ISR) and the delay differential of the second path.

Assuming that the undistorted pulse transmitted in the interval $-kT \leq t \leq -kT + T$ takes the following form:

$$s_k(t) = (2S)^{1/2} \cos(\omega_o t + \theta_k) , \qquad (2)$$

with S, ω_o, and θ_k is one of the values $2\pi j/m$, $0 \leq j \leq m-1$ representing respectively the signal power, the angular carrier frequency, and some phase associated with the pulse. The pulse being transmitted may be identified with k=0, That is

$$s_0(t) = (2S)^{1/2} \cos(\omega_0 t + \theta_o) . \qquad (3)$$

The received signal observed in the same interval $0 \leq t \leq T$ assuming first that the differential delay is less than a bit length, is given by

$$r(t) = h(t) * s_0(t) + n(t) = r_1(t) + r_2(t) + r_3(t) + n(t) \qquad (4)$$

where

$$r_1(t) = (2S)^{1/2} \cos(\omega_0 t + \theta_0) \text{ in } \quad 0 \leq t \leq T$$

is the direct-path response of the present pulse,

$$r_2(t) = A(2S)^{1/2} \cos[\omega_0 (t - \tau_d) + \theta_0], \text{ in } \tau_d \leq t \leq T$$

is the delayed response of the present pulse due to the second path,

$$r_3(t) = A(2S)^{1/2}\cos[\omega_0(t-\tau_d) + \theta_1] \quad \text{in } 0 \le t \le \tau_d$$

is the response of the second path due to the previous pulse sent in $-T \le t \le 0$, and $n(t)$ is the additive noise, assumed to be white gaussian with $n(t) = 0$.

The receiver calculates the following:

$$\alpha = (2)^{1/2} \int_0^T r(t)\cos(\omega_0 t + \theta_0)\,dt$$

$$= 2(S)^{1/2}\int_0^T \cos^2(\omega_0 t + \theta_0)\,dt$$

$$+ 2A(S)^{1/2}\int_{\tau_d}^T \cos(\omega_0 t + \theta_0)\cos[\omega_0(t-\tau_d) + \theta_0]\,dt$$

$$+ 2A(S)^{1/2}\int_0^{\tau_d} \cos(\omega_0 t + \theta_0)\cos[\omega_0(t-\tau_d) + \theta_1]\,dt$$

$$+ (2)^{1/2}\int_0^T n(t)\cos(\omega_0 t + \theta_0)\,dt \ .$$

$$= (S)^{1/2}T\left[1 + A\,\frac{T-\tau_d}{T}\cos\omega_0\tau_d + A\frac{\tau_d}{T}\cos(\omega_0\tau_d - \theta_1 + \theta_0)\right]$$

$$+ (2)^{1/2}\int_0^T n(t)\cos(\omega_0 t + \theta_0)\,dt \ . \qquad (5)$$

The probabilities of θ_1 and θ_0 depend on the message structure.

The ensemble average of the quantity α is given by

$$\bar{\alpha} = (S)^{1/2} T \left[1 + A\frac{T-\tau_d}{T} \cos \omega_0 \tau_d + A\frac{\tau_d}{T} \cos(\omega_0 \tau_d - \theta_1 + \theta_0)\right]. \quad (6)$$

For the binary case, $m = 2$, we have

$$\alpha_0 = \bar{\alpha}\Big|_{\theta_1 = \theta_0} = (S)^{1/2} T (1 + A \cos \omega_0 \tau_d) \quad (7)$$

as the average value of α when $\theta_1 = \theta_0$, and

$$\alpha_1 = \bar{\alpha}\Big|_{\theta_1 = \theta_0 + \pi} = (S)^{1/2} T \left[1 + A\left(\frac{T-2\tau_d}{T}\right) \cos \omega_0 \tau_d\right] \quad (8)$$

when $\theta_1 = \theta_0 + \pi$.

The corresponding variances will then be

$$\text{var } \alpha_0 = \overline{(\alpha - \alpha_0)^2}$$

$$= 2 \int_0^T \int_0^T \overline{n(t_1)\, n(t_2)} \cos(\omega_0 t_1 + \theta_0) \cos(\omega_0 t_2 + \theta_0)\, dt_1\, dt_2$$

$$= 1/2\ N_0 T, \quad (9)$$

and

$$\text{var } \alpha_1 = \text{var} \alpha_0 = 1/2\ N_0 T, \quad (10)$$

where N_0 is the noise power density in watts per hertz.

The output signal-to-noise ratios for this case may be defined as

$$(SNR)_0 = \frac{\alpha_0^2}{2 \text{ var } \alpha_0} = \frac{E}{N_0} (1 + A \cos\omega_0\tau_d)^2 , \qquad (11)$$

and and

$$(SNR)_1 = \frac{\alpha_1^2}{2 \text{ var } \alpha_1} = \frac{E}{N_0} \left[1 + A\left(\frac{T-2\tau_d}{T}\right) \cos \omega_0 \tau_d\right]^2 \qquad (12)$$

where $E = ST$.

From (5), we see that the first two terms of α are essentially deterministic when θ_0 and θ_1 are assumed. The distribution of the random variable α is, thus, basically the same as that of the noise term. That is, α is gaussian with the mean and variance given respectively by (7) or (8) and (9) or (10). Thus, the probability of bit error when $\theta_1=\theta_0$ is

$$P_{e0} = \frac{1}{\sqrt{2\pi \text{ var } \alpha_0}} \int_{-\infty}^{0} e^{-(\alpha-\alpha_0)^2/2 \text{ var } \alpha_0} \, d\alpha$$

$$= 1/2 \text{ erfc} \left(\frac{\alpha_0}{\sqrt{2 \text{ var } \alpha_0}}\right) = 1/2 \text{ erfc} \left[\sqrt{(SNR)_0}\right] , \qquad (13)$$

where

$$\text{erfc}(t) = \frac{2}{\sqrt{\pi}} \int_t^{\infty} e^{-u^2} \, du \quad . \qquad (14)$$

Similarly, the probability of bit error when $\theta_1=\theta_0+\pi$ is

$$p_{e1} = 1/2 \ \text{erfc}\left[\sqrt{(SNR)_1}\right] . \qquad (15)$$

For the case where θ_1 and θ_2 have equal probabilities and are uncorrelated, the total error probability is

$$p_e = 1/2 \ p_{e0} + 1/2 \ p_{e1} = 1/4\left[\text{erfc}\sqrt{(SNR)_0} + \text{erfc}\sqrt{(SNR)_1}\right] . \qquad (16)$$

For illustrative purposes, we present in figures 1a and 1b $(SNR)_0$ and $(SNR)_1$ for $E/N_0=100$ (20 dB), A = 1 (0 dB), and $\omega_0 T = 20\pi$. It is seen that maximum values of $4(E/N_0) = 400$ (26.02 dB) for $(SNR)_0$ occur at $\tau_d = i(0.1T)$, $i = 0, 1, \ldots, 10$, while minimum values of zero ($-\infty$ dB) for $(SNR)_0$ occur at $\tau_d = (2i-1)(0.05T)$, $i = 0, 1, \ldots, 10$. On the other hand, the places at which maximum and minimum values for $(SNR)_1$ occur are rather more involved, depending on whether τ_d is less or greater than T/2 (See tables 1 and 2).

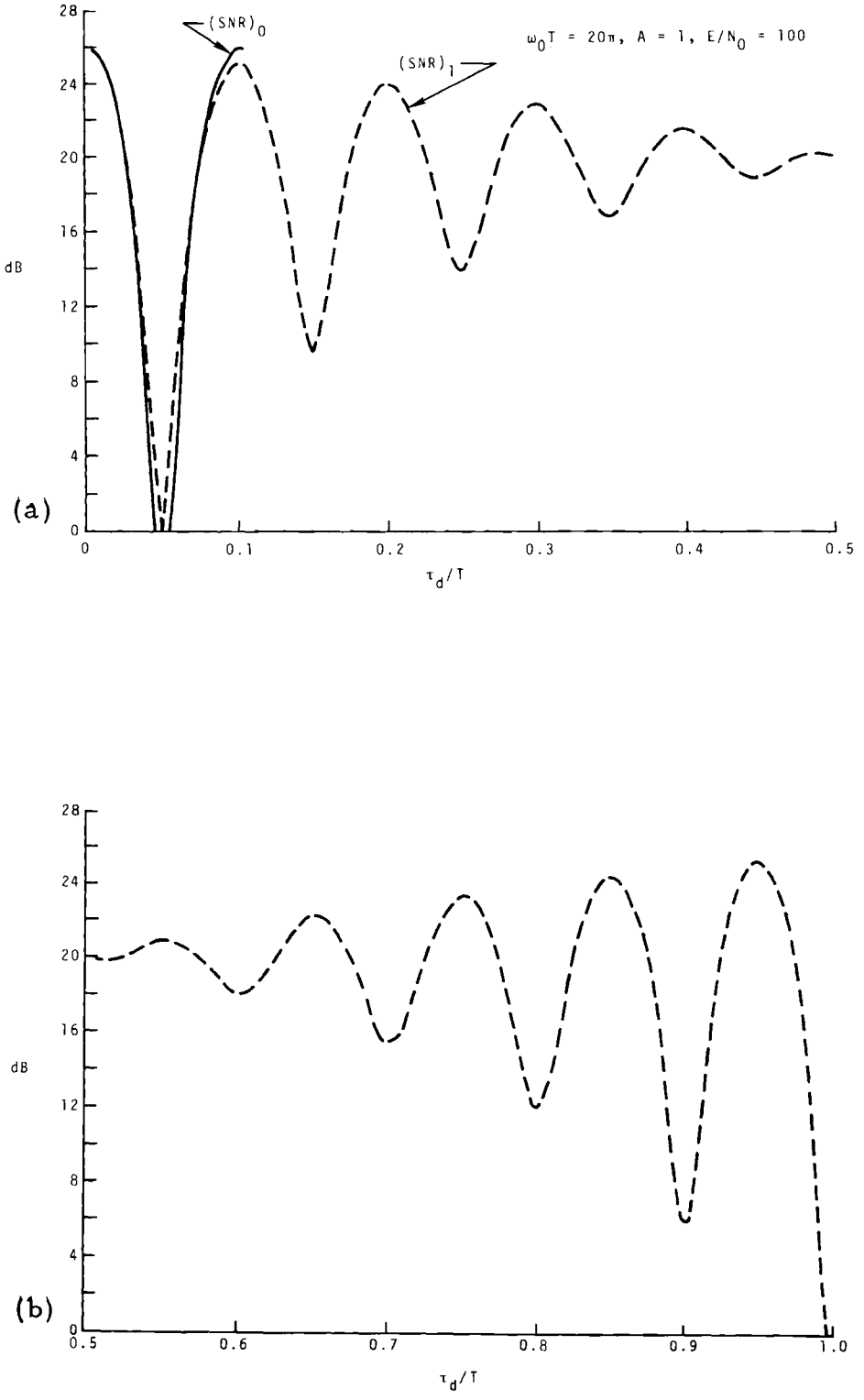

Figure BIII-1. Signal to noise ratio as a function of the ratio of delay τ_o to bit length T. $(SNR)_o$ is periodic with period 0.1, and p_e is symmetric about 0.5.

Table 1. Maximum values of $(SNR)_1$

Max $(SNR)_1$ is Approximately	That Occurs Approximately at τ_d
$2.0^2(E/N_0) = 400$	0
$1.8^2(E/N_0) = 324$	0.1 T
$1.6^2(E/N_0) = 256$	0.2 T
$1.4^2(E/N_0) = 196$	0.3 T
$1.2^2(E/N_0) = 144$	0.4 T
$(1.02)^2(E/N_0) =$	0.48 T
$1.1^2(E/N_0) = 121$	0.55 T
$1.3^2(E/N_0) = 169$	0.65 T
$1.5^2(E/N_0) = 225$	0.75 T
$1.7^2(E/N_0) = 289$	0.85 T
$1.9^2(E/N_0) = 361$	0.95 T

Table 2. Minimum values of $(SNR)_1$

Min $(SNR)_1$ is Approximately	That Occurs Approximately at τ_d
$0.1^2(E/N_0) = 1$	0.05 T
$0.3^2(E/N_0) = 9$	0.15 T
$0.5^2(E/N_0) = 25$	0.25 T
$0.7^2(E/N_0) = 49$	0.35 T
$0.9^2(E/N_0) = 81$	0.45 T
$0.98^2(E/N_0) =$	0.52 T
$0.8^2(E/N_0) = 64$	0.60 T
$0.6^2(E/N_0) = 36$	0.70 T
$0.4^2(E/N_0) = 16$	0.80 T
$0.2^2(E/N_0) = 4$	0.90 T
$= 0$	T

It is also clear that $(SNR)_0 = (SNR)_1 = E/N_0$ when $\omega_0\tau_d = (2i-1)\pi/2$, or $\tau_d = (2i-1)T/40$, $i = 0, 1, \ldots$.

Associated curves for p_{e0} and p_{e1} when $E/N_0=100$, $A=1$, and $\omega_0 T=20\pi$ are given in figure 2 for the range $0 \le \tau_d \le 0.1T$.

Figures 3 and 4 give p_e as a function of E/N_0 for various values of τ_d/T.

Graphs of $(SNR)_0$ and $(SNR)_1$ similar to those of figure 1 with $A=1/2$ (-6 dB) are given in figures 5a and 5b, from which we see that $\max(SNR)_0 = \max(SNR)_1 = 1.5^2(E/N_0) = 225$ (23.52 dB), and that $\min(SNR)_0 = \min(SNR)_1 = 0.5^2(E/N_0) = 25$ (13.98 dB). Thus, the worst probability of error which can happen for this case is

$$\max p_e = 1/2 \operatorname{erfc}(5) = 7.67 \times 10^{-13}.$$

From the forms of eqs (11) and (12) it is seen that delays τ_d, longer than T result in the same signal to noise ratios as a function of the fractional part of τ_d/T and the only change in the probability of error comes from the probabilities that $(SNR)_0$ and $(SNR)_1$ occur.

Additionally, if a distribution of delays is known, the average probability of error can be obtained by averaging p_e of (16).

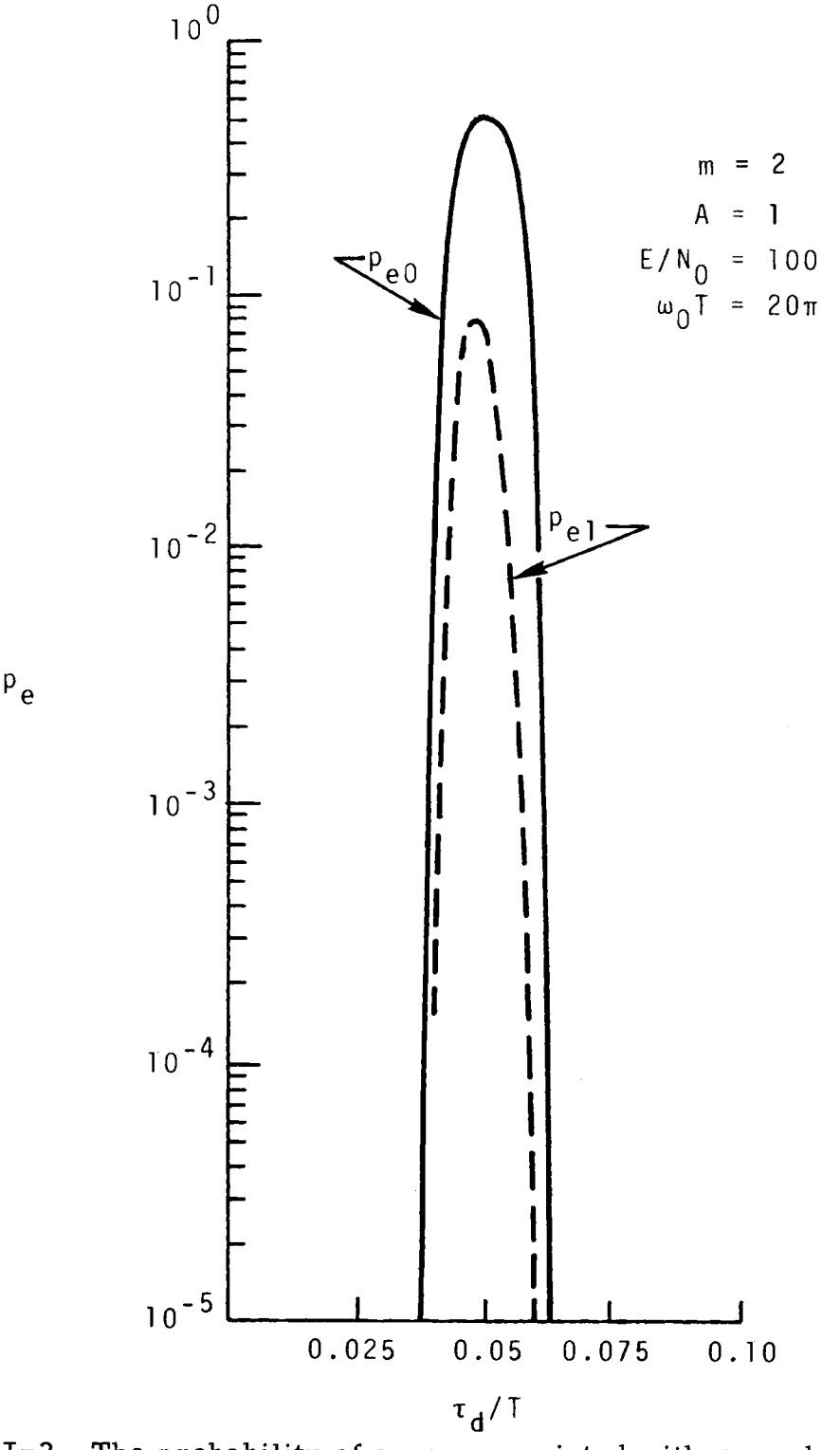

Figure BIII-2. The probability of error associated with α_o and α_1 as a function of the ratio of delay τ_d to bit length T. p_{eo} is periodic and p_{el} is symmetric corresponding to figure 1.

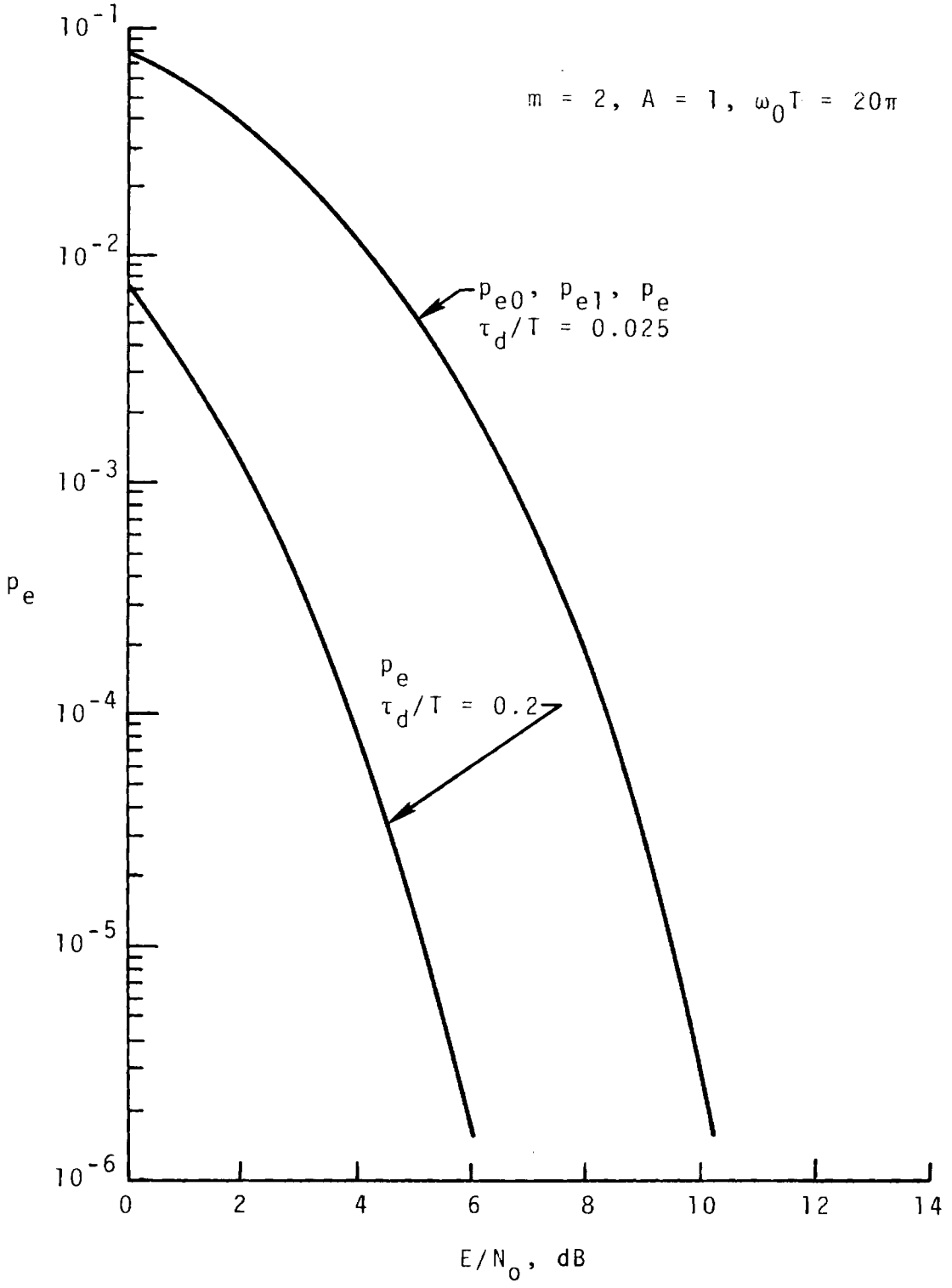

Figure BIII-3. Total probability of error for two values of τ_d/T.

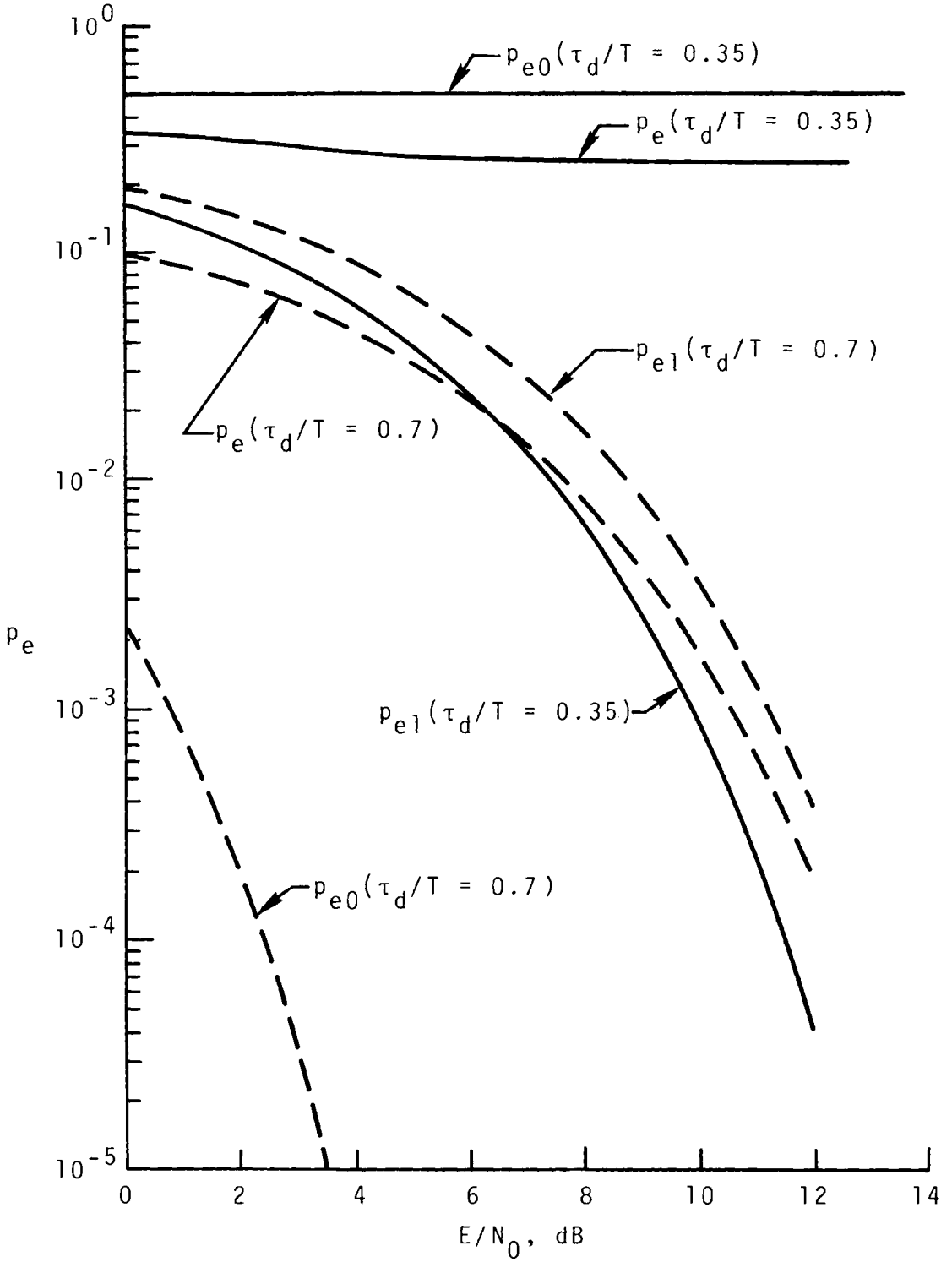

Figure BIII-4. The probability of error p_{eo} and p_{el} associated with α_o and α_1, and the total probability of error p_e for two cases, one where p_{eo} dominates and the other where p_{el} dominates.

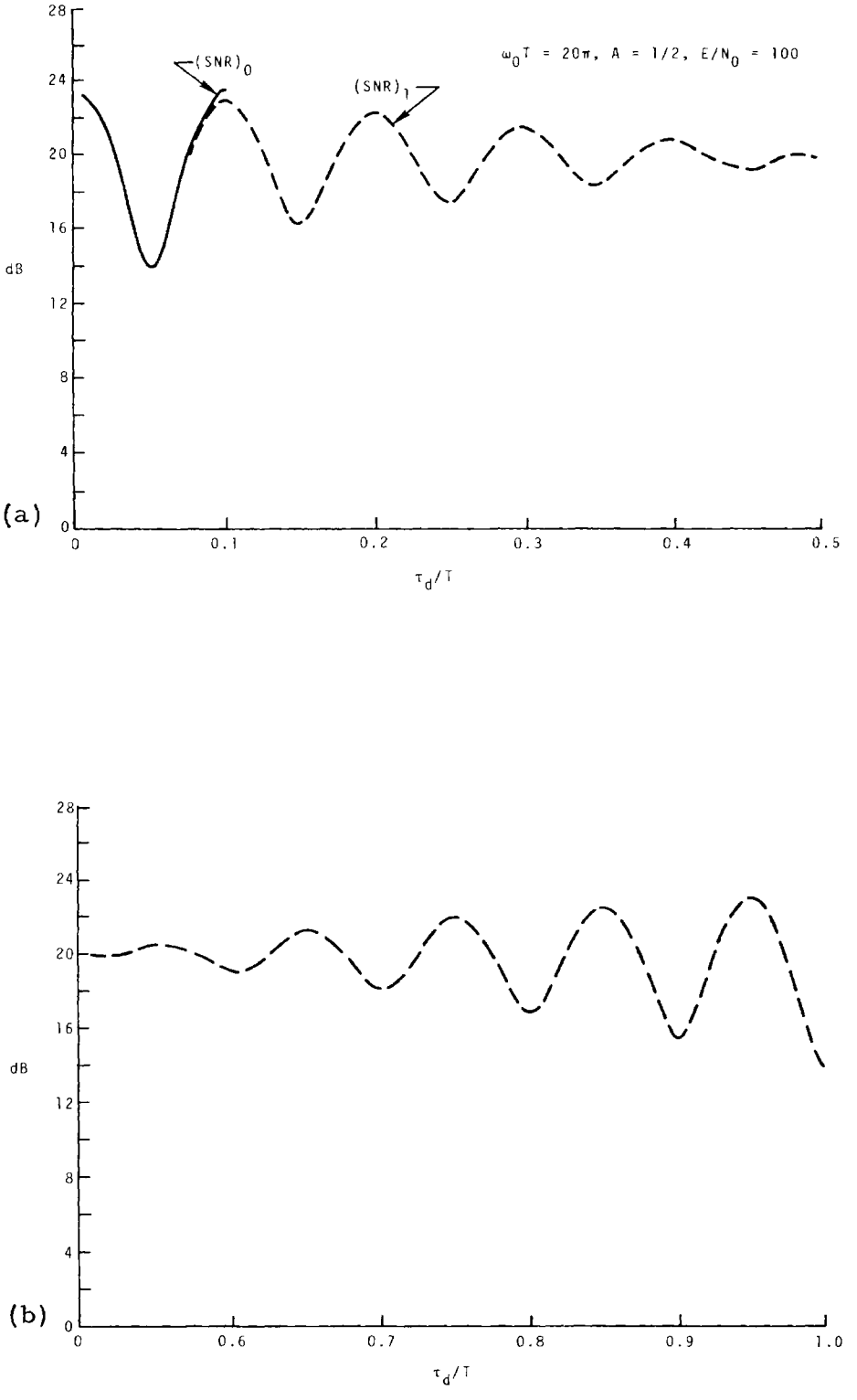

Figure BIII-5. Signal to noise ratio as a function of the ratio of delay τ_o to bit length T. $(SNR)_o$ is periodic with period 0.1, and p_e is symmetric about 0.5.

BIII-C. Two Paths with Time Spread

For the more general case that includes a spread in the second path, we replace the shifted impulse function $\delta(t-\tau_d)$ in the second term of (1) by the following function:

$$h_2(t-\tau_d) = \frac{\lambda}{\sqrt{\pi}\,N}\, e^{-\lambda^2(t-\tau_d)^2}, \quad -t_0+\tau_d \le t \le t_0+\tau_d, \tag{17}$$

where $2t_0$ represents the spread width, and N is a normalization constant defined as

$$N = \int_{-t_0+\tau_d}^{t_0+\tau_d} h_2(t-\tau_d)dt = \frac{1}{\sqrt{\pi}}\int_{-\lambda t_0}^{\lambda t_0} e^{-u^2}\,du$$

$$1-\mathrm{erfc}(\lambda t_0) = \mathrm{erf}(\lambda t_0). \tag{18}$$

Note that N approaches unity as t_0 or λ approaches infinity. However, in reality, t_0 should be finite and satisfy the following conditions:

$$-t_0+\tau_d > 0 \text{ and } t_0+\tau_d < T\,. \tag{19}$$

The parameter λ in (17) may be considered as a measure of closeness between $h_2(t-\tau_d)$ and $\delta(t-\tau_d)$. In fact, as $\lambda \to \infty$, $N \to 1$, and $h_2(t-\tau_d) \to \delta(t-\tau_d)$.

Again, if the pulse $s_0(t)$ given in (3) is transmitted, the part of the received signal corresponding to $r_2(t)$ discussed previously becomes

$$r_2'(t) = A\, s_0(t) * h_2(t - \tau_d)$$

$$= A \int_{-t_0+\tau_d}^{t_0+\tau_d} s_0(t - \tau)\, h_2(\tau - \tau_d)\, d\tau$$

$$= \frac{\sqrt{2s}A\lambda}{2N} \quad I_1 \cos\left[\omega_0(t - \tau_d) + \theta_0\right] \quad , \tag{20}$$

where A has the same meaning as before, namely, the interference-to-signal voltage ratio,

$$I_1 = \int_{-t_0}^{t_0} \cos \omega_0 u\, e^{-\lambda^2 u^2}\, du$$

$$= \frac{\sqrt{\pi}B}{2\lambda}\, e^{-\omega_0^2/4\lambda^2} \tag{21}$$

and

$$B = \operatorname{erf}(\lambda t_0 - j\frac{\omega_0}{2\lambda}) - \operatorname{erf}(-\lambda t_0 - j\frac{\omega_0}{2\lambda}) \quad . \tag{22}$$

Combining (20), (21), and (22), we obtain

$$r_2'(t) = AB(2S)^{1/2}(2N)^{-1} e^{-\omega_0^2/4\lambda^2} \cos[\omega_0(t-\tau_d)+\theta_0]. \tag{23}$$

We note that $r_2'(t)$ is the same as $r_2(t)$ except for the constant factor $B(2N)^{-1}e^{-\omega_0^2/4\lambda^2}$ and that $r_2'(t)$ reduces to $r_2(t)$ as λ is increased indefinitely, because under this condition, $N \to 1$, $B \to 2$, and $e^{-\omega_0^2/4\lambda^2} \to 1$.

If the direct path represented by $\delta(t)$ remains unchanged, the total received signal in the interval $0 \le t \le T$ should then be

$$r(t) = (2S)^{1/2} \cos(\omega_0 t + \theta_0) + r_2'(t) + r_3'(t) + n(t), \tag{24}$$

where $n(t)$ is the additive noise, $r_2'(t)$ is given in (22), and

$$r_3'(t) = AB(2S)^{1/2}(2N)^{-1} e^{-\omega_0^2/4\lambda^2} \cos[\omega_0(t-\tau_d) + \theta_1]. \tag{25}$$

With the receiver performing the same process as that in (5), we have the corresponding statistical average of the processed signal:

$$\bar{\alpha} = \sqrt{S}\, T \left\{ 1 + \frac{AB}{2N} e^{-\omega_0^2/4\lambda^2} \left[\left(\frac{T-\tau_d}{T}\right) \cos \omega_0 \tau_d + \frac{\tau_d}{T} \cos(\omega_0 \tau_d + \theta_0 - \theta_1) \right] \right\}. \tag{26}$$

This is the same as (6), if in (6) we replace A by $A' = \frac{B}{2N} e^{-\omega_0^2/4\lambda^2}$. When $\theta_0 = \theta_1$ for the binary case, we obtain

$$\alpha_0' = \sqrt{S}\ T\ [1 + \frac{AB}{2N}\ e^{-\omega_0^2/4\lambda^2}\ \cos \omega_0 \tau_d\ ] \ . \tag{27}$$

Similarly, with $\theta_0 \neq \theta_1$, we have

$$\alpha_1' = \sqrt{S}\ T\ [1 + \frac{AB}{2N}\ e^{-\omega_0^2/4\lambda^2}\ (\frac{T-2\tau_d}{T})\ \cos \omega_0 \tau_d]. \tag{28}$$

Comparing (27) and (28) respectively with (7) and (8), we conclude that the effect due to the path spread is completely accounted for by the factor

$$\frac{B}{2N}\ e^{-\omega_0^2/4\lambda^2}\ , \tag{29}$$

which will essentially be used to modify the actual interference-to-signal voltage ratio A.

Before giving quantitative results for the factor in (29), we need a further simplification for B in (22) since it involves the error function with complex argument. Fortunately, an expansion into separate real and imaginary parts is available [Abramowitz and Stegun, p. 299, 1964]:

$$\begin{aligned} \mathrm{erf}(x+jy) = \mathrm{erf}(x) &+ \frac{e^{-x^2}}{2\pi x}\ [(1 - \cos 2xy) + j \sin 2xy] \\ &+ \frac{2}{\pi}\ e^{-x^2} \sum_{n=1}^{\infty} \frac{e^{-\frac{1}{4}n^2}}{n^2 + 4x^2}\ [f_n(x,y) + j\, g_n(x,y)], \end{aligned} \tag{30}$$

where

$$f_n(x,y) = 2x - 2x \cosh ny \cos 2xy + n \sinh ny \sin 2xy, \quad (31)$$

and

$$g_n(x,y) = 2x \cosh ny \sin 2xy + n \sinh ny \cos 2xy, \quad (32)$$

Noting that the real and imaginary parts of erf(x+jy) in (30) are respectively odd and even functions of x, we obtain

$$\begin{aligned} B &= \operatorname{erf}(\lambda t_0 - j\frac{\omega_0}{2\lambda}) - \operatorname{erf}(-\lambda t_0 - j\frac{\omega_0}{2\lambda}) \\ &= 2\,\mathrm{Re}\left[\operatorname{erf}(\lambda t_0 - j\frac{\omega_0}{2\lambda})\right] \\ &= 2\operatorname{erf}(\lambda t_0) + \frac{e^{-\lambda^2 t_0^2}}{\pi\lambda t_0}(1 - \cos\omega_0 t_0) \\ &\quad + \frac{4}{\pi} e^{-\lambda^2 t_0^2} \sum_{n=1}^{\infty} \frac{e^{-\frac{1}{4}n^2}}{n^2 + 4\lambda^2 t_0^2} f_n(\lambda t_0, -\frac{\omega_0}{2\lambda}), \end{aligned} \quad (33)$$

where

$$\begin{aligned} f_n(\lambda t_0, -\frac{\omega_0}{2\lambda}) &= 2\lambda t_0 (1 - \cosh\frac{n\omega_0}{2\lambda} \cos\omega_0 t_0) \\ &\quad + n \sinh\frac{n\omega_0}{2\lambda} \sin\omega_0 t_0 . \end{aligned} \quad (34)$$

Now we are ready to make an analysis for B in (33) with a given value for λt_0.

On the one hand, when λt_0 is large and at the same time t_0 is also a large fraction of T so that λ is relatively small [representing a case for which $h_2(t-\tau_d)$ deviates substantially from the shifted impulse response function $\delta(t-\tau_d)$] and $\frac{\omega_0}{2\lambda} > 5$, the hyperbolic sine and cosine functions in (34) may be approximately replaced by $\frac{1}{2} e^{n\omega_0/2\lambda}$. Thus,

$$f_n(\lambda t_0, -\frac{\omega_0}{2\lambda}) \cong C_n e^{n\omega_0/2\lambda} \quad , \tag{35}$$

where

$$C_n = -\lambda t_0 \cos \omega_0 t_0 + \frac{n}{2} \sin \omega_0 t_0 \quad . \tag{36}$$

The infinite series in (33),

$$\sum_{n=1}^{\infty} \frac{e^{-\frac{1}{4}n^2}}{n^2 + 4\lambda^2 t_0^2} f_n(\lambda t_0, -\frac{\omega_0}{2\lambda}) \cong \sum_{n=1}^{\infty} C \frac{e^{-\frac{1}{4}n^2 + \frac{n\omega_0}{2\lambda}}}{n^2 + 4\lambda^2 t_0^2} \quad , \tag{37}$$

will then be determined by a few dominating terms near

$$n \cong \omega_0/\lambda \quad . \tag{38}$$

Under this condition, we have

$$\left| \sum_{n=1}^{\infty} \frac{e^{-\frac{1}{4}n^2}}{n^2 + 4\lambda^2 t_0^2} f_n \right| \sim \left| \frac{C}{\left(\frac{\omega_0}{\lambda}\right)^2 + 4\lambda^2 t_0^2} e^{\omega_0^2/4\lambda^2} \right| \gg 1 \quad . \tag{39}$$

Then

$$B \sim \frac{4}{\pi}\left[\frac{C_n}{\left(\frac{\omega_0}{\lambda}\right)^2 + 4\lambda^2 t_0^2}\right] e^{-\lambda^2 t_0^2 + \frac{\omega_0^2}{4\lambda^2}}, \qquad (40)$$

and the factor in (29) becomes approximately

$$\frac{C}{\left(\frac{\omega_0}{\lambda}\right)^2 + 4\lambda^2 t_0^2} e^{-\lambda^2 t_0^2} . \qquad (41)$$

Here we see clearly that the magnitude of (41) is a small quantity and its sign will oscillate depending on $\omega_0 t_0$. The small magnitude implies that the intersymbol interference has essentially no effect on the direct-path communication, even when the interference-to-signal voltage ratio A is significant. As an example, let us consider the case of $\lambda t_0 = 2.5$,

$$\omega_0 T = (2\pi) \times 100, \text{ and } t_0 = 0.5\,T.$$

We now have

$$\lambda T = 5,\ \omega_0/\lambda = 40\pi,\ N = 0.9996,\ \omega_0 t_0 = 100\pi,$$

and

$$\frac{B}{2N} e^{-\omega_0^2/4\lambda^2} \cong -0.6788 \times 10^{-6} . \qquad (42)$$

which is indeed negligible.

On the other hand, when both λt_0 and λ are large such that $\frac{\omega_0}{2\lambda} \ll 1$, corresponding to a case that $h_2(t-\tau_d)$ is much closer to $\delta(t-\tau_d)$, the first few terms under the summation sign in (33) would be sufficient to represent the infinite series. Furthermore, since the factor $e^{-\lambda^2 t_o^2}$ appears at both the second and third term in (33), it is apparent that $\text{erf}(\lambda t_0)$ should constitute the dominant term. Thus

$$B \cong 2\,\text{erf}(\lambda t_0) = 2N \quad , \tag{43}$$

and

$$\frac{B}{2N} e^{-\omega_0^2/4\lambda^2} \cong e^{-\omega_0^2/4\lambda^2} \cong 1 - (\omega_0/2\lambda)^2 \quad . \tag{44}$$

which is very close to unity, giving only a minor modification to the actual interference-to-signal voltage ratio A. This means that, under this condition, the analysis considered previously for the ideal case of no path spread still holds approximately true.

Detailed variations of $B(2N)^{-1} e^{-\omega_o^2/4\lambda^2}$ versus t_0 for $\lambda t_0 = 2.5$ are presented in figure 6. For comparison purpose, a similar example with $\lambda t_0 = 1.0$ is also included in figure 6.

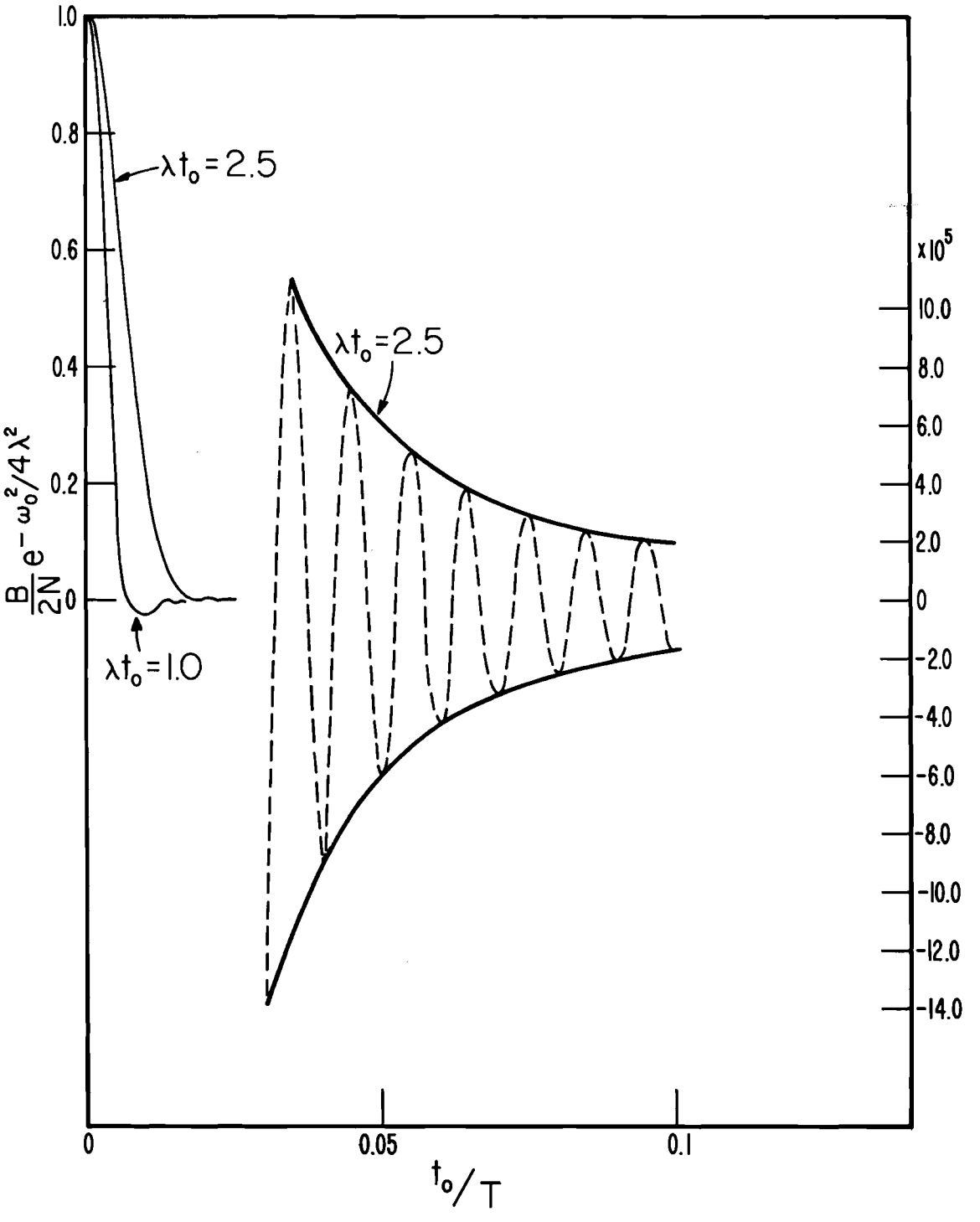

Figure BIII-6. The factor by which the amplitude of the second path is reduced as a function of the spread. The expanded scale for the oscillating portion of the curve is on the right.

BIII-D A SCATTERING FUNCTION MODEL*

BIII-D.1 INTRODUCTION

We assume here a coherent quadriphase shift key system with the form of the transmitted signal as in (2), with m=4.

The receiver processes the received waveform (fig. 7) by deriving two quadrature quantities

$$\alpha = \sqrt{2} \int_0^T r(t) \cos \omega_0 t \, dt,$$
$$\beta = \sqrt{2} \int_0^T r(t) \sin \omega_0 t \, dt. \tag{45}$$

As in the preceeding two cases, we assume a direct component s(t), a multipath component i(t) and noise n(t), so that the received signal is given by

$$r(t) = s(t) + n(t) + i(t). \tag{46}$$

The noise n(t) is assumed to be white Gaussian with autocorrelation function

$$E[n(t) \quad n(t+\tau)] = 1/2 \quad N_0 \, \delta(t) \tag{47}$$

The interference term i(t) depends on the statistical properties of the scattering mechanism. In general, we can

*The remainder of this chapter is exerpted from M. T. Ma, M. Nessenbergs, and R. H. Ott, Performance of Coherent QPSK Modems Over Time-Varying Channels with Random Intersymbol Interference Due to Scatter, Office of Telecommunications Technical Memorandum (1972), with permission from the authors.

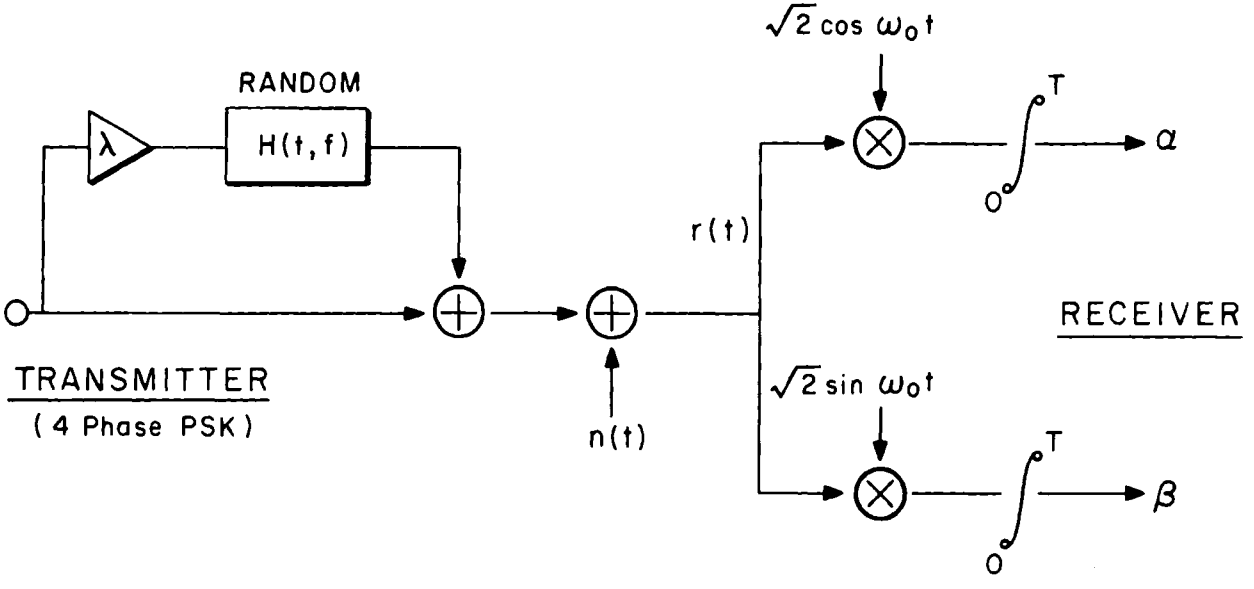

Figure BIII-7. The channel model.

say that it must be a superposition of the scattered contributions of all preceeding digits,

$$i(t) = \sum_{k=0}^{\infty} i_k(t), \tag{48}$$

where for all k=0, 1, 2, ...

$$i_k(t) = \sqrt{2\lambda S} \int_0^{\min(t + kT,\ T)} s_k(\tau - kT)\, h_3(t - \tau + kT,\ t)\, d\tau \ . \tag{49}$$

The time-varying impulse response $h_3(t-\tau,t)$ here depends on two variables. The argument t is the present time, while the argument $t-\tau$ is the delay from the occurrence of a unit impulse till present. Thus, τ is the time when the impulse occurs. It is postulated that $h(t,\tau)$ is a zero-mean homogeneous (i.e., wide-sense stationary in both arguments t and τ) Gaussian random process with specified scattering function $S(\Omega, \tau)$. When the scattering function is normalized

$$\int_{-\infty}^{\infty}\int_{-\infty}^{\infty} S(\Omega, \tau)\, d\Omega\, d\tau = 1,$$

the coefficient λ represents the interference-to-signal power ratio (ISR).

Conditioned on a fixed (yet arbitrary) modulating sequence $\theta=(\ldots,\theta_2,\theta_1,\theta_0)$ both α and β are random variables, with distribution determined by statistics of random $n(t)$ and $h(t,\tau)$. We claim that:

$$\text{(a)}\quad E\alpha = \sqrt{P}\ T\cos\theta_0, \tag{50a}$$

$$\text{(b)}\quad E\beta = \sqrt{P}\ T\sin\theta_0, \tag{50b}$$

$$\text{(c)}\quad \text{var}\,\alpha \cong \text{var}\,\beta \cong \tfrac{1}{2} N_0 T + \sigma^2, \tag{50c}$$

$$\text{(d)}\quad E\alpha\beta \cong 0, \tag{50d}$$

where σ^2 is to be determined. The proof of 50(a) and 50(b) is easy. From (45) and (46):

$$\begin{matrix}\alpha\\ \beta\end{matrix} = \sqrt{S}\ T \begin{matrix}\cos\\ \sin\end{matrix} \theta_0 + \sqrt{2}\int_0^T n(t) \begin{matrix}\cos\\ \sin\end{matrix} \omega_0 t\ dt$$

$$+ \sqrt{2}\int_0^T i(t) \begin{matrix}\cos\\ \sin\end{matrix} \omega_0 t\ dt, \tag{51}$$

and $En(t)=Ei(t)=0$ imply 50(a) and 50(b). Assertions 50(c) and 50(d) appear quite plausible, yet their proofs are lengthier and are omitted here. The remaining unknown in

(50) is σ^2; the derivation of this quantity is essential here--it is given in the next section.

From (50) we note that, being Gaussian, the random variables α and β must be independent. The random vector (α,β) is circularly symmetric in the (α,β)-plane about its mean $(E\alpha, E\beta)$. This symmetry plus the use of symmetric decision regions (fig. 8) implies that the decision problem is identical for all four phase θ_0 values.

BIII-D.2 DERIVATION OF σ^2

The variance of the interference term i(t) [see (50)] is

$$\sigma^2 = \int_0^T du \int_0^T dv \; E[i^*(u)\, i(v)] \cos \omega_0 (u - v), \tag{52}$$

where a series of repetitious substituions are next in order. First from (48)

$$E[i^*(u)\, i(v)] = \sum_{k=0}^{\infty} \sum_{\ell=0}^{\infty} E[i_k^*(u)\, i_\ell(v)], \tag{53}$$

then from (49)

$$E[i_k^*(u)\, i_\ell(v)] =$$

$$2\lambda P \int_0^{\min(u+kT,\, T)} du' \int_0^{\min(v+\ell T,\, T)} dv' \; s_k(u'-kT)\, s_\ell(v'-\ell T)\, E[h^*(u, u-u'+kT)\, h(v, v-v'+\ell T)], \tag{54}$$

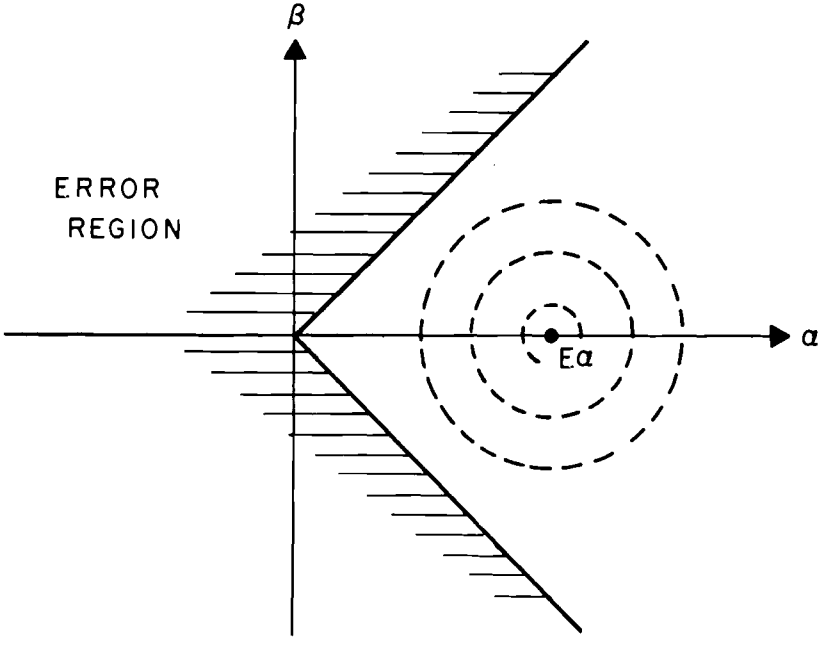

Figure BIII-8. The error region for QPSK.

and

$$E[h^{*}(u, u-u'+kT)\, h(v, v-v'+\ell T)] = \delta[(v-u)-(v'-u')+(\ell-k)T]\,\rho(v-u, u-u'+kT), \quad (55)$$

where the bivariate function $\rho(\mu,\tau)$ is merely an expedient abbreviation for an oft repeated function

$$\rho(\mu, \tau) = \int_{-\infty}^{\infty} S(\Omega, \tau)\, e^{i2\pi\Omega\mu}\, d\Omega. \quad (56)$$

We note that $\rho(\mu,\tau)$ is the non-impulsive part of one of the channel autocorrelation functions.

The impulse term in (55) only contributes when its argument vanishes. Since one always has $|v-u-v'+u'|<2T$, it follows that $|\ell-k|\leq 1$ are the only contributors in the double sum (53). When $\ell=k$, the limits of integration in (54) are shortened to $\max(0, v-u)\leq v'\leq \min(T+v-u, v+kT, T)$ and $\max(0, u-v)\leq u'\leq \min(T+u-v, u+kT, T)$, for v' and u', respectively. We obtain for all $k=0,1,2,\ldots$

$$E[i_k^{*}(u)\, i_k(v)] = 2\lambda P \int_{L}^{U} s_k(u-x)\, s_k(v-x)\, \rho(v-u, x)\, dx, \quad (57)$$

where the upper and lower limits are

$$U = \min(u,v)+kT,$$

$$L = \max(u, v, T-kT)+kT-T. \quad (58)$$

For QPSK waveforms, (57) yields

$$E[i_k^*(u)\, i_k(v)] \cong \lambda S \cos \omega_0 (u - v) \int_L^U \rho(v - u, x)\, dx, \tag{59}$$

where U and L are the same (58). The factor $\cos \omega_0 (u-v)$ appears for all $k=0,1,2,\ldots$ and, upon substitution in (52) and (53) yields $\cos^2 \omega_0 (u-v) = 1/2$ with an integral error term of the order of $1/\omega_0$. Thus the total contribution to σ^2 from the diagonal (i.e., $\ell = k$) terms is

$$\sigma_{di}^2 \cong \tfrac{1}{2} \lambda S \sum_{k=0}^{\infty} \int_0^T du \int_0^T dv \int_L^U dx\, \rho(v - u, x) \tag{60}$$

where U and L in (58) are functions of k.

When $\ell = k \pm 1$, a very similar approach works. Two departures from (60) are readily noted: (a) the message sequence $\{\theta_k\}$ does not cancel as it did in (59), (b) the integration limits must be modified. The non-diagonal contribution to σ^2 is

$$\sigma_{no\ di}^2 = \tfrac{1}{2} \lambda S \sum_{k=0}^{\infty} \cos(\theta_k - \theta_{k+1}) \int_0^T du \int_0^T dv \int_{L'}^{U'} dx\, \rho(v - u, x) \tag{61}$$

where

$$\begin{aligned} U' &= \text{mas}\ (u, v) + kT, \\ L' &= \min\ (u, v) + kT. \end{aligned} \tag{62}$$

The variance σ^2 is the sum of (60) and (61). In a form valid for all scattering functions it can be written as

$$\sigma^2 = \tfrac{1}{2}\lambda S \sum_{k=0}^{\infty} [A(k) + B(k) \cos(\theta_k - \theta_{k+1})] \tag{63}$$

where

$$A(k) = \int_0^T du \int_0^T dv \int_L^U dx \ \rho(v - u, x) ,$$

$$B(k) = \int_0^T du \int_0^T dv \int_{L'}^{U'} dx \ \rho(v - u, x) . \tag{64}$$

The common integrand $\rho(\mu, \tau)$ is determined by the scattering function $S(\Omega, \tau)$, see (56). The variance σ^2 is conditioned on a given sequence $\{\theta_k\}$, and varies as different messages are considered. In QPSK the four phases $\{0, \pi/2, \pi, 3\pi/s\}$ can be assumed to occur independently with equal probability, i.e., 1/4. We can then consider moments

$$E_\theta \sigma^2 = \frac{\lambda P}{2} \sum_{k=0}^{\infty} A(k) ,$$

$$\operatorname{var}_\theta \sigma^2 = \tfrac{1}{8} \lambda^2 P^2 \sum_{k=0}^{\infty} B^2(k) \tag{65}$$

and define an average σ^2 as $E_\theta \sigma^2$ and an rms σ^2 as $E_\theta \sigma^2 + \sqrt{\text{var}_\theta \sigma^2}$. Since both A(k) and B(k) are non-negative, we always have the worst-case and best-case bounds

$$\frac{\lambda P}{2} \sum_{k=0}^{\infty} [A(k) - B(k)] \leq \sigma^2 \leq \frac{\lambda P}{2} \sum_{k=0}^{\infty} [A(k) + B(k)] . \tag{66}$$

The sum in the right-hand side of (66) is easily shown to be

$$\sum_{k=0}^{\infty} [A(k) + B(k)] = \int_0^T du \int_0^T dv \, R_H (v - u, 0) \tag{67}$$

$$= E \left\{ \left[\int_0^T H(t, f) \, dt \right]^2 \right\} \tag{68}$$

BIII-D.3. TRUNCATED GAUSSIAN SCATTERING FUNCTION

An example of the medium scattering function is

$$S(\Omega, \tau) = \begin{cases} \dfrac{\exp\left\{ -\Omega^2 / 2\Omega_d^2 - (\tau - \tau_1)^2 / 2\tau_2^2 \right\}}{2\pi \Omega_d \tau_2 \, \Phi\left(\frac{\tau_1 - \tau_0}{\tau_2}\right)} & , \tau \geq \tau_0 \\ 0 & , \tau < \tau_0 \end{cases} \tag{69}$$

where $\Phi(x)$ is defined as

$$\Phi(x) = \frac{1}{\sqrt{2\pi}} \int_{-\infty}^{x} e^{-t^2/2} dt . \tag{70}$$

An "altitude chart" of $S(\Omega,\tau)$ is shown in figure 9 for τ_0 finite and τ_0 - . The standard deviation of $S(\Omega,\tau)$ along the Doppler shift axis is Ω while the standard deviation along the time delay axis is τ_2 if τ_0=- . The non-impulsive part of the channel auto correlation function is from (56)

$$\rho(u-v,\tau) = \begin{cases} \dfrac{\exp\left\{-2\pi^2\Omega_d^2(u-v)^2 - (\tau-\tau_1)^2/2\tau_2^2\right\}}{\sqrt{2\pi}\,\tau_2\,\Phi\left(\dfrac{\tau_1-\tau_0}{\tau_2}\right)}, & \tau \geq \tau_0 \\ 0, & \tau < \tau_0 \end{cases} \tag{71}$$

Since $\rho(u-v,\tau)$ is symmetric in u and v, assume v>u. Then it is not difficult to show from (64) that

$$A(k) = 2\int_0^T dv \int_0^v du \exp\left[-2\pi^2\Omega_d^2(u-v)^2\right] f_k(u,v) \tag{72}$$

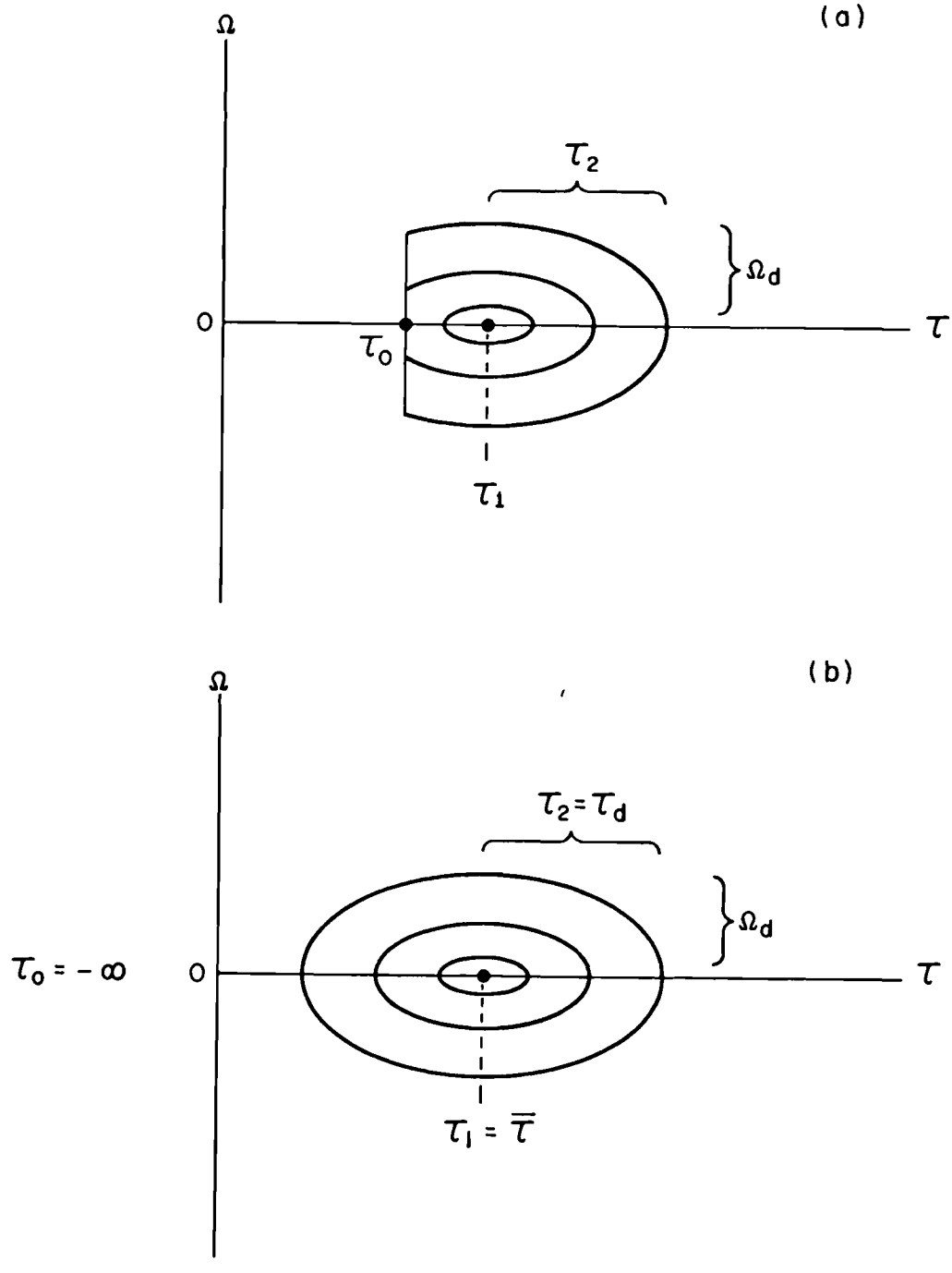

Figure BIII-9. The (a) truncated and (b) non-truncated scattering functions with Gaussian profiles.

$$B(k) = 2\int_0^T dv \int_0^v du \exp\left[-2\pi^2 \sigma_d^2 (u-v)^2\right] g_k(u, v) \tag{73}$$

with

$$f_0(u, v) = \begin{cases} 0 & , \tau_o > u \\ \dfrac{\Phi\left(\dfrac{u-\tau_1}{\tau_2}\right) - \Phi\left(\dfrac{\tau_0-\tau_1}{\tau_2}\right)}{\Phi\left(\dfrac{\tau_1-\tau_0}{\tau_2}\right)} & , 0 \le \tau_o \le u \\ \dfrac{\Phi\left(\dfrac{u-\tau_1}{\tau_2}\right) - \Phi\left(\dfrac{-\tau_1}{\tau_2}\right)}{\Phi\left(\dfrac{\tau_1-\tau_0}{\tau_2}\right)} & , \tau_0 < 0 \end{cases} \tag{74}$$

and for k=1,2,...

$$f_k(u, v) = \begin{cases} 0 & , \ \tau_0 > u + kT \\ \dfrac{\Phi\left(\dfrac{u + kT - \tau_1}{\tau_2}\right) - \Phi\left(\dfrac{\tau_0 - \tau_1}{\tau_2}\right)}{\Phi\left(\dfrac{\tau_1 - \tau_0}{\tau_2}\right)} & , \ v + kT - T \le \tau_0 \le u + kT \\ \dfrac{\Phi\left(\dfrac{u + kT - \tau_1}{\tau_2}\right) - \Phi\left(\dfrac{v_2 + kT - T - \tau_1}{\tau_2}\right)}{\Phi\left(\dfrac{\tau_1 - \tau_0}{\tau_2}\right)} & , \ \tau_0 < v + kT - T \end{cases} \tag{75}$$

and for $k = 0, 1, 2, \ldots$

$$g_k(u, v) = \begin{cases} 0 & , \ \tau_0 > v + kT \\ \dfrac{\Phi\left(\dfrac{\tau_1 - \tau_0}{\tau_2}\right) - \Phi\left(\dfrac{\tau_1 - kT - v}{\tau_2}\right)}{\Phi\left(\dfrac{\tau_1 - \tau_0}{\tau_2}\right)} & , \ u + kT \le \tau_0 \le v + kT \\ \dfrac{\Phi\left(\dfrac{\tau_1 - u - kT}{\tau_2}\right) - \Phi\left(\dfrac{\tau_1 - v - kT}{\tau_2}\right)}{\Phi\left(\dfrac{\tau_1 - \tau_0}{\tau_2}\right)} & , \ \tau_0 < u + kT \end{cases} \tag{76}$$

In this example with a Gaussian scattering function we find that (67) equals T^2 and that the variance (66) has a simple upper bound

$$\sigma^2 \leq \frac{\lambda P T^2}{2} \quad . \tag{77}$$

It is instructive to examine the behavior of the coefficients A(k) and B(k) for small τ_2. As an example, let $\Omega_d=0$, $\tau_0=0$, and $0<\tau_2<<T$. Then from (75) through (79), it follows that

$$A(0) = (T-\tau_1)^2 + \tau_2^2 + \ldots \tag{78}$$

$$A(1) = \tau_1^2 + \tau_2^2 + \ldots \tag{79}$$

$$B(0) = -2\tau_1^2 - 2\tau_2^2 + 2\ {}_1T + \ldots \tag{80}$$

with higher order coefficients exponential in $1/\tau_2$:

$$A(k) \propto e^{-T_2^{-2}} \quad , \quad k = 2, 3, \cdots$$

$$B(k) \propto e^{-T_2^{-2}} \quad , \quad k = 1, 2, \cdots \tag{81}$$

The variation of A(k) and B(k) for $T = 5 \times 10^{-9}$ and $0 \leq \tau_2 \leq T$ is shown in figure 10.

The results in figure 10 confirm the small τ_2 effects given in (78), (79) and (80).

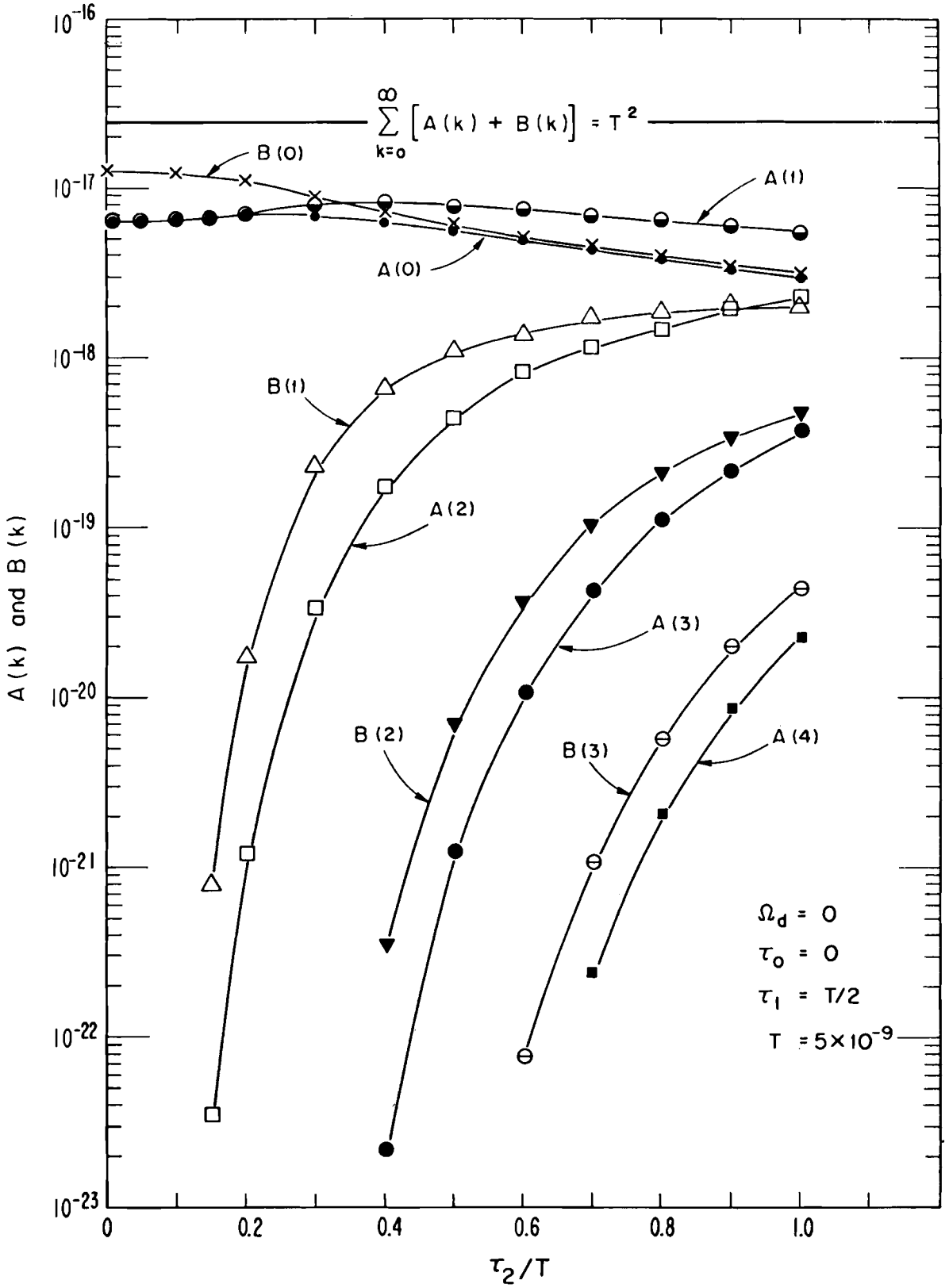

Figure BIII-10. The components of variance for small τ_2 .

These results will be used in the calculation of the output signal-to-noise ratio and probability of bit error.

BIII-D.4. OUTPUT SIGNAL-TO-NOISE RATIO

The output signal-to-noise ratio for the binary decision is defined as

$$SNR = \frac{|E\alpha|^2}{2 \text{ var } \alpha} \quad . \tag{82}$$

Using (50) and E=ST this becomes

$$SNR = \frac{E/N_0}{1 + \frac{2\sigma^2}{N_0 T}} \geq \frac{E/N_0}{1 + \lambda E/N_o} \tag{83}$$

In figure 11 we show a plot of the ouput signal-to-noise ratio in dB versus the input signal-to-noise ratio in dB for various values of the ISR ratio. There are three salient features to observe in figure 11: 1) as the ISR ratio λ goes to zero the output signal-to-noise ratio, approaches the straight line

$$\lim_{\lambda \to 0} SNR = E/N_0 \quad ; \tag{84}$$

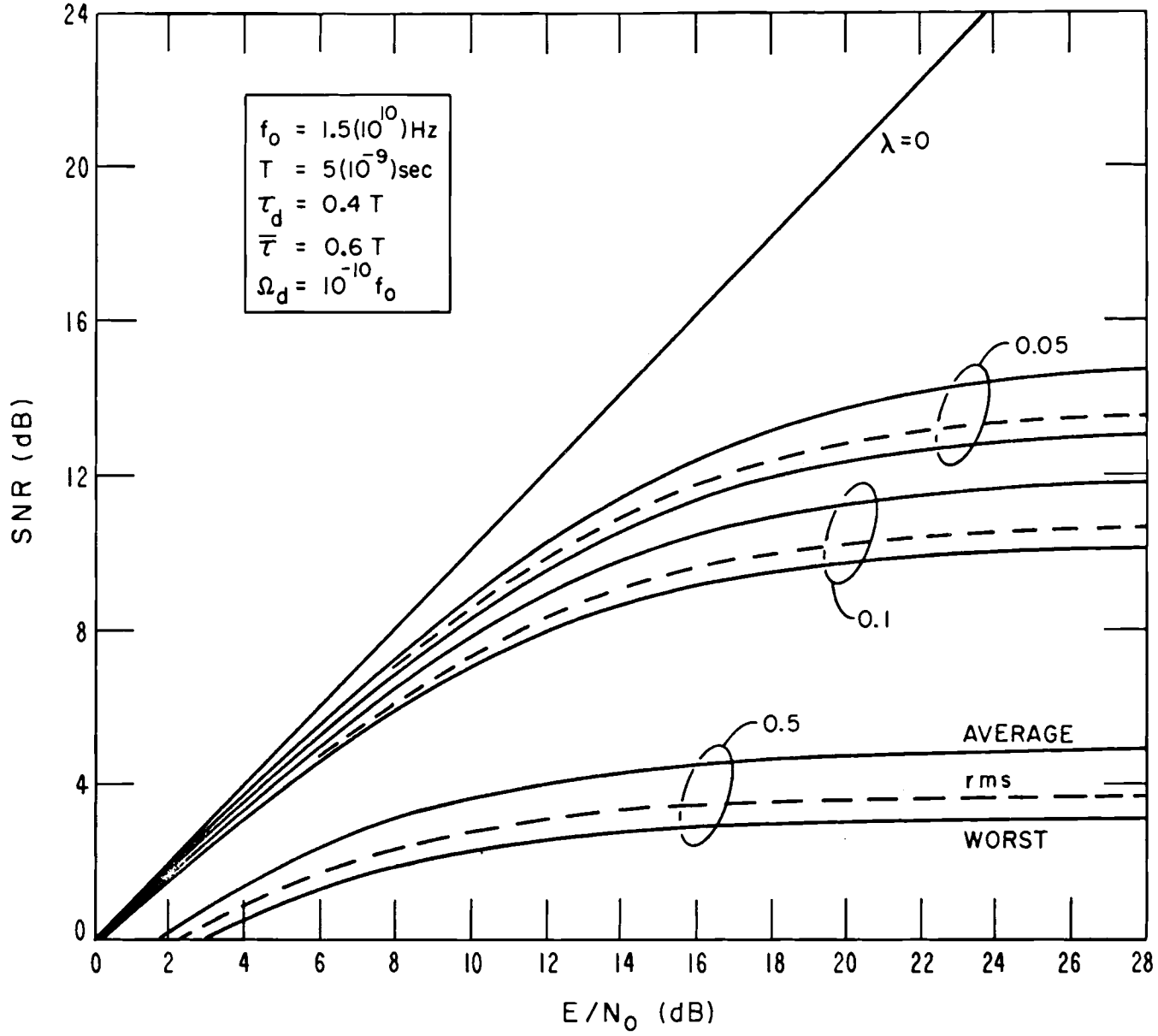

Figure BIII-11. The output SNR degradation due to intersymbol interference.

2) as the input signal-to-noise ratio E/N_0 becomes very large, the output signal-to-noise ratio has the asymptotic behavior

$$\lim_{N_0 \to 0} \mathrm{SNR} = \left\{ \frac{\lambda}{T^2} \sum_{k=0}^{\infty} \left[A(k) + B(k) \cos\left(\theta_k - \theta_{k+1}\right) \right] \right\}^{-1} \qquad (85)$$

which is independent of E/N_0 and cannot be less than λ^{-1}; 3) for a constant ISR ratio, the average output signal-to-noise ratio is greater than the RMS output signal-to-noise ratio which in turn is greater than the "worst" case. This is in agreement with the results in (65) and (66).

The insert in figure 11 shows that the calculations correspond to a non-truncated Gaussian scattering function, i.e., $\tau_0 = -\infty$. The three general features discussed above would remain unchanged if τ_0 were finite (truncated case).

BIII-D.5. ERROR PROBABILITY

From (50) the random vector (α, β) is circularly symmetric about the mean $(E\alpha, E\beta)$. From figure 8 a four-phase (i.e., two-bit) error will occur when the decision boundary (cross-hatched region) is crossed. The distance from the mean $(E\alpha, 0)$ to the decision boundary is $E\alpha/\sqrt{2}$. Thus, the probability of bit error is

$$P_e = \frac{1}{\sqrt{2\pi \,\mathrm{var}\,\alpha}} \int_{E\alpha/\sqrt{2}}^{\infty} e^{-y^2/2\,\mathrm{var}\,\alpha}\, dy, \qquad (86)$$

which becomes [see (48) (50), (82), and (83)]

$$P_e = 1 - \Phi(\mathrm{SNR}) \qquad (87)$$

The three salient features mentioned under the heading of output signal-to-noise ratio apply here equally well. In particular $\lim_{E/N_0 \to \infty} P_e$ is a non-zero constant determined by (85) and (87).

The probability of bit error is plotted in figure 12 as a function of the input signal-to-noise ratio, for various values of the ISR ratio, λ. Four parameters are constant for the six cases; i.e., $f_0=1.5\times10^{10}$ Hz, $T=5.0\times10^{-9}$ sec, $\tau_0=0$, $\Omega_d=0$ while τ_1 and τ_2 vary as

τ_1/T	τ_2/T
0.5	0.0001
0.5	0.5
0.5	1.0
0	0.08
0.4	0.036
1.5	0.12

The results in figure 12 are basically indistinguishable as the pair (τ_1, τ_2) is varied.

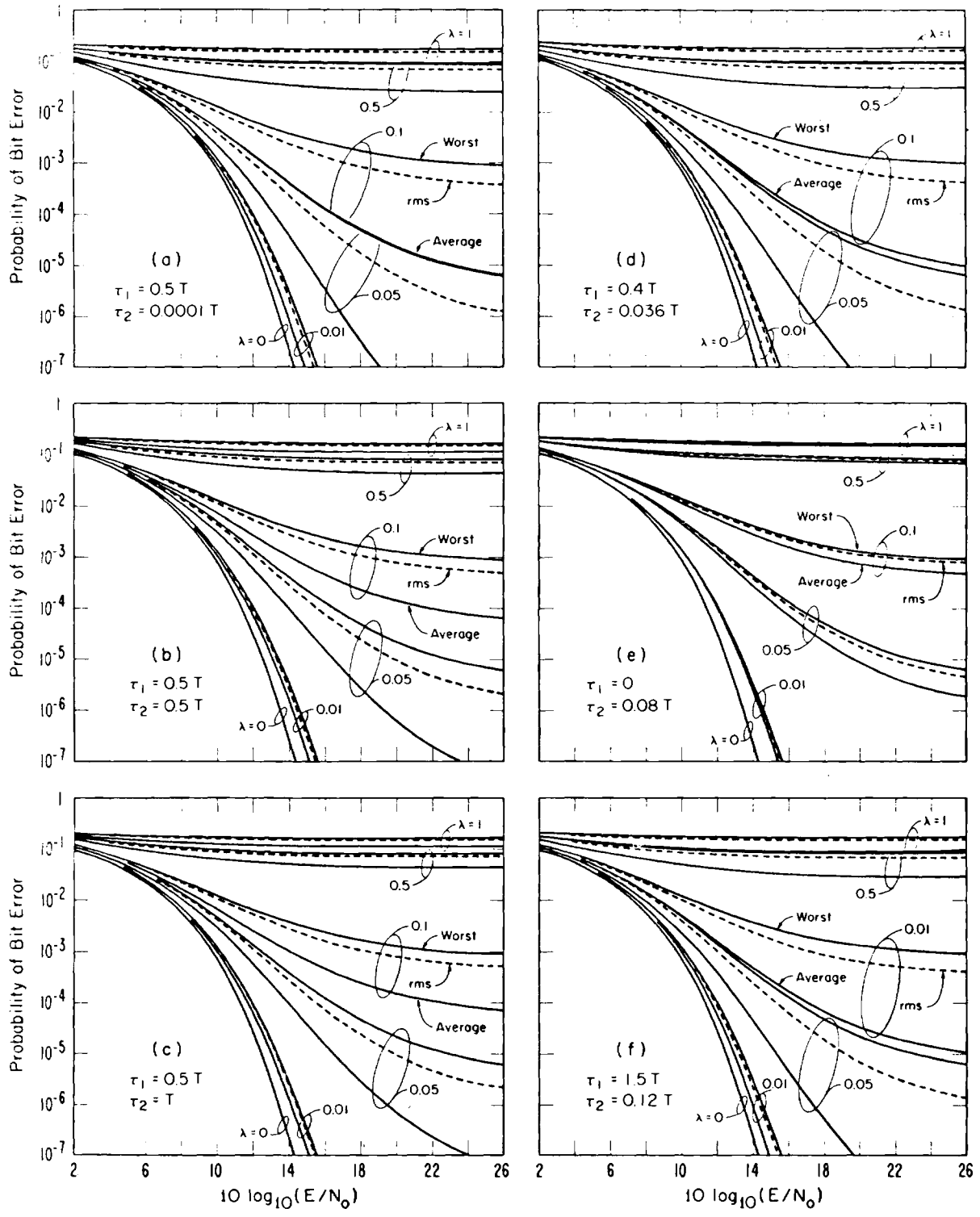

Figure BIII-12. The degradation of bit error probability for various parameter configurations.

ABRAMOWITZ, M., AND I.A. STEGUN (EDS.), (1964),
HANDBOOK OF MATHEMATICAL FUNCTIONS WITH FORMULAS, GRAPHS, AND MATHEMATICAL TABLES,
U.S. NATIONAL BUREAU OF STANDARDS, APPLIED MATHEMATICS SERIES, 55 (US.S GOVT. PRINTING OFFICE, WASHINGTON D.C. 20402).

BELLO, P.A. (1963),
CHARACTERIZATION OF RANDOMLY TIME-VARIANT LINEAR CHANNELS,
IEEE TRANS. COMMUNICATION SYSTEMS, CS-11, PP. 360-395.

DALY, R.F. (1970),
SIGNAL DESIGN FOR EFFICIENT DETECTION IN DISPERSIVE CHANNELS,
IEEE TRANS. INFORMATION THEORY, IT-16, PP. 206-213.

KAILATH, T. (1961),
COMMUNICATION VIA RANDOMLY VARYING CHANNELS,
PH.D. THESIS, MIT (CAMBRIDGE, MASS.)

KENNEDY, R.S. (1969),
FADING DISPERSIVE COMMUNICATIONS CHANNELS,
WILEY-INTERSCIENCE, NEW YORK, N. Y.

VAN TREES, H.L. (1968),
DETECTION, ESTIMATION AND MODULATION THEORY,
PART I, WILEY (NEW YORK, N. Y.)

YAGLOM, A.M. (1962),
AN INTRODUCTION TO THE THEORY OF STATIONARY RANDOM FUNCTIONS,
CHAPTER 2, PRENTICE HALL (ENGLEWOOD CLIFF, N.J.)

C. CAUSES OF MULTIPATH

This group of chapters pertains to the use of the physical parameters for the prediction or estimation of the types of multipath expected over nominal line-of-sight paths. For some problems it is sufficient to consider only simple geometric quantities, while for others, it is necessary to have knowledge of fine-scale structure which might be associated with atmospheric variations, changing sea state, detailed terrain structure, or combinations of these.

Mechanisms contributing to multipath problems which are considered here are reflections, scattering, refraction, diffraction and absorption.

Methods are given for estimating path length differences (relative delays), lobe modulation frequencies, and time variabilities associated with atmospheric changes, or other changes such as in sea state.

CHAPTER CI. SIMPLE TWO-RAY MODELS

CI-A. Introduction

This chapter deals with simple two-ray models for multipath where one ray connects the transmitting antenna with the receiving antenna via a direct path that is not obstructed by objects or terrain, and is called the "direct ray". The other ray is the "reflected ray" and it reaches the receiving antenna via a single reflection where the paths to and from the reflection surface are unobstructed. Specific limitations and conditions associated with particular models are provided as part of the discussion concerning them. Restrictions applicable to all models described are as follows:

1. Only the direct and reflected rays are involved.
2. Ray paths are unobstructed except for the reflecting surface which must obstruct (also changes direction) the reflected ray only.
3. The path length difference between the direct and reflected rays is sufficient to provide a relative path length difference of 0.03λ where λ is the wavelength (Rice et al., 1967, p. 5-6,

where the 0.06λ given should be changed to 0.03λ).

4. Antennas and reflecting surfaces must be separated by distances sufficient to allow free space antenna patterns to be used in determining the relative strength of phasors associated with the two rays.

Separations may be considered sufficient to overcome the last restriction if the reflecting surface and a point along the direct ray are in the "far-field" of each antenna. A commonly used formulation for the minimum far-field distance, d_{ff}, associated with an antenna having a maximum length, ℓ, and operating at a wavelength, λ, is (Jasik, 1961, p.34-14)

$$d_{ff} = 2\ell^2/\lambda \qquad (1)$$

where all lengths are expressed in the same units. With ℓ expressed in feet, ℓ_{ft}, and λ expressed using frequency in megahertz, f, (1) becomes

$$d_{ff} = 2 \times 10^{-3} f \ell_{ft}^2 \quad \text{ft.} \qquad (2)$$

Chapter topics include resultant signal representations (sec. CI-B), path length difference (sec. CI-C), and

effective reflection coefficient (sec. CI-D). A computer program for calculating lobing over a spherical earth is discussed in Chapter CII.

Except as specifically stated otherwise, units of length, time and frequency will be in kilometers, seconds and megahertz. This simplifies many of the formulations provided, in that the number of factors connected with unit conversions are greatly reduced. However, English units are used with graphs and formulas where such usage seems more practical. For convenience, the relationship between several units of measure are provided below:

1 ft = 3.048×10^{-4} km

1 s mi = 5280 ft

1 n mi = 1.852 km

1 n mi = 6076 ft

1 rad = 57.295779510^{o}

CI-B. Resultant Signal Representations

Resultant received signal representations in terms of phasors (sec. CI-B.1) and statistics (sec. CI-B.2) will be considered.

CI-B.1 Phasors

A two ray path is illustrated in figure 1 where r is the direct ray path length in kilometers, r_{12} is the reflected ray length in kilometers, g_{D12} is the complex voltage antenna gain (relative to isotropic) associated with the direct ray at terminal one or two and g_{R12} is the complex voltage antenna gain (relative to isotropic) associated with the reflected ray at terminal 1 or 2. Antenna heights in kilometers above the reflection plane, h_{12}, are also shown along with path distance, d, and grazing angle ψ. Note that the angle of incidence is equal to the angle of reflection (both are $\pi/2 - \psi$ rad). If the reflection surface is curved h_{12} are measured from a plane tangent to the reflection point and would not necessarily equal the antenna heights above the surface (see sec. CI-C.2).

Let the phasor characterizing the transmitted signal be

$$e_t = m(t) \exp(j\omega t) \quad V \tag{3}$$

where

$m(t)$ = complex modulation function in volts

$$\exp(j\omega t) = e^{j\omega t}, \tag{4}$$

$$j = \sqrt{-1}, \tag{5}$$

$$\Delta r = r_1 + r_2 - r = \frac{4 r_1 r_2 \sin^2 \psi}{r_1 + r_2 + r} \simeq 2 h_1 h_2 / d$$

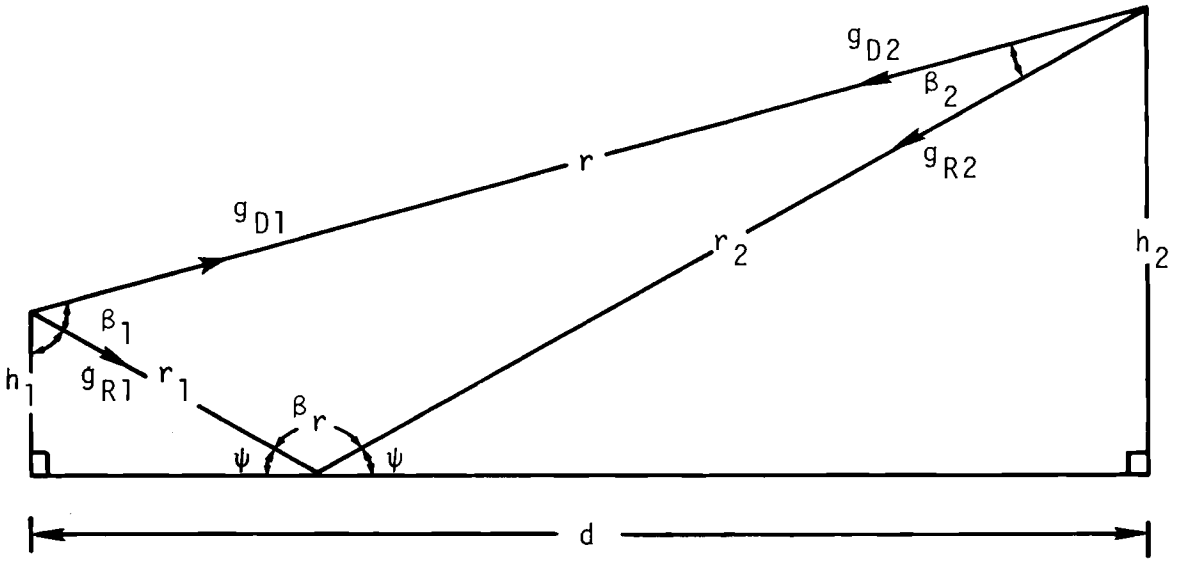

Figure CI-1. Flat air-less earth geometry. Note that the angle of incidence equals the angle of reflection so that the grazing angles, ψ, for r_1 and r_2 are equal.

ω = angular radio frequency in radians

and

t = time in seconds.

Then, the phasor characterizing the signal received via the direct path may be written as

$$e_D = \left(\frac{\lambda}{4\pi r}\right) \ell_D g_{D1} g_{D2} \, m(t - r/c) \exp\left[j(\omega t - \beta r)\right] \text{ V} \qquad (6)$$

where

$\left(\frac{\lambda}{4\pi r_{12}}\right)$ = free space voltage loss over direct ray path for isotropic antennas,

ℓ_D = voltage losses associated with antennas to measurement point coupling for direct ray

c = 2.997925×10^5 km/sec, propagation velocity (7)

β = $\omega/c = (2 \times 10^6) f$ rad/km, propagation constant (8)

f = radio frequency in megahertz

and all units of length are expressed in kilometers. The phasor characterizing the signal received via the reflected path may be written in a similar manner, i.e.,

$$e_R = \left(\frac{\lambda}{4\pi r_{12}}\right) \ell_R g_{R1} g_{R2} RDF_{\sigma h} F_A F_S \; m(t-r_{12}/c) \exp[j(\omega t - \beta r_{12})] \quad V \qquad (9)$$

where

$\left(\frac{\lambda}{4\pi r_{12}}\right)$ = free space voltage loss over reflected ray path for isotropic antennas,

ℓ_R = voltage losses associated with antenna to measurement point coupling for reflected ray,

R = Complex plane earth reflection coefficients (sec. CI-D.8)

D = divergence factor (sec. CI-D.1).

$F_{\sigma h}$ = surface roughness factor (sec. CI-D.7)

F_A = surface area factor (sec. CI-D.2),

and

F_S = surface shadow factor (sec. CI-C.6).

The resultant received voltage phasor, e_Σ, is

$$e_\Sigma = e_D + e_R \quad V \qquad (10)$$

and normalization to e_D yields

$$e_N = e_\Sigma / e_D \tag{11}$$

or

$$e_N = 1 + R_e \exp(-j\beta \Delta r) \tag{12}$$

where

$$R_e = \left[\frac{m(t - r_{12}/c)}{m(t - r/c)}\right] \left(\frac{r}{r_{12}}\right) \left(\frac{g_{R1}g_{R2}}{g_{D1}g_{D2}}\right) RD F_{\sigma h} F_A F_S \tag{13}$$

is the complex effective reflection coefficient (sec. CI-D), and

$$\Delta r = r_{12} - r \quad \text{km} \tag{14}$$

is the path length difference (sec. CI-C).

With R_e expressed in terms of its magnitude, $|R_e|$, and phase, ϕ_e, the magnitude of e_N squared can be expressed as

$$|e_N|^2 = 1 + |R_e|^2 - 2|R_e|\cos(\pi - \beta\Delta r + \phi_e) \tag{15}$$

or

$$|e_N|^2 = 1 + |R_e|^2 + 2|R_e|\cos(\beta\Delta r + \phi_e) \tag{16}$$

where the phasor diagram shown in figure 2 and the law of cosines is used to obtain (15).

Attenuation relative to free space propagation over the direct ray path with isotropic antennas, A, in decibels is obtained using

$$A = -10 \log |e_N|^2 \quad \text{dB} \tag{17}$$

where $\log = \log_{10}$ (common logarithm) and (15) can be used to express (17) as

$$A = \begin{cases} -10 \log [4 \sin^2(\beta \Delta r / 2)] & \text{if } R_e = -1 \\ -10 \log (1 + |R_e|^2 + 2|R_e| \cos \phi_T) & \text{otherwise} \end{cases} \quad \text{dB} \tag{18}$$

with $$\phi_T = \beta \Delta r + \phi_e \text{ rad.} \tag{19}$$

Maximum, A_M, and minimum, A_m, values for A are given by

$$A_M = \begin{cases} -20 \log |1 - |R_e|| & \text{if } |R_e| \neq 1 \\ \rightarrow \infty \text{ as } |R_e| \rightarrow 1 \end{cases} \quad \text{dB} \tag{20}$$

and

$$A_m = -20 \log (1 + |R_e|) \quad \text{dB} . \tag{21}$$

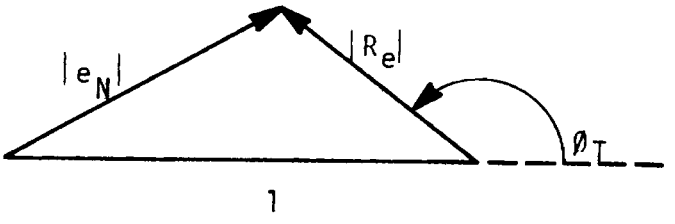

Figure CI-2. Phasor diagram, fixed phase.

Note that an effective reflection coefficient of unity will result in $A_M \rightarrow \infty$ and $A_m = -6$ dB. Curves that can be used to estimate A when R_e (sec. CI-D) and Δr (sec. CI-C) are known are provided in the next section.

Transmission loss, L, is the ratio, expressed in decibels, of the power radiated from the transmitting antenna to the power available at the terminals of an ideal (loss-less except for radiation resistance) receiving antenna (Rice et al., 1967, sec. 2). It may be determined using A from

$$L = L_{bf} + A - G_{D1} - G_{D2} \quad \text{dB} \qquad (22)$$

where L_{bf} is the free space basic (isotropic antennas) transmission loss for the direct path, and $G_{D1,2}$ is the decibel gain above isotropic in the direction of the direct ray of an ideal (loss-less) antenna at terminal 1 or terminal 2.

For lengths expressed in kilometers and frequency, f MHz, L_{bf} is given by (Rice et al., 1967, p. 2-7)

$$L_{bf} = 20 \log\left(\frac{4\pi r}{\lambda}\right) = 32.45 + 20 \log (fr) \quad \text{dB} \qquad (23)$$

With r expressed in nautical miles, r_{nm}, (22) becomes

$$L_{bf} = 37.8 + 20 \log (fr_{nm}) \quad \text{dB}. \qquad (24)$$

If the antenna gains used in (13) and (22) are for non-ideal antennas, transmission loss should be called system loss (Rice et al., 1967, sec. 2.1). However, since the heating losses associated with many antennas of interest is either not accurately known or negligible, the terminology distinction will not be pursued beyond this mention of it. Values of g_{12} in (13) are related to those of G_{12} in (22) by

$$G_{D12} = 20 \log |g_{D12}| \quad \text{dB} \tag{25}$$

and

$$|g_{D1,2}| = 10^{(G_{D1,2}/20)} \tag{26}$$

CI-B.2 Statistics

Attenuation variations associated with flight through a lobing pattern (see fig. 42, CII-5) formed by interference between the two rays can often be characterized by a cumulative distribution formulation that is very similar to the phasor formulation for A given in (18), but is easier to compute since the path length difference need not be calculated. That is,

$$A(p) = -10 \log|1+|R_e|^2+2|R_e|\cos(\pi p/100)| \quad \text{dB} \tag{27}$$

where A(p) is the attenuation that is not exceeded during p percent of the time.

Note that when a particular level of received power can be associated with specific A(p) values for the flight path section of interest, it would be exceeded p percent of the time so that p could be refered to as the time availability associated with the signal level. Values for A(p) correspond to specific received power levels when (a) the two ray model is valid (sec. CI-A), (b) the power radiated by the transmitter and losses associated with the receiving antenna system remain constant, and (c) all terms in (22) except A are essentially constant.

This formulation for A(p) is based on the conditions that for each flight path section of interest (a) $|R_e|$ is essentially constant and (b) the relative phase angle, $\emptyset_T$, associated with the phasor addition in (18) is a random variable with a uniform probability distribution over its 0 to 2π range, i.e., all angles occur with equal probability. Figure 3 illustrates the phasor relationships involved where possible $|R_e|$ phasor positions have a circular locus about the unity phasor. Values of A associated with $|R_e|$ phasors in the unshaded area are less than A(p). This area is p

percent of the total area bounded by the $|R_e|$ phasor rotation.

The median value of A(p) obtained from (27) with p = 50% is

$$A(50) = -10 \log (1 + |R_e|^2) \quad \text{dB.} \tag{28}$$

Values for A(50) are shown in figure 4 as a function of $|R_e|$ along with maximum, A_M, and minimum values for A_m obtained from (20) and (21). A relative phase angle $\emptyset$ of $\pi/2$ rad (90°) in (18) results in the same attenuation level as A(50).

$$A(p) = -20 \log|e_N(p)| = -10 \log |1+|R_e|^2+2|R_e| \cos(\pi p/100)| \quad \text{dB}$$

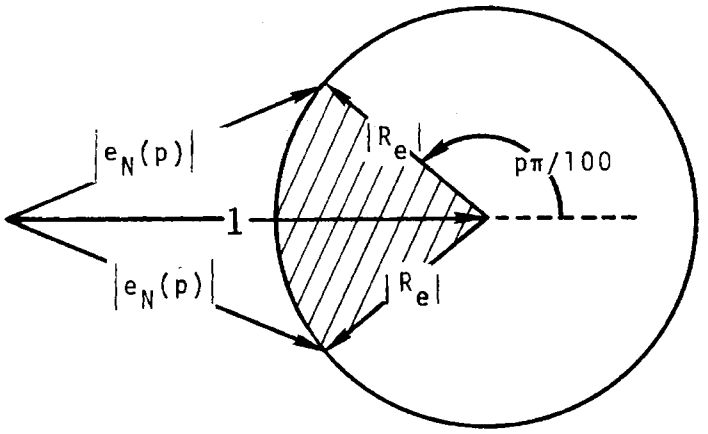

Figure CI-3. Phasor diagram, random phase. Values of $|e_N|$ for the unshaded area are $>|e_N(p)|$; i.e., $A < A(p)$ in unshaded area. The unshaded area is p percent of the total area covered by the $|R_e|$ phasor.

Normalized values, $A_N(p)$, of A(p) are shown in figure 5 as a function of p for several |Re| values. The attenuations are related by

$$A(p) = A_N(p) + A(50) \text{ dB}. \quad (29)$$

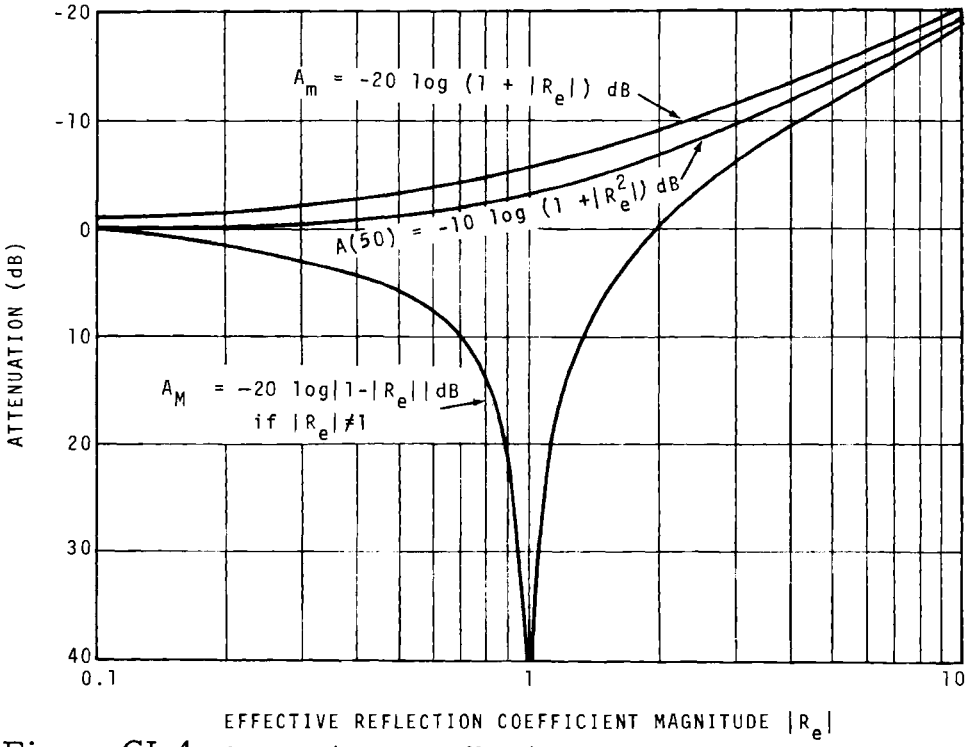

Figure CI-4. Attenuation vs. reflection coefficient, maximum phase opposition) and minimum (phase agreement) values of attenuation are shown as A_M and A_m, respectively. Median attenuation for a uniform distribution of phase is given by A(50).

Each curve is applicable to two $|R_e|$ values which are reciprocal to each other.

Figures 4 and 5 may be used with (29) to obtain values of A that would result from (18) by using them for

$$p = 100\, \phi_T/\pi \quad \% \tag{30}$$

and taking the resulting A(p) as A. For example, $\phi_T = \pi/4$ and $|R_e| = 1$ result in (a) p of 25% from (30), (b) A(50) of -3 dB from figure 4, and $A_N(25)$ of -2.3 dB from figure 5. These values used with (29) result in an A of -5.3 dB (-2.3-3).

When the geometry involved in a particular problem is such that the path length difference is likely to be more than a few wavelengths and the relative terminal locations are not accurately known within a few wavelengths, then these figures may be used to estimate the probability P_A that a particular attenuation level will not be exceeded via

$$P_A = p/100 \tag{31}$$

where p goes with the A(p) level of interest. For example, $|R_e| = 1$ and A(p) = 20 dB result in (a) A(50) = -3 dB from figure 4, (b) $A_N(p) = A(p) - A(50) = 20 + 3 + 23$ dB via a rearrangement of (29), (c) p = 98% from figure 5, and (d) $p_A = 0.98$ from (31). Equations (31) and (27) can be combined to provide a formulation for p_A; i.e.,

$$P_A = \pi^{-1} \text{Cos}^{-1} \left\{ \frac{10^{-[A(p)/10]} - 1 - |R_e|^2}{2\,|R_e|} \right\} \quad . \qquad (32)$$

CI-C PATH LENGTH DIFFERENCE

Relative attenuation associated with interference between direct and reflected rays calculated via (18) depends on Δr since (18) includes the relative phase of the two components.

Geometrical relationships involved in the calculation of the path length difference Δr, are discussed in this section for simple cases (sec. CI-C.1) and the spherical surface case (sec. CI-C.2). The concepts of Fresnel zone clearance (sec. CI-C.3) and lobing frequency (sec. CI-C.4) are also discussed since they are closely related to Δr.

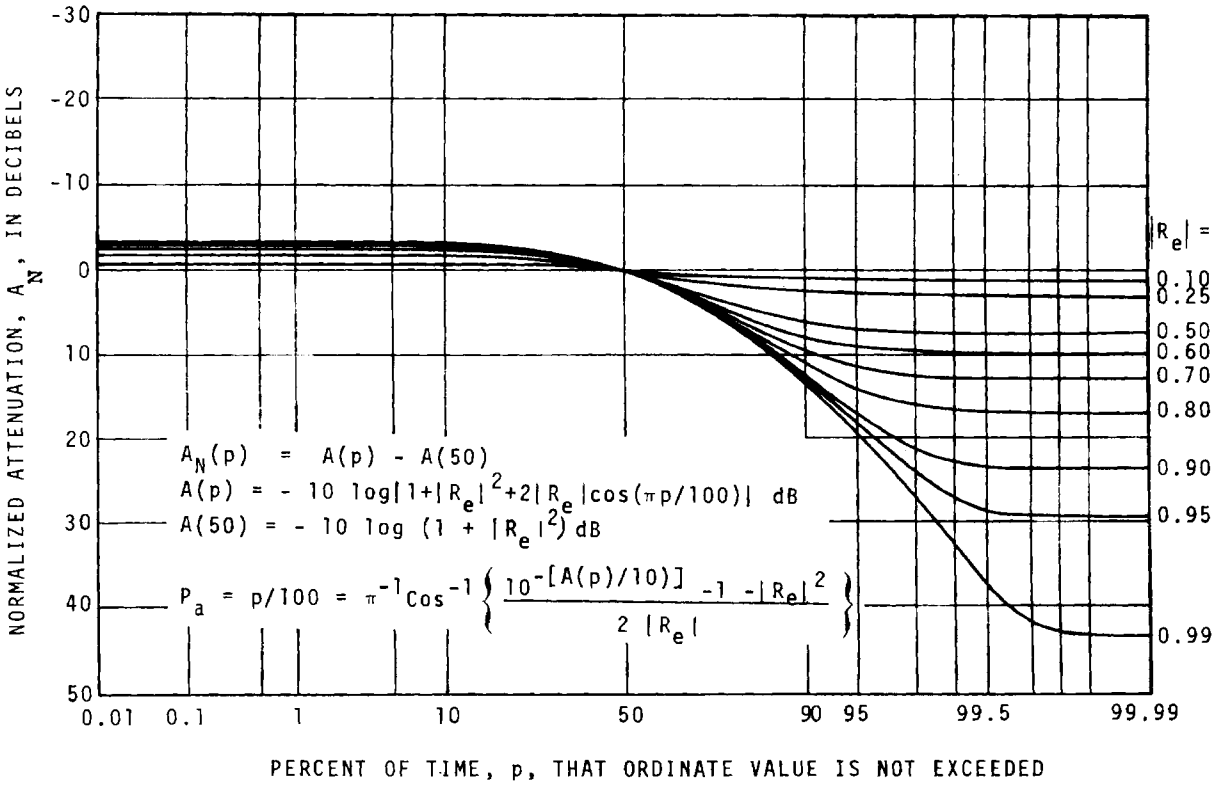

Figure CI-5. Normalized attenuation versus percent of time. Attenuation not exceeded for p percent of the time is given by $A(p) = A(50) + A_N(p)$ dB.

CI-C.1 Simple Geometries

Equation (14), $\Delta r = r_{12} - r$, can be used to calculate Δr if r_{12} and r (see fig. 1) are known with sufficient precision. However, it can involve the difference between large numbers that are nearly equal since Δr is required to a fraction of a wavelength; i.e., at 100 MHz accuracies on the order of a foot (2×10^{-4} n mi) are required so that a 100 n mi path would require r_{12} and r to be known to seven significant figures.

A formulation for Δr that avoids this precision problem can be derived using the law of cosines with the triangle of figure 1. That is,

$$r^2 = r_1^2 + r_2^2 - 2r_1 r_2 \cos(\pi - 2\psi) \quad km^2, \tag{33}$$

$$r^2 = r_1^2 + r_2^2 + 2r_1 r_2 (1 - 2\sin^2\psi) \quad km^2, \tag{34}$$

and

$$r^2 = r_{12}^2 - 4r_1 r_2 \sin^2\psi \quad km^2, \tag{35}$$

but

$$\Delta r = \frac{(r_{12} - r)(r_{12} + r)}{(r_{12} + r)} = \frac{r_{12}^2 - r^2}{(r_{12} + r)} \quad km \tag{36}$$

so that use of (35) in (36) yields

$$\Delta r = \frac{4r_1 r_2 \sin^2\psi}{(r_{12} + r)} \quad km \ . \tag{37}$$

Equation (37) is very useful since it not only avoids the precision problem, but is exact. It can be used to derive alternate expressions for specific situations; e.g., when $r_{12} \simeq r$

$$\Delta r \simeq \left\{ \begin{array}{ll} 2r_1 \sin^2\psi & \text{if } r_1 << r_2 \\ r_1 \sin^2\psi & \text{if } r_1 = r_2 \\ \dfrac{2r_1 b}{(1+b)} \sin^2\psi & \text{if } br_1 = r_2 \end{array} \right\} \quad km \tag{38}$$

where b is a positive constant.

Special cases where the reflecting point is known (sec. CI-C.1.1), or the reflecting plane is fixed (sec. CI-C.1.2) will be considered in the remainder of this section.

CI-C.1.1 Reflecting Point Known

Situations considered here are those where Δr can be estimated from knowledge of r_1, ψ and the relative size of r_2 with respect to r_1; i.e., $r_{12} \simeq r$ and $r_1 << r_2$ or $br_1 = r_2$ so that Δr can be calculated via (38).

The relative size of r_2 with respect to r_1 and r are assumed to be specified directly. Values for ψ however, may be specified directly or in terms of the angles β_{12} or β_r shown in figure 1. These angles are related as follows

$$\psi = (\pi - \beta_r)/2 \quad \text{rad}, \tag{39}$$

$$\psi = \left\{ \begin{array}{l} 0.5\,\beta_1 \text{ if } r_1 << r_2 \\ \beta_1 \quad \text{if } r_1 = r_2 \\ 0.5\,\beta_2 \text{ if } r_2 << r_1 \\ 0.5(\beta_1 + \beta_2) \text{ otherwise} \end{array} \right\} \text{ rad} \tag{40}$$

$$\sin\beta_1 = b \sin\beta_2. \tag{41}$$

As an example, suppose $r_1 << r_2$, r_1 = 0.3048 km (1000 ft), $\beta_1 = \pi/2$ rad (90°) then Δr is calculated using (40), and (38) as follows:

$$\psi = 0.5\,\beta_1 = \pi/4 \text{ rad} \qquad (45^\circ),$$

and $$\Delta r = 2r_1 \sin^2\psi = (2)(0.3048)\sin^2(\pi/4) = 0.3048 \text{ km}.$$

If it is assumed that $R_e = -1$, the simple formulation of (18) can be used to estimate attenuation; e.g., for a frequency of 100 MHz, (8) and (18) result in

$$\beta = \omega/c = (2\pi \times 10^8) / (2.9979 \times 10^5) = 2095.9 \text{ rad/km}$$

$$\beta\Delta r/2 = (2.095.9)(0.3048) / 2 = 319.42 \text{ rad},$$

and

$$A = -10 \log[4\sin^2(\beta\Delta r/2)] = -4.6 \text{ dB}.$$

CI-C.1.2 Reflecting Plane Fixed

For a fixed reflecting plane as shown previously in figure 1 (37) can be expressed in terms of the antenna heights in kilometers above the reflecting plane, h_{12}, i.e.

$$\Delta r = 4h_1h_2/(r_{12} + r) \quad \text{km} . \qquad (42)$$

Similarly, when $r_{12} \simeq r$, (38) can be written as

$$\Delta r = \left\{ \begin{array}{l} 2h_1 \sin\psi \quad \text{if} \quad h_1 << h_2 \\ h_1 \sin\psi \quad \text{if} \quad h_1 = h_2 \\ \dfrac{2h_1 b}{(1+b)} \sin\psi \quad \text{if} \quad bh_1 = h_2 \end{array} \right\} \qquad \text{km.} \tag{43}$$

When the path distance, d, in kilometers is much greater than either antenna height (42) becomes

$$\Delta r \simeq 2h_1 h_2 / d \qquad \text{km} . \tag{44}$$

When $R_e = -1$, maximum values of A or lobing nulls occur when Δr has a value Δr_n given by

$$\Delta r_n = N\lambda \qquad \text{km} \tag{45}$$

where N is a positive integer (zero included). Similarly, lobing peaks (A = -6 dB) occur when Δr has a value Δr_p given by

$$\Delta r_p = M\lambda / 2 \qquad \text{km} \tag{46}$$

where M is a positive non-zero integer. As implied by (45), the number of nulls, N , encountered for d increasing from zero with fixed antenna heights would be the maximum value of Δr, which occurs at d = 0, divided by λ; i.e.,

$$N_n = (2/\lambda) \text{ lesser of } \{h_1 \text{ or } h_2\} . \tag{47}$$

For $r_{12} \simeq r$ and $R_e = -1$, the grazing angles that correspond to lobing nulls, ψ_n, and lobing peaks, ψ_p, can be obtained using (43), (45) and (46). The resulting formulas are

$$\psi_n \simeq \left\{ \begin{array}{l} \mathrm{Sin}^{-1}\left[\lambda N/(2h_1)\right] \text{ if } h_1 \ll h_2 \\ \mathrm{Sin}^{-1}(\lambda N/h_1) \text{ if } h_1 = h_2 \\ \mathrm{Sin}^{-1}\left[\frac{\lambda N(1+b)}{2h_1 b}\right] \text{ if } bh_1 = h_2 \end{array} \right\} \quad \text{rad} \qquad (48)$$

and

$$\psi_p \simeq \left\{ \begin{array}{l} \mathrm{Sin}^{-1}\left[\lambda M/(4h_1)\right] \text{ if } h_1 \ll h_2 \\ \mathrm{Sin}^{-1}\left[\lambda M/(2h_1)\right] \text{ if } h_1 = h_2 \\ \mathrm{Sin}^{-1}\left[\frac{\lambda M(1+b)}{4h_1 b}\right] \text{ if } bh_1 = h_2 \end{array} \right\} \quad \text{rad} \; . \qquad (49)$$

For $r_{12} \simeq r \simeq d$, fixed frequency and antenna heights and $R_e = -1$, (44), (45), and (46) can be used to determine the distances d_n and d_p at which nulls or peaks occur. The resulting formulas are

$$d_n \simeq 2h_1h_2/N\lambda \quad \text{km} \qquad (50)$$

and

$$d_p \simeq 4h_1h_2/M\lambda \quad \text{km.} \qquad (51)$$

Distance between nulls, Δd can be obtained by using (44) for d and d + Δd; i.e.,

$$\frac{2h_1h_2}{d} - \frac{2h_1h_2}{d + \Delta d} = \lambda \quad \text{km} \qquad (52)$$

or

$$\Delta d \simeq \lambda d^2/(2h_1h_2) \quad \text{km} \qquad (53)$$

when $\Delta d << d$.

For $r_{12} \simeq r \simeq d$, fixed frequency, h_1 and d, and $R_e = -1$, (44), (45), and (46) can be used to determine the values for h_2 at which nulls, h_{2n}, and peaks, h_{2p}, occur. The resulting formulas are

$$h_{2n} \simeq N\lambda d/(2h_1) \quad \text{km} \qquad (54)$$

and

$$h_{2p} \simeq M\lambda d/(4h_1) \quad \text{km} . \qquad (55)$$

Height between nulls, Δh_2, can be obtained by using (44) for $h_2+\Delta h_2$ and h_2; i.e.,

$$\frac{2h_1(h_2 + \Delta h_2)}{d} - \frac{2h_1h_2}{d} \simeq \lambda \quad \text{km} \qquad (56)$$

or

$$\Delta h_2 \simeq d\lambda/(2h_1) \quad \text{km} \qquad (57)$$

For $r_{12} \simeq r \simeq d$, fixed antenna heights and path distance, and $R_e = -1$, (44), (45), and (46) can be used to determine the frequencies at which nulls, f_n, and the peaks, f_p, occur. The resulting formulas are

$$f_n \simeq 150\ Nd/(h_1h_2) \quad \text{MHz} \qquad (58)$$

and

$$f_p \simeq 75\ Md/(h_1h_2) \quad \text{MHz}. \qquad (59)$$

Frequency between nulls, Δf, can be obtained by using (44) such that the Δr at $f + \Delta f$ is one wavelength longer than the Δr at f; i.e.,

$$1 \simeq 2h_1h_2\ (f + \Delta f - f)/(dc) \qquad (60)$$

or

$$\Delta f \simeq 150\ d/h_1h_2) \quad \text{MHz}. \qquad (61)$$

Though the equations given here apply only to restricted conditions, they can be used to provide insight for situations where the required conditions are not completely realized. The more complex case for reflection from a spherical surface is discussed in section CI-C.2.

CI-C.2 Spherical Surface Geometry

Several methods are presented that can be used to determine Δr when reflection from a spherical surface is involved. Included are a graphical method (sec. CI-C.2.1), a Nomogram method (sec. CI-C.2.2) and computational methods (sec. CI-C.2.3).

CI-C.2.1 Graphical Method

This method is based on the use of charts to provide the relationships between antenna height grazing angle and the antenna to reflection point distance. Such charts are shown in figures 6 and 7 where figure 6 is applicable to antenna heights below 1000 ft and figure 7 is applicable to antenna heights up to 100,000 ft. These charts were produced by ray tracing through the continuous exponential atmosphere (sec. CIII-A; Bean and Dutton, 1966, sec. 3.8) that corresponds to a surface refractivity, N , of 301 N-units. Use of N = 301 N-units in the effective earth radius formulation of Rice, et al. (1967, sec. 4) results in an effective earth radius that is 4/3 of the actual earth radius.

Parameter values obtained from the charts are then converted to Δr via figure 8. This figure provides Δr

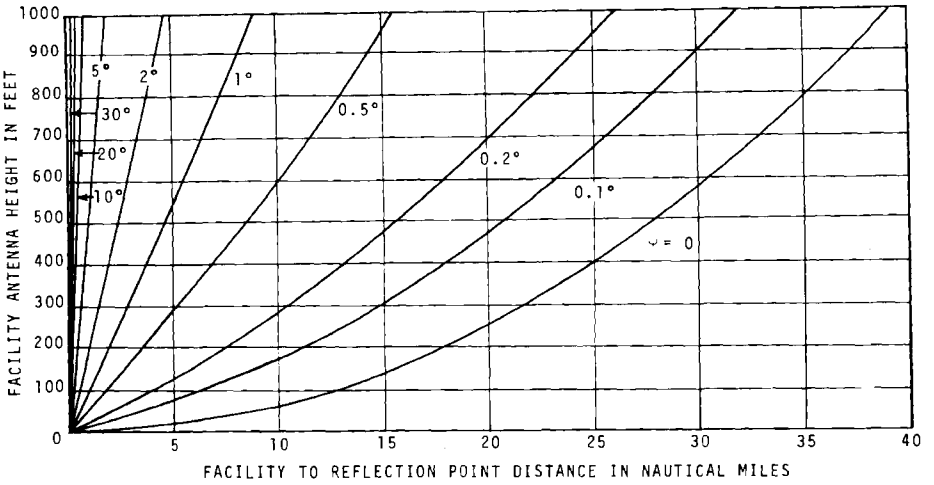

Figure CI-6. Height vs. distance to reflection point for low antennas. The grazing angle, ψ, is the complement to the angle of incidence or reflection which are equal.

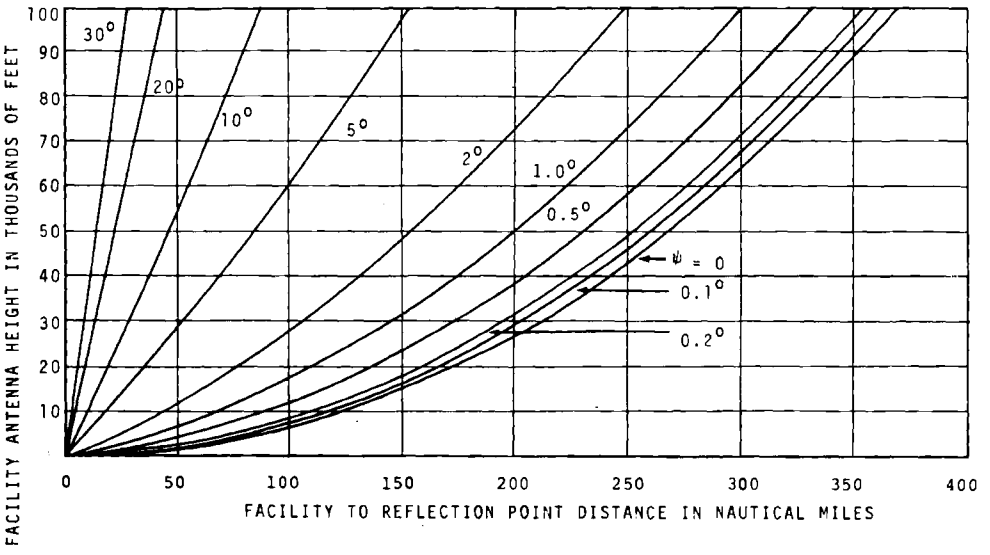

Figure CI-7. Height versus distance to reflection point for high antennas. The grazing angle, ψ, is the complement of the angle of incidence or reflection which are equal.

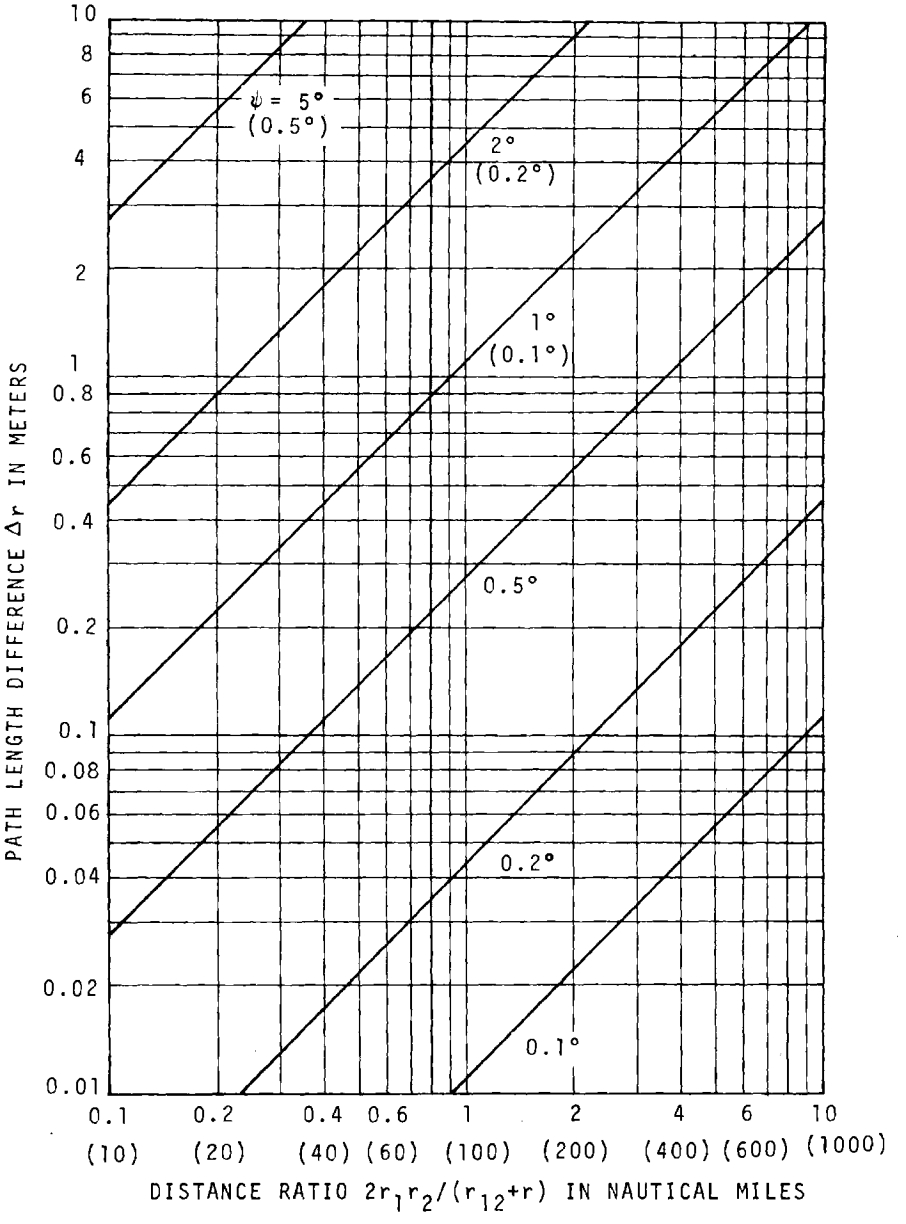

Figure CI-8. Path length difference versus distance ratio. Values of ψ in parenthesis go with distance ratio values in parenthesis. For $r_{12} \simeq r$, $2r_1r_2/(r_{12}+r) \simeq r_1r_2/r$. For $h_1 << h_2$, $r_1r_2/r \simeq r_1 \simeq d_1/\cos\psi \simeq d_1$ when $\psi < 10^o$. For $\psi < 10^o$, $r_1r_2/r \simeq d_1d_2/d$. For $h_1=h_2$, $r_1r_2/r = r_1 \simeq d_1/(2\cos\psi) \simeq 0.5d_1$ when $\psi < 10^o$.

versus the distance ratio $2r_1r_2/(r_{12}+r)$ for the same values provided on figures 6 and 7. The expression used to calculate Δr is

$$\Delta r = (7.408)\left[\frac{r_1 r_2}{r_{12}+r}\right] \sin^2\psi \quad \text{km} \qquad (62)$$

where the r's are in nautical miles. Except for the constant introduced for units conversion this expression is identical with (37). Alternate ways of expressing the ratio are provided in the caption of figure 8.

Although these figures can be used in several ways, the most straight-forward way is to start with antenna heights and grazing angle. For example, with H_1 = 100 ft, H_2 = 30,000 ft, and $\psi = 5^o$ use of figures 6 and 7 results in d_1= 0.15 n mi and d_2= 52 n mi. Then figure 8 can be read using $\frac{2r_1r_2}{r_{12}+r} \simeq d_1$ so that Δr=0.004 km. Finally, the great circle distance, d, between antennas is determined using

$$d = d_1 + d_2 \quad \text{n mi} \qquad (63)$$

which yields 52.15 n mi.

This approach is useful if Δr or attenuation, via (18), versus distance curves are desired, but requires use of iteration or interpolation when values for a specific d are needed. It is, of course, also limited to the special case

where N =301 N-units since figures 6 and 7 are based on this value.

CI-C.2.2 Nomogram Method

G.A. Hufford, (OT/ITS) has developed a nomogram that is useful in estimating r for reflection from a spherical earth (Norton, Hufford, Dougherty and Wilkerson, 1965). It was developed for situations where antenna heights H_{12} are much greater than the great circle path length, d, the effective earth radius, a, is much greater than d, and the parabolic approximation for the earth curvature is valid. The parabolic approximation is often used to estimate radio horizon distances (Bean and Dutton, 1966, p. 59).

The nomogram is given in figure 9. It provides estimates of the parameter D_h from values of

$$H = (H_2 - H_1) / (H_1 + H_2) \qquad (64)$$

and

$$\gamma/k = \frac{d^2}{4a(H_1 + H_2)} \qquad (65)$$

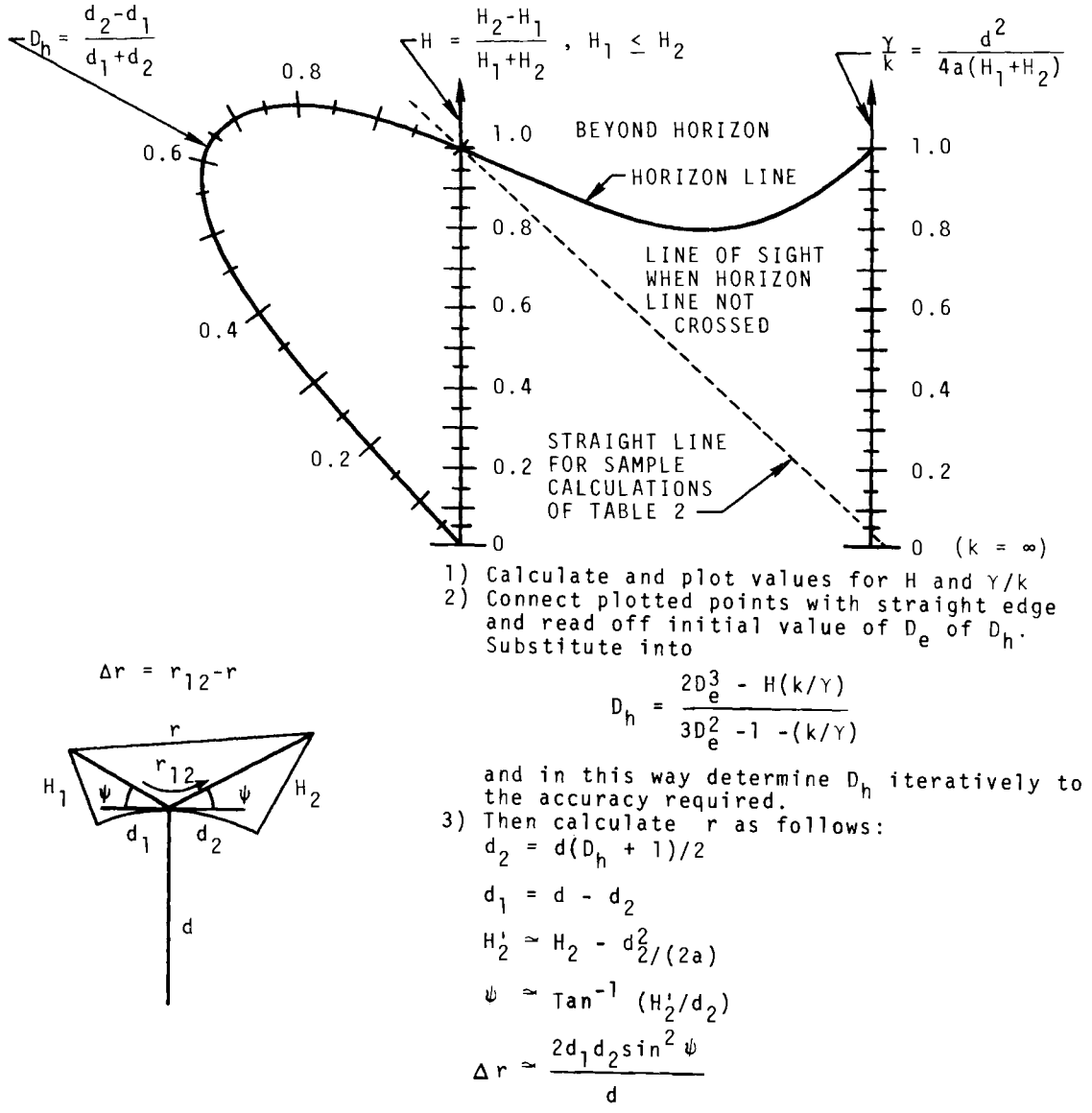

Figure CI-9. Nomogram for use in calculating path length difference.

where all lengths are expressed in the same units and $H_1 < H_2$ (switch subscripts if $H_2 \geq H_1$). After obtaining an initial estimate D_e of D_h from the nomogram, substitute into

$$D_h \simeq \frac{2D_e^3 - H(k/\gamma)}{3D_e^2 - 1 - (k/\gamma)} \qquad (66)$$

and use (66) iteratively until D_h is determined to the required accuracy. Values of d_{12}, ψ and Δr can be estimated from D_h, i.e.,

$$d_2 = d(D_h + 1)/2 \ , \qquad (67)$$

$$d_1 = d - d_2 \qquad (68)$$

$$H_2' \simeq H_2 - d_2^2/(2a), \qquad (69)$$

$$\psi \simeq \mathrm{Tan}^{-1}(H_2'/d_2), \qquad (70)$$

and

$$\Delta r \simeq 2d_1 d_2 \sin^2\psi/d \qquad (71)$$

When $d_2 >> d_1$, $d_2 \simeq d$, (71) becomes

$$\Delta r \simeq 2d_1 \sin^2\psi. \qquad (72)$$

The k in γ/k is the effective earth radius factor and is defined as the ratio of the effective earth radius a to the actual earth radius a_0, i.e.,

$$k = a/a_0 \tag{73}$$

and

$$a_0 \simeq \begin{cases} 6370 \text{ km} \\ 3960 \text{ s mi} \\ 3440 \text{ n mi} \end{cases} \tag{74}$$

Values for k can be estimated from surface refractivity (Rice, et al., 1967, sec. 4) or refractivity gradient (Dougherty, 1967, p. 6). A k value of 4/3 is frequently used to characterize average refractivity conditions.

In addition, certain k values can result in paths that are not line-of-sight. This condition is encountered when the straight edge used in reading the nomogram crosses the horizon line, and the results obtained from the nomogram should not be used.

Table 1 summarizes the values obtained using the nomogram for a sample problem with parameters similar to those used in the section CI-C.2.1 example.

Table 1. Example, Nomogram Use

Given Parameters

h_1 = 100 ft = 0.0348 km

h_2 = 30,000 ft = 9.144 km

d = 53.2 n mi = 92.6 km

a = 8493 km

Calculated Results

Equation	Parameter	Value	
(63)	H	0.993355	
(64)	γ/k	0.027099	
(65)	D_h	0.99	from nomogram
(65)	D_h	0.993972	1st iteration
(65)	D_n	0.9929729	2nd iteration
(65)	D_h	0.9929729	3rd iteration
(66)	d_2	92.227465 km	
(67)	d_1	0.3253538 km	
(68)	H_2'	8.642763 km	
(69)	ψ	0.09339100 rad.	
(70)	Δr	0.005639 km	

CI-C.2.3 Computational Methods

Geometry for reflection from a smooth earth is shown in figure 10. Rays are assumed to be straight lines and the earth spherical with effective radius a. Use of an effective earth radius is a first-order compensation for average ray bending associated with transmission through the atmosphere (Bean and Dutton, 1966, sec. 3.6; Rice et al., 1967, p. 6-14).

Given the effective earth radius a, antenna heights H_{12} and the path length d, the ray length difference (Δr) between the reflected ray ($r_{12}=r_1+r_2$) and the direct ray r may be calculated using (75) through (90) where all angles are in radians, and all lengths are measured in identical units, e.g., kilometers. The formulation is as follows

$$z_{1,2} = a + H_{1,2} \quad \text{km}, \tag{75}$$

$$\rho_{1,2} = a/z_{1,2}, \tag{76}$$

$$\theta = d/a \quad \text{rad}, \tag{77}$$

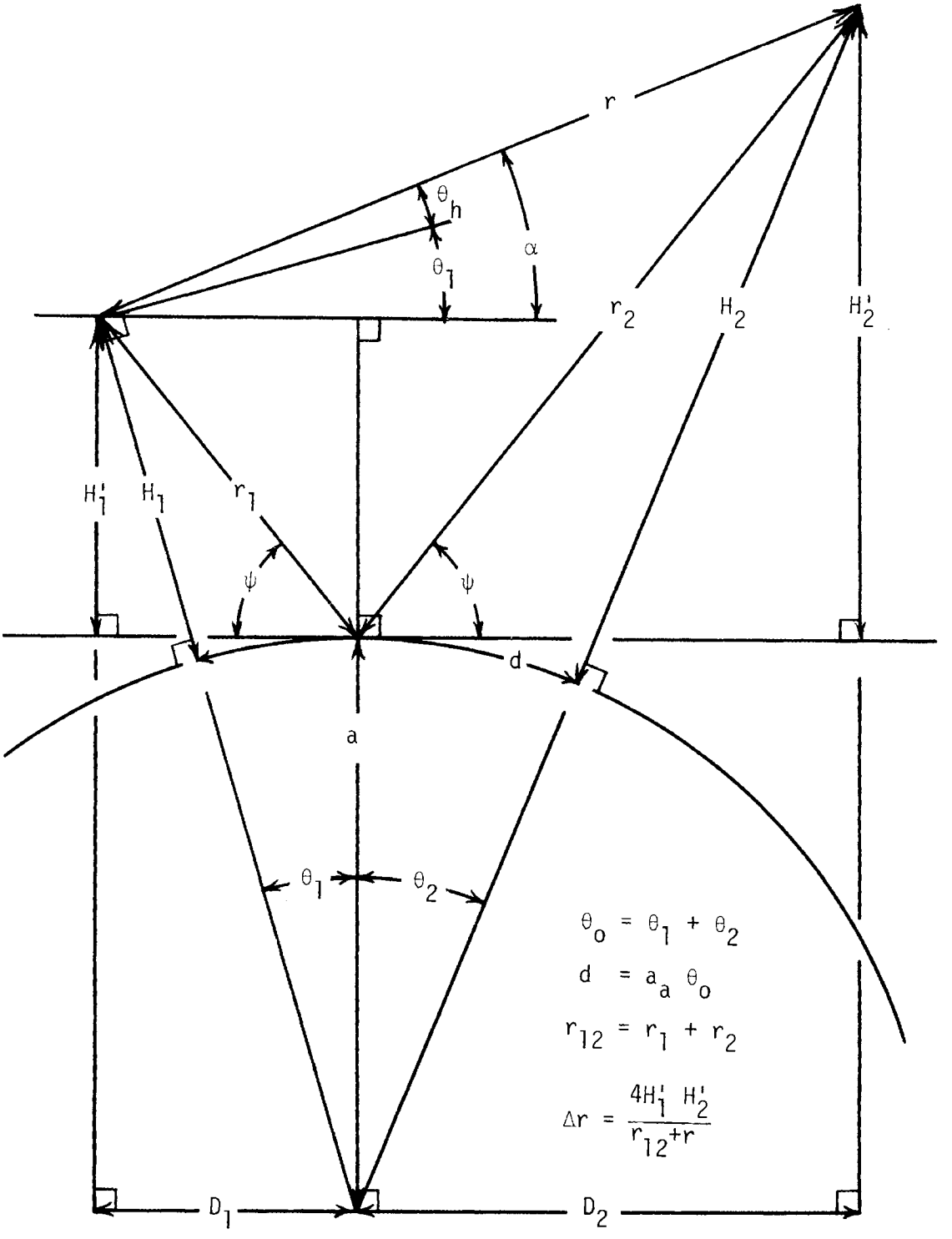

Figure CI-10. Spherical earth geometry. (not drawn to scale)

$$z = \rho_1^2 + \rho_2^2 + 2\rho_1\rho_2 \cos\theta \tag{78}$$

$$\phi = (1/3)\,\mathrm{Sin}^{-1}\left\{ \frac{(\rho_1^2 - \rho_2^2)\sin\theta}{[(4-z)/3]^{3/2}} \right\} \text{ rad} \tag{79}$$

$$t_{n=0,1,2} = 1 - \left(\frac{4-z}{3}\right)\sin^2(\phi + \frac{n\pi}{3}) \tag{80}$$

$$\psi = \mathrm{Tan}^{-1}\left[\frac{\cos\theta - (\sqrt{t_1} + \sqrt{t_2} - \sqrt{t_o})}{\sin\theta} \right] \text{ rad} \tag{81}$$

$$\theta_{1,2} = \mathrm{Cos}^{-1}(\rho_{1,2}\cos\psi) - \psi \text{ rad} \tag{82}$$

$$D_{1,2} = Z_{1,2}\sin\theta_{1,2} \text{ km} \tag{83}$$

$$D_o = D_1 + D_2 \text{ km} \tag{84}$$

$$H'_{1,2} = D_{1,2}\tan\psi \text{ km} \tag{85}$$

$$\alpha = \mathrm{Tan}^{-1}[(H'_2 - H'_1)/D_o] \text{ rad} \tag{86}$$

$$r = D_o/\cos\alpha \text{ km} \tag{87}$$

$$r_{12} = r_1 + r_2 = D_o/\cos\psi \text{ km} \tag{88}$$

$$\Delta r = 4H'_1 H'_2/(r_{12} + r) \text{ km.} \tag{89}$$

$$\Delta r \simeq 2H'_1H'_2/r \text{ km} \tag{91}$$

$$\Delta r \simeq 2H'_1H'_2/d \text{ km} \tag{92}$$

$$\Delta r_M = 4H_1H_2/(H_1+H_2 + H_2 - H_1) = 2H_1 \text{ km} \tag{93}$$

$$\Delta r_{AG} \simeq 2r_1\sin^2\psi = 2H'_1\sin\psi \text{ km} \tag{94}$$

These expressions are an exact solution for the geometry of figure 10 where $a \geq 0$ and $d \geq 0$. They were obtained by combining the relationship between d and ψ developed by L.E. Vogler (OT/ITS, informal communication, 1971) with a formulation previously given by Gierhart and Johnson (1969, sec. A.1). However, they are an approximate solution to the problem since the use of an effective earth radius does not provide an exact compensation for ray bending. Effective heights (sec. 5, Rice, et al., 1967, fig. 6.7) could be used to provide some correction. Additional compensation for ray bending could be made by letting the effective heights and radius approach actual values as ψ approaches $\pi/2$ (sec. 5; Gierhart and Johnson, 1973, sec. A.4.2). This method could be used to obtain curves of Δr versus d by performing calculations for various values of ψ and calculating d from

$$d = a\theta \ . \qquad (90)$$

Even with the aid of electronic computers it is frequently difficult to obtain $r_1+r_2=r_{12}$ and r with enough precision to calculate Δr from its fundamental definition

($\Delta r = r_{12} - r$), since it represents the difference between large and nearly equal parameters. The formula given in (89) avoids this problem. It is an alternate formulation of (37), and (89) is useful in developing approximate expressions for Δr.

For example, when $r_{12} \simeq r$

$$\Delta r \simeq 2H_1'H_2'/r \text{ km} \qquad (91)$$

with $H_1+H_2 \ll d$, $r \simeq d$ and (91) becomes

$$\Delta r \simeq 2H_1'H_2'/d \text{ km}, \qquad (92)$$

which is a frequently used formulation (Beckmann and Spizzichino, 1963, p. 225; Rice et al., 1967, p. 5-5). Note that (a) $H_1'=H_1$ and $H_2'=H_2$ when the reflecting surface between the antennas is flat, e.g., as $a \to \infty$ or when d is very much less than the total smooth earth radio horizon distance ($d \ll \sqrt{2aH_1} + \sqrt{2aH_2}$) and (b) maximum value Δr_m of Δr occurs at $d \simeq 0$ ($\psi = \pi/2$, $r_1 = H_1$, $r_2 = H_2$) and is given by

$$\Delta r_M = 4H_1H_2/(H_1+H_2+H_2-H_1) = 2H_1 \text{ km} \qquad (93)$$

where H_1 is the smaller antenna height ($H_1 < H_2$). For most air/ground applications, $r_1 \ll r_2$, $r_1 + r_2 \; r_2 \; r$, and

$$\Delta r_{AG} \simeq 2r_1 \sin^2 \psi = 2H_1' \sin \psi \quad \text{km} \;, \tag{94}$$

where H_1' may be approximated by H_1 giving

$$\Delta r_L = 2H_1 \sin \psi \geq \Delta r_{AG} \quad \text{km} \;, \tag{95}$$

or by

$$H_1' \simeq H_1 - d_1^2/2a \simeq H_1 - H_1^2/(2a \tan^2 \psi) \quad \text{km} \tag{96}$$

which yields another approximate expression for Δr, i.e.,

$$\Delta r_s = 2H_1[(1 - H_1/(2a \tan^2 \psi)] \sin \psi \leq \Delta r_{AG} \quad \text{km}. \tag{97}$$

These approximations are useful in placing bounds on Δr_{AG} since

$$\Delta r_s \leq \Delta r_{AG} \leq \Delta r_L \quad \text{km} \tag{98}$$

and

$$\Delta r_L - \Delta r_s = H_1^2 \cos(\psi) / (a \tan \psi) \; \text{km} \tag{99}$$

For the special case of equal antenna heights where $H_1=H_2$, $r_1=r_2=D_1 \sec\psi$ and $r=2D_1$ so that

$$\Delta r_{EH} \simeq d\,[\sec(\psi)-1] \text{ km} \qquad (100)$$

or

$$\Delta r_{EH} = r_1 + r_2 - r = 2D_1[\sec(\psi)-1] \text{ km} \qquad (101)$$

when $d \simeq 2D_1$.

A useful approximation for $\tan\psi$ was developed (L.E. Vogler, OT/ITS, informal communication, 1971) by expanding (81) as a power series in (1/a), i.e.,

$$\tan\psi \frac{H_1+H_2}{d} - \left(\frac{H_1^2+H_2^2}{ad}\right)\left[1 + \frac{d^2}{2(H_1+H_2)^2}\right] \qquad (102)$$

For air/ground ($H_1 << H_2$) applications, (102) becomes

$$\tan\psi_{AG} \simeq \frac{H_2}{d}\left[1 - \frac{H_2}{a}\right] - \frac{d}{2a} \simeq \frac{H_2}{d} - \frac{d}{2a} \qquad (103)$$

and for equal antenna heights ($H_1 = H_2$) it becomes

$$\tan\psi_{EH} \simeq \frac{2H_2}{d}\left[1 - \frac{H_2}{a}\right] - \frac{d}{4a} \simeq \frac{2H_2}{d} - \frac{d}{4a} \quad . \qquad (104)$$

Table 2 summarizes values obtained using the equations provided in this section for a sample problem with parameters similar to those used in the section CI-C.2.1 and section CI-C.2.2 (table 1) examples.

CI-C.3 Fresnel Zone Clearance

If rays are taken as straight lines, the locus of points about the terminal locations with constant r would form an ellipsoid. Figure 11 shows the ellipse associated with the great circle plane. The largest ellipse that can be drawn without intersecting terrain along the path has a Δr of Δr_F which is used to determine the order of Fresnel zone clearance, C_F, from

$$C_F = 2\,\Delta r_F/\lambda \qquad (105)$$

where λ is wavelength in the same units as Δr . First Fresnel zone clearance, $C_F \geq 1$, or 0.6 of the first Fresnel zone clearance, is often taken as sufficient to allow the mean transmission loss to be estimated by its free space value (ITT, 1970, p. 26-15). However, these criteria are usually applied with the earths curvature exaggerated such

Table 2. Example, Computational Methods[a]

Equation	Parameter	Value
(75)	Z_1	8493.630 km
(75)	Z_2	8502.744 km
(76)	ρ_1	0.9999964
(76)	ρ_2	0.9989246
(77)	θ	0.01090233 rad
(78)	Z	3.995566
(79)	$\emptyset$	1.412314 rad
(80)	t_0	0.9999707
(80)	t_1	0.9987279
(80)	t_2	0.9990846
(81)	ψ	0.9328764 rad
(82)	θ_1	3.834837×10^{-5} rad
(83)	D_1	0.3257169 km
(83)	D_2	92.37181 km
(84)	θ_2	0.010864 rad
(84)	D_0	92.69753 km
(85)	H_1'	0.03047381 km
(85)	H_2'	8.642233 km
(86)	α	9.263581 rad
(87)	r	93.09669 km
(88)	r_{12}	93.10235 km
(89)	Δr	0.565764 m

(a) Given parameters are as in table 1.

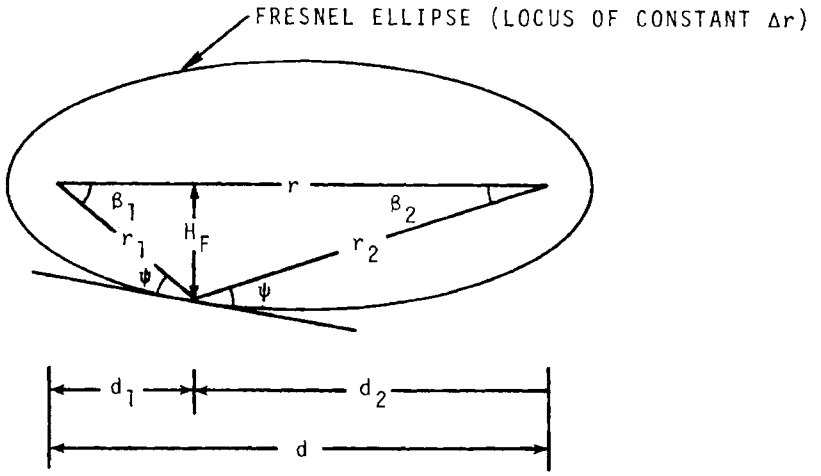

Figure CI-11. Fresnel zone ellipse.

as with an effective earth radius that is 2/3 of the actual radius.

In selecting antenna heights (or sites) to meet a Fresnel clearance requirement, it is convenient to use the Fresnel ellipse semi-height, H_F. A useful approximation for this height can be derived using (37) and (40) for the special case where the path length is very much greater than either antenna height; i.e., for $h_{1,2} \ll d$, $r_{1,2}\ r \simeq d$, $\sin\psi \simeq \psi$, $\sin\beta_{1,2} \simeq \beta_{1,2}$ and $r_{1,2} \simeq d_{1,2}$ so that

$$\Delta r_F = C_F\lambda/2 = \frac{4r_1r_2\sin^2\psi}{(r_{12} + r)} \simeq \frac{2d_1d_2\psi^2}{d} \text{ rad} \qquad (106)$$

$$\beta_{1,2} = \text{Sin}^{-1}\left(H_F/r_{1,2}\right) \simeq H_F/d_{1,2} \quad \text{rad} \qquad (107)$$

and $2\psi = \beta_1 + \beta_2$ from (40) can be combined to obtain

$$H_F \simeq \sqrt{d_1 d_2 C_F \lambda / d} \quad \text{km.} \tag{108}$$

At mid-path, H_F, has a maximum value, H_{MF}, given by

$$H_{MF} \simeq 0.5 \sqrt{d C_F \lambda} \quad \text{km} . \tag{109}$$

With height in feet, distance in nautical miles and frequency, f, in megahertz (108) and (109) become

$$H_F \simeq (2.44 \times 10^3) \sqrt{\frac{d_1[\text{n mi}]\, d_2[\text{n mi}]\, C_F}{d\,[\text{n mi}]\, f}} \quad \text{ft} \tag{110}$$

and

$$H_{MF} \simeq (1.22 \times 10^3) \sqrt{d[\text{n mi}]\, C_F / f} \quad \text{ft} . \tag{111}$$

For example, the maximum first Fresnel zone clearance semi-height for a 100 n mi path operating at 100 MHz is

$$H_{MF} \simeq (1.22 \times 10^3) \sqrt{(100)(1)/(100)} = 1,220 \text{ ft} .$$

CI-C.4 Lobing Frequency

Received signal level will vary with terminal location because of interference between the two waves, e.g., an

aircraft traveling toward a facility at constant altitude will experience signal strength variation of a periodic nature. The maximum number N_L of cycles (or lobes) associated with reflection from a smooth spherical earth (fig. 11) as an aircraft traverses a constant altitude radial path from a ground facility is given by

$$N_L = 1 + 0.5\,\lambda \text{ lesser of } \{H_1 \text{ or } H_2\} \qquad (112)$$

where $H_{1,2}$ and λ are in the same units. The +1 is included in (112) as an allowance for the phase variation associated with the reflection coefficient, e.g., this phase changes by about π rad for vertical polarization near the pseudo-Brewster angle. The +1 was not included in (47) since $R_e = -1$ (constant π phase shift at reflection) was assumed. Neither (112), (47) nor equations presented here for lobing frequency contain an allowance for signal level variations associated with antenna patterns. In fact, (112) is the only equation in this section that includes an allowance for the phase shift change at the pseudo-Brewster angle (sec. CI-D.8).

Estimates of the distance lobing frequency f_d can be made using

$$f_d \simeq (1.716 \times 10^{-3}) F_d f[\text{MHz}] |V_d[\text{kts}]| \text{ Hz} \qquad (113)$$

where F_d is the distance lobing factor discussed below, and V_d is the radial component of the aircraft velocity. In terms of the geometry of figure 10, Δr may be expressed as

$$\Delta r = \frac{4H'_1 H'_2}{r_{12} + r} = \frac{4H'_1 H'_2}{\sqrt{D_o + H'_1 + H'_2} + \sqrt{D_o + H'_2 - H'_1}} \text{ km} \qquad (114)$$

which can be used to obtain the approximation for F_d given by

$$F_d \simeq \left| \frac{\partial}{\partial d} (\Delta r) \right| \simeq \left| \frac{\partial}{\partial D_o} (\Delta r) \right| = \frac{D_o \Delta r}{r_{12} r} \qquad (115)$$

when H'_{12} are considered constant. Since Δr does not include phase changes associated with the reflection coefficients, $\frac{\partial}{\partial d}(\Delta r)$ in (115) is approximate. When $D_o \simeq r_{12} \simeq r \simeq d$, (115) becomes

$$F_d \simeq \Delta r / D_o \quad . \qquad (116)$$

Similarly, the height lobing frequency f_H associated with vertical ascent at a fixed distance can be estimated with

$$f_H \simeq (1.695 \times 10^{-5}) F_H f[\text{MHz}] |V_H[\text{ft/min}]| \text{ Hz} \qquad (117)$$

where F_H is the height lobing factor, and V_H is the vertical component of the aircraft velocity. Values of F_H may be obtained using (115) from

$$F_H \simeq \left| \frac{\delta}{\delta H_2}(\Delta r) \right| \simeq \left| \frac{\delta}{\delta H_2'}(\Delta r) \right| = 4H_1' \left| \frac{\delta}{\delta H_1'} \left(\frac{H_2'}{r_{12} + r} \right) \right| \qquad (118)$$

or

$$F_H \simeq \frac{F_d}{D_o} \left| \frac{H_1'(r - r_{12}) + H_2'(r + r_{12})}{r_{12} - r} - \frac{r_{12} r}{H_2'} \right| \qquad (119)$$

when $D_o \simeq r_{12} \simeq r \simeq d$

$$F_H \simeq \frac{F_d}{H_2' d} \left| \left(H_2'\right)^2 - d^2 \right| \qquad (120)$$

but $r \simeq d$ implies $d >> H_2'$ so that

$$F_H \simeq \frac{F_d d}{H_2'} \quad . \qquad (121)$$

For paths where $H_2 >> H_1$ and $H_2' = H_2 - d^2/(2a)$ (121) can be expressed as

$$F_H \simeq \frac{F_d d}{H_2 - d^2/(2a)} \qquad (122)$$

or if $H_1 \simeq H_2$

$$H_1' \simeq H_1 - d^2/(8a) \qquad \text{km} \qquad (123)$$

and

$$F_H \simeq \frac{F_d d}{H_1 - d^2/(8a)} \qquad (124)$$

Note that (124) applies to the case where only one aircraft is changing altitude. If both aircraft are changing altitude at the same rate, the F_H from (120) should be doubled.

The lobing frequency f_ℓ encountered by an aircraft is dependent upon (1) the location of the aircraft relative to the facility it is using, (2) the aircraft velocity, and (3) the radio frequency used. It is related to f_d and f_H by

$$f_\ell \leq f_d + f_H \qquad (125)$$

Here $<$ is needed because of the magnitude bars used in (113) through (120). It is possible for an aircraft to follow a flight pattern such that the lobing with distance is compensated for by lobing with height so that $f_\ell \simeq 0$ and $f_d + f_H > 0$, e.g., an aircraft flying the glide slope of a conventional instrument landing system in which the lobing structure is used to determine the desired flight path.

An estimate of the maximum value f_M of f_ℓ expected for a particular height combination can be made by assuming that $f_d >> f_H$ when F_d is near its maximum at a small d. From (37) and (115) it follows that

$$F_d \simeq \frac{4D_o r_1 r_2 \sin^2\psi}{r_{12} r(r_{12} + r)} \tag{126}$$

and since $D_o/r \leq 1$

$$F_d \simeq \frac{4r_1 r_2 \sin^2\psi}{r_{12}(r_{12} + r)} \tag{127}$$

which has a maximum value at d = 0 such that

$$F_d < \left\{ \begin{array}{l} 2\, H_1/H_2 \text{ if } H_1 \ll H_2 \\ 1 \text{ if } H_1 \simeq H_2 \\ 2\,(H_1 + H_2)^{-1} \text{ lesser of } \{H_1 \text{ or } H_2\} \text{ otherwise} \end{array} \right\} \tag{128}$$

An estimate of an upper bound for the maximum value f_M of f_ℓ can be obtained directly from (128) and (113) since $f_d >> f_H$ is assumed; i.e.,

$$f_M < (3.432 \times 10^{-3})\, f[\text{MHz}]\, |V_d[\text{kts}]|$$

$$\cdot \left\{ \begin{array}{l} H_1/H_2 \text{ if } H_1 \ll H_2 \\ 0.5 \text{ if } H_1 \simeq H_2 \\ (H_1 + H_2)^{-1} \text{ lesser of } \{H_1 \text{ or } H_2\} \text{ otherwise} \end{array} \right\} \text{Hz} \tag{129}$$

Lobing frequency is also referred to as lobe modulation frequency or Doppler beat modulation. Reed and Russell (1964, ch. 10) develop formulas using both the lobe and Doppler beat modulation and show that "... no fundamental difference exists between the lobe modulation and the Doppler-beat modulation concepts. They differ only in the treatment of the independent variable."

Dougherty (1967, sec. 4, app. A) has extended Gerks (1966) formulation of lobing frequency for air-to-air propagation between aircraft with relative horizontal motion to a more general formulation that considers vertical aircraft motion as well as horizontal. However, the formulation is based on equal aircraft altitudes and equal ascent rates. Dougherty's (1967) formulation will be summarized in the remainder of this section. Slight changes in his notation have been made to provide consistancy or avoid conflict with notation previously used here.

For aircraft with equal ascent rates, equal altitudes, and no relative horizontal motion, the number of lobes per second -- the number of variations from signal minimum to maximum and back to minimum per second -- is given by

$$n_h = 26.7\, f \left[\frac{H_{1,2}}{2d}\right] \left[1 - \frac{d^2}{8a_e H_{1,2}}\right] \left|\frac{d}{dt}\ (H_{1,2})\right| \text{ lobes/sec} \quad (130)$$

where f is frequency in megahertz $H_{1,2}$ is the altitude of aircraft 1 or 2 in kilometers which are equal in this case, d is great circle path distance between aircraft in kilometers, a_e is an effective earth radius in kilometers and $\frac{d}{dt}(H_{1,2})$ is the ascent rate in kilometers/second for aircraft 1 or 2 which are equal in this case. Figures 12 and 13 show n_h versus aircraft altitude for $\left|\frac{d}{dt}(H_{1,2})\right|$=0.0029 km/sec (~10 ft/sec) and f=4500 MHz. Figure 12 is applicable to aircraft separations, d, of 100, 300 and 500 km (54, 162 and 270 n mi) while figure 13 provides curves for separations of 207 and 400 km (112 and 216 n mi). Both figures are based on an exponential atmosphere above a smooth earth where the particular exponential atmospheres are defined by the surface refractivity, N , in N-units. The a_e values used with (130) to develop these curves were determined via ray tracing data for an exponential atmosphere (Bean and Thayer, 1959).

For aircraft at equal altitudes and no vertical motion, $\frac{d}{dt}(H_{1,2})=0$, the number of lobes per second is given by

$$n_d = 26.7\, f\left[\frac{H_{1,2}}{2d}\right]^2\left[1 + 2\left(\frac{d^2}{8a_e H_{1,2}}\right) - 3\left(\frac{d^2}{8a_e H_{1,2}}\right)^2\right]\left|\frac{d}{dt}(d)\right| \text{ lobes/sec.} \qquad (131)$$

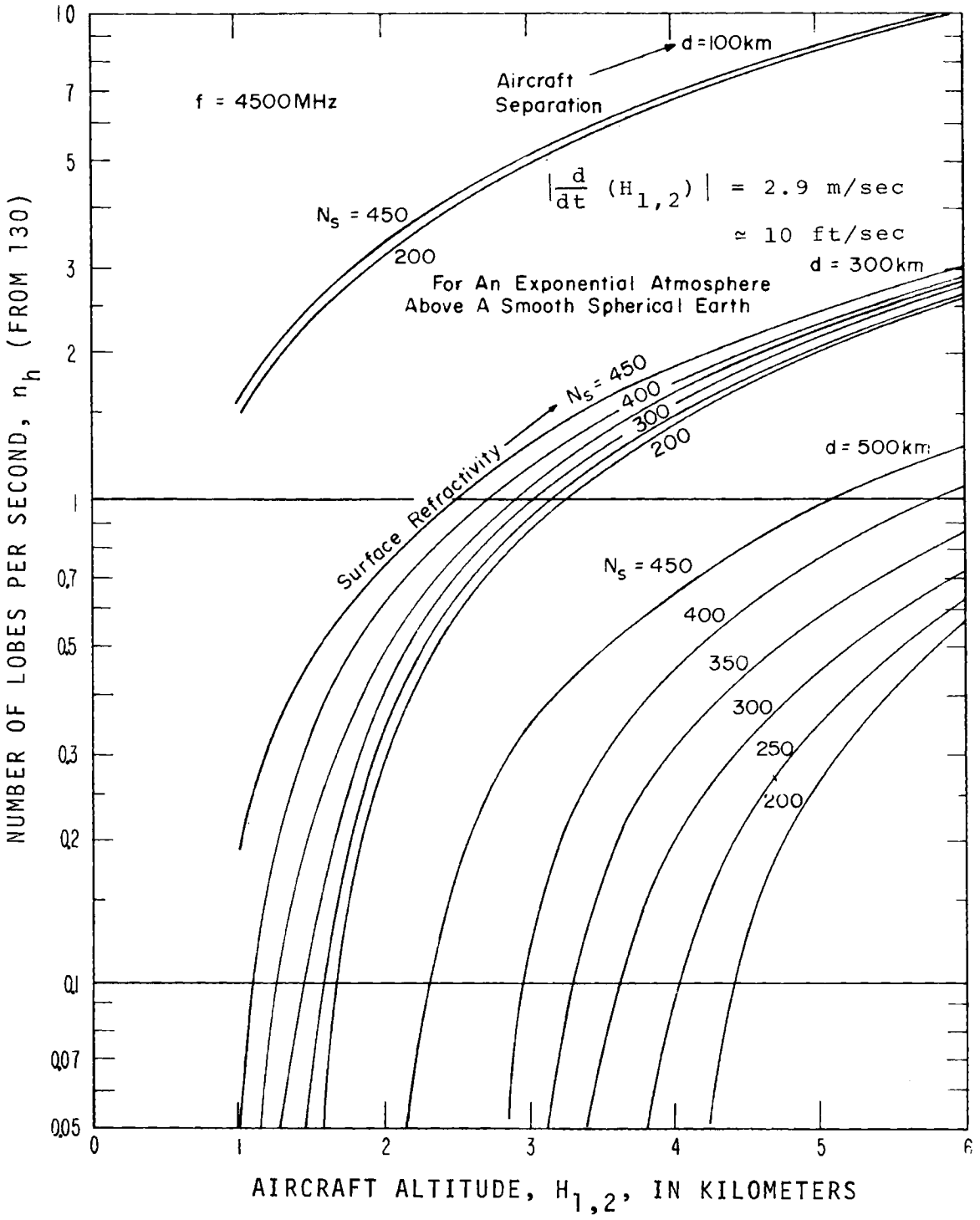

Figure CI-12. Lobing frequency for vertical displacement of both terminals, d = 100, 300, 500 km (Dougherty, 1967, fig. 12a).

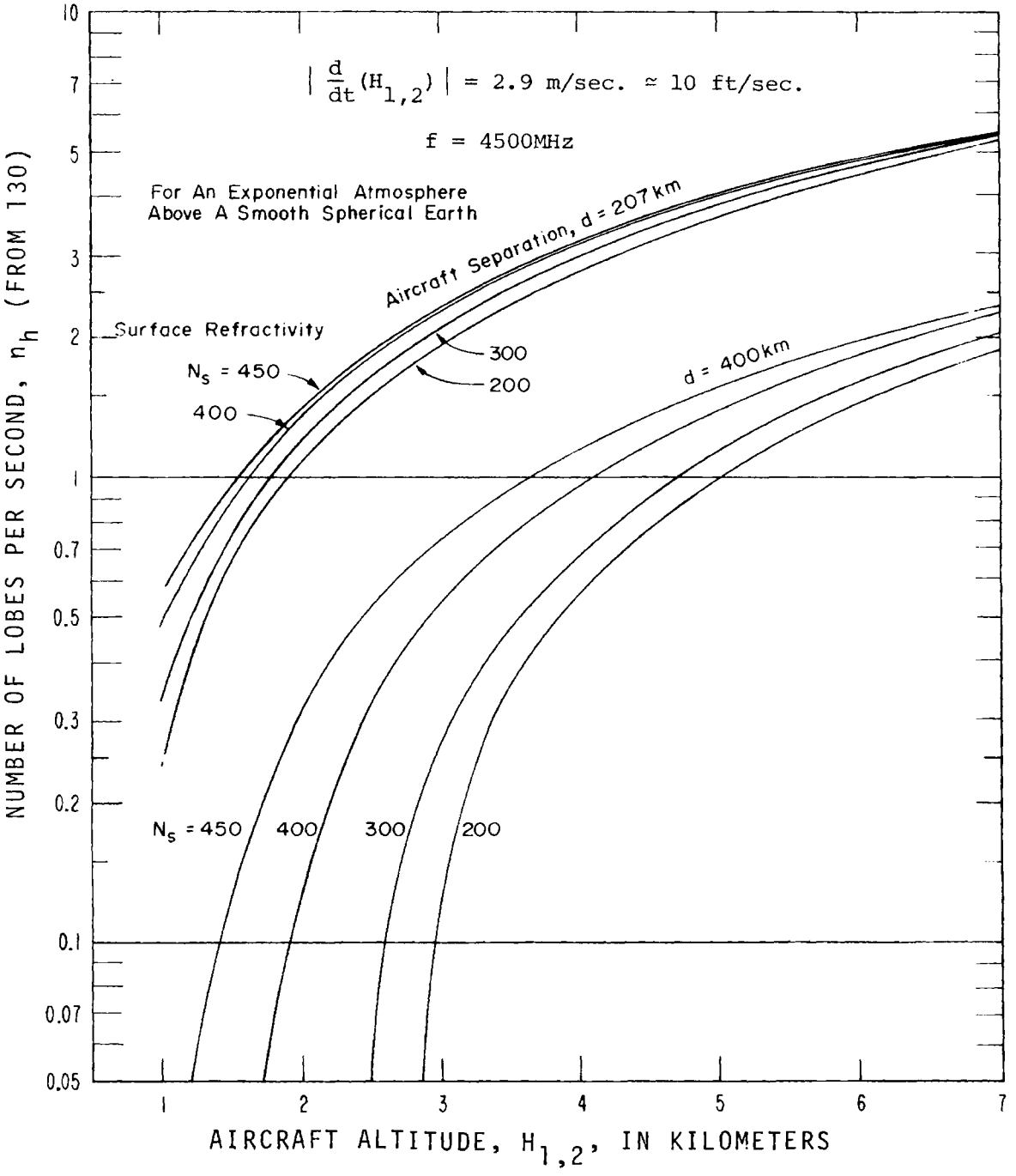

Figure CI-13. Lobing pattern for vertical displacement of antennas. (Dougherty, 1967, fig.12b).

The parameters and conditions for (131) are identical to those for (130) except that only relative horizontal motion, $\frac{d}{dt}(d)$, is allowed instead of vertical motion, $\frac{d}{dt}(H_{12})$. Figures 14 and 15 show n_d versus the great circle separation or distance, d, between aircraft for $|\frac{d}{dt}(d)|=0.1$ km/sec (~200 kts). Figure 14 is applicable to aircraft altitudes, $H_{1,2}$, of 1, 3.05 and 7 km (3.3, 10, and 23 thousand feet) while figure 15 provides curves for altitudes of 2 and 5 km (6.6 and 16 thousand feet).

Table 3 summarizes values obtained using the equations provided in this section for sample problems. One has air-to-ground parameters similar to those used in the section CI-C.2.2 (table 1) example, and the others have air-to-air parameters that allow the results to be compared with figures 12 and 14.

CI-D EFFECTIVE REFLECTION COEFFICIENT

The complex effective reflection coefficient, R_e, defined in section CI-B.1 by (13) for specular reflection may be written as

$$R_e = D F_A F_g F_m F_r F_s F_{\sigma h} R \qquad (132)$$

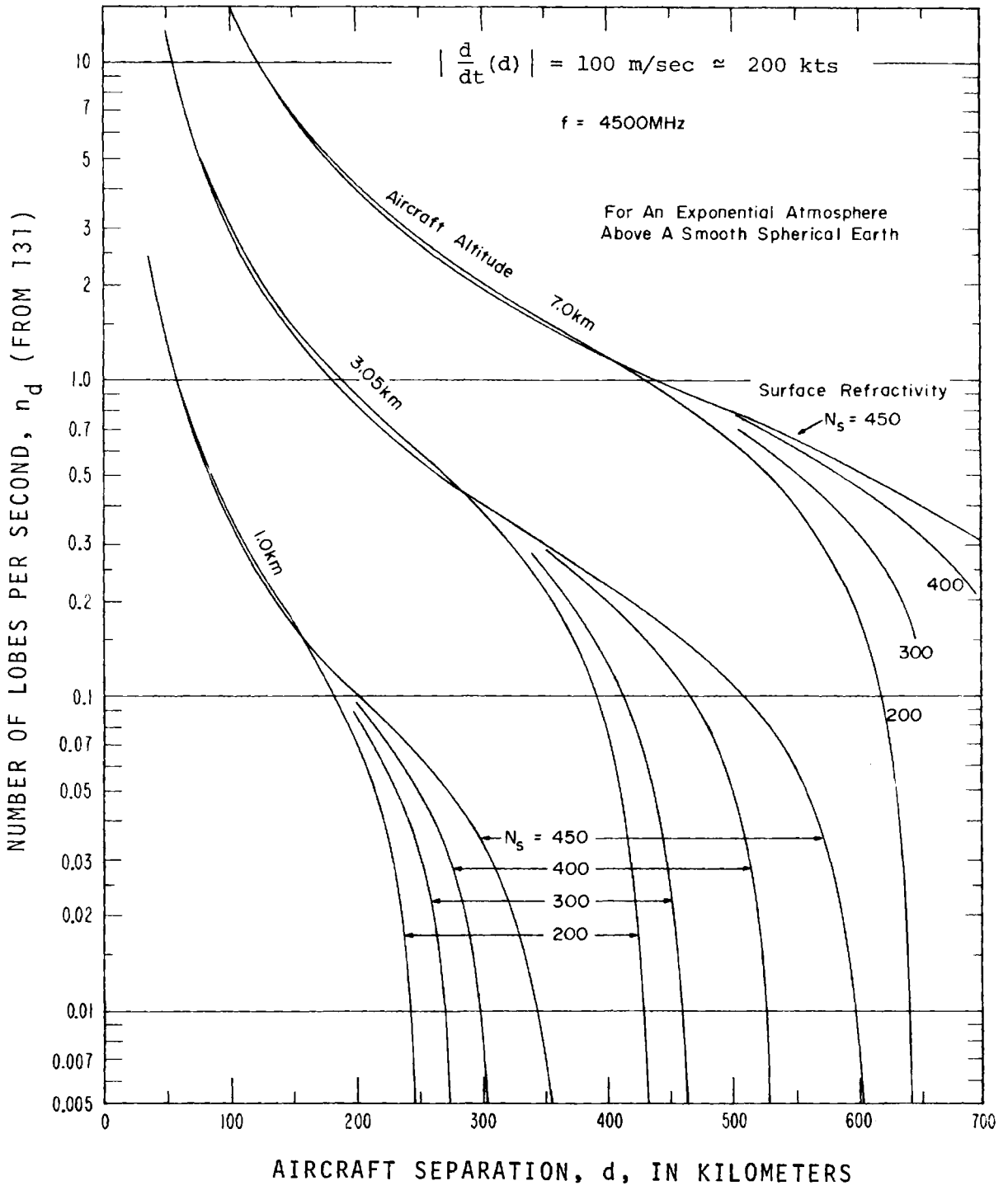

Figure CI-14. Lobing frequency for horizontal displacement of terminals, $H_{1,2}$ = 1, 3.05, 7 km (Dougherty, 1967; fig. 12c).

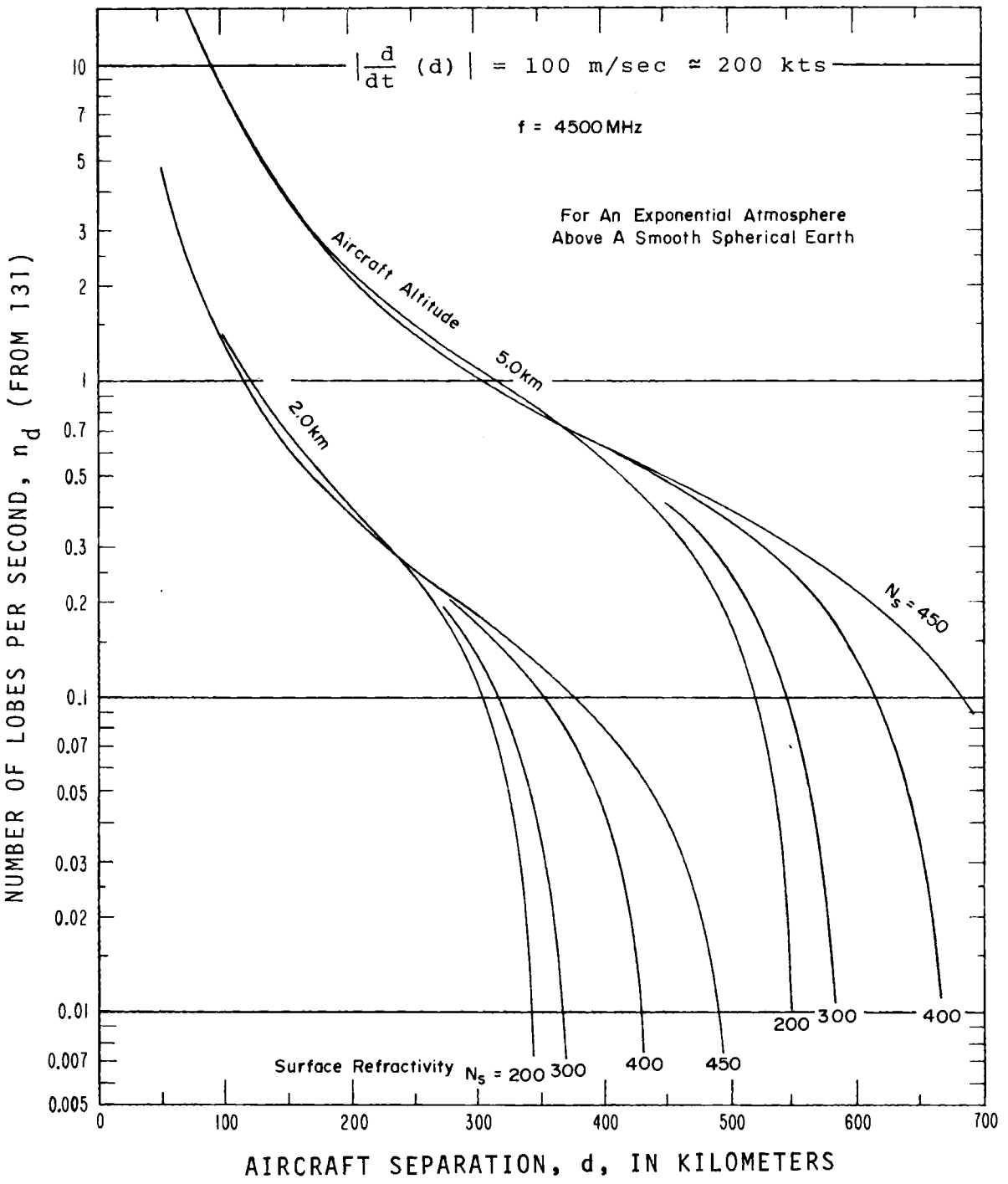

Figure CI-15. Lobing frequency for horizontal displacement of terminals, $H_{1,2}$ = 2, 5 km (Dougherty, 1967, fig. 12d).

where

D = divergence factor,
F_A = area factor,
F_g = complex antenna gain factor,
F_m = complex modulation factor,
F_r = ray length factor,
F_s = shadow factor,
$F_{\sigma h}$ = surface roughness factor,

and

R = complex plane earth reflection coefficient.

This division of R_e into factors is made for convenience. It allows R_e to be written in a compact form and the component factors to be discussed separately.

Maximum, minimum and nominal values for these factors are given in table 4 along with the section number in which the factors are discussed in greater detail. Note that the value of R_e can range over the whole complex plane, but has a nominal value of -1 for the conditions given with table 4.

Table 3. Example, Lobing Frequency

Given Parameters: V_d = 250 kts; V_H = 1000 ft/min
Other parameters as in table 2.

Equation	Parameter	Value
(115)	F_d	6.1×10^{-5}
(112)	f_d	0.04 Hz
(120)	F_H	6.5×10^{-4}
(116)	f_H	0.02 Hz
(124)	f_ℓ	0.06 Hz
(128)	f_M	4.6 Hz

Table 4. Reflection Factor Values

Factor	Maximum	Minimum	Nominal	Section
D	1	0	1[b]	CI-D.1
F_A	1	0	1[c]	CI-D.2
F_g[a]	∞	$-\infty$	1[d]	CI-D.3
F_m[a]	∞	$-\infty$	1[e]	CI-D.4
F_r	1	0	1[f]	CI-D.5
F_s	1	0	1[c]	CI-D.6
$F_{\sigma h}$	1	0	1[c]	CI-D.7
R[a]	1	-1	-1[g]	CI-D.8

(a) These factors are complex and can affect the phase of R_e.
(b) Normally 1 except for near grazing paths.
(c) Smooth spherical earth is assumed.
(d) Non-directional antennas are assumed.
(e) Modulation that is slow with respect to the relative transit time is assumed.
(f) Ray lengths assumed nearly equal.
(g) Horizontal polarization with a grazing angle (ψ of fig. 10) less than 6^o is assumed. Vertical polarization over average ground with $\psi < 0.6^o$ could also be assumed.

For many practical problems involving aircraft it is sufficient to use

$$R_e \simeq -F_{\sigma h} \tag{133}$$

Few problems will require the calculation of all factors.

A scaler effective reflection coefficient, R_{ed}, for diffuse reflection can be defined in a similar fashion; i.e.,

$$R_e = D F_A |F_g| |F_m| F_r F_{sd} F_{\sigma hd} \tag{134}$$

where

F_{sd} = diffuse shadow factor.
$F_{\sigma hd}$ = diffuse roughness factor,

and magnitude bars are used around F_g and F_m since R_{ed} is not complex. Although R_{ed} ranges from 0 to ∞, for many practical problems involving aircraft it will have a maximum value of 0.4 that occurs when $|R_e| \ll R_{ed}$ and it is sufficient to use

$$R_{ed} \simeq F_{\sigma hd} . \tag{135}$$

Phase associated with diffuse reflection is random so that R_{ed} is treated as a scaler and the methods involving phasor combinations (sec. CI-B.1) should not be used with R_{ed}. However, the statistical methods of section CI-B.2 can be used with R_{ed} by replacing $|R_e|$ with R_{ed} or a combination, R_{eed}, of R_e and R_{ed} made using

$$R_{eed} = \sqrt{|R_e|^2 + R_{ed}^2} \tag{136}$$

Factors F_{sd} and $F_{\sigma hd}$ are discussed with F_s (sec. CI-D.6) and $F_{\sigma h}$ (sec. CI-D.7), respectively. Decreasing values of F_s or $F_{\sigma h}$ are often accompanied by increasing values of F_{sd} or $F_{\sigma hd}$.

CI-D.1 Divergence Factor

The divergence factor, D, is used in (132) to allow for the divergence of energy reflected from a curved surface in the effective reflection coefficient formulation. It is defined by Reed and Russell (1964, p. 103) "as the ratio of the field strength obtained after reflection from a plane surface, the radiated power, total axial distance, and type of surface being the same in both cases, and the solid angle being a small elemental angle approaching zero in magnitude."

Figure 16 illustrates the geometry for reflection from a plane earth and a spherical earth where the relative location of the source reflecting point and reference plane are identical. It also shows the relative size of the ray bundle on the reference plane for each case. The divergence factor is related to the reference plane area associated with the spherical earth reflection, A_s, and the plane earth reflection, A_p, by

$$D = \sqrt{A_p/A_s} \quad . \tag{137}$$

Deviations of expressions for D in terms of the geometry of figure 10 are beyond the scope of this text, but such developments are provided by Beckmann and Spizzichino (1963,

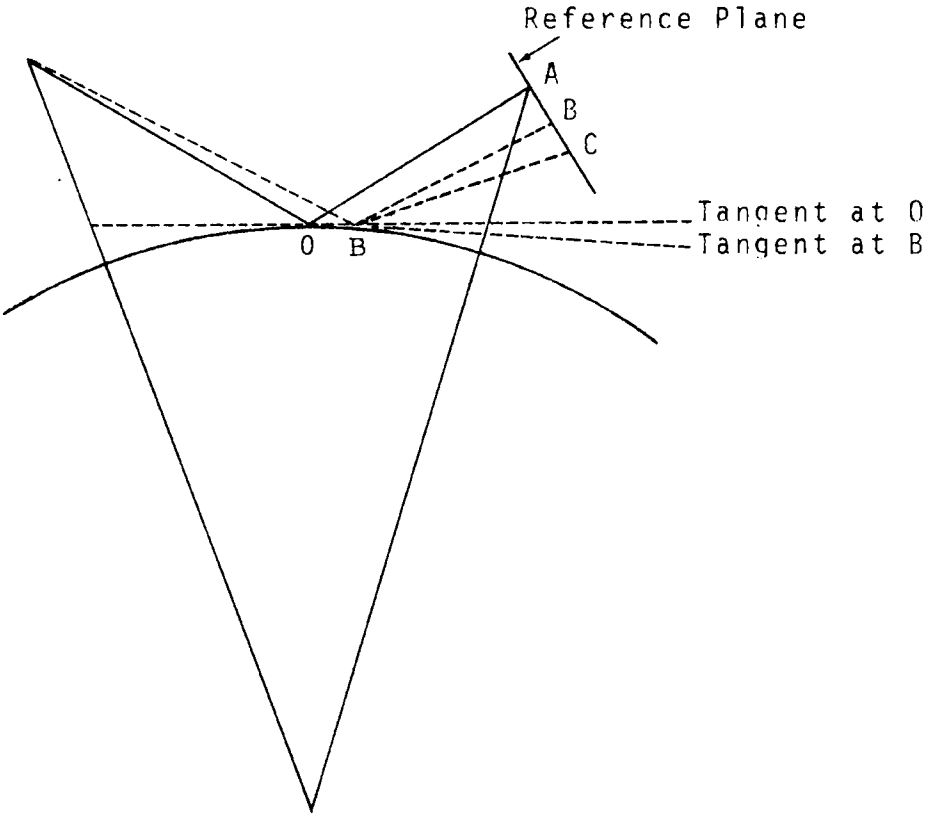

Figure CI-16. Sketch illustrating divergence. Line length AB indicates ray bundle size at the reference plane for reflection from a plane surface and AC corresponds to reflection from the curved surface.

sec. 11.3), Kerr (1964, sec. 5.2), Reed and Russell (1964, sec. 4.27), Riblet and Barker (1948), and Van der Pol and Bremmer (1939). An exact expression for D that is very similar to the formula provided by Beckmann and Spizzichino (1963, p. 223) may be developed by extending Riblet and Barker (1948, eq 13) to the special case where principal

radii of curvature of the reflecting surface at the reflection point are within, a_p, and normal, a_n, to the plane of incidence. This expression is

$$D = \left[1 + \frac{2r_1 r_2}{a_p (r_1 + r_2) \sin\psi} \right]^{-1/2} \left[\frac{2r_1 r_2 \sin\psi}{a_n (r_1 + r_2)} \right]^{-1/2} \qquad (138)$$

where the ray lengths r_1 and r_2 along with the grazing angle ψ are shown in figures 10 and 16.

For the spherical earth case (fig. 10) $a_p = a_n = a$ so that (138) may be expressed as

$$D = \left[1 + \frac{2R_r (1 + \sin^2 \psi)}{a \sin\psi} + \left(\frac{2R_r}{a} \right) \right]^{-1/2} \qquad (139)$$

where

$$R_r = \left\{ \begin{array}{ll} r_1 & \text{if } r_2 >> r_1 \\ r_1/2 & \text{if } r_1 \simeq r_2 \\ \dfrac{r_1 r_2}{(r_1 + r_2)} & \text{otherwise} \end{array} \right\} \text{ km} . \qquad (140)$$

Values for ψ may be obtained from (81), and $r_{1,2}$ determined using

$$r_{1,2} = \left\{ \begin{array}{ll} H_{1,2} & \text{if } \psi \simeq 90^{\circ} \\ D_{1,2}/\cos\psi & \text{otherwise} \end{array} \right\} \text{ km.} \qquad (141)$$

When r_1 and r_2 are less than 650 km (350 n mi) the third term of (139) can be neglected without altering D by more than 1% (Riblet and Barker, 1948, eq 25) so that

$$D \simeq \left[1 + \frac{2R_r(1 + \sin^2\psi)}{\sin\psi} \right]^{-1/2} . \qquad (142)$$

An antenna elevation of at least 240 km (80,000 ft) is required for r_1 or r_2 to exceed 650 km.

Figure 17 shown R_r/r_1 versus r_2/r_1 for $r_2 \geq r_1$. Note that $R_r \simeq r_1$ (i.e., $0.99r_1 \leq R_r \leq r_1$) when $r_2/r_1 > 100$ (i.e., $r_2 \geq r_1$). This figure can also be used for $r_2 \leq r_1$ by reversing the roles taken by the two variables; i.e., let r_2 be the smaller ray length and r_1 the larger.

Values for D are shown in figure 18 as a function of R_r and ψ. This figure is based on an a value in (139) of

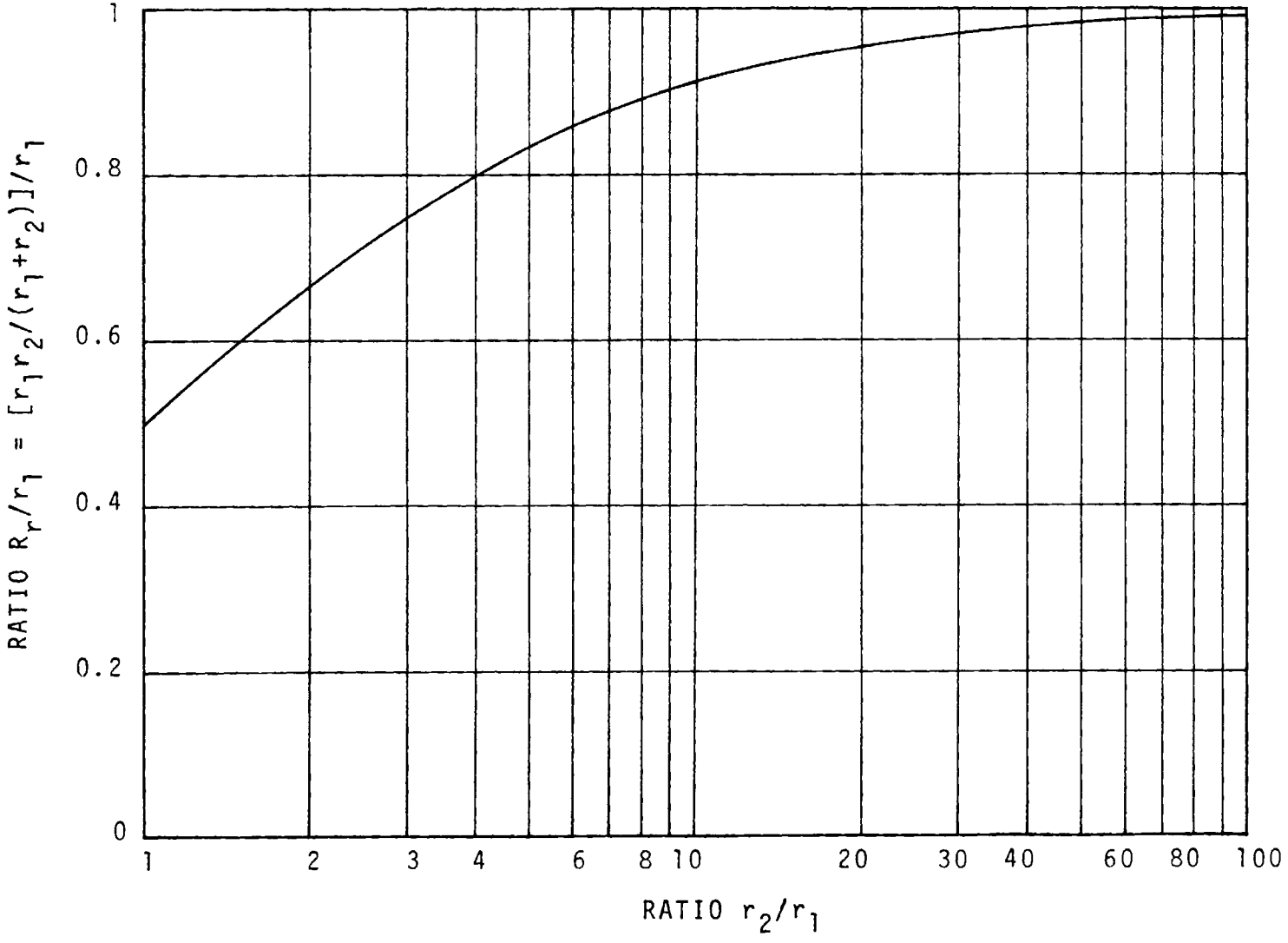

Figure CI-17. Curve showing R_r/r_1 versus r_2/r_1

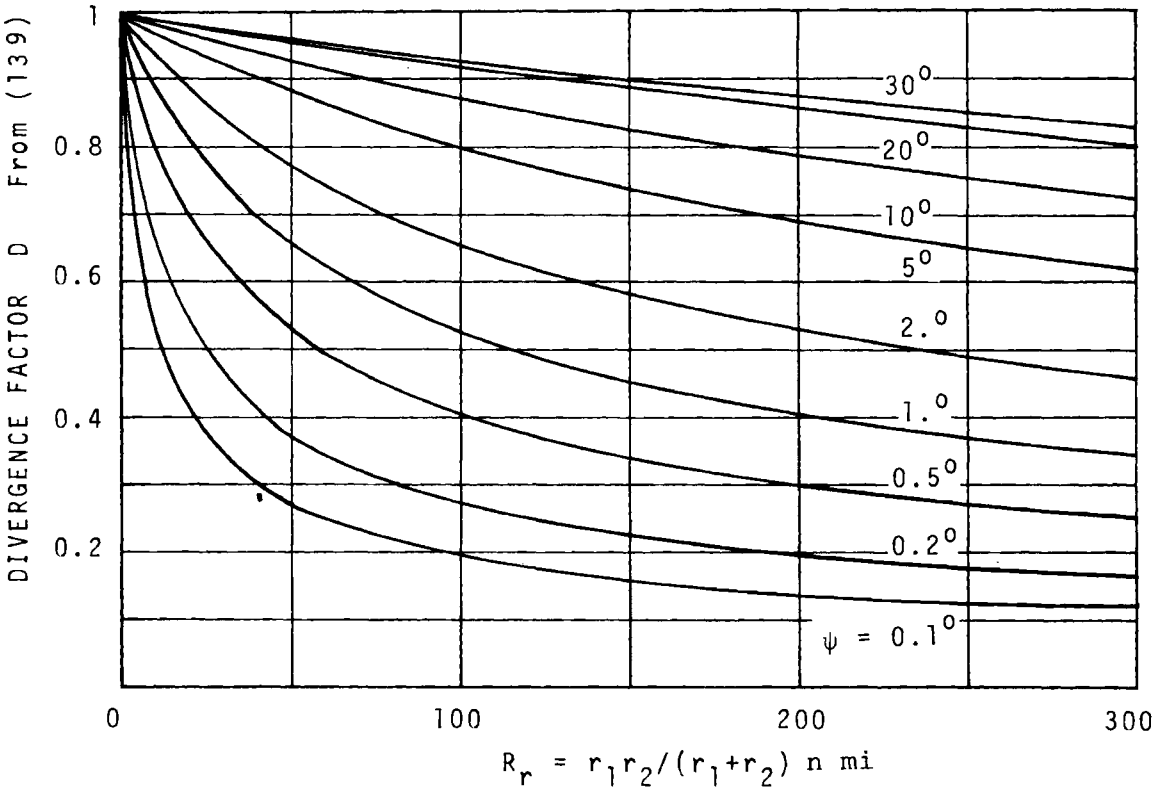

Figure CI-18. Divergence factor as a function of R_r and ψ for a 4/3 earth (a = 4586 n mi).

4586 n mi which corresponds to an effective earth radius factor 4/3 [see discussion following eq (74)]. However, it can be used for other values of a by reading the abscissa at an effective R_{re} value given by

$$R_{re} = \frac{(4586) R_r}{a} \quad \text{n mi} \qquad (143)$$

since R_r in figure 18 is in nautical miles. For example, $r_1 = 2.5$, $r_2 = 10$, $\psi = 1^o$, a = 45.86 nmi result in $R_r = 2$, from figure 17, $R_{re} = 200$ nmi from (138) and D = 0.41 from figure 18.

CI-D.2 Area Factor

The area factor, F_A, as used in (132) allows an adjustment for the size of the reflecting surface to be made. It is used (i.e., $\neq 1$) only when the reflecting area is smaller than the first Fresnel zone associated with a first terminal image to second terminal path so that rays reaching the receiving antenna via the reflector are essentially in phase. Figure 19 illustrates this Fresnel zone for a plane reflector. First Fresnel zone dimensions can be estimated using formulations such as those provided by Beckmann and Spizzichino (1963, sec. 12A), Kerr (1964, p. 413), Norton and Omberg (1947), or Rice et al. (1967, p. III-4), but such calculations are as complicated as the calculation of F_A.

Calculation of F_A involves the area of the reflector, A km²; wavelength λ km from (7); grazing angle from (39), (40), (70), (81) or (102); and the ray length product-sum ratio of figure 17, $r_1 r_2/(r_1+r_2) = R_r$ km; i.e.,

$$F'_A = (A \sin \psi)/(\lambda R_r) \qquad (144)$$

and

$$F_A = \begin{cases} 1 \text{ if } F'_A > 1 \\ F'_A \quad \text{otherwise} \end{cases} . \qquad (145)$$

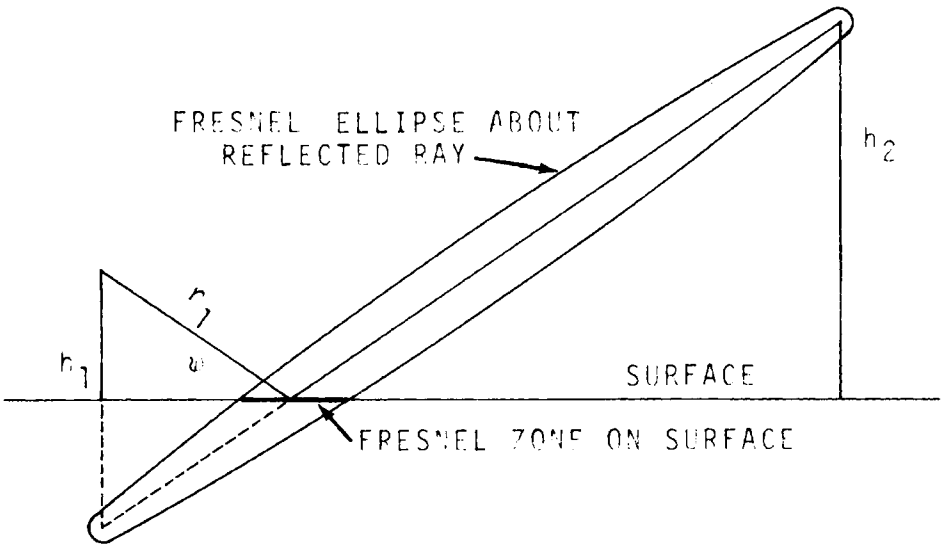

Figure CI-19. Fresnel zone on reflecting surface.

For example, R_r = 1 km, λ = 0.001 km, A = 0.001 km^2 and ψ = $\pi/6$ rad (30°) result in F_A = 0.5.

Since this formulation is based on a plane reflector, it should be used with caution when curved surfaces are involved. In fact F'_A is given by

$$F'_A = \sqrt{p_r/p_f} \qquad (146)$$

where p_r is the power (watts) received via a passive repeater path (perfect reflector that is smaller than first Fresnel zone) and p_f is the power that would be received over a similar path in free space. Transmitter power, p_t

watts, transmitting antenna voltage gain, g_t , effective area of the receiving antenna, A_{er} km², and the total path length, r_1+r_2 km are used to calculate p_f via

$$p_f = \frac{p_t g_t^2 A_{er}}{4\pi (r_1 + r_2)^2} \text{ W.} \tag{147}$$

Similarly, p_r can be expressed as

$$p_r = \left(\frac{p_t g_t^2 A_e}{4\pi r_1^2} \right) \left(\frac{g^2 A_{er}}{4\pi r_2^2} \right) \text{ W} \tag{148}$$

where A_e km² is the effective cross-section of the reflector with A that is perpendicular to r_1 (also r_2), and g is the reflector voltage gain corresponding to A_e ; i.e.,

$$A_e = A \sin \psi \text{ km}^2 \tag{149}$$

and

$$g^2 = 4\pi A_e / \lambda^2 . \tag{150}$$

The first factor of (148) may be taken as the power intercepted and reflected by the repeater, and the second factor represents transmission from the repeater to receiver. Substitution of (149) and (150) into (148) gives

$$p_r = \frac{p_t A_{er}}{4\pi} \left(\frac{g_t A \sin\psi}{r_1 r_2 \lambda} \right)^2 \quad W \qquad (151)$$

which when used with (147) in (146) will yield (144). Beckmann and Spizzichino (1963, eq 3, p. 381) provide a formulation very similar to (144).

An expression for transmission loss, L_{pr} dB, across the passive repeater path can be obtained by using (150) with an expression for A_r in terms of the receiving antenna voltage gain, g_r ; i.e.,

$$g_r^2 = 4\pi A_{er}/\lambda^2 \qquad (152)$$

and

$$L_{pr} = 10 \log (p_t/p_r) = 10 \log \left(\frac{4\pi r_1 r_2}{g_t g_r A \sin\psi} \right)^2 \quad dB \qquad (153)$$

Note that the frequency sensitive factors in (153) are the antenna gains so that L_{pr} is independent of frequency when fixed antenna gains such as 1 (isotropic) are assumed.

CI-D.3 Gain Factor

The complex antenna gain factor, F_g, is used in (132) to allow for situations where the antenna gains effective for the direct ray path differ from those for the reflected ray path. Figure 1 illustrates the two-ray path and indicates the gains involved. These are the complex voltage antenna gains (relative to isotropic) associated with the direct ray at terminal one or two, g_{D12}, and those associated with the reflected ray, g_{R12}.

Since these gains are, in general, complex quantities it is necessary that a common phase reference be used at each antenna; e.g., g_{D1} and g_{R1} must have a common reference so that they have the correct relative phase. In many practical applications the direct and reflected rays will leave (or arrive) at elevation angles where the relative phase is either expected to be near zero or is unknown so that the complex nature of these gains is largely academic.

These gains are called voltage gain since they have dimensions of volt/volt and contain relative phase information. Decibel gain values are related to these gain as in (25) and (26) for g_{D12}, or as

$$G_{R1,2} = 20 \log |g_{R1,2}| \text{ dB} \qquad (154)$$

$$|g_{R1,2}| = 10^{(G_{R1,2}/20)} \qquad (155)$$

for $g_{R1,2}$ The isotropic antennas to which the antenna gain are referenced should be appropriately polarized with the same reference used for both terminal antennas. For example, the reference antenna should be circularly polarized when a circuit with a circularly polarized and a linearly polarized antenna is considered so that the gain of the linearly polarized antenna would be about 3 dB below the value it would have if a linearly polarized reference were used.

The formulation for F_g is simply the factor in (13) that involves the antenna gains; i.e.,

$$F_g = \begin{cases} 1 \text{ for omnidirectional antennas and/or circular polarization} \\ \dfrac{g_{R1}\, g_{R2}}{g_{D1}\, g_{D2}} \quad \text{otherwise} \end{cases} \tag{156}$$

where omnidirectional implies that for the radiation angles of interest $g_{R1} = g_{D1}$ and $g_{R2} = g_{D2}$. As an example

$g_{R1} = 1 + j = \sqrt{2}\angle 45^\circ$, $g_{R2} = -j = 1\angle -90^\circ$, $g_{D1} = 1$ and $g_{D2} = 1-j = \sqrt{2}\angle -45^\circ$

would result in $F_g = (\sqrt{2}/\sqrt{2})\angle 45-90+45 = 1\angle 180^\circ = -1$.

The parameter F_{Vg} is similar to F_g except that F_{Vg} involves gains g_{VR12}, and g_{VD12} that are measured with respect to a linearly polarized antenna oriented in the plane of incidence (normally vertical polarization), i.e.,

$$F_{vg} = \left\{ \begin{array}{l} 1 \text{ for omnidirectional antennas} \\ \\ \dfrac{g_{vR1}\, g_{vR2}}{g_{vD1}\, g_{vD2}} \end{array} \right\} . \qquad (157)$$

Also

$$F_{hg} = \left\{ \begin{array}{l} 1 \text{ for omnidirectional antennas} \\ \\ \dfrac{g_{hR1}\, g_{hR2}}{g_{hD1}\, g_{hD2}} \end{array} \right\} \qquad (158)$$

where the subscript h implies a linearly polarized reference antenna oriented normal to the plane of incidence. These parameters will be used later (sec. CI-D.8) in a formulation for complex plane earth reflection coefficients for circular polarization.

CI-D.4 Modulation Factors

The complex modulation factor, F_m, is used in (132) since the time delay associated with the reflected ray path can result in situations where the modulation received via the direct ray signal differs significantly from that received via the reflected ray signal. It is the factor in (13) that involves the complex modulation function, m(t); i.e.,

$$F_m = \left\{ \begin{array}{l} 1 \text{ if the highest frequency in } m(t) < c/\Delta r \\ \left[\dfrac{m(t-r_{12}/c)}{m(t-r/c)} \right] \quad \text{otherwise} \end{array} \right\} \tag{159}$$

where $m(t-r_{12}/c)$ and $m(t-r/c)$ are values for m(t) at times $t-r_{12}/c$ and $t-r/c$. Values for r_{12}, r, c, and Δr may be obtained from (87), (88), (7), and (37), respectively. For example, $F_m = 1$ when the highest frequency in m(t) is 5 kc provided that $\Delta r_m << c/5000 = 60 \text{ km} = 2\text{x}10^4$ ft.

CI-D.5 Ray Length Factor

The ray length factor, F_r, is used in (132) to allow for situations where the free space path loss associated with the reflected ray may be significantly greater than that associated with the direct ray. It is a factor in (13) that involves the ray length ratio; i.e.,

$$F_r = \frac{r}{r_{12}} \tag{160}$$

CI-D.6 Shadow Factor

Theoretical solutions to scattering from rough surfaces frequently neglect shadowing (Beckmann and Spizzichino, 1963, p. 28). Figure 20 illustrates a situation where some portions of a reflecting surface are not illuminated by incoming rays. In cases where significant portions of the reflecting surface are not visible to both the receiving and transmitting antenna the reflection coefficient should be reduced to allow for shadowing. This reduction is introduced into the effective reflection coefficient formulation of (132) by the shadow factor term, F_s. For a smooth flat surface or normal incidence $F_s = 1$, and $F \rightarrow 0$ as the angle of incidence $(\pi/2-\psi)$ becomes large for either a rough surface or a smooth earth, i.e., $F \rightarrow 0$ as $\psi \rightarrow 0$. However, ray theory becomes invalid as $\psi \rightarrow 0$ (sec. CI-A).

In the context of effective reflection coefficients, the shadow factor can be taken as the probability that a random point within the first Fresnel zone on the reflecting surface will be illuminated. Equivalently, the shadow factor represents the fraction of first Fresnel zone area which is illuminated. Beckmann's (1965, eq 17) formulation for the shadowing function can be used to express F_s in

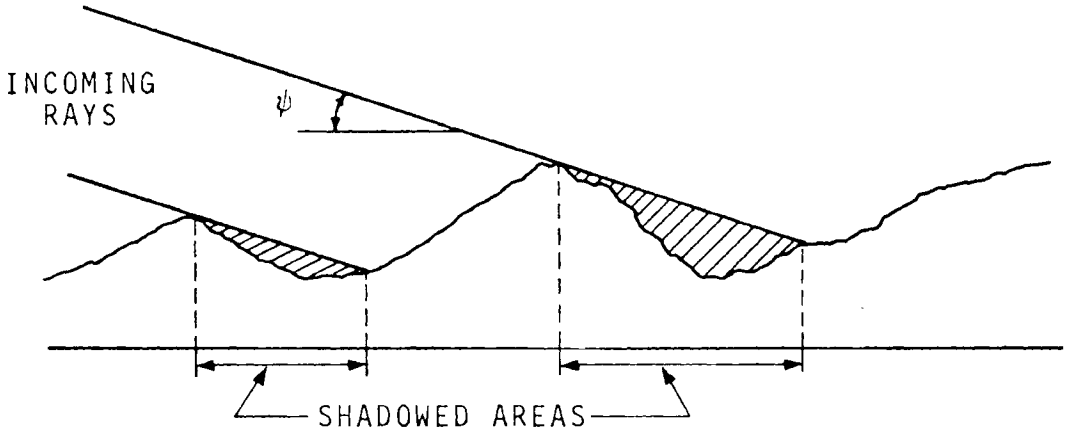

Figure CI-20. Shadowing of a reflecting surface.

terms of the grazing angle, ψ, and the variance of terrain slopes, $|B''(0)|$, within the first Fresnel zone; i.e.,

$$F_s = \exp\{(-0.25 \cot\psi) \operatorname{erfc}[(\tan\psi)/(\sqrt{2}|B''(0)|)]\} \quad (161)$$

where the complementary error function, erfc $[\psi]$, is related to the error function, erf $[\chi]$, by

$$\operatorname{erfc}[\chi] = 1 - \operatorname{erf}[\chi] \quad (162)$$

and values for erf $[\chi]$ can be obtained from Abromowitz and Stegun (1964, table 7.1). This formulation is based on a stationary terrain process in which the terrain slope is a normally distributed random variable with a zero-mean, and

the assumption that interdiction by terrain of rays reflected from illuminated portions of the terrain is negligible.

Curves provided by Beckmann (1965, fig. 2) are helpful in evaluating (161). For example, $\psi = 10^{o}$ and $|B''(0)| = \sqrt{2}/5$ result in $F_s = 0.73$ when Beckmann (1965, fig. 2) is used; i.e.,

Beckmann's θ = angle of incidence = $90^{o}-\psi=80^{o}$

Beckmann's $k = [\sqrt{2}|B''(0)|]^{-1} = 5$

and

Beckmann's $S(\theta) = F_s = 0.73$.

Calculation via (159) for the same parameters yields $F_m = 0.74$; i.e.,

$(\tan \psi)/(\sqrt{2}\ |B''(0)|) = 0.882$

erf (0.88) = 0.787

erfc (0.88) = 1 - 0.787 = 0.213,

and $(0.25 \cot \psi)$ erfc (0.88) = 0.302

$F_s = \exp(-0.302) = 0.74$.

Because of the complexity associated with the determination of F_s and the frequent lack of sufficient statistical information concerning the reflecting surface, $F_s = 1$ is frequently assumed and the surface roughness

factor, $F_{\sigma h}$ (sec. CI-D.7) is taken as a sufficient factor to allow for reflecting surface irregularities. When the extent of the first Fresnel zone area that is visible from both antennas can be determined from geometrical considerations it can be taken as the A in (144) and F neglected (i.e., $F_s = 1$) so that shadowing would be considered as part of the area factor, F_A (sec. CI-D.2). More information concerning shadowing can be obtained from sources such as Beckmann (1965), Sancer (1969) and Smith (1967).

CI-D.7 Surface Roughness Factors

The surface roughness factors $F_{\sigma h}$ and $F_{\sigma hd}$ are used in (132) and (134), respectively, to allow for roughness of the reflecting surface in these effective reflection coefficient formulations. Each is defined as the magnitude ratio of the reflection coefficient for the rough surface with respect to a smooth surface where, except for roughness, surface characteristics that affect reflection are identical for both surfaces. Specular components (deterministic phase) of the reflections are used in defining $F_{\sigma h}$. In defining $F_{\sigma hd}$ the numerator is taken as the diffuse component of the reflection coefficient for the rough surface case and the denominator is the smooth surface specular component.

Relatively simple formulations for these factors can be provided in terms of wavelength, λ m, grazing angle, ψ , and the root-mean-square (rms) deviation of surface excursions within the limits of the first Fresnel zone in the dominant reflecting plane (Longley and Rice, 1968, p. 3-23; Rice et al., 1967, sec. 5.2.2). That is

$$F_{\sigma hd} = \exp(-2\pi\delta), \tag{163}$$

$$F_{\sigma hd} = \begin{cases} 0.01 + 9.46\,\delta^2 & \text{if } \delta < 0.00325 \\ 6.15\,\delta & \text{if } 0.00325 \le \delta \le 0.0739 \\ 0.45 + \sqrt{0.000843 - (\delta - 0.1026)^2} & \text{if } 0.0739 < \delta < 0.1237 \\ 0.601 - 1.06\,\delta & \text{if } 0.1237 \le \delta \le 0.3 \\ 0.01 + 0.875 \exp(-3.88\,\delta) & \text{otherwise} \end{cases} \tag{164}$$

and

$$\delta = \sigma_h \sin(\psi)/\lambda \qquad (165)$$

where σ_h and λ are in the same units, i.e., meters. Figure 21 shows surface roughness factors versus δ. Wavelength can be obtained from frequency via (7) and methods for estimating ψ have been provided; e.g., (40), (48), (70), (81) and (102). Estimates of σ_h for various terrain types and sea states are provided in tables 5 and 6.

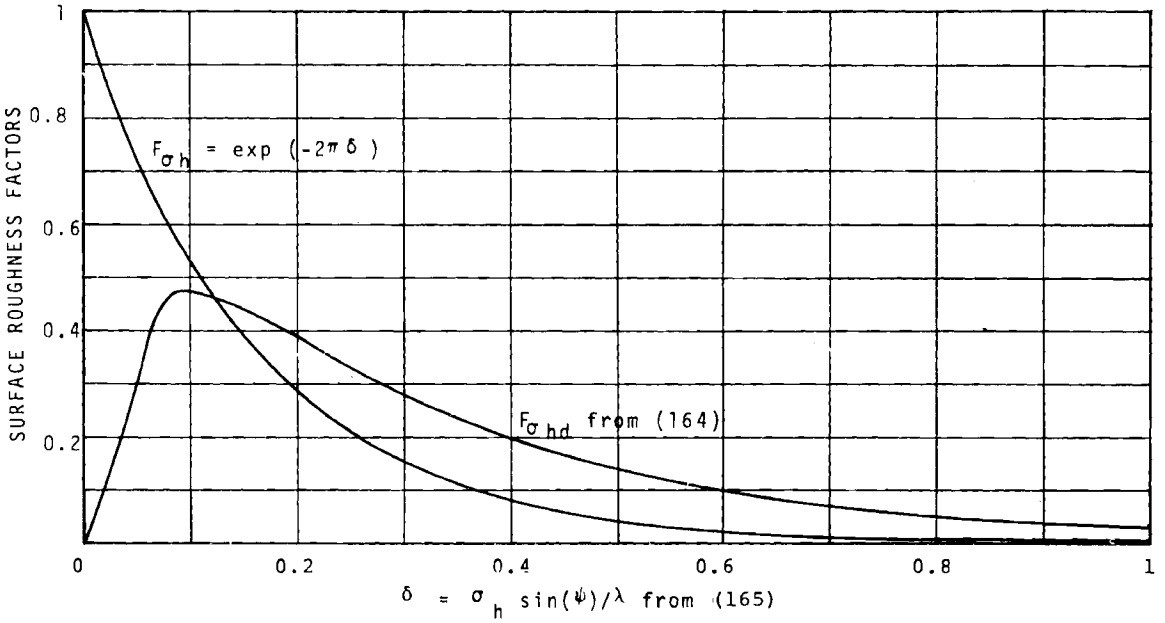

CI-21. Surface roughness factors versus δ.

Table 5. Estimates of σ_h for Terrain Types[a]

Terrain Type	Δh[b] meters (feet)	σ_h[c] meters (feet)
Very smooth plains	0-5 (0-20)	0-1.8 (0-6)
Smooth plains	5-20 (20-70)	1.8-5.4 (6-18)
Slightly rolling plains	20-40 (70-130)	5.4-8.9 (18-29)
Rolling plains	40-80 (130-260)	8.9-14.0 (29-46)
Hills	80-150 (260-490)	14.0-20.3 (46-67)
Mountains	150-300 (490-980)	20.3-29.2 (67-96)
Rugged mountains	300-700 (980-2300)	29.2-41.7 (96-137)
Extremely rugged mountains	>700 (>2300)	>41.7 (>137)

(a) The values given here are based on Longley and Rice (1968), table 1, eqs. 3, 3.6a and 3.6b).

(b) Metric values were converted then rounded to the nearest 10 ft or two significant figures.

(c) Metric values were calculated then rounded to the nearest foot.

Table 6 Estimates of σ_h for Sea States

Sea[a] State Code	Descriptive Terms[a]	Average Wave Height Range m (ft)	$H_{1/3}$[b] m (ft)	σ_h[c] m (ft)
0	Calm (glassy)	0 (0)	0 (0)	0 (0)
1	Calm (rippled)	0 - 0.1 (0 - 0.33)	0.09 (0.3)	0.002 (0.08)
2	Smooth (wavelets)	0.1-0.5 (0.33-1.6)	0.43 (1.4)	0.11 (0.35)
3	Slight	0.5-1.25 (1.6-4.0)	1 (3.3)	0.25 (0.82)
4	Moderate	1.25-2.5 (4 - 8)	1.9 (6.1)	0.46 (1.5)
5	Rough	2.5-4 (8-13)	3 (10)	0.76 (2.5)
6	Very Rough	4-6 (13-20)	4.6 (15)	1.2 (3.8)
7	High	6-9 (20-30)	7.9 (26)	2 (6.5)
8	Very high	9-14 (30-46)	12 (40)	3 (10)
9	Phenomenal	>14 (>46)	>14 (>45)	3.3 (11)

(a) Based on international meteorological code (Naval Weather Service, 1972, code 3700)

(b) Estimated significant wave heights (average of highest 1/3), $H_{1/3}$, data from Sheets and Boatwright (1970, Table 1).

(c) Estimated using a formulation provided by Moskowitz (1964, eq 1) with $H_{1/3}$ estimates.

The σ_h values provided in table 5 are based on a relationship between the terrain parameter Δh and σ_h developed by Longley and Rice (1968, eqs. 3, 3.6a and 3.6b), i.e.,

$$\Delta h_d = h[1-0.8 \exp(-0.02\, d)] \quad m, \qquad (166)$$

and

$$\sigma_h = \begin{cases} 0.039\, \Delta h_d & \text{if } \Delta h_d \leq 4 \\ 0.78\, \Delta h_d \exp[-0.5(\Delta h_d)^{1/4}] & \text{otherwise} \end{cases} \quad m \qquad (167)$$

where d is path length in kilometers. In using (167) to provide values for table 1, d was assumed to be large enough that $\Delta h_d \cong \Delta h$. Longley and Rice (1968, table 1) was used to relate Δh to terrain types. Values for Δh can also be obtained from path profile data (Longley and Rice, 1968, annex 2). In accordance with Longley and Rice (1968, p. 3-23) Δh and Δh_d are defined as follows:

Δh — an asymptotic value of Δh which is is used to characterize terrain.

Δh_d — interdecile range of terrain heights above and below a straight line fitted to elevations above sea level.

In figures 22, 23 and 24 various $F_{\sigma h}$ formulations are compared with each other and experimental data. In each case the format was selected to provide easy comparison with

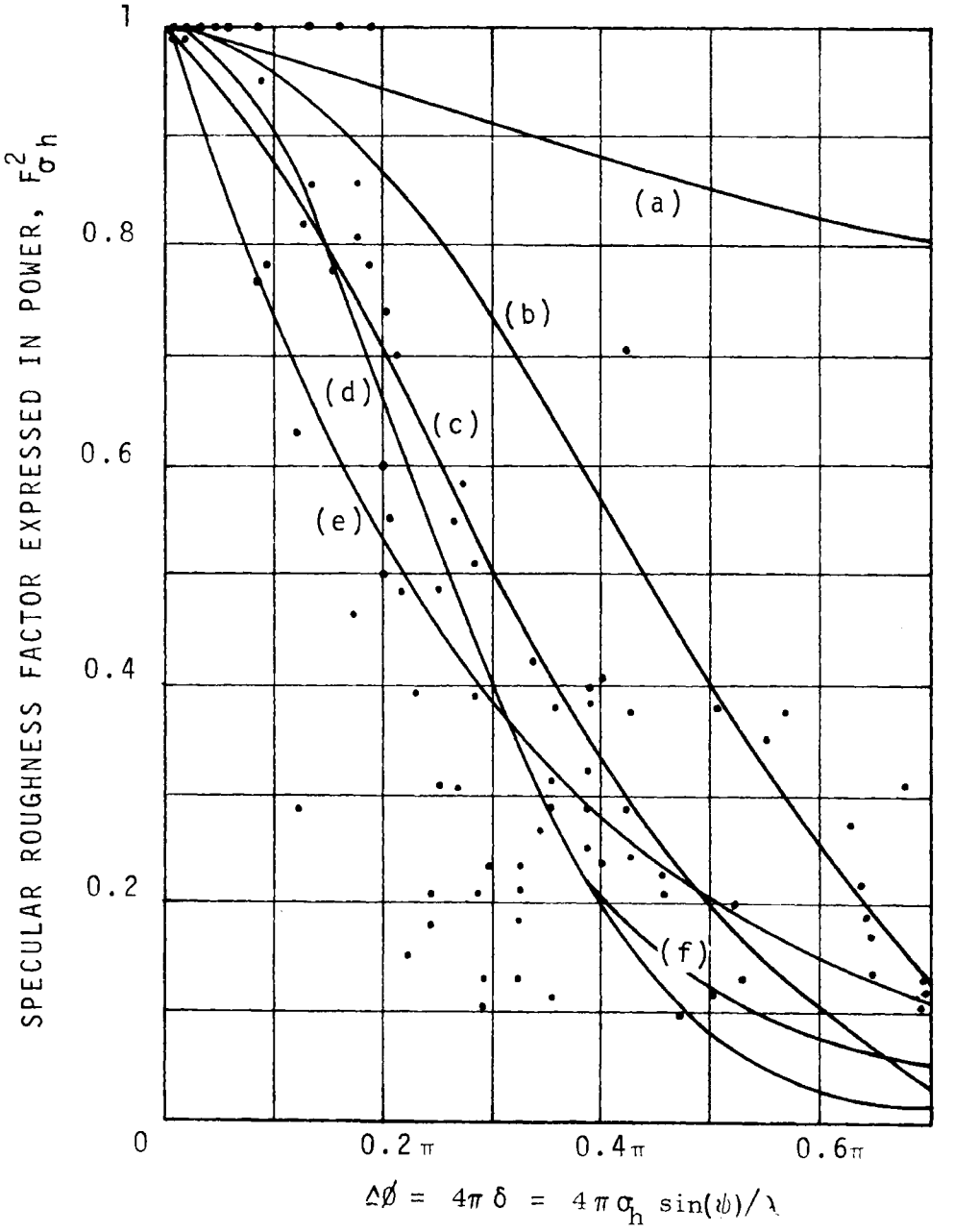

Figure CI-22. Comparison of $F_{\sigma h}$ formulations, Beckmann and Spizzichino (1963, fig. 14.1) data. Formulations are (a) exp (-1.2δ) from Rice et al. (1967, eq. 5.1); (b) $[\sin(\Delta\phi)/\Delta\phi]^2$ for uniformly distributed surface; (c) $(1-\Delta\phi/\pi)\ [\sin(\Delta\phi)/\Delta\phi]^2$ for first Fresnel zone of a uniformly distributed surface; (d) exp $(-\Delta\phi)^2$ for a normally distributed surface; (e) exp $(-\Delta\phi)$ from Longley and Rice (1968, eq. 3.5), also $(F_{\sigma h})^2$ from (163); and (f) a curve fit to data by Beard (1961, fig. 2). Equations used for (b), (c) and (d) were obtained from Beckmann and Spizzichino (1963, fig. 12.1).

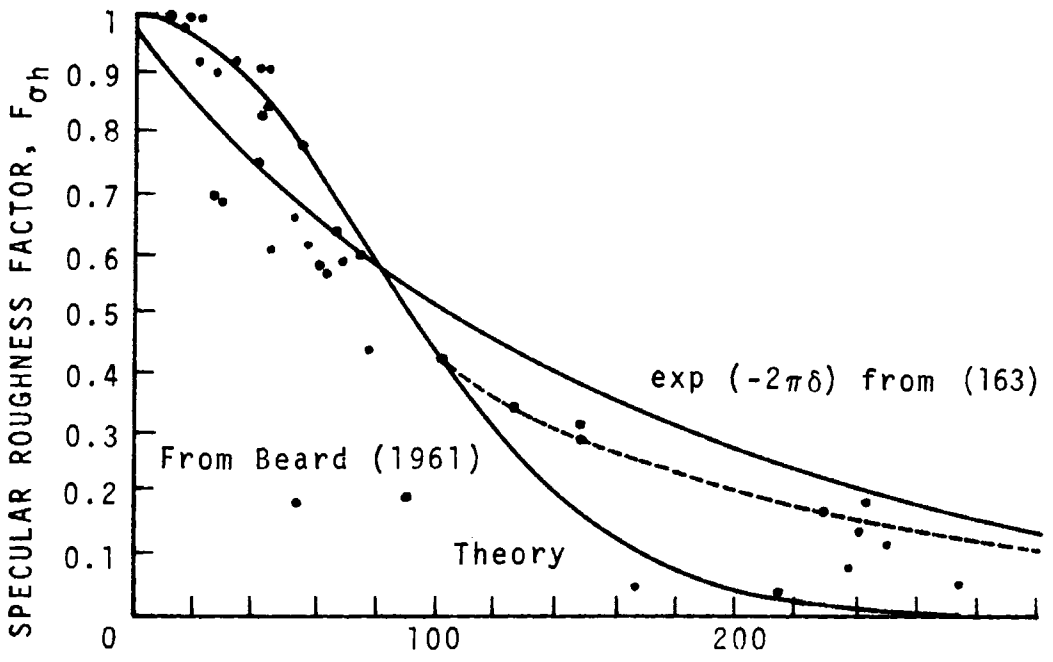

Figure CI-23. Comparison of $F_{\sigma h}$ formulations, Beard (1961, fig. 2).

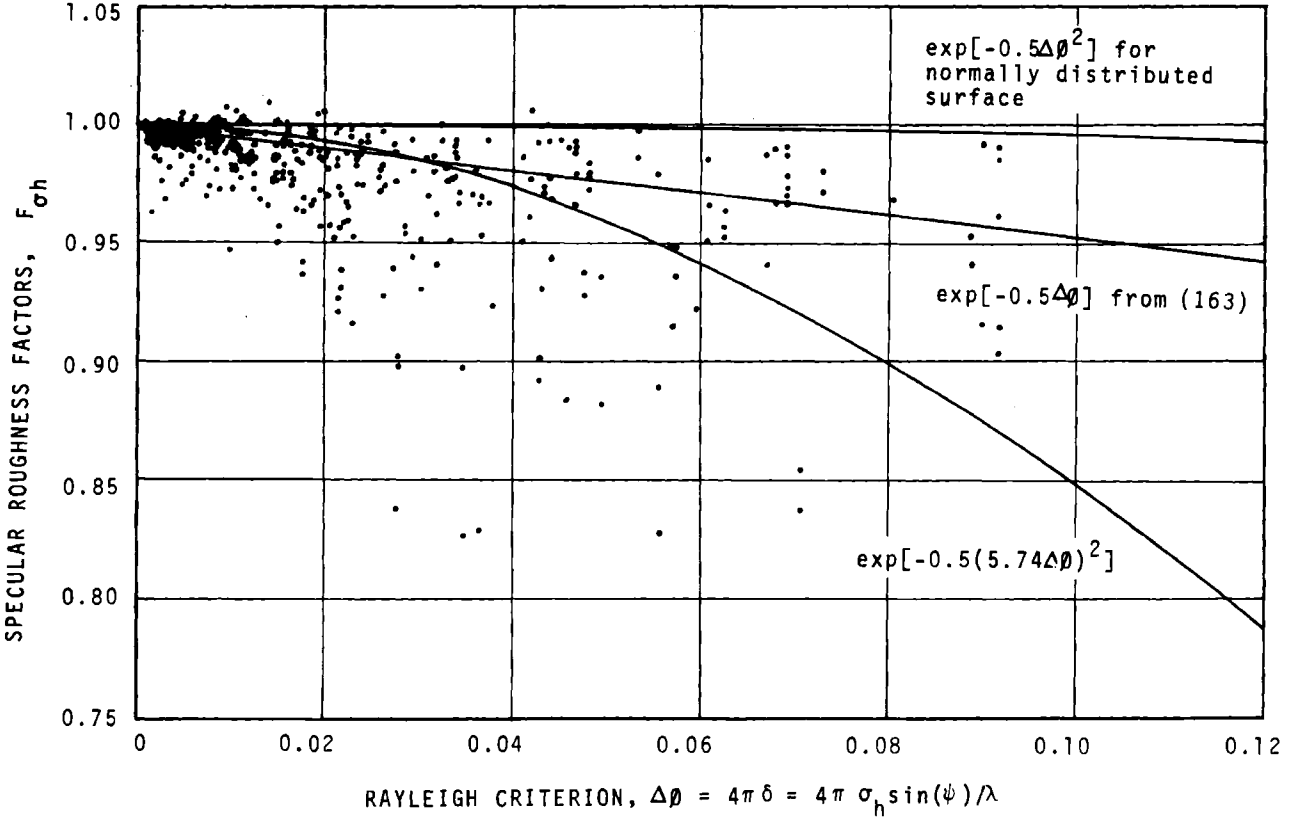

Figure CI-24. Comparison of F_{σ_h} formulations Montgomery (limited distribution ESSA Tech. Memo. ERLTM-ITS 158, "A note on selected definitions of effective antenna heights," Jan. 1969).

the data given in the source document. Figure 25 shows a comparison of $F_{\sigma hd}$ obtained using (164) with data presented by Beard (1961, fig. 4). Since (164) is largely based on a curve fit to Beard's empirical curve the agreement shown in the figure is as expected. From these figures it is obvious that significant deviations from predicted values can occur. Both roughness factors should be considered as estimated rms values.

Values for σ_h provided in table 6 were estimated using significant wave height, $H_{1/3}$ m, estimates from Sheets and Boatwright (1970, table 1) with a formulation given by Moskowitz (1964, eq. 1); i.e.,

$$\sigma_h = 0.25\ H_{1/3} \quad \text{m} \qquad (168)$$

where σ_h and $H_{1/3}$ have the same units.

As an example, $\sigma_h = 0.76$ m (corresponding to slightly rolling plains, table 5, or a rough sea, table 6) $\psi = 5^o$ and $\lambda = 0.1847$ m corresponding to 1600 MHz), when used in (165) yield $\delta = 0.353$. Figure 21 gives $F_{\sigma h} = 0.11$ and $F_{\sigma hd} = 0.23$, and (163) and (164) yield $F_{\sigma h} = 0.1$ and $F_{\sigma hd} = 0.23$, i.e.,

$$(2\pi)\ (0.353) = 2.22$$
$$F_{\sigma h} = \exp(-2.22) = 0.11$$
$$(-3.88)\ (0.353) = 1.37$$
$$\exp\ (-1.37) = 0.254$$
$$F_{\sigma hd} = 0.01 + (0.875)\,(0.254) = 0.23$$

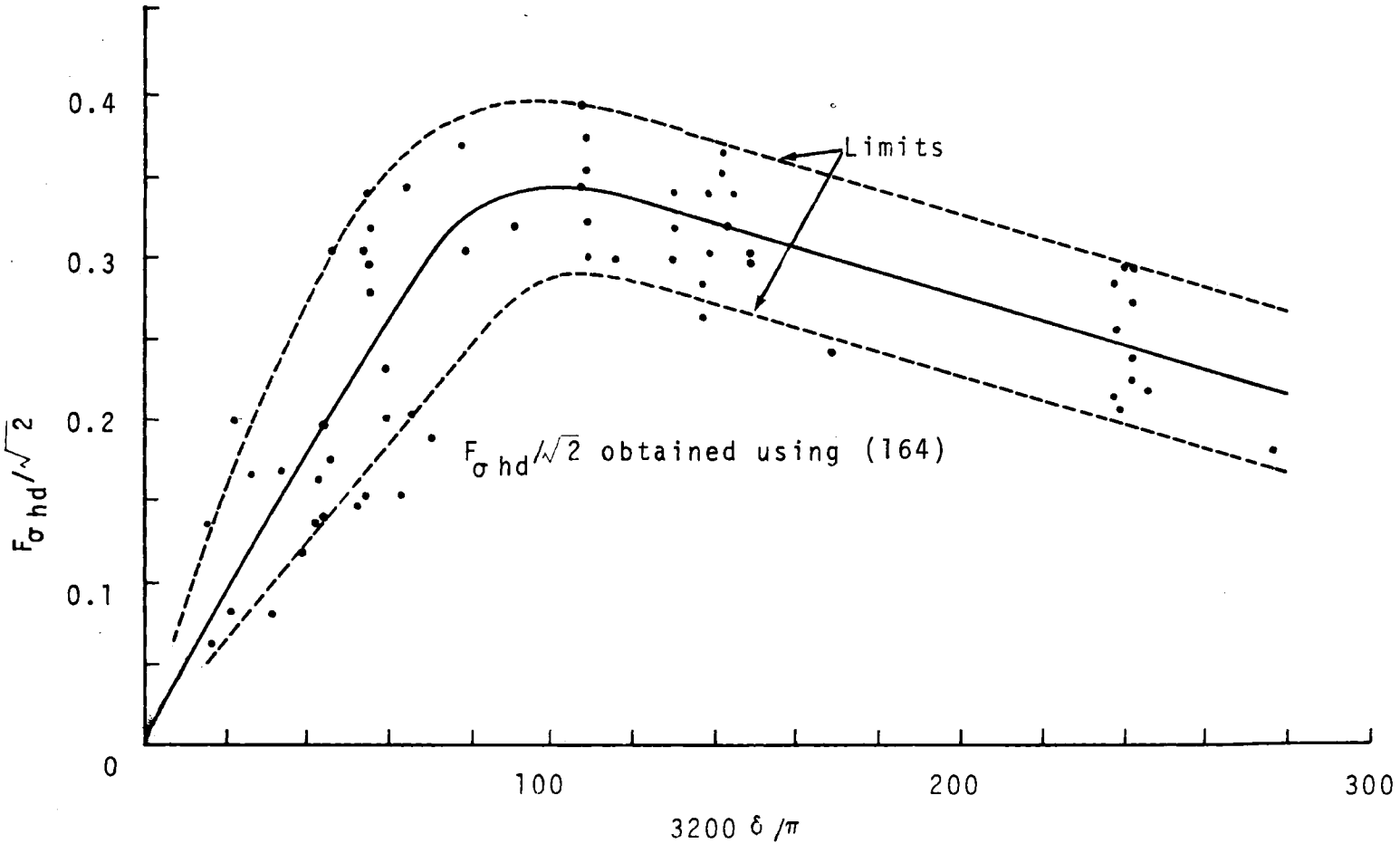

Figure CI-25. Comparison of $F_{\sigma\ hd}$ with data (Beard, 1961, fig. 4)

CI-D.8 Plane Earth Reflection Coefficient

Values for the complex plane earth reflection coefficient, R, used in (132) depend on the relative dielectric constant, ϵ and conductivity, σ mho/m, along with wavelength, λ m, grazing angle, ψ, and polarization (Beckmann and Spizzichino, 1963, p. 219; Kerr, 1964, p. 396; Reed and Russell, 1964, p. 88, and Rice et al., 1967, sec. III.1). For vertical polarization (electric field in the plane of incidence) and horizontal (electric field normal to plane of incidence) R is given by

$$R = R_v \exp -j(\pi - c_v) = \frac{\epsilon_c \sin(\psi) - Y}{\epsilon_c \sin(\psi) + Y} \qquad (169)$$

and

$$R = R_h \exp -j(\pi - c_n) = \frac{\sin(\psi) - Y}{\sin(\psi) + Y} \qquad (170)$$

respectively where

$$Y = \sqrt{\epsilon_c - \cos^2\psi} \qquad (171)$$

and the complex relative dielectric constant, ϵ_c, is defined as

$$\epsilon_c = \epsilon - j\ 1.799 \times 10^4\, \sigma / f \qquad (172)$$

For circular (or elliptical) polarization linear polarization gain factors (sec. CI-D.3) and reflection coefficients are combined, i.e.,

$$R = R_c \exp -j(\pi - c_c) \qquad (173a)$$

or

$$R = 0.5 [F_{hg} R_h \exp -j(\pi - c_h) \pm F_{Vg} R_V \exp -j(\pi - c_V)] \qquad (173b)$$

where "+" is used for antennas with the same polarization sense (e.g., both right-handed) and "-" is used otherwise.

Nominal values for dielectric constant, ϵ, and conductivity, σ, mho/m, are provided in table 7 along with values for water of static dielectric constant, ϵ_s, relaxation time, T μs and ionic conductivity, σ_i. Figures 26 through 29 show complex plane earth reflection coefficients versus the tangent of the grazing angle, ψ, for vertical polarization and figures 30 through 33 show similar information for horizontal polarization.

For a perfect dielectric ($\sigma = 0$ so that $\epsilon_c = \epsilon$) the numerator of (169) will go to zero when $\psi = \psi_B$ where

$$\psi_B = \mathrm{Sin}^{-1} \sqrt{1/(\epsilon + 1)} \qquad (174)$$

so that R =0 for vertical polarization. This critical angle is called the Brewster angle and a similar angle associated with reflection from a surface that has non-zero conductivity is called the pseudo Brewster angle (Rice et al., 1967, sec. III.1). Equation (174) may be used to estimate the pseudo Brewster angle when $\epsilon > 60\lambda\sigma$. Figures

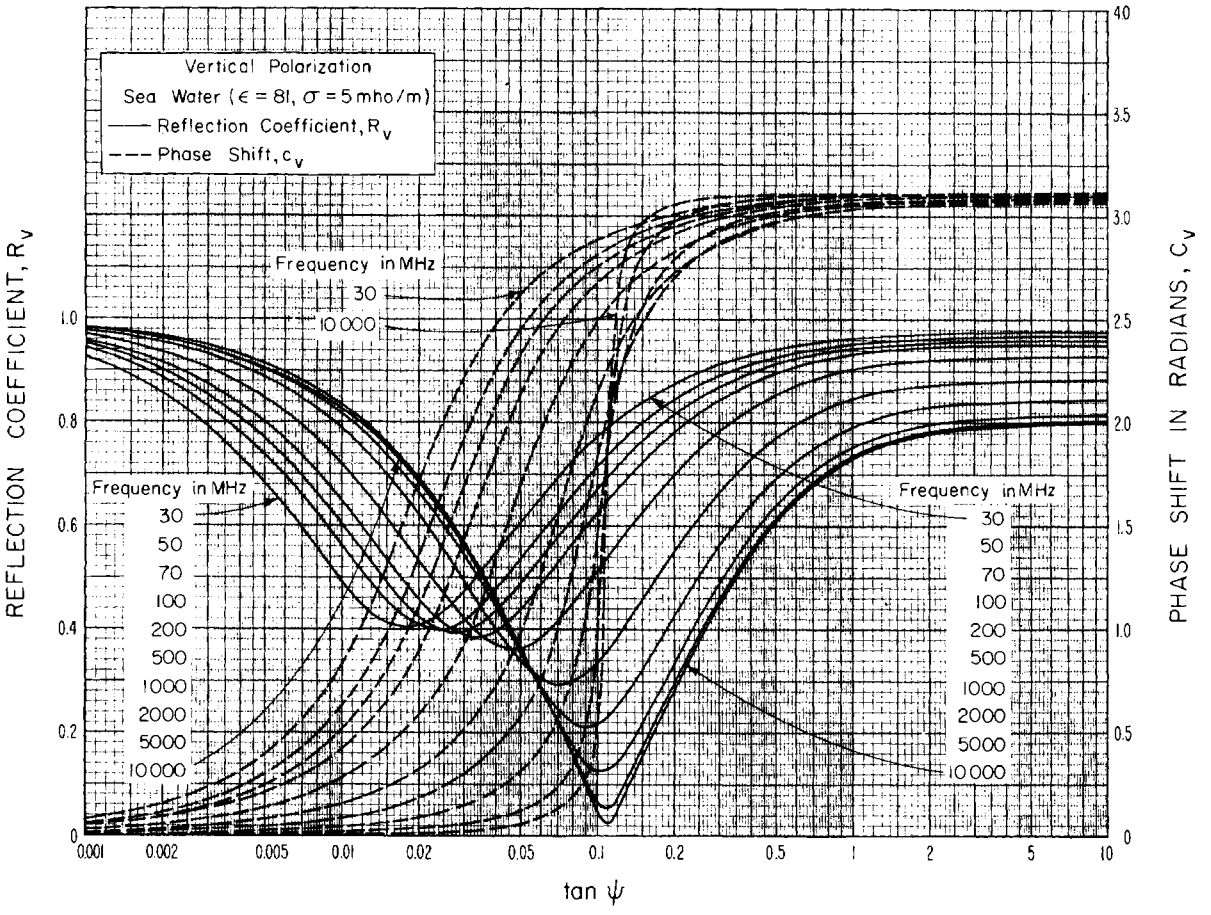

Figure CI-26. Complex plane earth reflection coefficients, $R_v \exp j(\pi - C_v)$ for vertical polarization over sea water.

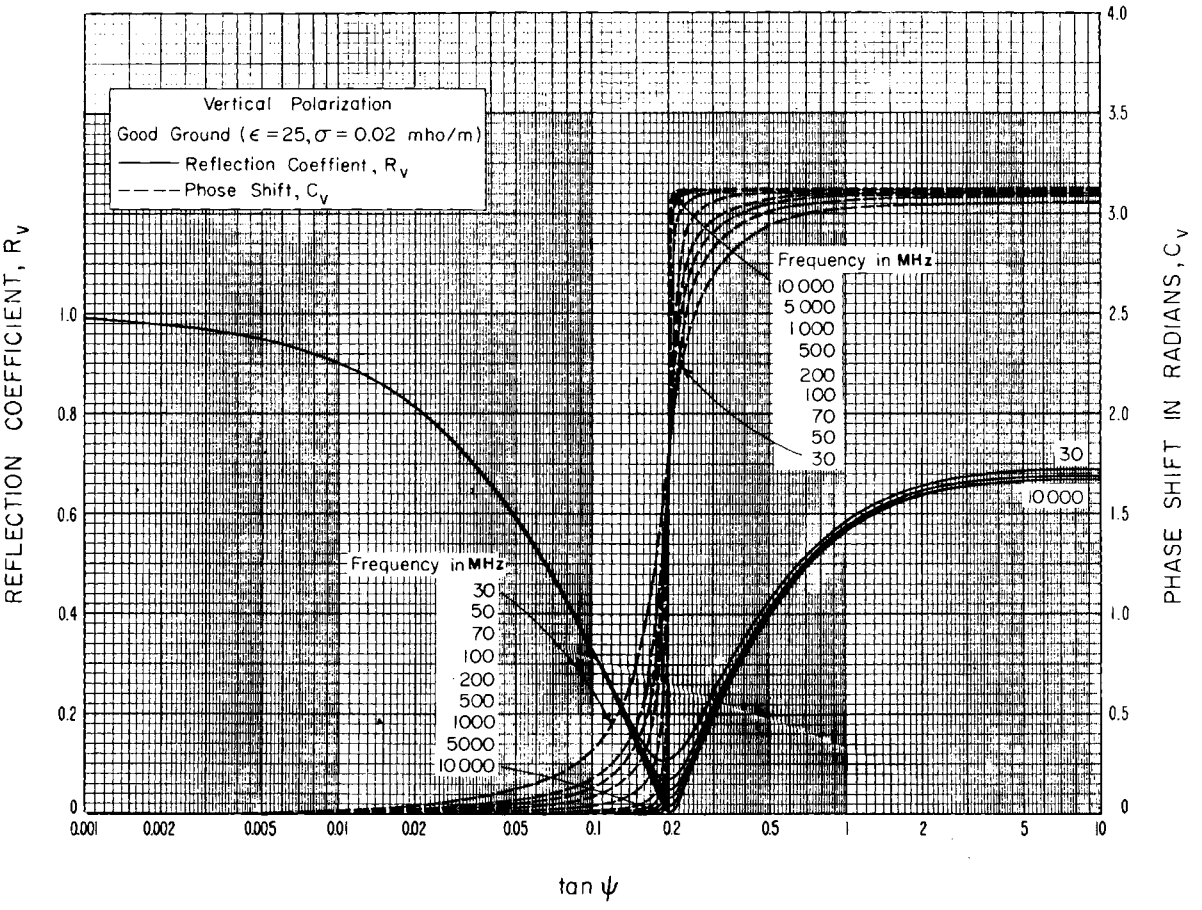

Figure CI-27. Complex plane earth reflection coefficient, $R_v \exp j(\pi - C_v)$ for vertical polarization over good ground.

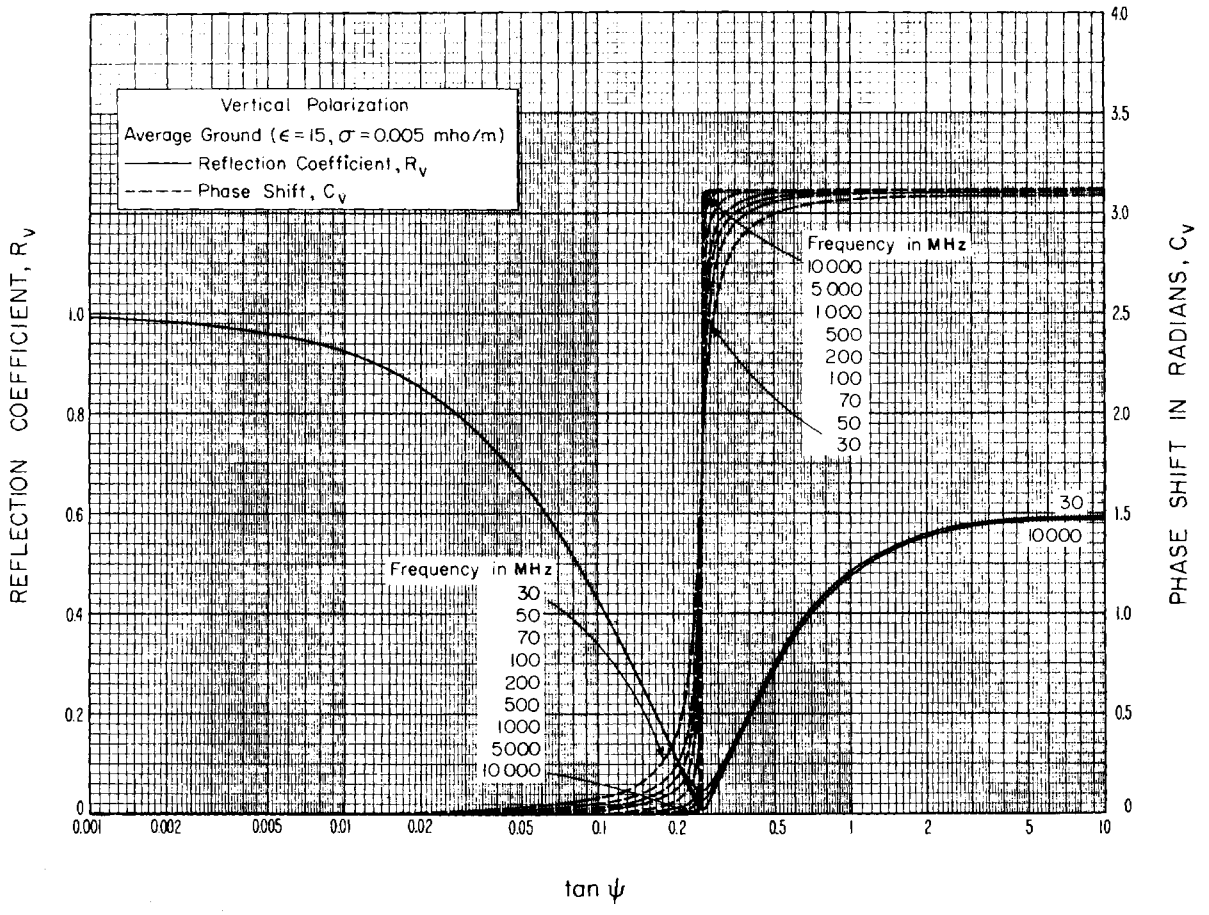

Figure CI-28. Complex plane earth reflection coefficient, $R_v \exp j(\pi - C_v)$ for vertical polarization over average ground

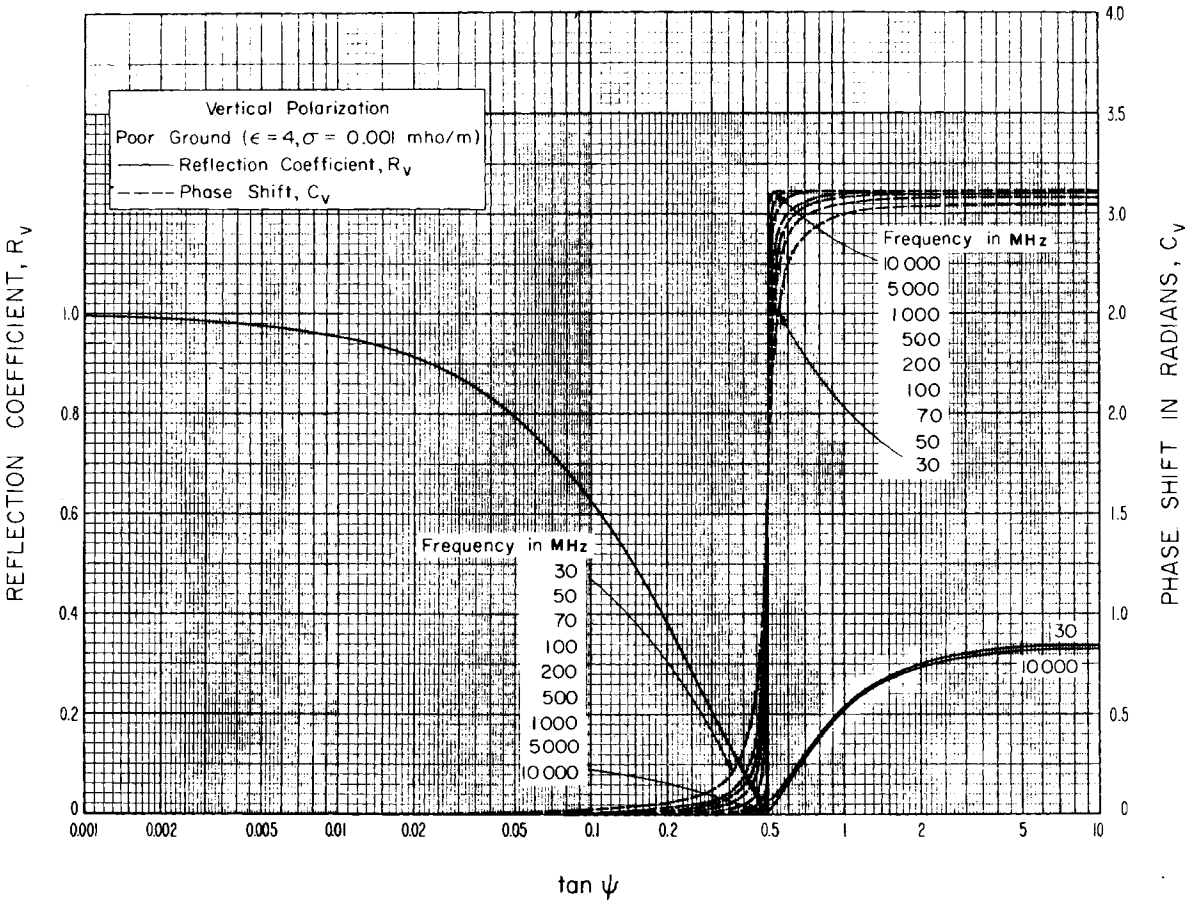

Figure CI-29. Complex plane earth reflection coefficient, $R_v \exp j(\pi - C_v)$ for vertical polarization over poor ground.

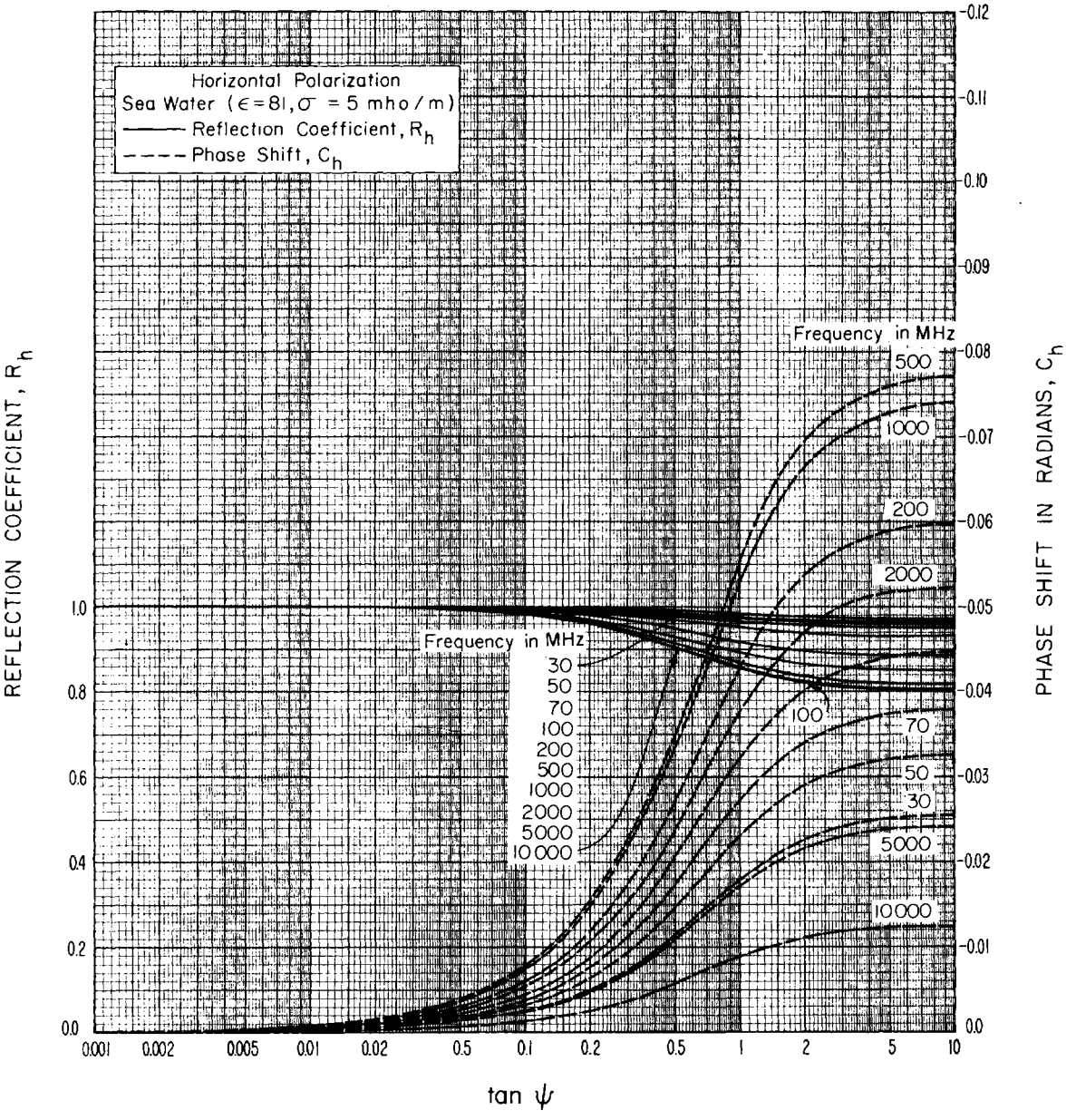

Figure CI-30. Complex plane earth reflection coefficient, $R_h \exp j(\pi - C_h)$ for horizontal polarization over sea water.

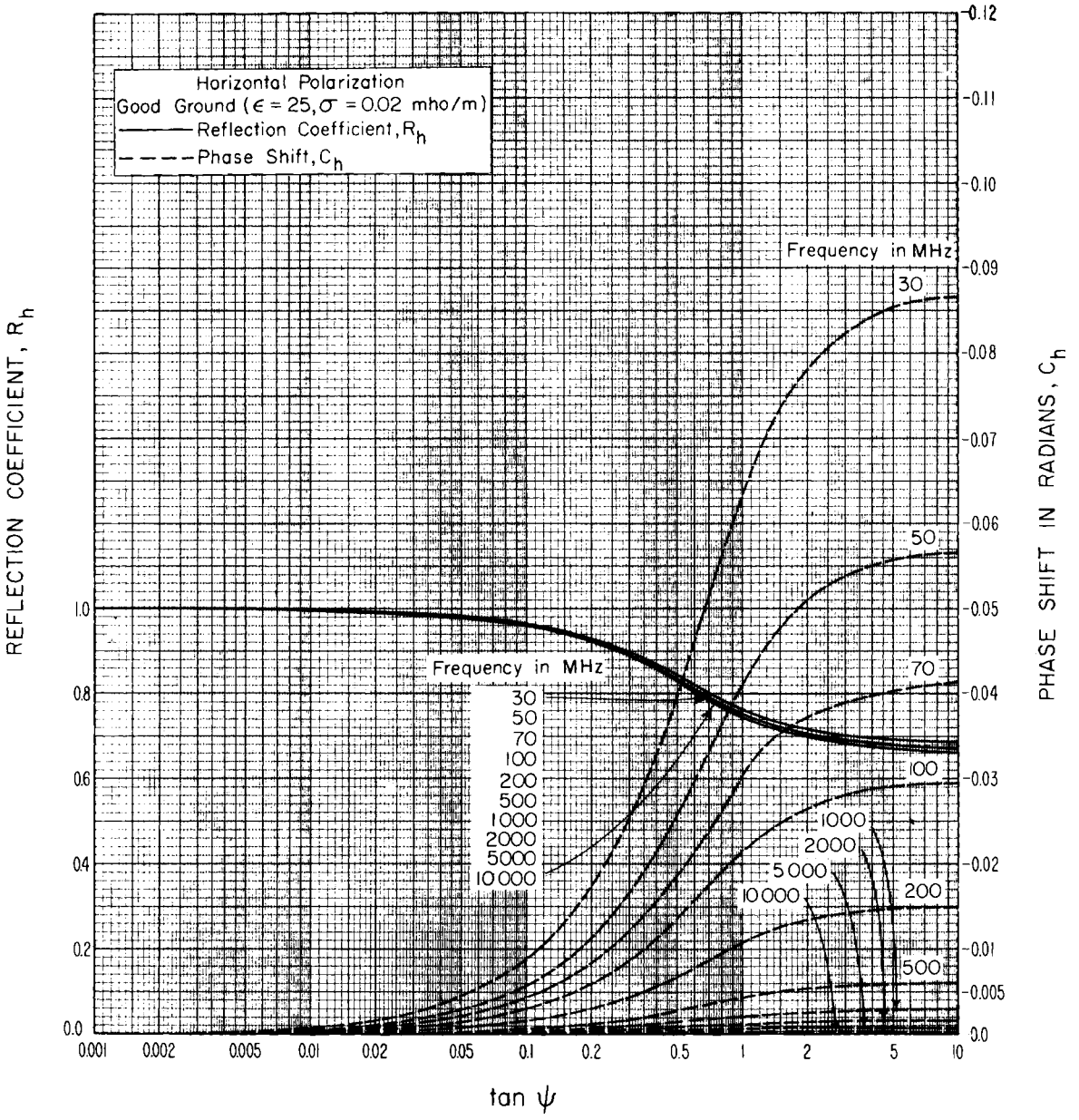

Figure CI-31. Complex plane earth reflection coefficient, $R_h \exp j(\pi - C_h)$ for horizontal polarization over good ground.

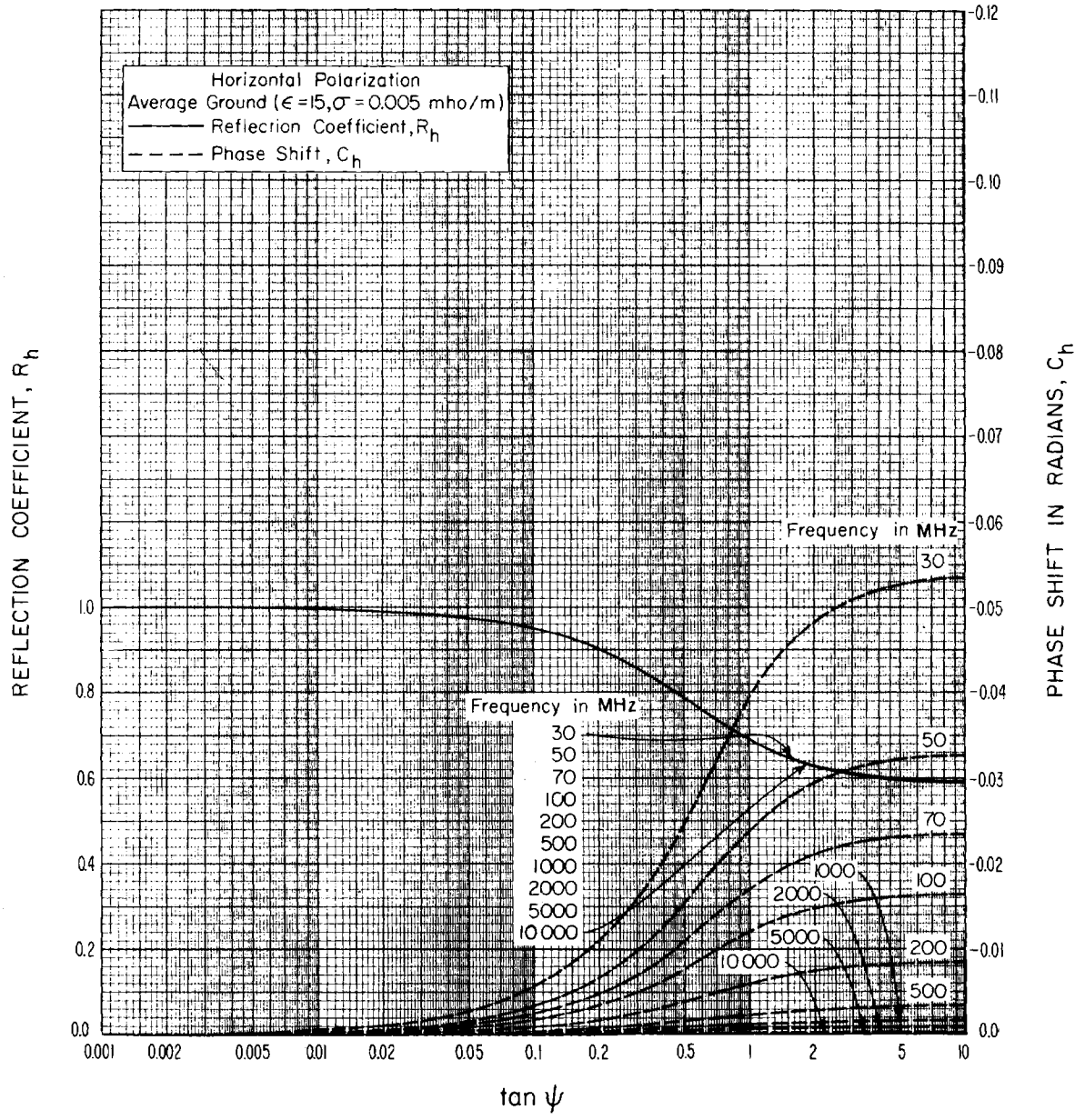

Figure CI-32. Complex plane earth reflection coefficient, $R_h \exp j(\pi - C_h)$ for horizontal polarization over average ground.

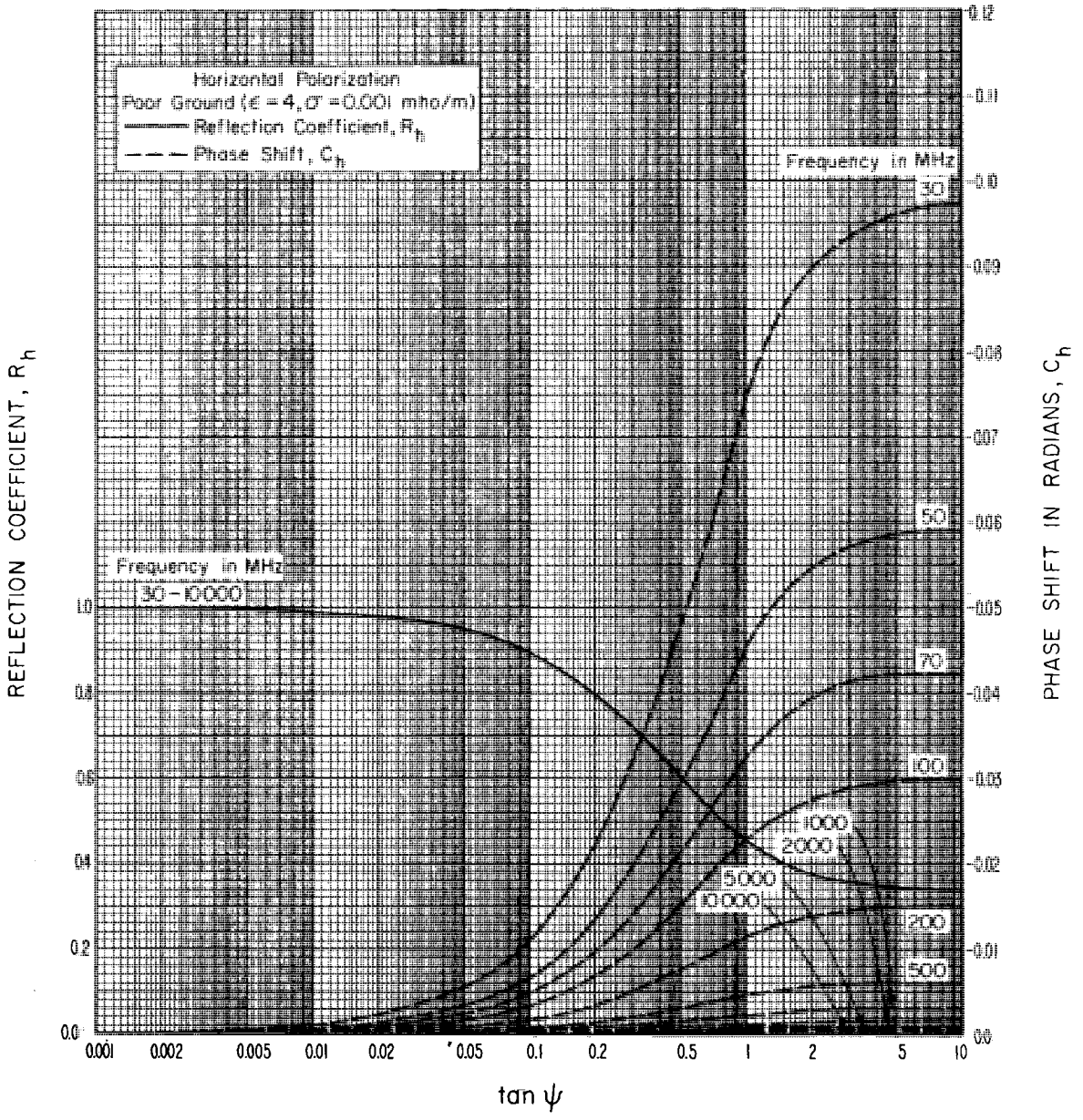

Figure CI-33. Complex plane earth reflection coefficient, $R_h \exp j(\pi - C_h)$ for horizontal polarization over poor ground.

26 through 29 clearly show the dip in the reflection coefficient for vertical polarization associated with the pseudo Brewster angle along with the abrupt change in phase that occurs as ψ goes through its critical value. This change in phase, which does not occur for horizontal polarization, will change the rotation sense of circularly polarized waves that are reflected from the surface; i.e., when a circularly polarized wave is reflected its rotation sense will remain unchanged only if the grazing angle is less than the pseudo Brewster angle.

For water ϵ and σ may be estimated from (Saxton and Lane, 1952).

$$\epsilon = \frac{\epsilon_s - \epsilon_0}{1 + (2\pi ft)^2} + \epsilon_0 \qquad (175)$$

and

$$\sigma = f^2 T(\epsilon - \epsilon_o)/2863 + \sigma_i \text{ mho/m} \qquad (176)$$

where ϵ_s is the static dielectric constant, $\epsilon_0 = 4.9$ is the dielectric constant representing the sum of electronic and atomic polarizations, f MHz is frequency, T μs is relaxation time, and σ_i mho/m is the ionic conductivity. Values of ϵ_s, T, and σ_i obtained using Saxton and Lane (1952) are provided in table 7 for fresh water and sea water.

Table 7. Surface Types and Nominal Constants

Surface Type	ϵ	σ mho/m
Poor Ground	4	0.001
Average Ground	15	0.005
Good Ground	25	0.02
Fresh Water	81	0.01
Sea Water	81	5
Concrete	5	0.01
Metal	1	10^6

For Fresh Water

	0°C	10°C	20°C
ϵ_s	88	84	80
$T\mu s$	1.87×10^{-5}	1.36×10^{-5}	1.01×10^{-5}
σ_i mho/m	0.01	0.01	0.01

For Sea Water

	0°C	10°C	20°C
ϵ_s	75	72	69
$T\mu s$	1.69×10^{-5}	1.21×10^{-5}	9.2×10^{-6}
σ_i mho/m	3.0	4.1	5.4

Figures 34 and 35 show ϵ and σ for water versus frequency, respectively. Reflection coefficients for water are shown in figure 36 for vertical polarization and in figure 37 for horizontal polarization.

Table 8 summarizes values obtained using the equations provided in this section for a sample problem.

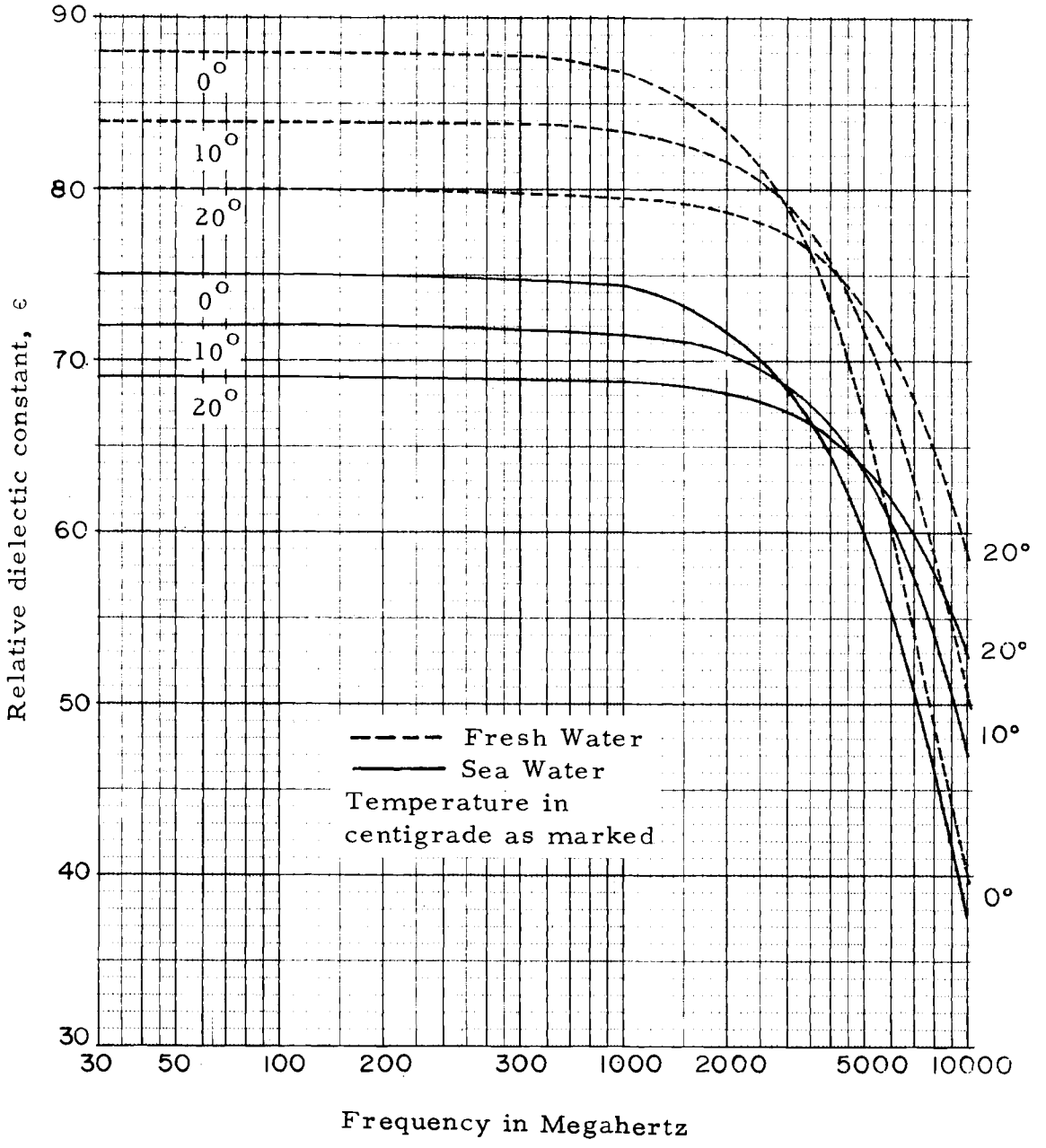

Figure CI-34. Relative dielectric constant for water versus frequency.

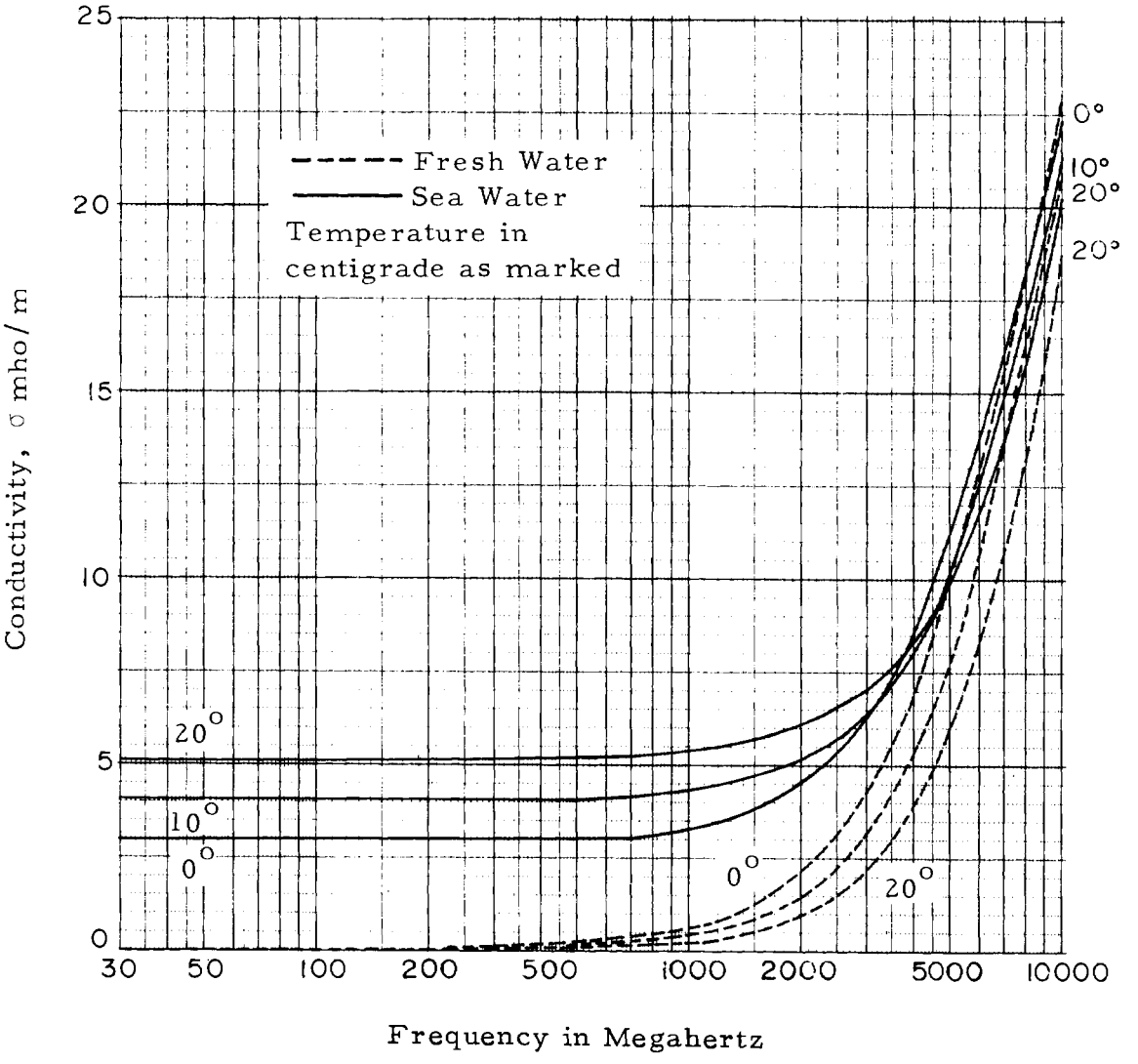

Figure CI-35. Conductivity for water versus frequency.

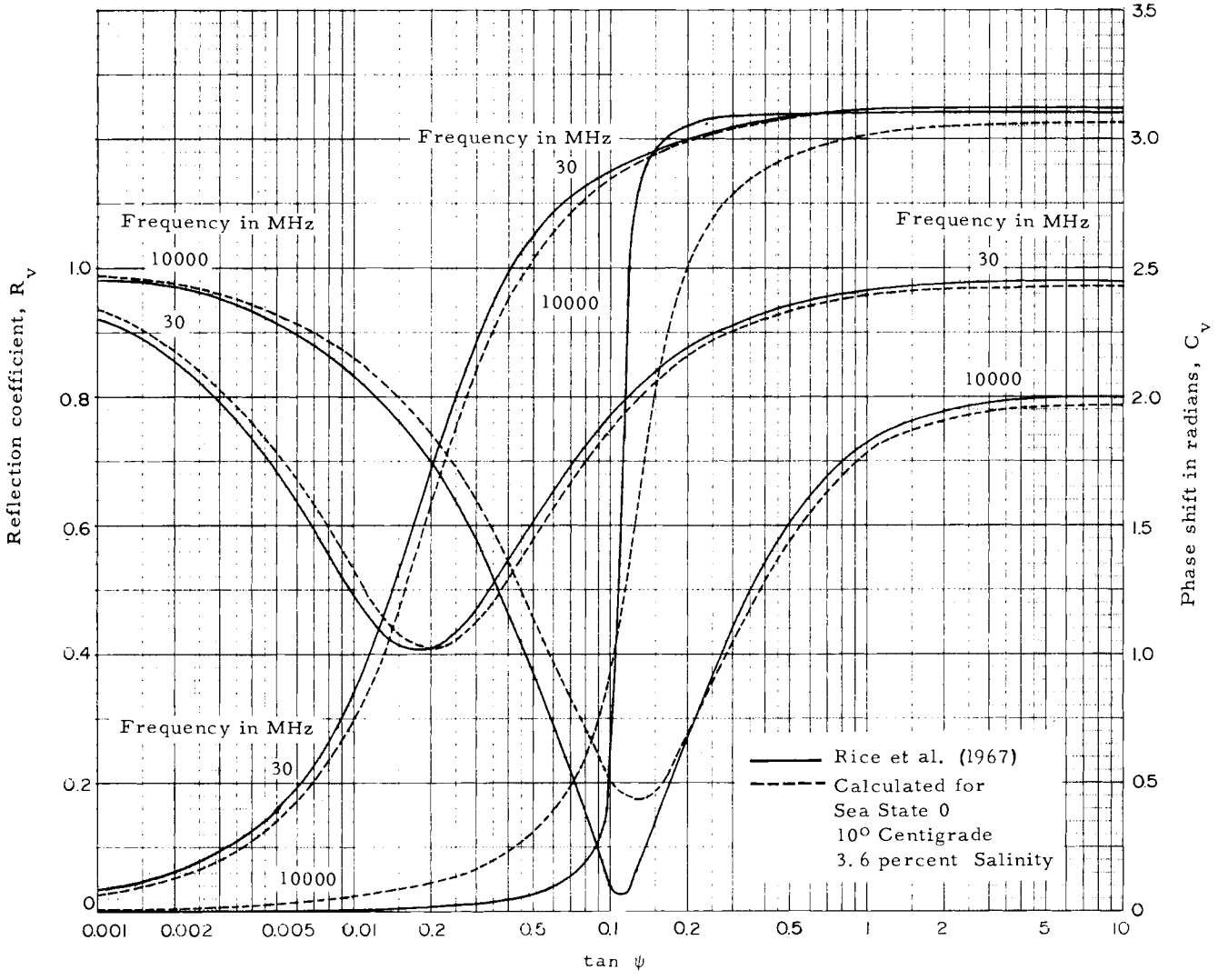

Figure CI-36. Comparison of reflection coefficients for sea water, vertical polarization.

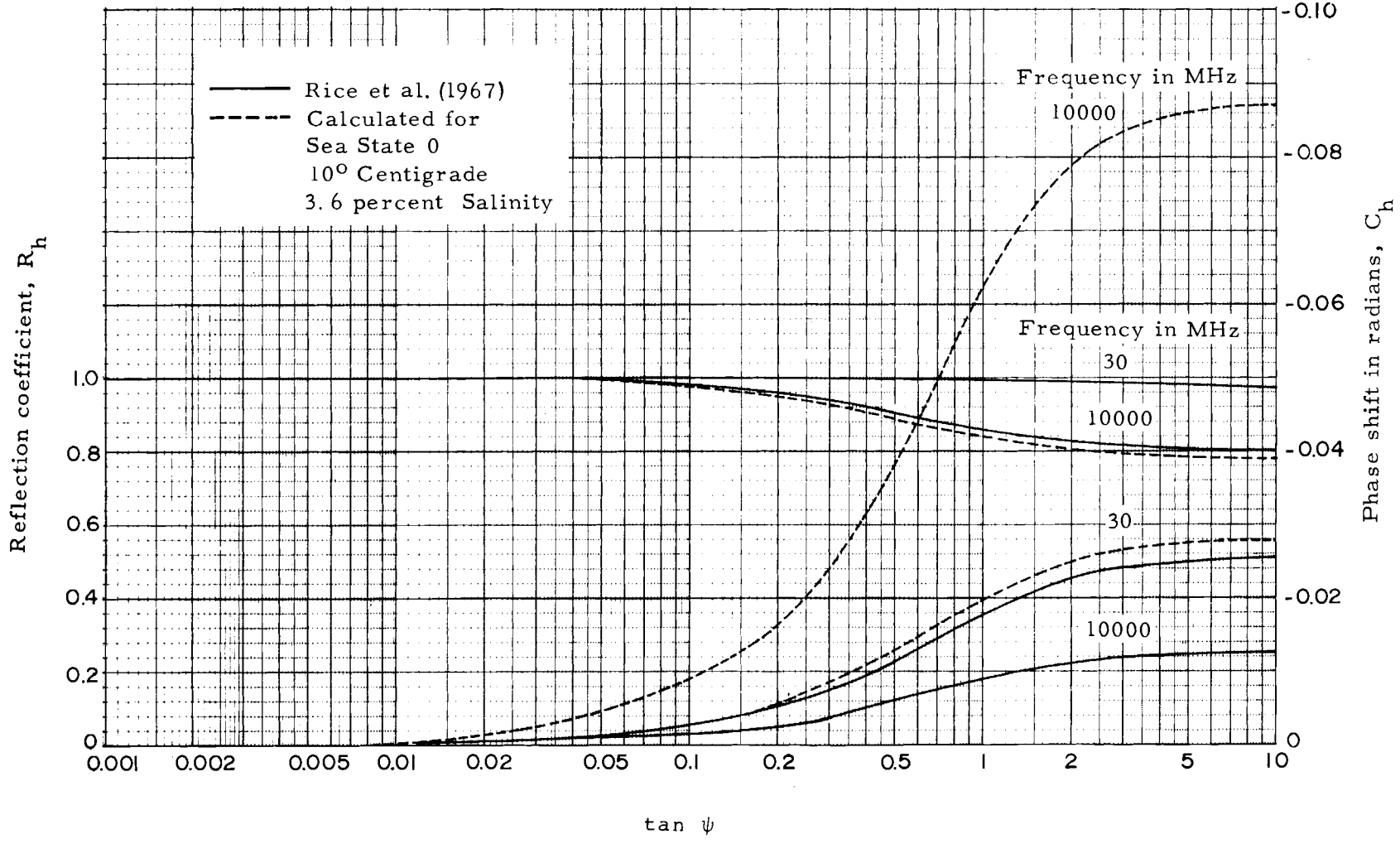

Figure CI-37. Comparison of reflection coefficients for sea water, horizontal polarization.

Table 8. Example, Plane Earth Reflection Coefficient

Given:

Same sense isotropic circularly polarized antennas, a 10°C sea water reflecting surface, f = 10 GHz and $\psi = 11.31°$ ($\tan\psi = 0.2$) define the conditions for these sample calculations of the plane earth reflection coefficient are provided.

Determined:

From table 7: $\epsilon_s = 72$, $T = 1.21 \times 10^{-5}$ μs, and $\sigma_i = 4.1$ mho/m.

From text near table 7: $\epsilon_o = 4.9$, $1 + (2\pi fT)^2 = 1.578$.

From (175): $\epsilon = [(72 - 4.9)/1.578] + 4.9 = 47.42$,

$$Tf^2(\epsilon - \epsilon_o) = 1.21\times10^{-5} \times 10^8(47.42 - 4.9) = 5.145\times10^4$$

From (176): $\sigma = (5.145\times10^4/2863) + 4.1 = 22.07$ mho/m,

$$1.799\times10^4\ \sigma/f = 1.799\times10^4(22.07)/10^4 = 39.70$$

From (172): $\epsilon_c = 47.42 - j\,39.70$,

$$\epsilon_c - \cos^2\psi = 47.42 - j\,39.70 - 0.962 = 46.46 - j\,39.70$$
$$= 61.11 \angle -40.51°$$

From (171): $Y = \sqrt{61.11 \angle -40.51°} = 7.817 \angle -20.26°$

$$= 7.333 - j\,2.707$$

$$\epsilon_c \sin\psi = (47.42 - j\,39.70)(0.1961) = 9.299 - j\,7.785$$

$$\epsilon_c \sin(\psi) - Y = 9.299 - j7.785 - 7.333 + j2.707 = 1.966 - j5.078$$
$$= 5.445 \angle -68.84°$$

$$\epsilon_c \sin(\psi) + Y = 9.299 - j7.785 + 7.333 - j2.707 = 16.63 - j10.49$$
$$= 19.66 \angle -32.24°$$

$$[\epsilon_c \sin(\psi) - Y]/[\epsilon_c \sin(\psi) + Y] = (5.445/19.66) \angle -68.84° + 32.24°$$
$$= 0.2770 \angle -36.6°$$

From (169): $R_v \exp -j(\pi - c_v) = 0.2770 \angle -36.6°$

$$= 0.2770 \exp -j(\pi - 2.503)$$
$$= 0.2224 - j\,0.1651$$

Table 8. (continued)

$$\sin(\psi) - Y = 0.1961 - 7.333 + j\,2.707 = -(7.137 - j\,2.707)$$

$$= -7.633 \angle -20.77^\circ$$

$$\sin(\psi) + Y = 0.1961 + 7.333 - j\,2.707 = 7.529 - j\,2.707$$

$$= 8.001 \angle -19.78^\circ$$

$$[\sin(\psi) - Y]/[\sin(\psi) + Y] = (-7.633/8.001) \angle -20.77^\circ + 19.78^\circ$$

$$= -0.9540 \angle -0.99^\circ$$

From (170): $R_h \exp -j(\pi - c_h) = -0.9540 \angle -0.99^\circ$

$$= 0.9540 \exp -j(\pi - 0.01728)$$

$$= -0.9539 + j\,0.01648$$

$$F_{hg} R_h \exp -j(\pi - c_h) + F_{vg} R_v \exp -j(\pi - c_v)$$

$$= (1)(-0.9539 + j\,0.01648) + (1)(0.2224 - j\,0.1651)$$

$$= -0.7315 - j\,0.1486$$

$$= -0.7464 \angle 11.48^\circ$$

From (173): $R = (0.5)(-0.7464 \angle 11.48^\circ)$

$$= -0.3732 \angle 11.48^\circ$$

$$= 0.3732 \exp -j(\pi - 0.2004)$$

Angle to exp $-j(\pi - c)$ conversions are made as follows:

Vertical polarization:

$$\angle -36.6^\circ => -\pi 36.6/180 \text{ rad} = -(\pi - c_v) = c_v - \pi$$

$$c_v = \pi(-36.6/180 + 1) = 2.503 \text{ rad}$$

Horizontal polarization:

$$-\angle -0.99^\circ => \pi(1 - 0.99/180) = c_h - \pi$$

$$c_h = 2\pi - (0.99/180)\pi$$

Drop the 2π.

$$c_h = -(0.99/180)\pi = -0.01728 \text{ rad}$$

Circular polarization:

$$-\angle 11.48^\circ => \pi(1 + 11.48/180) = c_c - \pi$$

$$c_c = 2\pi + (11.48/180)\pi$$

Drop 2π.

$$c_c = 0.2004 \text{ rad}$$

CI-E. REFERENCES

ABRAMOWITZ, M., AND I.A. STEGUM (1964),
HANDBOOK OF MATHEMATICAL FUNCTIONS,
NBS APPL. MATH. SERIES 5-5
(GPO, $6.50)

BEAN, B.R., AND E.J. DUTTON (1966),
RADIO METEOROLOGY,
NBS MONO. 92
(GPO, $2.75)

BEAN, B.R., AND G.D. THAYER (1959),
CRPL EXPONENTIAL REFERENCE ATMOSPHERE,
NATIONAL BUREAU OF STANDARDS, NBS MONOGRAPH NO. 4, OCT., 1959.
(U.S. GOVT. PRINTING OFFICE, WASH. D.C., 20402, PRICE $0.45)

BEARD, C.I. (1961),
COHERENT AND INCOHERENT SCATTERING OF MICROWAVES FROM THE OCEAN
IRE TRANS. ANT. PROP. AP-9 (5), 470-483.

BECKMANN, P. (1965),
SHADOWING OF RANDOM ROUGH SURFACES,
IEEE TRANS. ANT. PROP. AP-13, NO.3, 384-388

BECKMANN, P. AND A. SPIZZICHINO (1963),
THE SCATTERING OF ELECTROMAGNETIC WAVES FROM ROUGH SURFACES,
PERGAMON PRESS, NEW YORK.

DOUGHERTY, H.T. (1967),
MICROWAVE FADING WITH AIRBORNE TERMINALS,
ESSA TECH. REPT. IER58-ITSA55, OCTOBER, 1967.
(U.S. GOVT. PRINTING OFFICE, WASH. D.C. 20402, PRICE 50 CENTS)

GERKS, I.H. (1966),
THEORETICAL ANALYSIS OF MULTIPATH PROPAGATION,
INCLUDED AS ENCLOSURE B IN 'AN INVESTIGATION OF AIRBORNE
MICROWAVE MARCOM RELAY FINAL REPORT,' VOL. 2,
COLLINS RADIO CO.,
(523-055 8526-001A3M SEG WRIGHT PATTERSON AFB)

GIERHART, G.D., AND M.E. JOHNSON (1969),
TRANSMISSION LOSS ATLAS FOR SELECT AERONAUTICAL SERVICE
BANDS FROM 0.125 TO 15.5 GHZ,
ESSA TECH. REPT. ERL 111-ITS 79
(GPO, $1.25)

GIERHART, G.D., AND M.E. JOHNSON (1973),
COMPUTER PROGRAMS FOR AIR/GROUND PROPAGATION AND
INTERFERENCE ANALYSIS, 0.1 TO 20 GHZ,
DOT REPT. FAA-RD-73-103
(NTIS, AD-770 335)

JASIK, H. (1961),
ANTENNA ENGINEERING HANDBOOK
(MC GRAW-HILL, NEW YORK, N.Y.)

KERR, D.E. (1964),
PROPAGATION OF SHORT RADIO WAVES,
M.I.T. RADIATION LABORATORY SERIES 13
(BOSTON TECHNICAL PUBLISHERS, INC., LEXINGTON, MASS.)

LONGLEY, A.G., AND P.L. RICE (1968),
PREDICTION OF TROPOSPHERIC RADIO TRANSMISSION LOSS OVER
IRREGULAR TERRAIN, A COMPUTER METHOD-1968,
ESSA TECH. REPT. ERL 79-ITS 67
(GPO, $0.70)

MONTGOMERY, J.L. (1969),
A NOTE ON SELECTED DEFINITIONS OF EFFECTIVE ANTENNA HEIGHTS
ESSA TECH. MEMO. ERLTM-ITS 158, LIMITED DISTRIBUTION

MOSKOWITZ, L. (1964),
ESTIMATES OF THE POWER SPECTRUMS FOR FULLY DEVELOPED SEAS
FOR WIND SPEEDS OF 20 TO 40 KNOTS,
J. GEOPHYS. RES. 69, NO.24, 5161-5179

NAVAL WEATHER SERVICE COMMAND (1972),
INTERNATIONAL METEOROLOGICAL CODES
(NEWSFD, ASHEVILLE, N.C.)

NORTON, K.A., AND A.C. OMBERG (JAN. 1947),
THE MAXIMUM RANGE OF A RADAR SET,
PROC. IRE 35, NO. 1, 4-24

NORTON, K.A., L.E. VOGLER, W.V. MANSFIELD,
AND P.J. SHORT (1955),
THE PROBABILITY DISTRIBUTION OF THE AMPLITUDE OF A CONSTANT
VECTOR PLUS A RAYLEIGH-DISTRIBUTED VECTOR,
PROC. IRE 43, NO. 10, 1354-1361

REED, H.R., AND C.M. RUSSELL (1964),
ULTRA HIGH FREQUENCY PROPAGATION
(BOSTON TECHNICAL PUBLISHERS, INC., LEXINGTON MASS. 02173)

RIBLET, H.J., AND C.B. BARKER (1948),
A GENERAL DIVERGENCE FORMULA,
J. APPL. PHYSICS 19, 63-70

RICE, P.L., A.G. LONGLEY, K.A. NORTON, AND A.P. BARSIS, (1967),
TRANSMISSION LOSS PREDICTIONS FOR TROPOSPHERIC COMMUNICATIONS
CIRCUITS,
NBS TECH. NOTE 101, VOLS. 1 AND 2
(NTIS, AD 687 820 AND AD 687 821)

SANCER, M.I. (1969),
SHADOW-CORRECTED ELECTROMAGNETIC SCATTERING FROM A RANDOMLY
ROUGH SURFACE,
IEEE TRANS. ANT. PROP. AP-17, NO. 5, 577-585

SAXTON, J.A. AND J.A. LANE (1952),
ELECTRICAL PROPERTIES OF SEA WATER,
WIRELESS ENGR. 29, 269-275.

SHEETS, H.E., AND V.T. BOATWRIGHT, JR. (1970),
HYDRONAUTICS,
(ACADEMIC PRESS, NEW YORK, N.Y.)

SMITH, B.G. (1967),
GEOMETRICAL SHADOWING OF A RANDOM ROUGH SURFACE,
IEEE TRANS. ANT. PROP. AP-15, NO.5, 668-671

VAN DER POL, BALTH., AND H. BREMMER (1939),
FURTHER NOTE ON THE PROPAGATION OF RADIO WAVES
OVER A FINITELY CONDUCTING SPHERICAL EARTH,
PHIL. MAG. 27, 261-275

CII COMPUTER PROGRAM "LOBING OVER SPHERICAL EARTH"

CII-A. INTRODUCTION

A propagation model for two-path multipath (direct and reflected) over a spherical earth based on the formulations previously described (secs. CI-B.1, CI-B.2, and CI-C) has been incorporated into a computer program. This program is written in FORTRAN for a digital computer (CDC 3800) at the Department of Commerce Laboratories, Boulder, Colorado. Since it utilizes the cathode ray tube microfilm plotting capability at the Boulder facility, substantial modification would have to be made for operation at any other facility. Average running time is a few seconds per set of input parameters. Information on input parameter requirements and output produced is provided in sections CII-B and CII-C, respectively.

The computer program, "LOBING," is similar to the power density program described by Gierhart and Johnson (1973). Their program provides statistical information on propagation for a wider variety of propagation paths in that it is not limited to line-of-sight propagation over a spherical earth. However, program LOBING provides more

information relevant to the lobing structure associated with two-path multipath over a spherical earth.

CII-B INPUT PARAMETERS

The computer program may be operated with nine or more separate model parameters specified. Most parameters not specifically specified as input will be set to initial conditions incorporated into the program or estimated from parameters that are specified. However, three primary parameters must be specified by the user. These are facility antenna height, frequency, and aircraft altitude. Parameters that may be specified as input are summarized in table 1 along with the acceptable value range (or options available), and the value (or option) selected in lieu of a specified parameter. For convenience, parameters are listed in table 1 in the same order as the parameter sheet produced by the computer (fig. 3). Graph format parameters (lower portion of table 1) are not reproduced on the parameter sheet. Sample graphs are provided in section CII-C.

Blank spaces are provided in table 1 so that copies of it can be used to specify input requirements for program

Table 1. Parameter Specification[a]

Parameter	Range	Value
Primary Parameters, Specification Required		
Aircraft altitude above mean sea level (msl)	Elevation facility antenna and 300,000 ft-msl	_____ ft-msl
Facility antenna height above (msl)	1.5 ft and 2,000 ft-msl	_____ ft-msl
Frequency	100 to 20,000 MHz	_____ MHz
Secondary Parameters, Assumed, Computed, Estimated, or Specified		
Absorption (at surface): Oxygen options	Calculated* or specified	_____ dB/km
Water vapor options	Calculated* or specified	_____ dB/km
Effective altitude correction factor options	Via ray tracing* or specified	_____ ft
Effective reflection surface elevation above msl	At msl* or specified <facility antenna elevation	_____ ft-msl
Facility antenna type options	JTAC directive isotropic*, or specified	_____
Main beam gain	to 60 dB[b]	_____ dB
Polarization options	Horizontal* or vertical	_____
Refractivity: Effective earth's radius[b]	4240 to 6070 n mi[b]	_____ n mi
or minimum monthly mean (msl)[b]	250 to 400 N-units (301 N-units)*	_____ N-units
Spectral parameters: Bandwidth as a fraction of carrier frequency	0 to 0.2	_____
Surface type options	Poor, average* or good ground, fresh or sea water, concrete, metal	_____
Sea state[b]	0-Glassy*, 1-rippled, 2-smooth, 3-slight, 4-moderate, 5-rough, 6-very rough, 7-high, 8-very high, 9-phenomenal	_____
or rms wave height[b]	0 to 50 m	_____ m
Temperature[b]	0, 10*, or 20°C	_____ °C
Terrain Parameter, Δh	0* or greater	_____ ft

Graph options (check graphs desired); Lobing _____; Reflection coefficient _____; Path length difference _____; Time delay _____; Normalized distance lobing frequency _____; Normalized height lobing frequency _____; Reflection point _____; Elevation angle _____; Elevation angle difference _____; Spectral point _____.

Range of Parameters for Graph Formats

	Ordinate				Abscissa			
	Lower	Upper	Increment	Units	Left Side	Right Side	Increment	Units
Lobing				dB				n mi
Reflection coefficient								n mi
Path length difference				m				n mi
Time delay				nsec				n mi
Normalized lobing frequency with distance				Hz/THz-Kt				n mi
Normalized lobing frequency with height				Hz/THz-ft/min				n mi
Reflection point				n mi				n mi
Elevation angle				deg				n mi
Elevation angle difference				deg				n mi

Spectral plot lobe _____ to lobe _____, counting from the horizon

(a) Copies of this table may be used to provide data for computer runs by utilizing the blanks provided in the value column. The units of measure following each blank will be assumed for the values placed in the blanks if other units are not provided.

(b) Specification of this parameter is conditional, see text.

(*) Values or options that would be assumed when specific designations are not made are flagged by asterisks.

runs. The units of measure following each blank are the units that will be assumed for values placed in the blanks if other units are not provided. Where values (or options) are not specified, the values (or options) marked by asterisks will be used. Parameters listed in the table are discussed below.

Aircraft Altitude

As shown in figure 1, this altitude is measured above mean sea level. The propagation model is not valid for antennas located below the surface, or if the aircraft

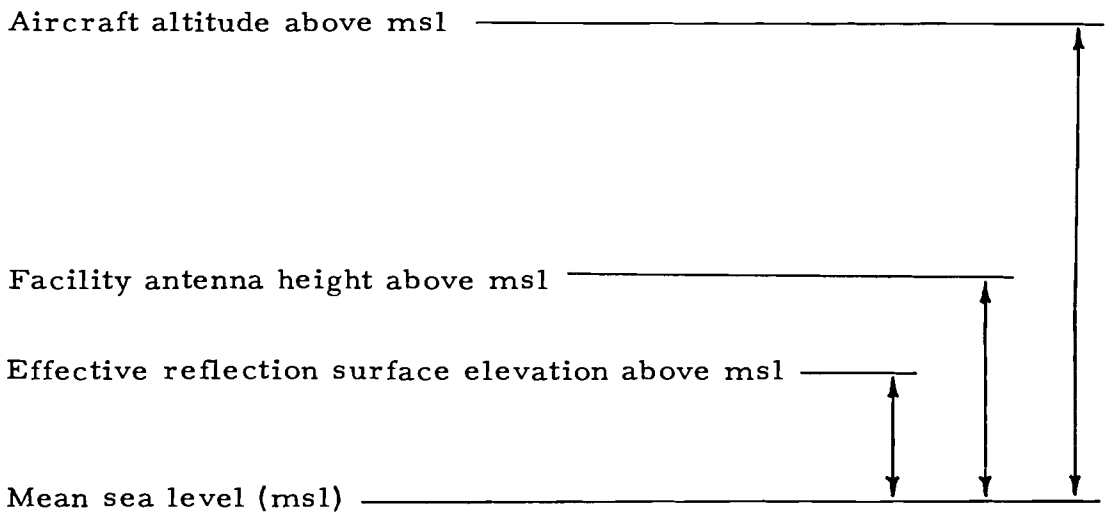

Figure CII-1. Antenna heights and surface elevations.

altitude is (a) less than the facility antenna elevation above msl; (b) less than 1.5 ft where surface wave contributions that are not included in the model could become important; (c) less than the effective reflecting surface elevation plus 500 ft, where the model may fail to give proper consideration to the aircraft radio horizon; or (d) greater than 300,000 ft, where ionospheric effects not included in the model may become important. Use of such aircraft heights may give incorrect results.

Facility Antenna Height

As shown in figure 1, this height is measured above msl. The propagation model is not valid for antennas below the effective reflection surface or if the height is (a) less than 1.5 ft, for which surface wave contributions not included in the model could become important, or (b) greater than 9,000 ft, for which the model may include too much ray bending.

Frequency

Caution should be used if the frequency is (a) less than 100 MHz, when neglected ionospheric effects may become important; (b) greater than 5 GHz, when neglected attenuation and/or scattering from hydrometeors (rain, etc.)

may become important; and (c) greater than 17 GHz, when the estimates made for atmospheric absorption may be inaccurate. For frequencies less than 200 MHz or greater than 100 GHz, the program should be used with extreme caution.

Absorption (at surface) Oxygen and Water Vapor Options

The program will calculate surface oxygen and water vapor absorption rates if values are not specified. These calculations involve interpolation between values taken from Rice et al. (1967, fig. 3.1). Metric units (dB/km) are used for these parameters, since this allows values printed on the parameter sheet to be checked directly against sources of such information (Rice et al., 1967, fig. 3.1; Bean and Dutton (1966), sec. 7.3; Kerr, 1964, ch. 8).

Effective Altitude Correction Factor Options

If not specified, this factor is calculated by ray tracing through a continuous exponential atmosphere (sec. CVI-G; Bean and Dutton, 1966). This factor is used in correcting for the excessive bending associated with the effective earth radius method of ray bending compensation when high (>9,000 ft) antennas are used (fig. CIII-2; Rice et al., 1967). However, values provided by Rice et al.,

(1967, fig. 6.7) are based on ray tracing through a three part atmosphere (Bean and Dutton, 1966, sec. 3.7).

Effective Reflection Surface Elevation Above msl

As shown in figure 1, this elevation is measured above msl. If not specified, it will be taken as msl. This factor is used when the terrain from which reflection is expected is not at msl.

Facility Antenna Type Options

These options involve the antenna gain pattern of the facility antenna in the vertical plane. Patterns are currently built into the program for isotropic and "JTAC directive" [JTAC, 1970, p. 51; Gierhart and Johnson, 1973, eq (67)]. Program modifications can easily be made to accommodate other patterns that are specified in terms of gain versus elevation angle.

Antenna pattern data are used to provide information on gain relative to the main beam only. The extent to which the facility's main beam antenna gain exceeds that of an isotropic antenna is included as input data.

Main Beam Gain

The facility antenna's main beam gain is specified in decibels greater than isotropic. Since the isotropic

pattern option selection (above) does not determine gain it is possible to specify a uniform vertical pattern ("isotropic") with gain.

Polarization Options

The option selected for polarization (horizontal) when a specific option is not selected will frequently result in poorer propagation conditions for typical line-of-sight air/ground links.

Refractivity

Values for the minimum monthly mean surface refractivity referred to mean sea level, N_0, may be obtained from figure 2. Specification of N_0 outside the 250 to 400 N-unit range will result in N_0 being set to 301. The surface refractivity, N_s, is calculated from N_0 [Rice et al., 1967, eq (4.3)] and an effective earth radius calculated [Rice et al., 1967, eq (4.4)]. An N_s of 301 N-units corresponds to an effective earth radius factor of 4/3 (Rice et al., 1967, fig. 4.2). An option to input the effective earth radius directly is available; the program will then calculate N_s and N_0.

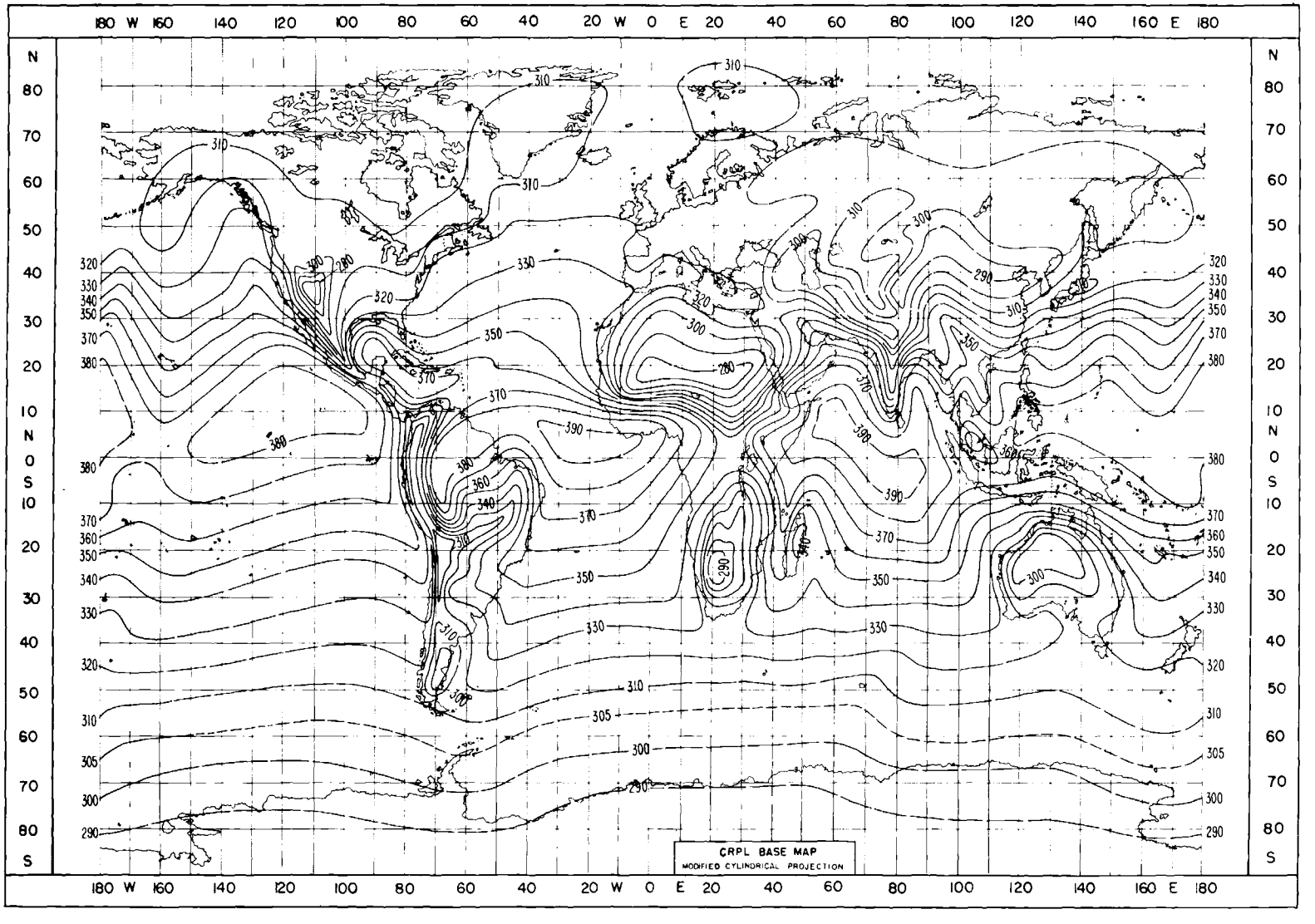

Figure CII-2. Surface refractivity map (Rice et al., 1967). Minimum mean surface refractivity values are referred to mean sea level, N_o N-units.

Spectral Parameters

Defining lobe 1 as the first maximum on the lobing graph (fig. 5) and numbering consecutively toward the origin, any five consecutive lobes can be selected, up to lobe 10, to obtain plots of the effects of the fading on a signal with a flat spectrum of bandwidth B, specified as a fraction of the carrier frequency. Since, for the lobing graph, four points are calculated to determine each lobe, the spectra for these same four points are calculated for the corresponding spectra.

Surface Type Options

These options fix the conductivity and dielectric constants associated with the effective reflecting surface. Values associated with each option are given in table 1.

Sea State

If fresh or sea water is chosen, an allowance may be made for water by specifying sea state or σ_h. Table CI-6 shows the relationship of sea state to σ_h.

Values for σh provided in table CI-6 were estimated using significant wave height, $H_{1/3}$ m, estimates from Sheets and Boatwright (1970, table 1) with a formulation given by Maskowitz [1964, eq (1)]. However, σ_h in meters may be specified directly when it is desired.

Temperature

The dielectric constants and the conductivity of water vary with salinity and temperature (sec. CI-D.8). The program allows specification of either fresh water or average sea water (3.6% NaCl) along with a choice of three temperatures; 0°, 10°, or 20°C.

Terrain Parameter Δh

This parameter is used to characterize irregular terrain. Values for it may be calculated from path profile data (Longley and Rice, 1968, annex 2), or estimated using table CI-5. This parameter is used only to obtain estimates of the surface roughness factor (sec. CI-D.7).

Graph Options

Any combination of the graphs described in section CII-C may be produced in a particular program run.

Graph Grid Scaling

Limits and scaling increments for the graphs of section CII-C may be specified. For the spectral graph one must specify the beginning and ending lobe, counting from the radio horizon. Also for this graph one must specify the bandwidth as a function of carrier frequency (sec. CII-C.10).

CII-C Output Generated

The computer produces a listing of parameters associated with a particular run and microfilm plots of computed parameter values versus the facility-to-aircraft great circle distance. These outputs are provided for each parameter set input to the computer and are tied to each other by a run code which is the date and time at which calculations for a particular set started. Only those graphs desired are plotted and the program will bypass portions of the output that are not desired. This is controlled by input codes.

A sample parameter sheet is shown in figure 3.

Graphs produced during the run are summarized on a graph list (fig. 4) that is produced at the time of the run. Items in this list may be used as figure captions. Although the run made to produce figure 4 includes all current graphic options, all graphs (as mentioned above) need not be produced on each run. Samples of the various graphs will be given along with a brief discussion of each in the sequence implied on figure 4. Some additional examples are provided in section CII-B.11.

PARAMETERS FOR ITS PROPAGATION MODEL MAY 74
05/03/74 10:38:03 SUN

AIR-GROUND LINE-OF-SIGHT FOR ISOTROPIC AIRBORNE ANTENNA
REQUIRED OR FIXED

AIRCRAFT ANTENNA ALTITUDE: 30000 FT ABOVE MSL
FACILITY ANTENNA HEIGHT: 100.0 FT ABOVE MSL
FREQUENCY: 1600 MHZ

SPECIFICATION OPTIONAL

ABSORPTION: OXYGEN 0.00832 DB/KM*
WATER VAPOR 0.00000 DB/KM*
EFFECTIVE AIRCRAFT CORRECTION FACTOR: 1199 FT*
EFFECTIVE REFLECTION SURFACE ELEVATION ABOVE MSL:
0 FT
FACILITY ANTENNA TYPE: ISOTROPIC
MAIN BEAM GAIN: 0 DI
POLARIZATION: HORIZONTAL
REFRACTIVITY:
EFFECTIVE EARTH RADIUS: 4980 N MI*
MINIMUM MONTHLY MEAN: 301 N-UNITS AT SEA LEVEL
SPECTRAL PARAMETERS:
BANDWIDTH AS A FRACTION OF CARRIER FREQUENCY:
1.00-002
BEGINNING LOBE: 1 ENDING LOBE: 4
COUNTING FROM THE HORIZON
SURFACE TYPE: SEA WATER
STATE: 0
CALM (GLASSY)
0.00 FT RMS WAVE HEIGHT*
TEMPERATURE: 10 DEG CENTIGRADE
3.5 PERCENT SALINITY
TERRAIN PARAMETER: 0 FT

* COMPUTED OR ESTIMATED VALUE

Figure CII-3. Sample parameter sheet.

GRAPH LIST

05/03/74 10:38:03 RUN

GRAPH 1: TRANSMISSION LOSS (DB) OF THE FIRST TEN LOBES INSIDE THE RADIO HORIZON WITH LIMITING VALUES ASSOCIATED WITH CONSTRUCTIVE AND DESTRUCTIVE INTERFERENCE AND FREE SPACE LOSS VERSUS PATH DISTANCE (N MI)

GRAPH 2: EFFECTIVE REFLECTION COEFFICIENT VERSUS PATH DISTANCE (N MI)

GRAPH 3: PATH LENGTH DIFFERENCE (M) OR THE EXTENT BY WHICH THE LENGTH OF THE REFLECTED RAY EXCEEDS THAT OF THE DIRECT RAY VERSUS PATH DISTANCE (N MI)

GRAPH 4: TIME LAG (NSEC) OF TRANSMISSION VIA THE SURFACE REFLECTION PATH RELATIVE TO THE DIRECT PATH VERSUS PATH DISTANCE (N MI)

GRAPH 5: NOLF (HZ/THZ-KTS) OR THE NORMALIZED DISTANCE LOBING FREQUENCY VERSUS PATH DISTANCE (N MI)

GRAPH 6: NHLF (HZ/THZ-FT/MIN) OR THE NORMALIZED HEIGHT LOBING FREQUENCY VERSUS PATH DISTANCE (N MI)

GRAPH 7: DISTANCE (N MI) FROM FACILITY TO REFLECTION POINT VERSUS PATH DISTANCE (N MI)

GRAPH 8: ELEVATION ANGLE (DEG) OF THE DIRECT RAY AT THE FACILITY ABOVE THE HORIZONTAL VERSUS PATH DISTANCE (N MI)

GRAPH 9: AMOUNT (DEG) BY WHICH THE ELEVATION ANGLE OF THE DIRECT RAY AT THE FACILITY EXCEEDS THAT OF THE REFLECTED RAY VERSUS PATH DISTANCE (N MI)

GRAPH 10: SPECTRAL PLOT OR THE FADING ACROSS FLAT SPECTRA OF BANDWIDTH (PERCENT OF CARRIER FREQUENCY) CORRESPONDING TO THE LOBING STRUCTURE

Figure CII-4. Sample graph list.

CII-C.1 Lobing Graph

Figure 5 shows a sample of the "LOBING" graph. Transmission loss is plotted against path distance for (a) lobing (solid curve) caused by interference between direct and reflected rays for the first 10 lobes inside the radio horizon, (b) limiting values associated with constructive (low loss, upper curve with small dots) and destructive (high loss, lower curve with small dots) interference, and (c) free space (curve with large dots).

Antenna gains are included in transmission loss since it is the difference (dB) between power radiated (dBW), and the power available (dBW) at the terminals of an ideal receiving antenna (no internal losses), but in the sample run presented here, transmission loss is the same as basic transmission loss because isotropic antennas were assumed. Relative antenna gains, surface parameters (dielectric constant, conductivity, and roughness), frequency and grazing angle (ψ of fig. 10, sec. CI-D) are included in the effective reflection coefficient formulation used in interference calculations (CI-C). The reduction in spacing between the limiting curves at about 10 n mi and at the far distances is caused by a small reflection coefficient (CII-C.2).

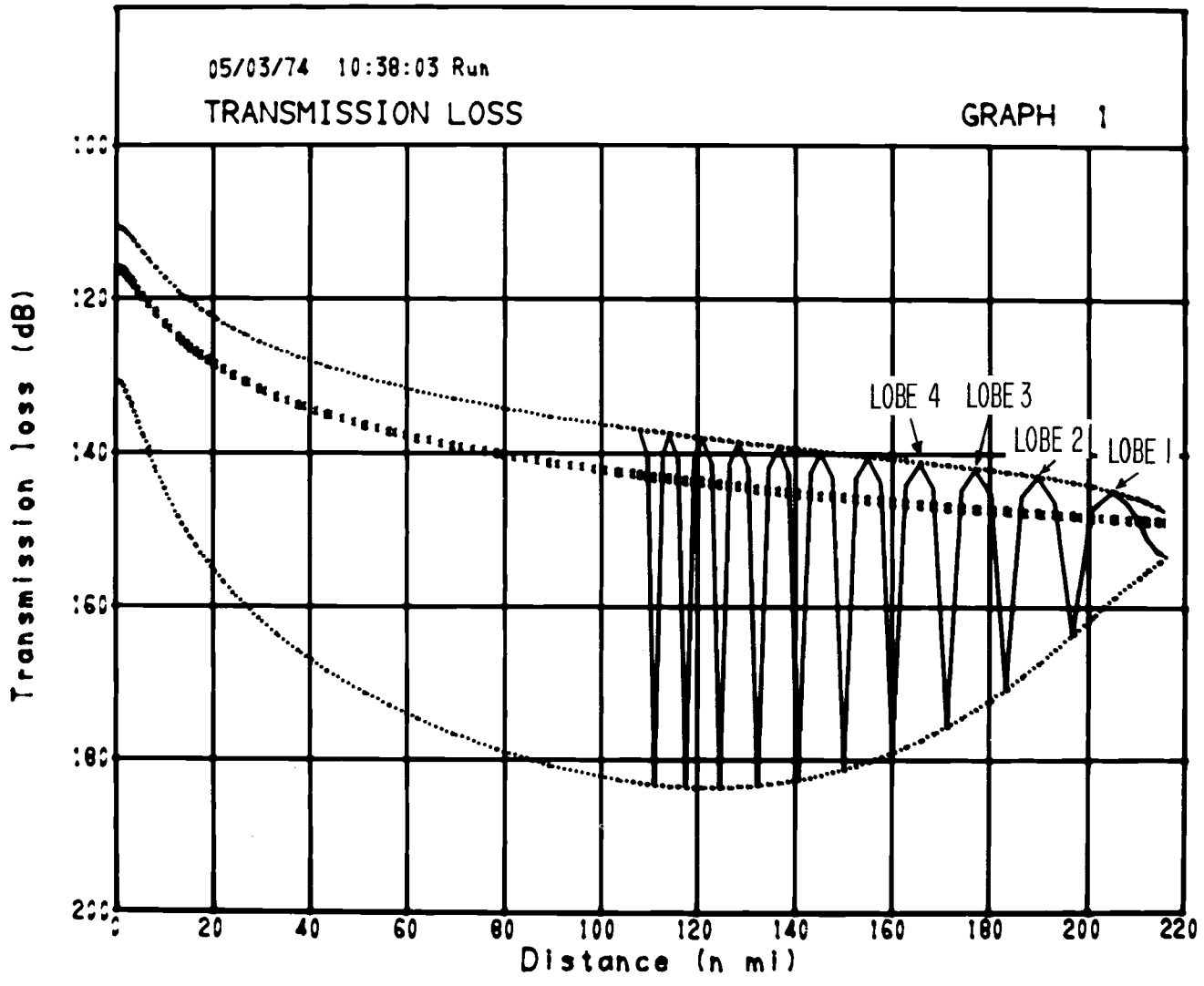

Figure CII-5. Sample lobing graph. Transmission loss (dB) of the first ten lobes inside the radio horizon with limiting values associated with constructive and destructive interference and free space loss versus path distance (n mi).

There is a test built into the program that limits the maximum transmission loss to its free space value plus 40 dB.

CII-C.2 Reflection Coefficient Graph

Figure 6 shows a sample of the "REFLECTION COEFFICIENT" graph. Effective reflection coefficient is plotted against path distance.

Relative antenna gains, surface parameters (dielectric constant, conductivity and roughness), frequency and grazing angle (ψ of fig. 10, sec. CI-D) are included in the calculation of effective reflection coefficient (sec. CI-D). The drop in reflection coefficient at the near distances is associated with the path length reduction factor (CI-D.5). The drop in reflection coefficient at the far distances is caused by the divergence factor (CI-D.1).

CII-C.3 Path Length Difference Graph

Figure 7 shows a sample of the "PATH LENGTH DIFFERENCE" graph. The extent by which the length of the reflected ray exceeds that of the direct ray (Δr of sec. CI-C) is plotted against path distance.

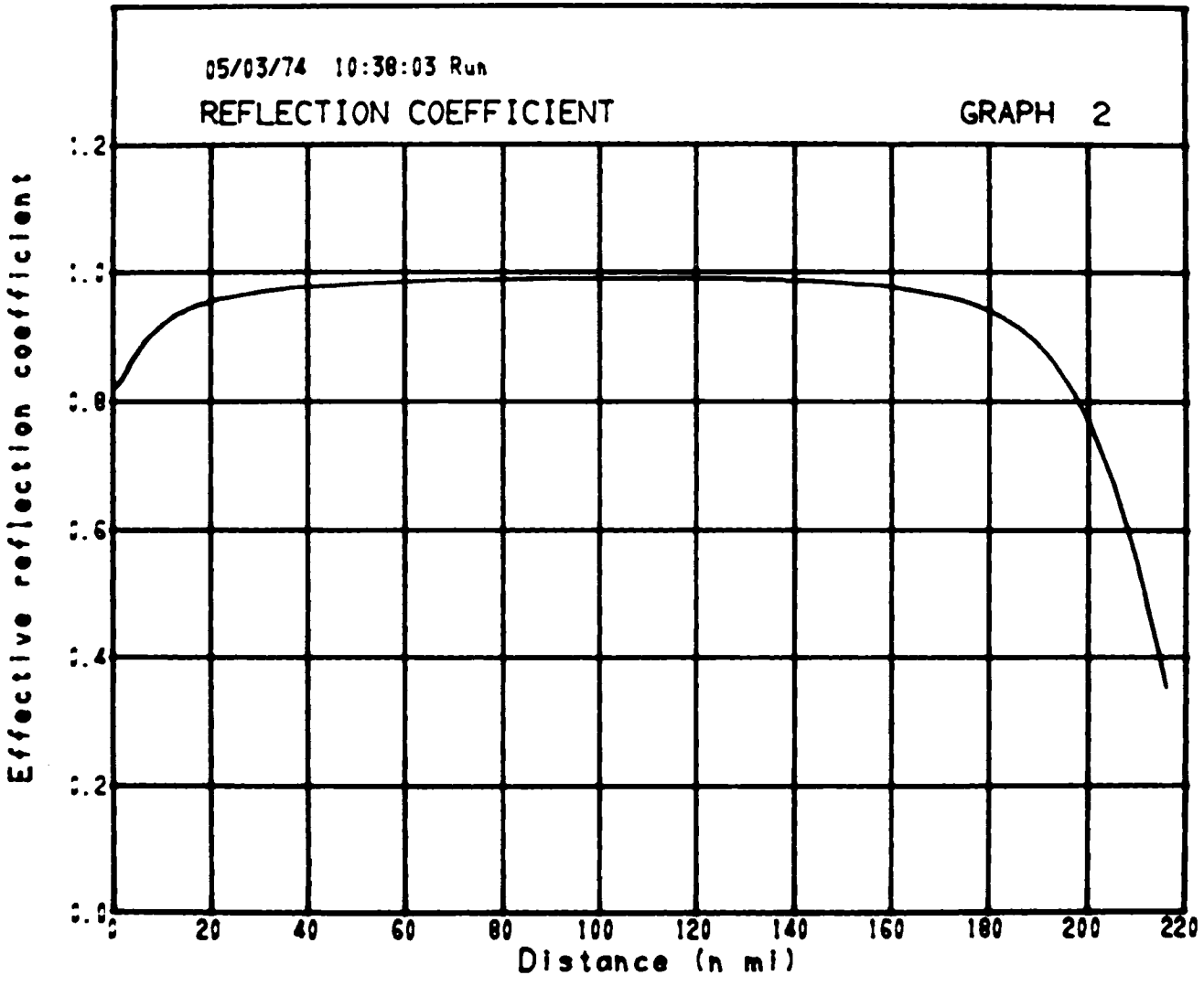

Figure CII-6. Sample reflection coefficient graph. Effective reflection coefficient versus path distance (n mi).

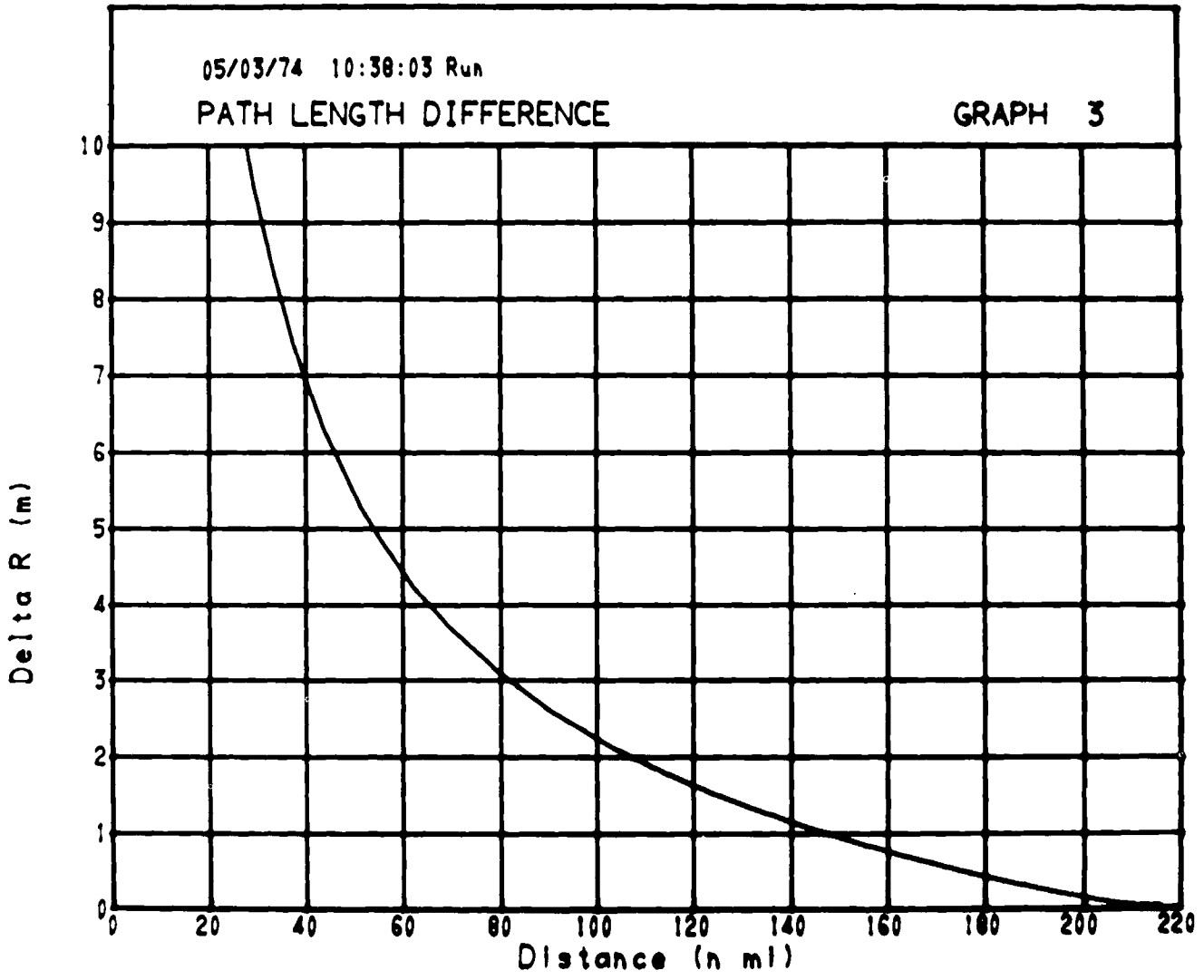

Figure CII-7. Sample of path length difference graph. Path length difference (m) or the extent by which the length of the reflected ray exceeds that of the direct ray versus path distance (n mi).

CII-C.4 Time Delay Graph

Figure 8 shows a sample of the "TIME DELAY" graph. The time delay of transmission via the surface reflection path relative to the direct path is plotted against path distance.

CII-C.5 Normalized Distance Lobing Frequency Graph

Figure 9 shows a sample of the "NORMALIZED DISTANCE LOBING" graph. Lobing frequency, f_d Hz, for the parameters of figure 1 and an aircraft traveling directly toward (or away from) the facility may be determined from values of normalized distance lobing frequency, NDLF Hz/THz-kt, read from this graph, radio frequency, f THz (1 THz=10^6 MHz) and the magnitude of its velocity $|V_d|$ kts, i.e.,

$$f_d = \text{NDLF [Hz/THz-kts]} \; f \text{ [THz]} \; |V_d| \text{ [kts]} \quad \text{Hz} \qquad (1)$$

so that $f_d = 4.0 \times 10^{-2}$ Hz when NDLF = 0.10 Hz/THz-kt (at a distance of 50 nmi), f = 1.6×10^{-3} THz, and $|V_d|$ = 250 kts which may be compared with $f_d = 4.2 \times 10^{-2}$ Hz obtained using more approximate methods in table 3 (sec. CI-D).

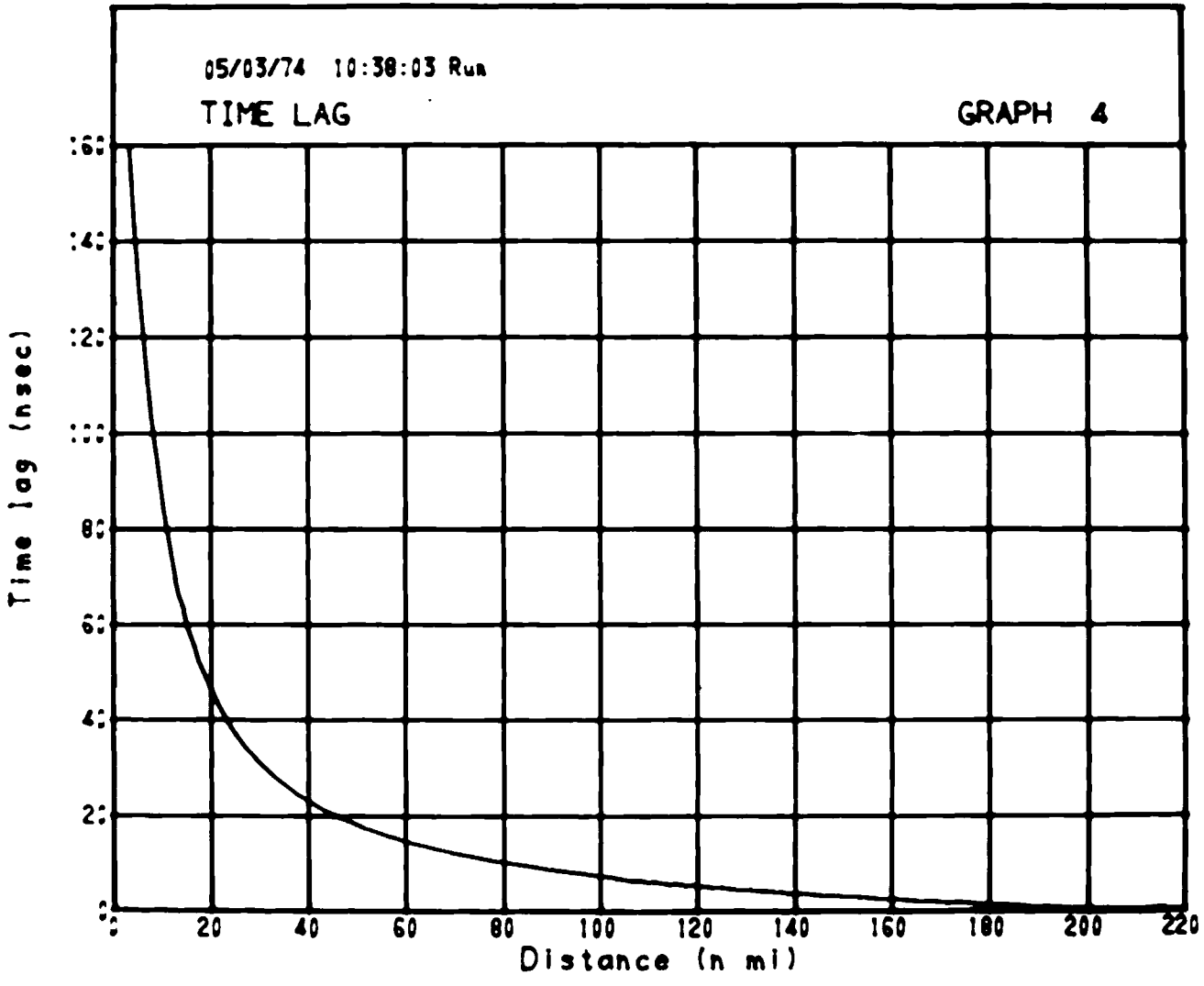

Figure CII-8. Sample time lag graph. Time lag (nsec) of transmission via the surface reflection path relative to the direct path versus path distance (n mi).

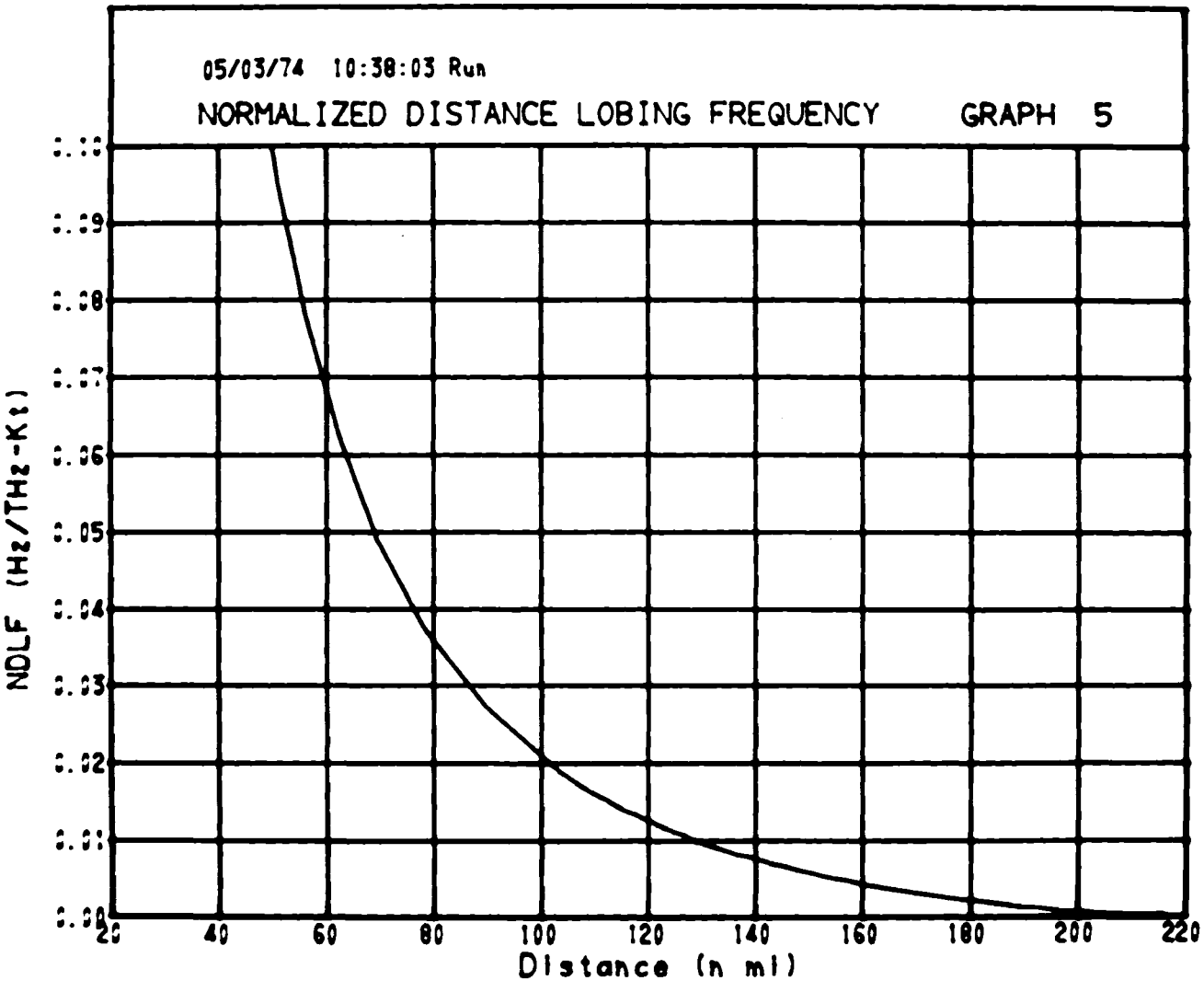

Figure CII-9. Sample normalized distance lobing frequency graph. NDLF(Hz-THz-kts) versus path distance (n mi).

CII-C.6 Normalized Height Lobing Frequency Graph

Figure 10 "NORMALIZED HEIGHT LOBING FREQUENCY" shows a sample of the graph. Lobing frequency, f_h Hz, for the parameters of figure 3 and an aircraft in vertical ascent (or descent may be determined from values of normalized lobing frequency, DHLF Hz-min/THz-ft, read from this graph, radio frequency, f THz, and the magnitude of the ascent rate $|V_h|$ Hz-min/THz-ft, i.e.;

$$f = \text{NHLF}\ [\text{Hz-min/THz-ft}]\ f[\text{THz}]|V_h|\ [\text{ft/min}] \quad \text{Hz} \quad (2)$$

so that $f_h = 1.8 \times 10^{-2}$ when NHLF = 1.1×10^{-2} Hz-min/THz-ft (at a distance of 50 nmi), f = 1.6×10^{-3} THz, and $|V_h| = 10^3$ ft/min which may be compared with $f_h = 1.8 \times 10^{-2}$ Hz obtained using more approximate methods in table 3.

CII-C.7 Reflection Point Graph

Figure 11 shows a sample of the "REFLECTION POINT" graph. Distance (d_1 of fig. 9, sec. CI) from facility-to-reflection point is plotted against path distance.

CII-C.8 Elevation Angle Graph

Figure 12 shows a sample of the "ELEVATION ANGLE" graph. The elevation angle (θ_h of fig. 10, sec. CI) of the direct ray at the facility in degrees above horizontal is plotted against path distance.

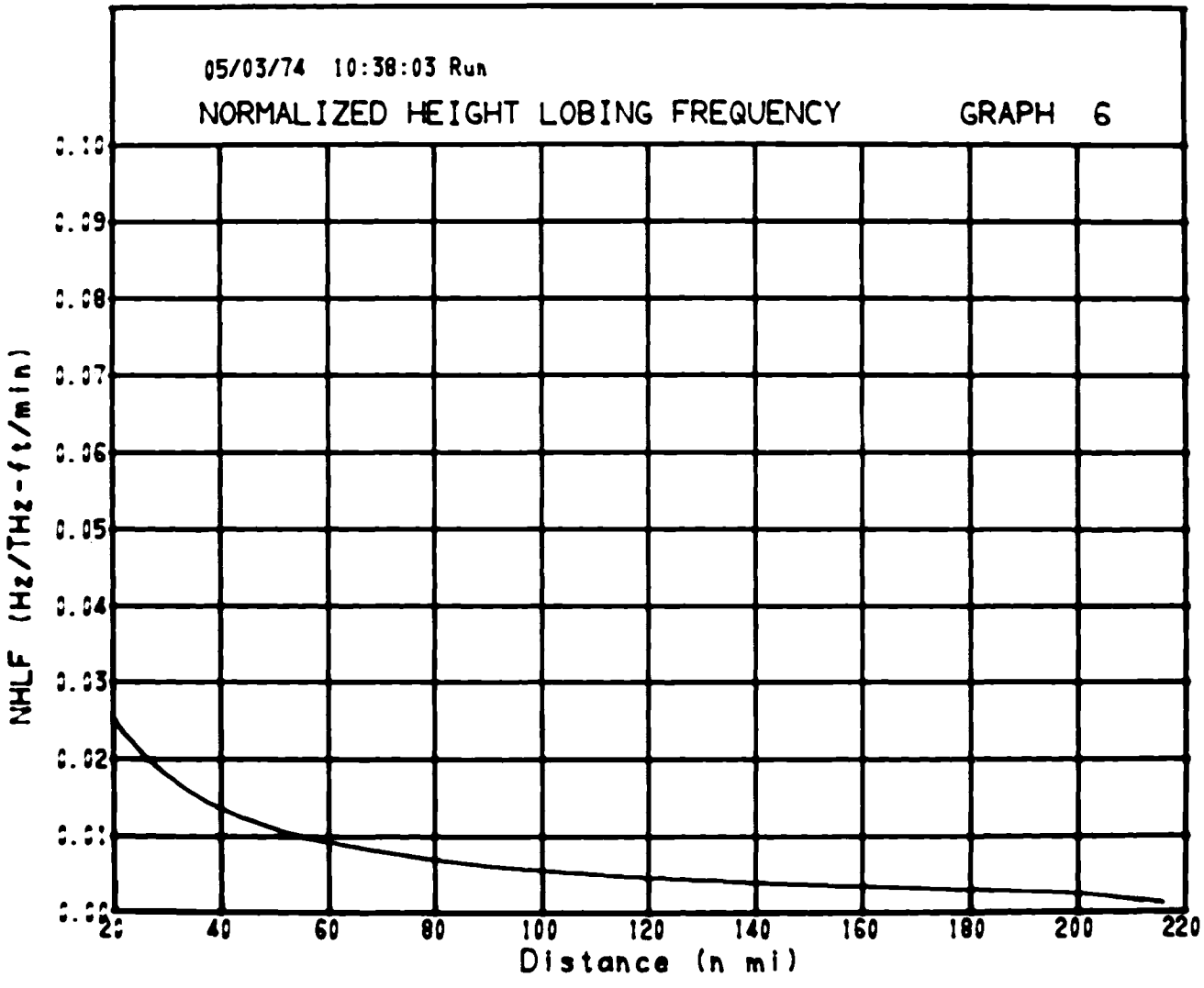

Figure CII-10. Sample normalized height lobing frequency graph. NHLF(Hz/THz-ft/min) versus path distance (n mi).

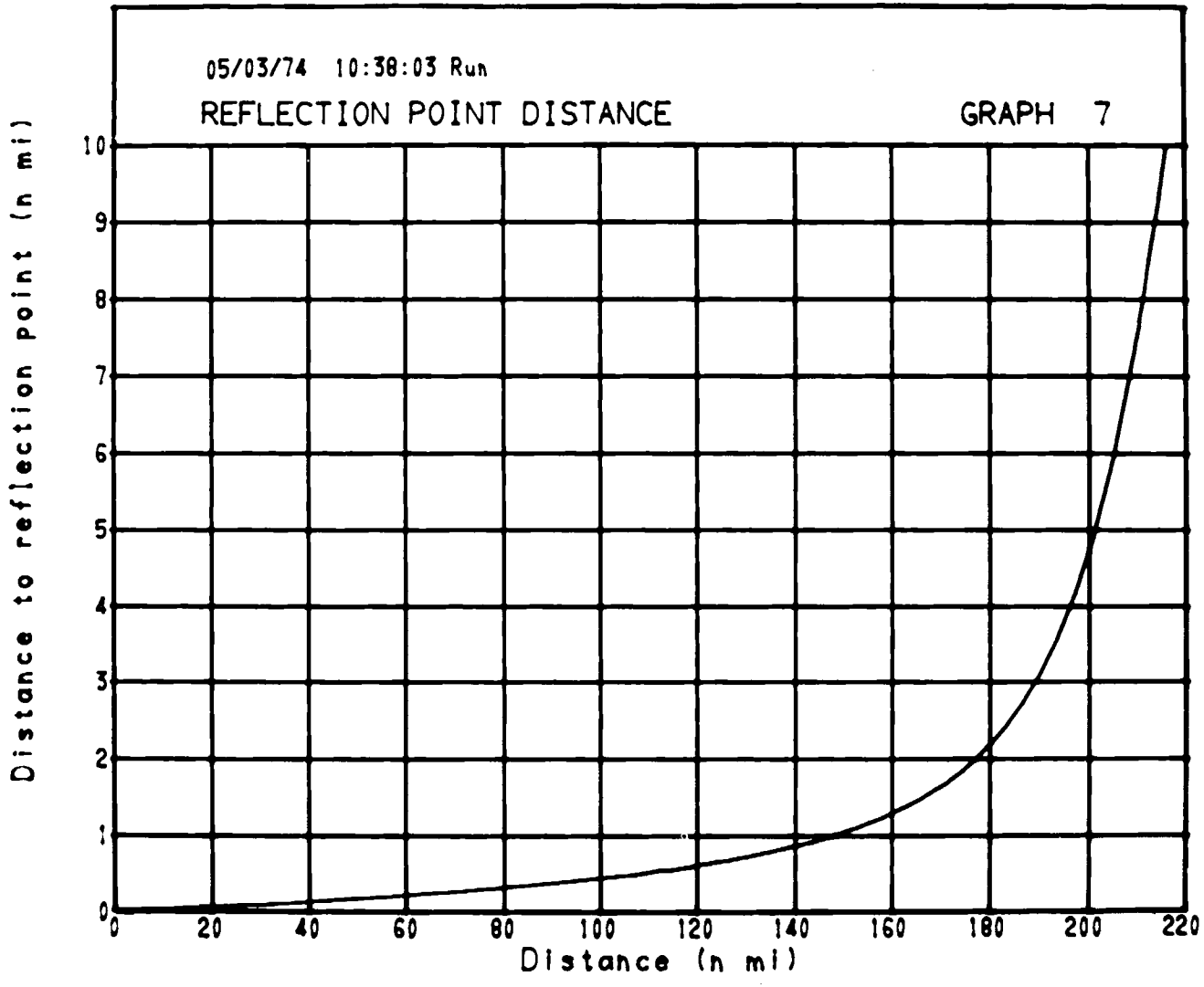

Figure CII-11. Sample reflection point graph. Distance (n mi) from facility to reflection point versus path distance (n mi).

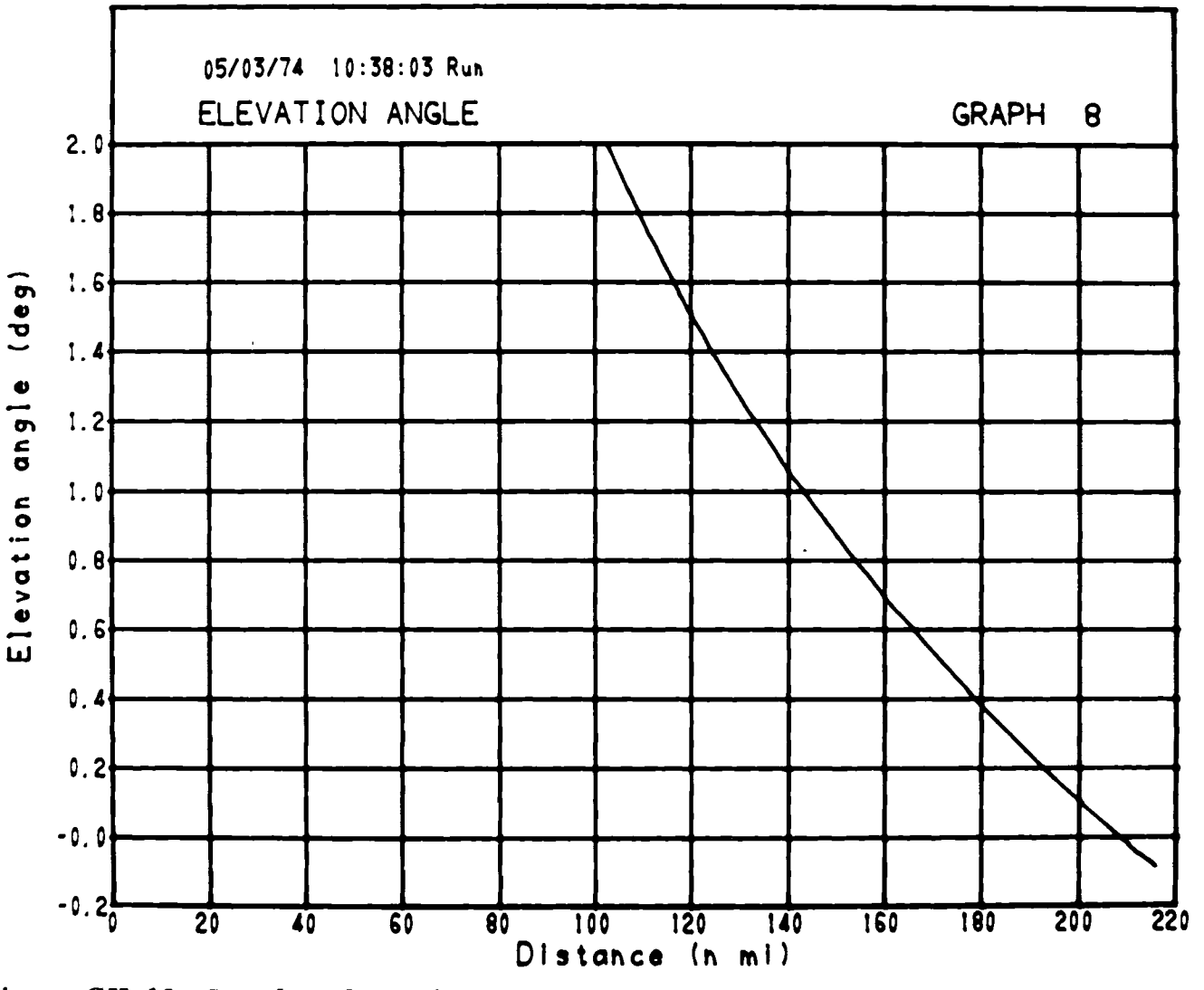

Figure CII-12. Sample elevation angle graph. Elevation angle (deg) of the direct ray at the facility above the horizontal versus path distance (n mi).

CII-C.9 Elevation Angle Difference Graph

Figure 13 shows a sample of the "ELEVATION ANGLE DIFFERENCE" graph. The amount by which the elevation angle at the facility of the direct ray exceeds that of the reflected ray (elevation angle difference) is plotted against path distance.

CII-C.10 Spectral Graph

Figure 14 shows one spectrum corresponding to each point calculated for the lobing graph, figure 5, between the lobes chosen, in this figure lobes 1-4 as labeled in figure 5. Each spectrum is of bandwidth 2Bf , where B is a fraction of the carrier frequency. The scale along the diagonal axis is proportional to the distance shown for that point on the lobing graph, and maximum range is 43 dB, the height of lobe 4 above the origin.

CII-C.11 Additional Examples

Several additional graphs are included in this section to illustrate the effect of the divergence factor and the pseudo Brewster angle.

The divergence factor (sec. CI-D.1) is used to allow for the divergence of energy reflected from a curved surface

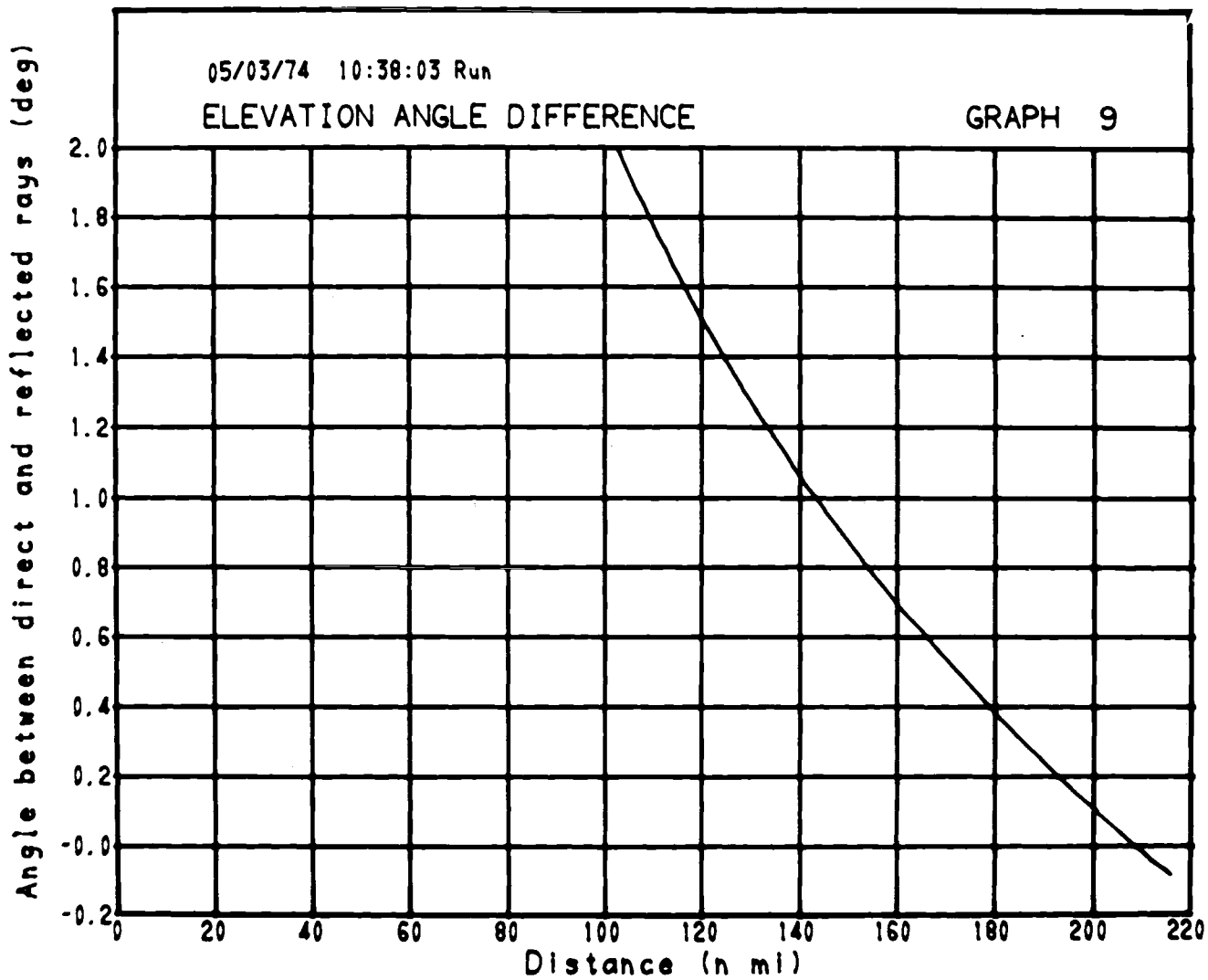

Figure CII-13. Sample elevation angle difference graph. Amount (deg) by which the elevation angle of the direct ray at the facility exceeds that of the reflected ray versus path distance (n mi).

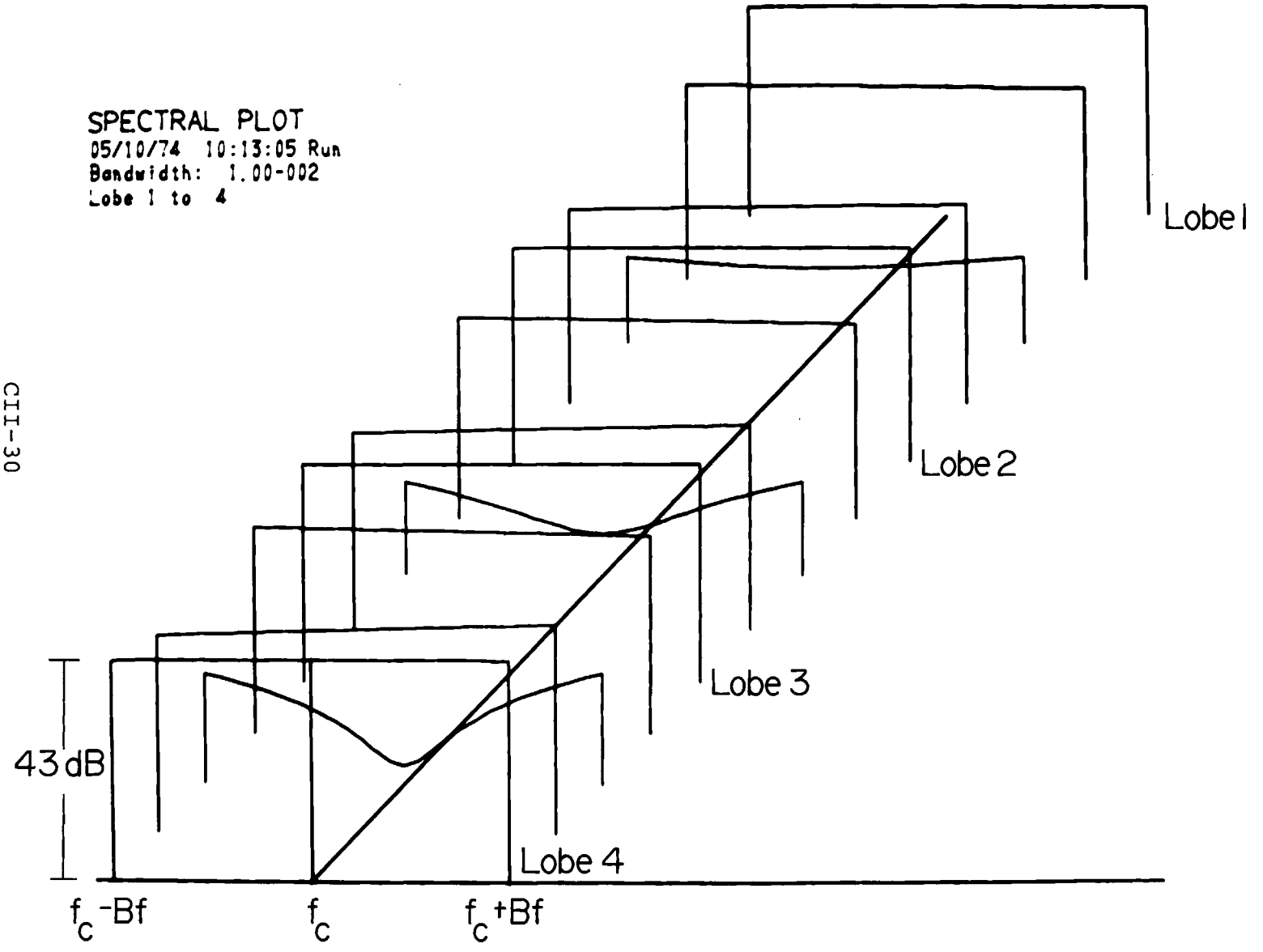

Figure CII-14. Sample spectral plot. Fading across flat spectra of Bandwidth B (2 percent of carrier frequency f_c) corresponding to the lobing structure shown in figure 5.

in the effective reflection coefficient formulation [sec. CI-D, eq (132)]. It decreases the effective reflection coefficient so that lobing is less pronounced than it would be otherwise. This is illustrated by a comparison of figure 15 with figure 6, and of figure 16 with figure 5. These graphs were all calculated for identical parameters (fig. 3), but divergence was neglected (taken as unity) in the calculations for figures 15 and 16. Divergence has its most pronounced effect at low grazing angles (near the radio horizon) and becomes more important as antenna heights are increased. However, it does not depend on frequency.

The plane earth reflection coefficient for vertical polarization goes through a minimum and encounters a radical phase shift as the grazing angle passes through a critical value known as the pseudo Brewster angle [CI-D.8, eq (174), figs. 26 through 29]. Figure 17 shows the dip in reflection coefficient for calculations made for vertical polarization and a facility antenna height of 10 ft where the other parameters are as given in figure 3. Figure 18 shows the corresponding lobing graph where the effect of the reflection coefficient magnitude and phase change is clearly visible.

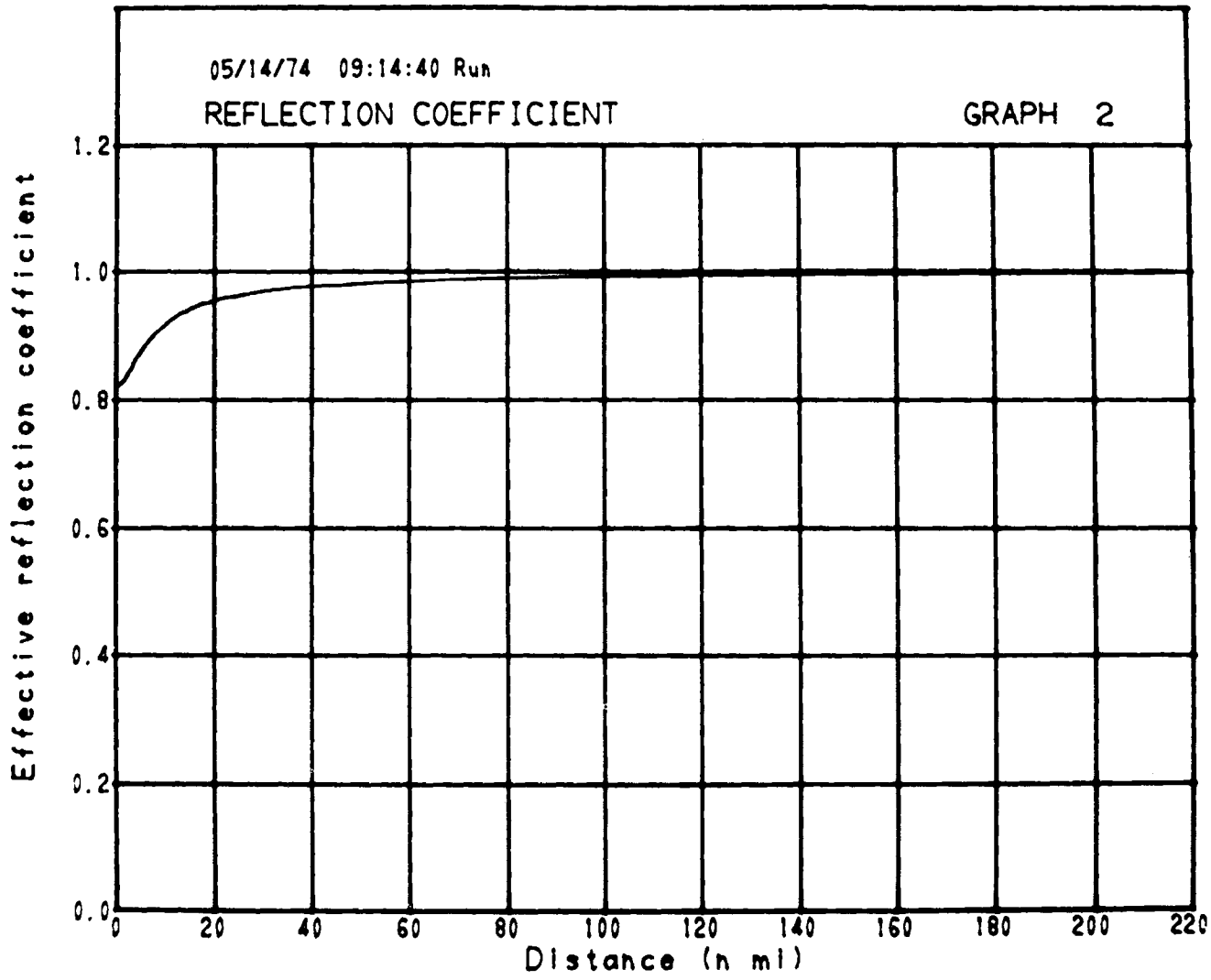

Figure CII-15. Effective reflection coefficients without divergence (c.f., fig. 6).

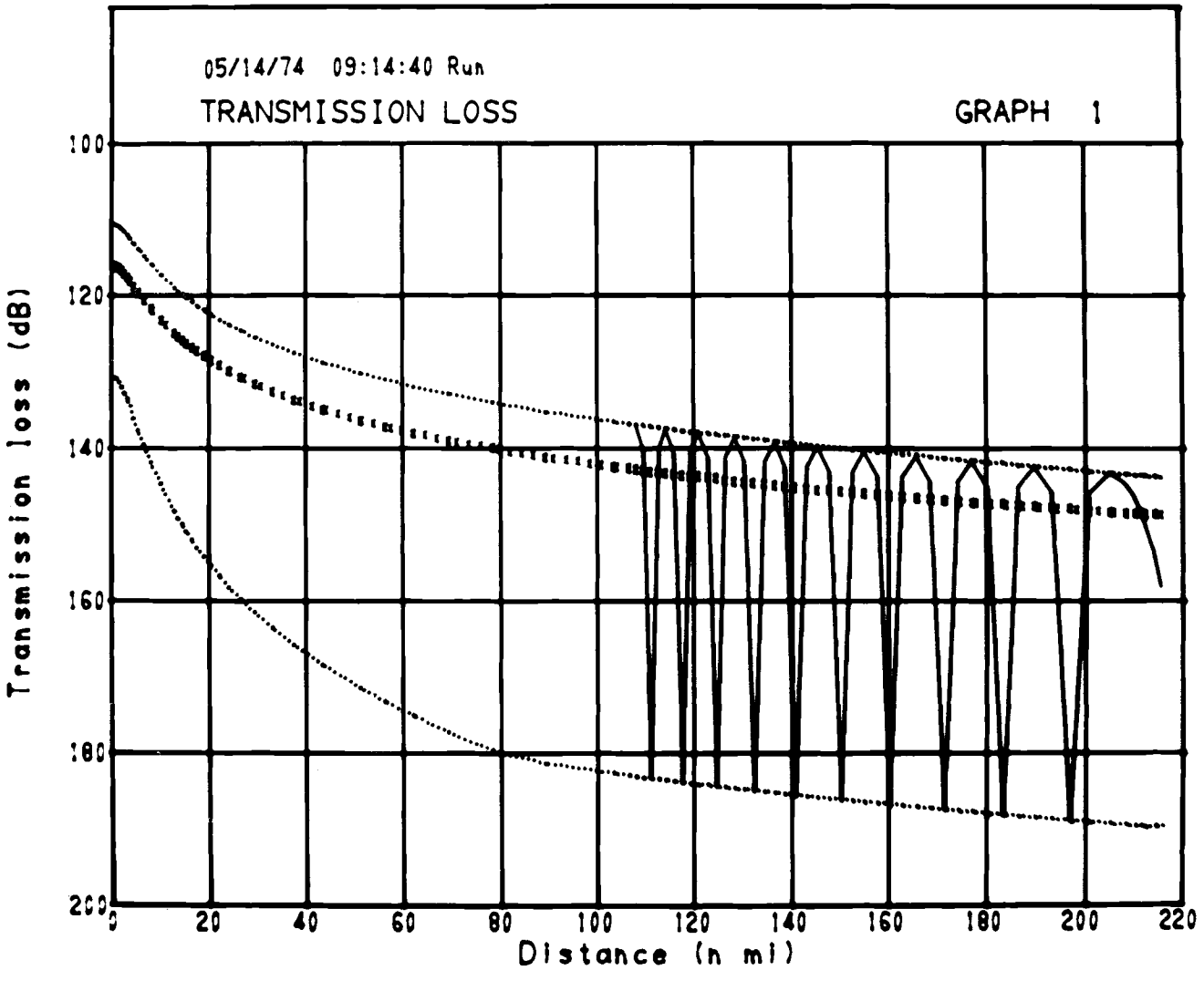

Figure CII-16. Lobing without divergence (c.f., fig. 5).

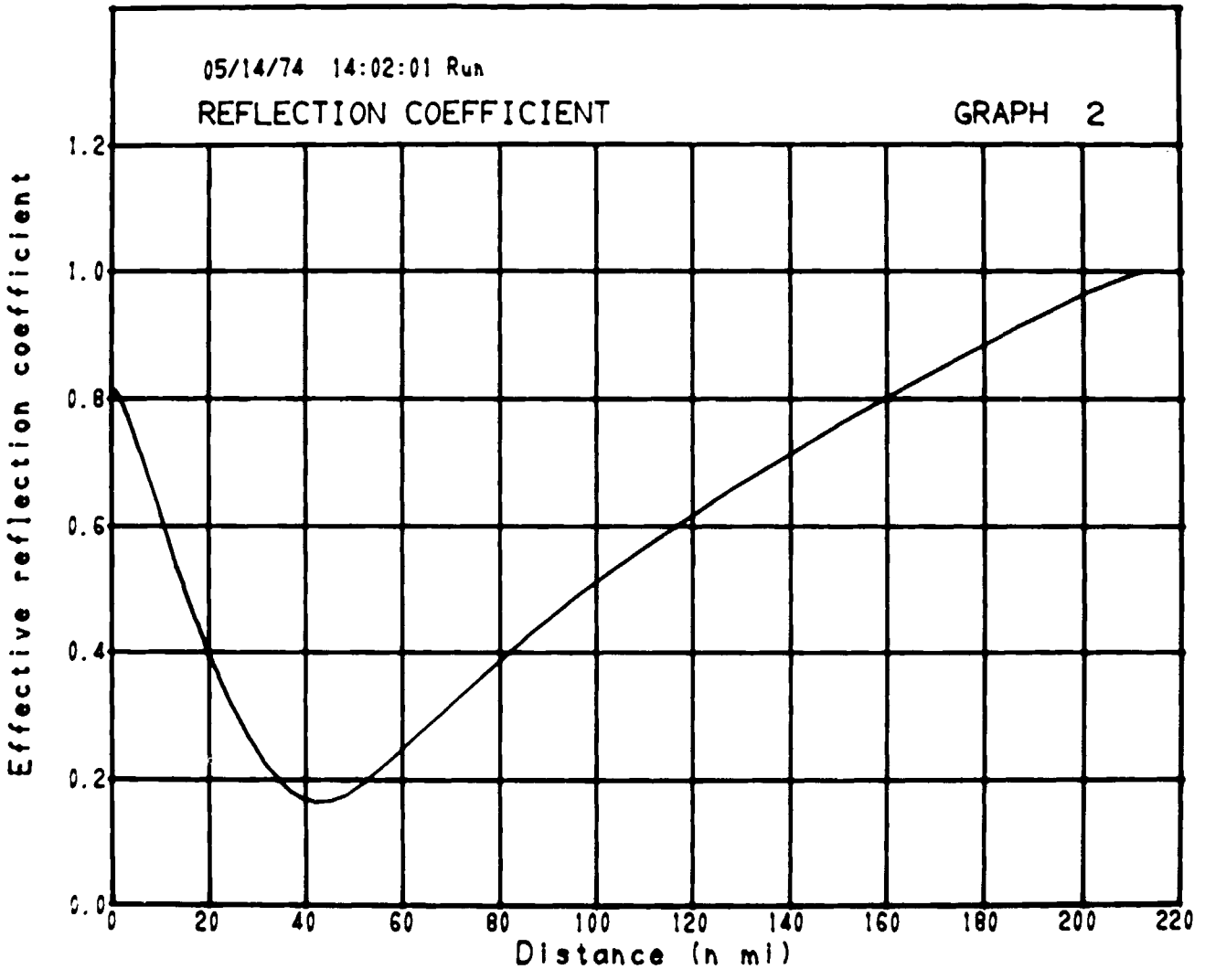

Figure CII-17. Reflection coefficients for vertical polarization and a facility antenna height of 10 ft (other parameters as per fig. 3).

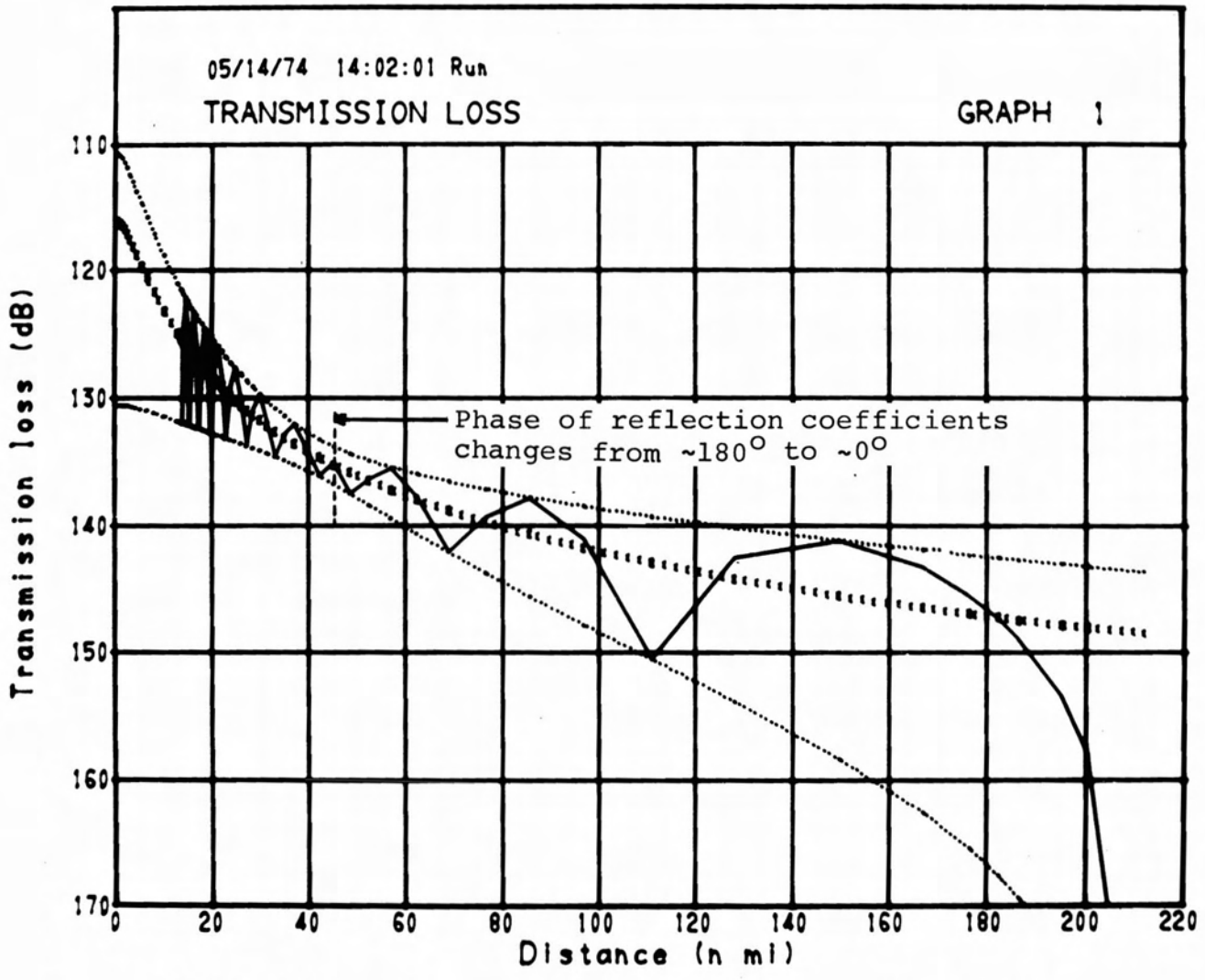

Figure CII-18. Lobing for vertical polarization and a facility antenna height of 10 ft (other parameters as per fig. 3).

CII-D. REFERENCES

BEAN, B.R., AND E.J. DUTTON (1966), RADIO METEOROLOGY, NBS MONOGRAPH 92 (GPO, $2.75)

GIERHART, G.D., AND M.E. JOHNSON (1973), COMPUTER PROGRAMS FOR AIR/GROUND PROPAGATION AND INTERFERENCE ANALYSIS, 0.1 TO 20 GHZ, DOT REPT. FAA-RD-73-103 (NTIS, AD-770 335)

JTAC (1970), RADIO SPECTRUM UTILIZATION IN SPACE, JOINT TECHNICAL ADVISORY COMMITTEE (INSTITUTE OF ELECTRICAL AND ELECTRONICS ENGINEERS, NEW YORK, N.Y. 10017).

KERR, D.E. (1964), PROPAGATION OF SHORT RADIO WAVES, M.I.T. RADIATION LABORATORY SERIES 13 (BOSTON TECHNICAL PUBLISHERS, INC., LEXINGTON, MASS.)

LONGLEY, A.G., AND P.L. RICE (1968), PREDICTION OF TROPOSPHERIC RADIO TRANSMISSION LOSS OVER IRREGULAR TERRAIN, A COMPUTER METHOD - 1968, ESSA TECH. REPT. ERL 79-ITS 67 (GPO, $0.70)

MOSKOWITZ, L. (1964), ESTIMATES OF THE POWER SPECTRUMS FOR FULLY DEVELOPED SEAS FOR WIND SPEEDSOOF 20 TO 40 KNOTS, J. GEOPHYS. RES. 69, NO. 24, 5161-5179.

RICE, P.L., A.G. LONGLEY, K. A. NORTON, AND A.P. BARSIS, (1967), TRANSMISSION LOSS PREDICTIONS FOR TWOPOSPHERIC COMMUNICATIONS CIRCUITS, NBS TECH. NOTE 101, VOLS. 1 AND 2 (NTIS AD 687 820 AND AD 687 821).

SHEETS, H.E., AND V.T. BOATWRIGHT, JR. (1970), HYDRONAUTICS (ACADEMIC PRESS, NEW YORK, N.Y.)